# TABLE OF CONTENTS

# LIST OF FIGURES

# LIST OF TABLES

# LIST OF ELECTRONIC APPENDICES

---

## Appendix A – Pyrrhotite Mineralogy

A1: D \ Appendix A \ A1 Pyrrhotite Mineral Chemistry.xls

## Appendix B – Pyrrhotite Reactivity

B1: D \ Appendix B \ B1 Open Circuit Potential.xls

B2: D \ Appendix B \ B2 Cyclic Voltammetry.xls

B3: D \ Appendix B \ B3 Reagent Dosages for Oxygen Uptake.xls

B4: D \ Appendix B \ B4 Calculation and Repeatability of the $O_2$ uptake factor.pdf

B5: D \ Appendix B \ B5 $O_2$ Uptake.xls

## Appendix C – Pyrrhotite Microflotation

C1: D \ Appendix C \ C1 Microfloat Feed Liberation.xls

C2: D \ Appendix C \ C2 Reagent Dosages for Microfloats.xls

C3: D \ Appendix C \ C3 Pyrrhotite Microflotation.xls

# LIST OF ABBREVIATIONS

| | |
|---|---|
| AA | Atomic absorption spectroscopy |
| AMD | Acid mine drainage |
| AES | Auger electron spectroscopy |
| ARXPS | Angle resolved x-ray photoelectron spectroscopy |
| BET | Brunauer, Emmett, Teller |
| BIC | Bushveld Igneous Complex |
| BMS | Base metal sulfide |
| BSE | Back scattered electron |
| CCN | Copper Cliff North |
| Ccp | Chalcopyrite |
| CMC | Carboxymethycellulose |
| DETA | Diethylenetriamine |
| EBSD | Electron back scattered diffraction |
| EDTA | Ethylenediaminetetraacetic acid |
| EMP | Electron microprobe |
| FTIR | Fourier transform infrared spectroscopy |
| Hex | Hexagonal |
| HRTEM | High resolution transmission electron microscopy |
| LA ICP-MS | Laser ablation inductively coupled plasma mass spectrometry |
| LIMS | Laser ion mass spectrometry |
| M | Metal |
| Mag | Magnetite |
| Mag Po | Magnetic pyrrhotite |
| Mon | Monoclinic |
| MSB | Massive Sulfide Body (Nkomati) |
| MLA | Mineral Liberation Analyser |
| MMZ | Main Mineralized Zone (Nkomati) |
| MSS | Monosulfide solid solution |

| | |
|---|---|
| Non-mag Po | Non-magnetic Pyrrhotite |
| ORP | Oxidation reduction potential |
| Ortho | Orthorhombic |
| PDA | Personal digital assistant |
| Pent | Pentlandite |
| PGE | Platinum group elements |
| PGM | Platinum group minerals |
| PIXE | Particle induced x-ray emission |
| Po | Pyrrhotite |
| Py | Pyrite |
| QEMSCAN | Quantitative evaluation of minerals by scanning electron microscopy |
| QXRD | Quantitative powder x-ray diffraction |
| RPL | Reflected polarised light |
| SEM | Scanning electron micoscope |
| SCE | Standard calomel electrode |
| SHE | Standard hydrogen electrode |
| SIBX | Sodium isobutyl xanthate |
| SIC | Sudbury Igneous Complex |
| SNPX | Sodium normal propyl xanthate |
| TETA | Triethylenetriamine |
| ToF SIMS | Time of flight secondary ion mass spectroscopy |
| Tr | Troilite |
| Wt | Weight |
| X | Xanthate |
| $X_2$ | Dixanthogen |
| XANES | X-ray absorption near-edge structure spectroscopy |
| XMCD | X-ray magnetic circular dichroism |
| XPRL | Cross polarised reflected light |
| XPS | X-ray photoelectron spectroscopy |
| X-ray CT | X-ray computed tomography |
| XRD | X-ray diffraction |

# GLOSSARY

The following definitions are given within the context of this study:

| | |
|---|---|
| Anhedral | Textural term to describe a mineral grain that does not show a well developed crystal form |
| Antiferromagnetic | Magnetic state of a material where opposing magnetic moments are equal and result in no net magnetic character |
| Archean | Geological time period 2.5 billion years before present |
| Disseminated | Textural description of an ore consisting of fine grains of valuable minerals dispersed throughout the bulk of the rock |
| *En echelon* | Textural term to describe very closely spaced, overlapping and parallel to sub-parallel structural features |
| Euhedral | Textural term to describe a mineral grain that shows well developed crystal form |
| Exsolution | Unmixing of two phases from a solid solution |
| Ferrimagnetic | Magnetic state of a material where opposing magnetic moments are unequal and result in a net magnetic character |
| Greenstone belt | Ancient geological structure comprised of metamorphosed volcanic rocks with associated sedimentary rocks |
| "Hexagonal" pyrrhotite | Common reference to non-magnetic NC pyrrhotite used in the literature. When quoted here, it is in reference to the terminology used by the authors of a particular study, even though 5C pyrrhotite is shown to be orthorhombic. |
| Liberated | A particle with greater than 95% surface area exposed |
| Liberation | Proportion of the surface area of a particle which is exposed |
| Locked | Mineral grain that is entirely enclosed by other grains and has no exposed surface area |
| Middlings | Mineral grain that is partially liberated |

| | |
|---|---|
| Orogenic | Mountain building |
| Paramagnetic | Magnetic state of a material where the orientation of magnetic moments is completely random |
| Petrogenesis | Origin of rocks |
| Petrography | Description of rock textures |
| Proterozoic | Geological time period from 1.5 billion to 542 million years before present |
| Subhedral | Textural term to describe a mineral grain that shows partially developed crystal form |
| Superstructure | Pyrrhotite structure based upon multiple repeats of the smaller NiAs unit cell |

# Chapter 1

# INTRODUCTION

---

## 1.1 Introduction

Pyrrhotite $Fe_{(1-x)}S$ is one of the most commonly occurring metal sulfide minerals and is recognised in a variety of ore deposits including nickel-copper, lead-zinc, and platinum group element (PGE). Since the principal nickel ore mineral, pentlandite, almost ubiquitously occurs coexisting with pyrrhotite, the understanding of the behaviour of pyrrhotite during flotation is of fundamental interest. For many nickel processing operations, pyrrhotite is rejected to the tailings in order to control circuit throughput and concentrate grade and thereby reduce excess sulfur dioxide smelter emissions (e.g. Sudbury; Wells *et al.*, 1997). However, for platinum group element processing operations, pyrrhotite recovery is targeted due to its association with the platinum group elements and minerals (e.g. Merensky Reef; Penberthy and Merkle, 1999; Ballhaus and Sylvester, 2000). Therefore, the ability to be able to manipulate pyrrhotite performance in flotation is of great importance. It can be best achieved if the mineralogical characteristics of the pyrrhotite being processed can be measured and the relationship between mineralogy and flotation performance is understood.

The pyrrhotite mineral group is non-stoichiometric and has the generic formula of $Fe_{(1-x)}S$ where $0 \leq x < 0.125$. Pyrrhotite is based on the nickeline (NiAs) structure and is comprised of several superstructures owing to the presence and ordering of vacancies within its structure. Numerous pyrrhotite superstructures have been recognised in the literature, but only three of them are naturally occurring at ambient conditions (Posfai *et al.*, 2000; Fleet, 2006). This includes the stoichiometric FeS known as troilite which is generally found in extraterrestrial localities, but on occasion, has also been recognised in some nickel deposits (e.g. Voisey's Bay, Bushveld Igneous Complex; Liebenberg, 1970; Naldrett *et al.*, 2000). The commonly occurring magnetic pyrrhotite is correctly known as 4C pyrrhotite, has an ideal composition $Fe_7S_8$ and monoclinic crystallography (Powell *et al.*, 2004). Non-magnetic pyrrhotite is formally described as *N*C pyrrhotite where *N* is an integer between 5 and 11 (Morimoto *et al.*,

1970). Non-magnetic NC pyrrhotite has a range of ideal compositions varying from $Fe_9S_{10}$, $Fe_{10}S_{11}$ to the least iron deficient composition of $Fe_{11}S_{12}$. Although NC pyrrhotite is generally known as "hexagonal pyrrhotite", it has been argued to be pseudohexagonal and may actually be monoclinic or orthorhombic (Carpenter and Desborough, 1964; Morimoto *et al.*, 1970; Koto *et al.*, 1975; Posfai *et al.*, 2000).

Pyrrhotite is known to be a reactive mineral which is highly prone to oxidation (Rand, 1977; Belzile *et al.*, 2004). The downstream consequences of this during minerals beneficiation may be quite severe, an example of which is the Nickel Rim site in Sudbury described by Johnson *et al.* (2000). The Nickel Rim site is actively suffering from the release of low pH waters, high concentrations of iron, and dissolved metals such as nickel and aluminium and will likely suffer from this continual discharge for at least another half century. Pyrrhotite from the Sudbury ore deposit was acknowledged as the source of the acid mine drainage (AMD). However, in terms of flotation, the reactivity of pyrrhotite towards excessive oxidation may have a detrimental effect on its flotation performance due to the formation of hydrophilic iron hydroxides that render surfaces of pyrrhotite particles less floatable. Therefore, the influence of pyrrhotite mineralogy upon oxidation and oxidation rates is also of interest.

Accounts in the literature are somewhat contradictory, but more frequently attribute monoclinic pyrrhotite to be the more reactive phase (e.g. Vanyukov and Razumovskaya, 1979; Yakhontova *et al.,* 1983; both in Russian and quoted by Janzen, 1996). More recently, using ToF-SIMS, Gerson and Jasieniak (2008) similarly showed that the oxidation rate of monoclinic pyrrhotite was greater than "hexagonal" pyrrhotite. Orlova *et al.* (1988) however (in Russian, quoted by Janzen, 1996), suggested that "hexagonal" pyrrhotite was more reactive. Janzen (1996) showed no correlation between pyrrhotite crystal structure and oxidation rate. Kwong (1993) suggested that the oxidation rate of pyrrhotite enriched in trace metals was slower than those with low nickel and cobalt contents. In the leaching study of Lehmann *et al.* (2000) it was shown that "hexagonal" pyrrhotite from two Australian locations was less susceptible to cyanide leaching than monoclinic pyrrhotite.

Accounts in the literature with respect to the flotation behaviour of magnetic and non-magnetic pyrrhotite are similarly quite varied. According to Iwasaki (1988), it was noted by Harada (1967; In Japanese) that samples of freshly ground monoclinic pyrrhotite were more floatable than "hexagonal" pyrrhotite although the reverse occurred on more oxidised

samples. Kalahdoozan (1996) showed that synthetic "hexagonal" pyrrhotite exhibited better xanthate adsorption and flotation recovery at a higher pH (≥ 10), whereas at a lower pH (7 - 8.5) monoclinic pyrrhotite was more floatable. Using pyrrhotite samples derived from the Mengzi lead zinc ore deposit, M.F. He *et al.* (2008) also showed that monoclinic pyrrhotite was more floatable than "hexagonal" pyrrhotite. Others such as Lawson *et al.* (2005) and Wiese *et al.* (2005) have demonstrated that differences in flotation performance between different pyrrhotite types exist. Lawson *et al.* (2005) showed a difference in pyrrhotite recovery between non-magnetic and magnetic circuits of the Sudbury ore where pyrrhotite depression was targeted. Similarly, results of batch flotation tests performed on Bushveld Merensky Reef ores by Wiese *et al.* (2005) have shown that the recovery of pyrrhotite from Merensky Reef ore from one location was greatly increased when copper sulfate was used as an activator during flotation, whereas for ore from another location the effect of copper sulfate addition on pyrrhotite recovery was minor. It is probable that these differences in recovery may have been due to the differences in pyrrhotite mineralogy.

Various process mineralogy studies on a range of operations have shown the benefit achieved by concentrators when a complete characterisation of the ore was undertaken in conjunction with experimental tests to determine its metallurgical performance (Bojecevski *et al.*, 1998; Baum *et al.*, 2006; Charland *et al.*, 2006; Brough, 2008). This suggests that in order to be able to successfully optimise or control the behaviour of an ore during flotation, a comprehensive understanding of its mineralogy and relationship to flotation behaviour is needed. It is probable that the lack of agreement in studies comparing pyrrhotite flotation and oxidation to crystallography and trace metal content may be due to the fact that only limited aspects of the pyrrhotite mineralogy were examined.

## 1.2 Aim of this Study

The aim of this process mineralogy study was to develop the relationship between pyrrhotite mineralogy and flotation performance based on a thorough characterisation of pyrrhotite from selected nickel and platinum group element ore deposits in terms of its crystallography, mineral association, mineral chemistry and mineral reactivity. By linking key characteristics of pyrrhotite mineralogy and reactivity to variations in the flotation performance through carefully controlled microflotation experiments of magnetic, non-magnetic and mixed pyrrhotite, an understanding of the reasons and mechanisms behind these differences in pyrrhotite flotation performance was sought. An additional goal of importance was to show which mineralogical measurements have shown the most potential in developing the relationship between pyrrhotite mineralogy and flotation performance.

## 1.3 Key Questions

The objectives of this work were met by addressing the following key questions:

(i) How does the mineral association, mineral chemistry and crystallography vary between magnetic and non-magnetic pyrrhotite?

(ii) How does ore deposit formation affect the mineralogy of pyrrhotite?

(iii) How does the reactivity of magnetic and non-magnetic pyrrhotite differ? Can these differences be accounted for in terms of the:
a) crystallography
b) mineral chemistry
c) mineral association of pyrrhotite?

(iv) How does the flotation performance of magnetic and non-magnetic pyrrhotite differ? Can these differences be accounted for in terms of the:
a) crystallography
b) mineral chemistry
c) mineral association of pyrrhotite?

## 1.4 Scope of Research

Since the fields of ore geology and mineral processing are extremely diverse, the scope and boundaries of this process mineralogy study are illustrated by figure 1.1. The only mineralogical components of ore geology that are relevant, are the petrography, mineral chemistry and crystallography of pyrrhotite from selected nickel and platinum group element ore deposits. Pyrrhotite crystallography is only investigated in terms of the unit cell dimensions in order to determine pyrrhotite superstructures and does not extend to any molecular modelling of the stability of the pyrrhotite crystal structure. The focus of this study is on pyrrhotite mineralogy and therefore excludes additional silicate and oxide minerals.

Mineral reactivity, which is considered to be a consequence of the interaction of pyrrhotite with the environment, is considered, but only selected measurements are investigated in order to determine differences in the reactivity of magnetic and non-magnetic pyrrhotite towards oxidation. These measurements include the use of open circuit potential, cyclic voltammetry and oxygen uptake. Specialised techniques such as XPS and ToF-SIMS also provide detailed information on the reactivity of mineral surfaces and with the addition of EDTA are considered as potential areas for further research focus (see recommendations in Chapter 8). Although some previous studies have compared the reactivity of different pyrrhotite types using flow through reactor experiments in order to determine oxidation rate constants (e.g. Janzen, 1996), reactivity measurements in this study are used as a characterisation method in order to develop the relationship between mineralogy and flotation performance.

Within the field of mineral processing, the separation process of flotation is the primary focus in this study. Pyrrhotite flotation performance is measured using carefully controlled microflotation experiments. Therefore, aspects relating to the breakage such as the comminution method, particle size distribution and liberation characteristics of both valuable and gangue minerals will not be focussed upon. However, the liberation of pyrrhotite will be of interest in terms of its mineral association to pentlandite. Other aspects of flotation such as the presence of a froth phase, pulp rheology, circuit performance and flotation scale up also fall beyond the scope of this study.

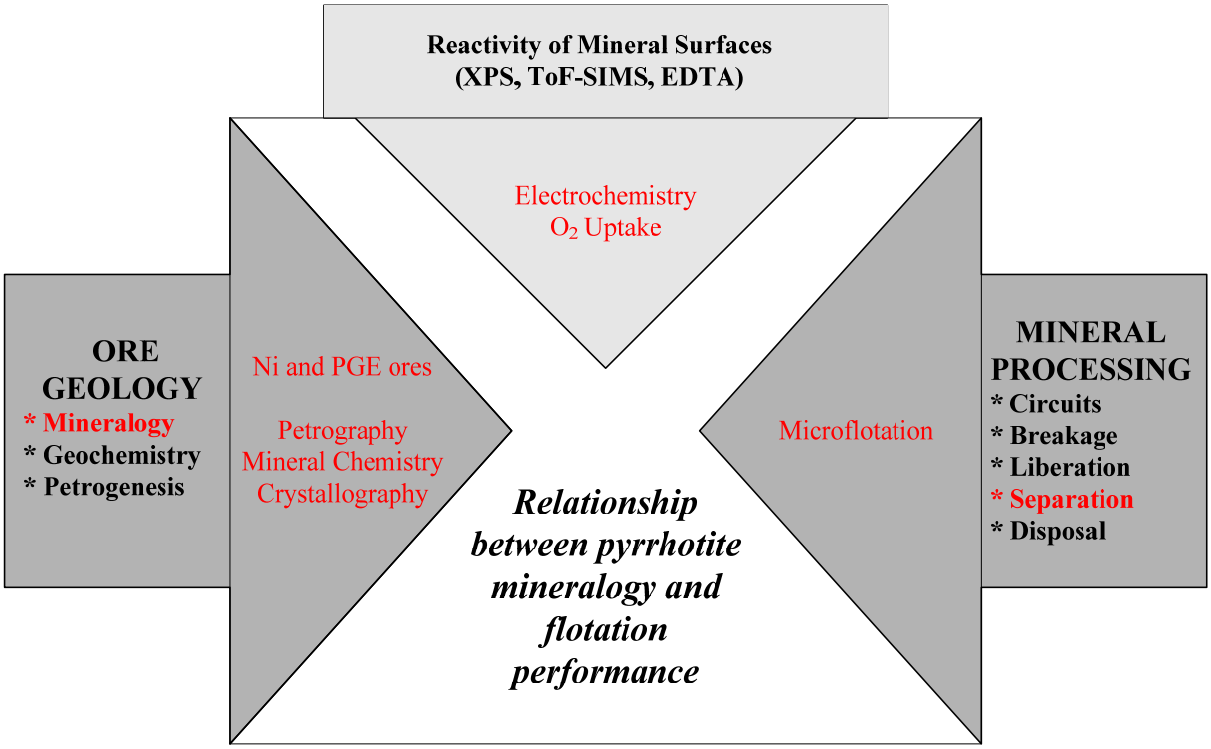


**Figure 1.1:** Schematic of the scope of research in this study with key areas of interest highlighted in red.

## 1.5 Organisation of the Thesis

The body of this thesis is divided into eight chapters starting with the Introduction where the background, scope of the thesis and key questions are presented in Chapter 1. This is followed by a critical review of the literature in Chapter 2 on pyrrhotite ore deposits, pyrrhotite mineralogy, the electrochemical properties of pyrrhotite, pyrrhotite flotation and the field of process mineralogy. Chapter 3 describes sampling and analytical methods. The results are then divided into three chapters; Chapter 4 describes the mineralogical characterisation of the pyrrhotite samples, Chapter 5 describes the reactivity of the pyrrhotite samples and Chapter 6 describes the flotation of the pyrrhotite samples. A discussion and linkage of these results in order to determine the effect of pyrrhotite mineralogy on flotation performance is given in Chapter 7. Some final conclusions as well as several recommendations for further research are given in Chapter 8. The complete set of results from the various experiments is given in the Appendices.

# Chapter 2

# LITERATURE REVIEW

## 2.1 Overview of Pyrrhotite Ore Deposits

Pyrrhotite is one of the most commonly occurring sulfide minerals, with associations to nickel deposits, platinum group element deposits, as well as copper lead zinc type deposits. Geologically, nickel ore deposits are classified according to their mode of occurrence and petrogenesis and are broadly classified into those related to magmatic events and the laterite deposits. The laterite deposits are generally found in equatorial or paleoequatorial locations. Magmatic sulfide deposits can be described as those nickel copper and platinum group element sulfide deposits which have formed through the interaction of mantle material with continental crust. Following the classification scheme of Naldrett (1989) they can be further subdivided into groups according to their association with:

i). Synvolcanic deposits often associated with greenstone belts e.g. Kambalda, W. Australia.
ii). Rifted plate margins and ocean basins e.g. Thompson Belt, Manitoba, Canada.
iii). Intrusions in cratonic areas e.g. Noril'sk Talnakh, Russia; Bushveld Igneous Complex, South Africa and the Sudbury Igneous Complex, Canada.
iv). Intrusions in orogenic belts: e.g. Aberdeenshire, Scotland.

The literature reviewed here, is focused on pyrrhotite occurrences selected for this study. These are related to the stratiform deposits occurring as intrusions in cratonic areas (Bushveld Igneous Complex, Sudbury Igneous Complex) and as those in association with Archean greenstone belts (Tati greenstone belt).

### 2.1.1 Bushveld Igneous Complex, South Africa

The Bushveld Igneous Complex in South Africa is one of the worlds largest economic platinum group element resources with estimates of 204 and 116 million ounces of proven reserves for platinum and palladium, respectively (Cawthorn, 1999). The layered complex has an aerial extent on the order of 65 000 $km^2$ and is thought to extend into Botswana to the Molopo Farms Complex (Eales and Cawthorn, 1996). The Proterozoic Bushveld Complex is comprised of various limbs, shown in figure 2.1, that formed during the Bushveld Super-Event. The economic horizon of the Complex is known as the Rustenburg Layered Suite (SACS, 1980), a transitional layered series representing the influx of multiple injections of magma into the continental crust. Within the Critical Zone of the Rustenburg Layered Suite occurs the Upper Group Chromitite (UG2) Reef, which is stratigraphically overlain by the Merensky Reef as illustrated by the stratigraphic column in figure 2.2. Both reefs are exploited for their PGE content, although the base metal sulfides (BMS) are recovered as a by product from the Merensky Reef. A third reef type known as Platreef is also exploited for PGEs. The Platreef is restricted to the Northern limb of the Complex, whereas the Merensky Reef and UG2 Reef are present in both the Eastern and Western limbs.

Pyrrhotite samples for characterisation in this study are derived from the Merensky Reef named after Dr Hans Merensky, who first discovered the in-situ location and recognised the importance of this platinum group element bearing ore body in 1924 (Cawthorn, 1999). The terminology “Merensky Reef” is generally used to represent the economic mining cut situated within the basal section of the “Merensky Cyclic Unit”. It should be noted that any description of the Merensky Reef will not adequately capture the variation in lithology and texture of the reef along strike due to its heterogenous character (Farquhar, 1986; Leeb-Du Toit, 1986; Viljoen and Hieber, 1986; Viljoen *et al.*, 1986; Viring and Cowell, 1999). The footwall of the Merensky cyclic unit is comprised of a norite to anorthosite with a sharp contact to the overlying thin basal chromitite layer (~1 cm thick). Sandwiched between the basal chromitite and an upper chromitite layer (known as the Merensky chromitite) is a feldspathic pegmatoidal pyroxenite. The thickness of this pegmatoidal layer varies quite considerably from mine to mine. In some locations on the Western limb, this pegmatoidal layer is absent (e.g. Impala platinum mines; Leeb-Du Toit, 1986) whereas towards the northern most mines of the Western limb (e.g. Northam Platinum Mine; Viring and Cowell, 1999) this pegmatoidal pyroxenite layer may be up to several metres thick. The Merensky

chromitite is typically a few centimetres in thickness. Overlying the Merensky chromitite, is a pyroxenite which gradually changes into norite and even anorthosite (Farquhar, 1986; Leeb-Du Toit, 1986; Viljoen and Hieber, 1986; Viljoen *et al.*, 1986; Viring and Cowell, 1999).

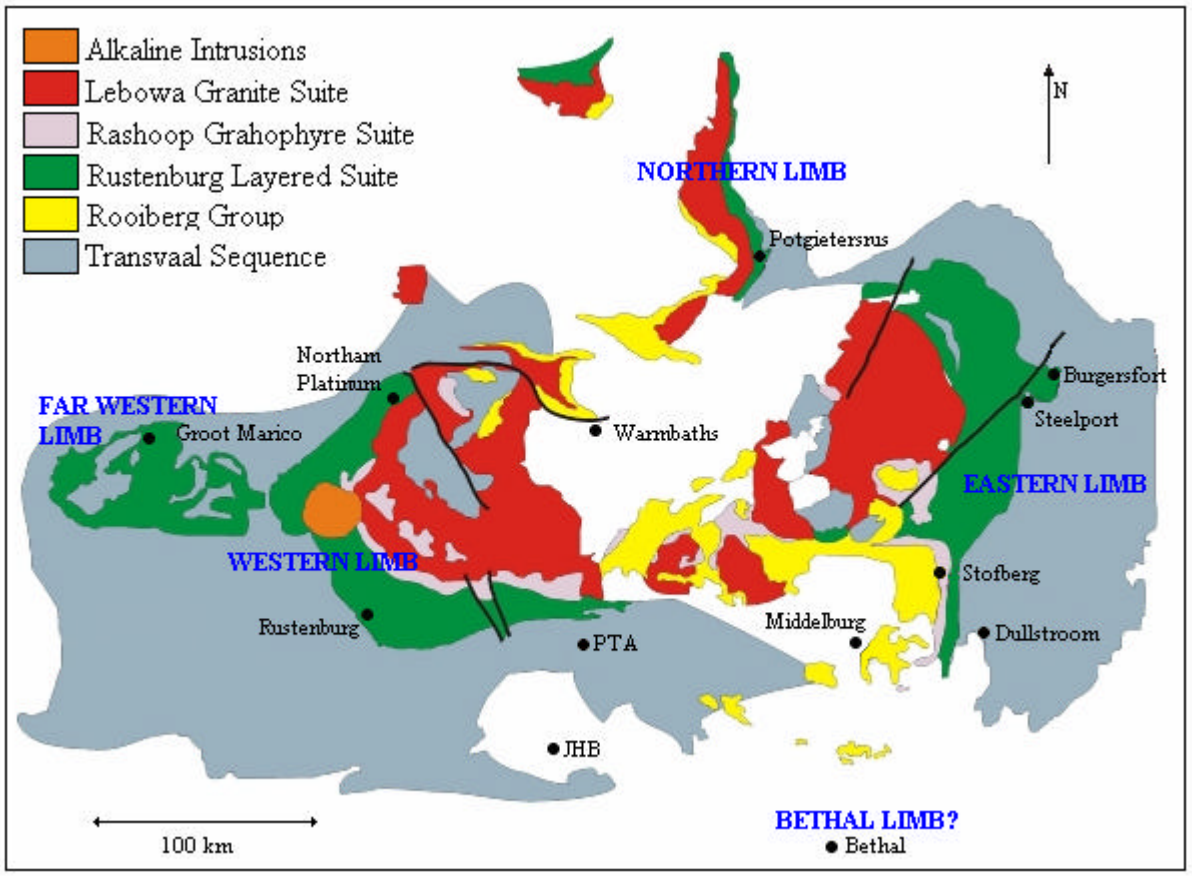


**Figure 2.1:** Map of the Bushveld Igneous Complex, illustrating the location of the Rustenburg Layered Suite, host to the Merensky Reef, in the Bushveld Igneous Complex. From: Brough (2008).

Base metal sulfides and associated platinum group minerals are typically interstitial to the coarse grained pyroxene and plagioclase and are enriched within the vicinity of the Merensky chromitite. The sulfides generally constitute a few weight percent of the Merensky Reef. The observed sulfides are pyrrhotite, pentlandite, chalcopyrite and pyrite in decreasing order of abundance and typically occur as multi-mineralic granular aggregates. Lesser cubanite, mackinawite, sphalerite, bornite, vallerite and troilite have also been recognised (Liebenberg, 1970). Platinum group mineralization at 5-7 g/t (Cawthorn *et al.*, 2002) occurs as either discrete platinum group minerals such as sulfides, tellurides, arsenides and alloys or in solid solution with the sulfides (Kinloch, 1982; Schouwstra *et al.*, 2000; Cabri *et al.*, 2008). In the study of Ballhaus and Sylvester (2000), concentrations of the platinum group elements

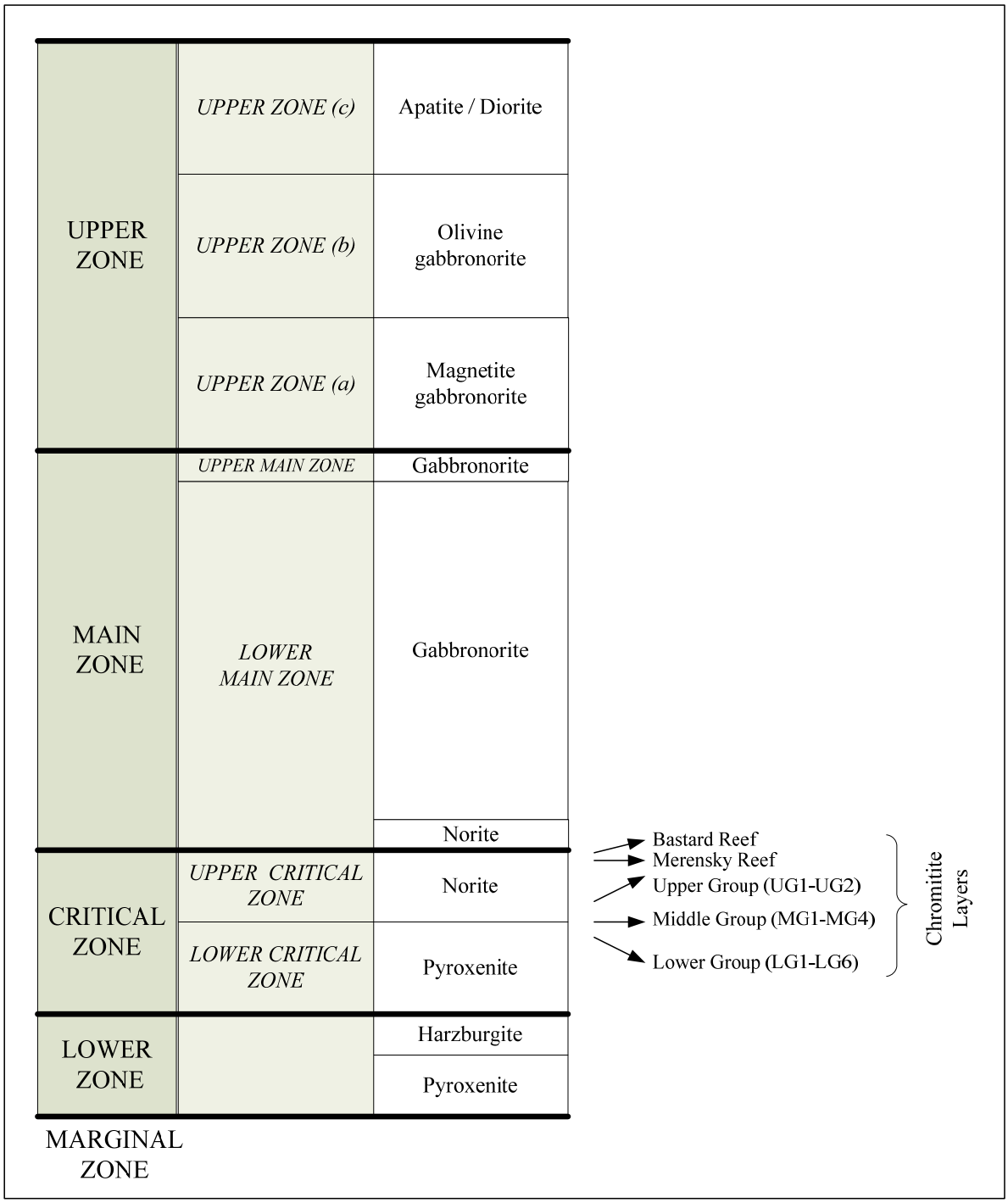


**Figure 2.2:** Generalised stratigraphy of the Rustenburg Layered Suite, of the Bushveld Igneous Complex. The stratigraphic position of the Merensky Reef is also shown. Adapted from Eales and Cawthorn (1996).

were detected in both pyrrhotite and pentlandite. Osmium, iridium and ruthenium in particular, were detected in solid solution with pyrrhotite.

### 2.1.2 Uitkomst Complex, South Africa

The Uitkomst Complex in South Africa is situated in the Mpumalanga Province near Badplaas. Mining of the economic mineralisation in the Uitkomst Complex takes places at the Nkomati Nickel Mine. The Uitkomst Complex is situated just east of the Eastern Limb of the Bushveld Complex as shown in figure 2.3a. Since it is similar in age and character to the Bushveld Igneous Complex, it has been argued to be related to the Bushveld Igneous Complex (Gauert *et al.*, 1995; Gauert, 2001). As illustrated by figure 2.3b and c, the Uitkomst Complex is an elongate intrusion that consists of a series of defined lithological units of gabbros, harzburgites, gabbronorites and pyroxenites that form a trough-like shape 750 m in thickness and between 650 and 1600 m in width (Gauert, 2001). A series of mineralised zones exist and which are summarised in table 2.1. In the past, mining was concentrated within the massive sulfide body (MSB) located beneath the Basal Gabbro in the Uitkomst Complex. Currently mining is focused on exploiting the more disseminated ores located in the Main Mineralised Zone (MMZ) and the Chromititic Peridotite Mineralised Zones.

Sulfide mineralization in the Uitkomst Complex occurs in a variety of textural types that includes disseminated sulfides, net-textured sulfides, local concentrations of sulfides and as massive sulfide ore (Gauert *et al.*, 1995; van Zyl, 1996). The most common sulfide minerals are pyrrhotite, pentlandite, chalcopyrite and pyrite in decreasing order of abundance. Minor sulfide minerals present are digenite, mackinawite, galena, sphalerite, millerite and arsenopyrite. The oxide minerals, magnetite, ilmenite and chromite are common. Enrichment of the PGE also occurs as discrete platinum-palladium tellurides (merenskyite, michenerite, testibiopalladite) or as the arsenides (sperrylite). Unlike the platinum group mineralisation in the Merensky Reef, platinum-palladium sulfide minerals are not common (Theart and de Nooy, 2001).

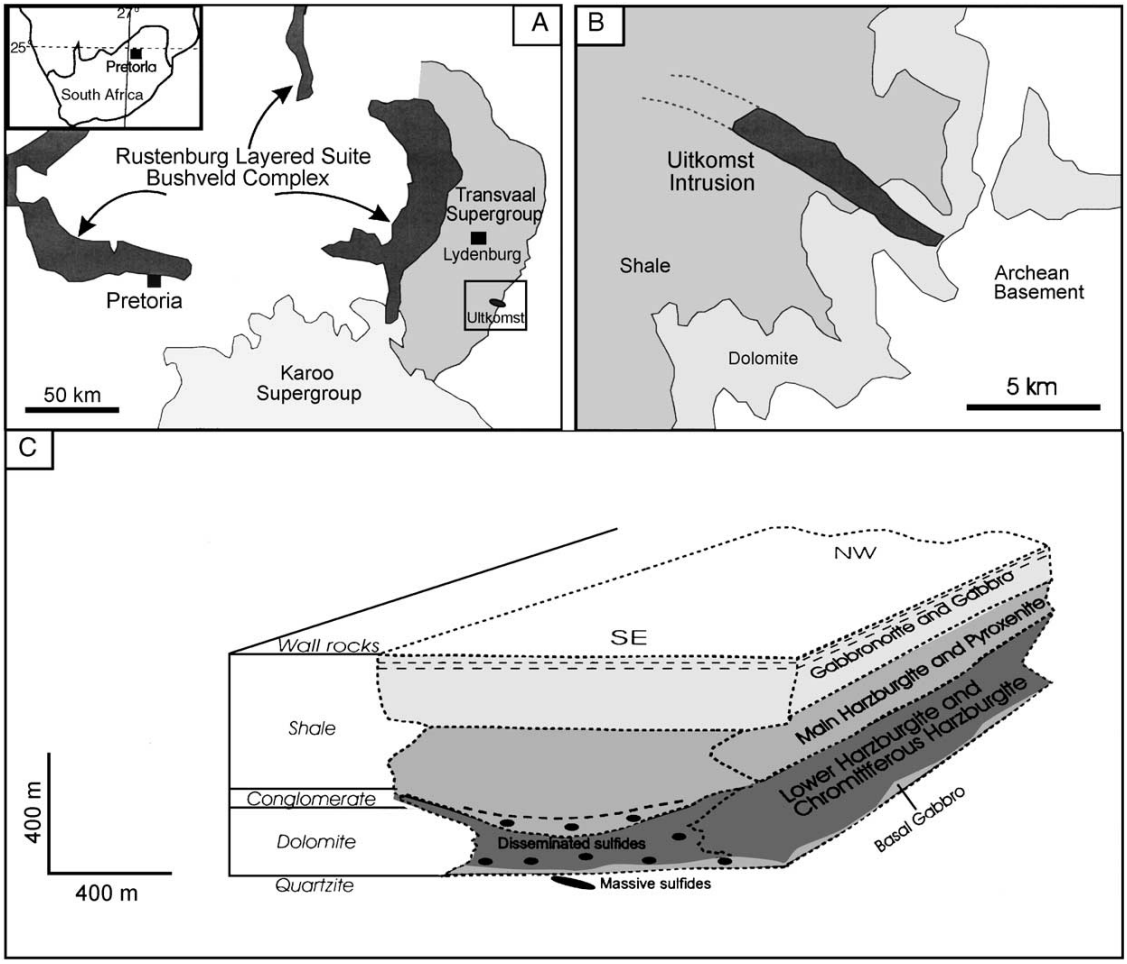


**Figure 2.3**: (a) Location of the Uitkmost Complex in relation to the Bushveld Complex in South Africa. (b) Strike of the Uitkomst intrusion and (c) Cross section of the Uitkomst intrusion showing the location of massive and disseminated sulfides. From: Li *et al.* (2002).

**Table 2.1:** Stratigraphy of the Uitkomst Complex with associated sulfide mineralisation. Adapted from: Theart and de Nooy (2001).

| Group | Unit | Thickness (m) | Mineralisation |
|---|---|---|---|
| Main | Gabbronorite | 262 | - |
| | Upper Pyroxenite | 66 | - |
| | Peridotite/Harzburgite | 264 | - |
| | Massive Chromitite | (0-6) | - |
| Basal | Chromititic Peridotite | 35 | Chromititic Peridotite Mineralised Zone (PCMZ) |
| | Lower Pyroxenite | 37 | Main Mineralised Zone (MMZ) |
| | Basal Gabbro | 35 | Basal Mineralised Zone (BMZ) |
| (Basement) | Massive Sulfide Body (MSB) | 26 | Upper Stringer Zone<br>Massive Stringer Zone<br>Lower Stringer Zone |

### 2.1.3 Phoenix Deposit, Botswana

The Phoenix ore deposit forms part of the Archean Tati greenstone belt situated near Francistown in Botswana as shown in figure 2.4a. In addition to the Phoenix sulfide deposit, the Selkirk and Tekwane sulfide deposits have been recognised (Figure 2.4b). The greenstone belt has been subjected to lower greenschist and lower amphibolite facies metamorphism and comprises a series of meta-volcanics, meta-sedimentary rocks and granitoids. The Phoenix ore body is hosted by meta-gabbronorite, whereas the Selkirk and Tekwane ore bodies are hosted by a granular meta-gabbro (Johnson, 1986; Maier *et al.*, 2008). Mineralisation at Phoenix occurs as a series of elongate north-south and east-west trending lenses of massive sulfide ore. These lenses are typically only 1.5 m in diameter although are tens of metres in length (Johnson, 1986; Maier *et al.*, 2008). Sulfide minerals present include pyrrhotite, pentlandite and chalcopyrite with lesser sphalerite, molybdenite and galena. The Selkirk and Tekwane deposits are similar in mineralogy to Phoenix, except that they are characterised by the presence of magnetite and pyrite.

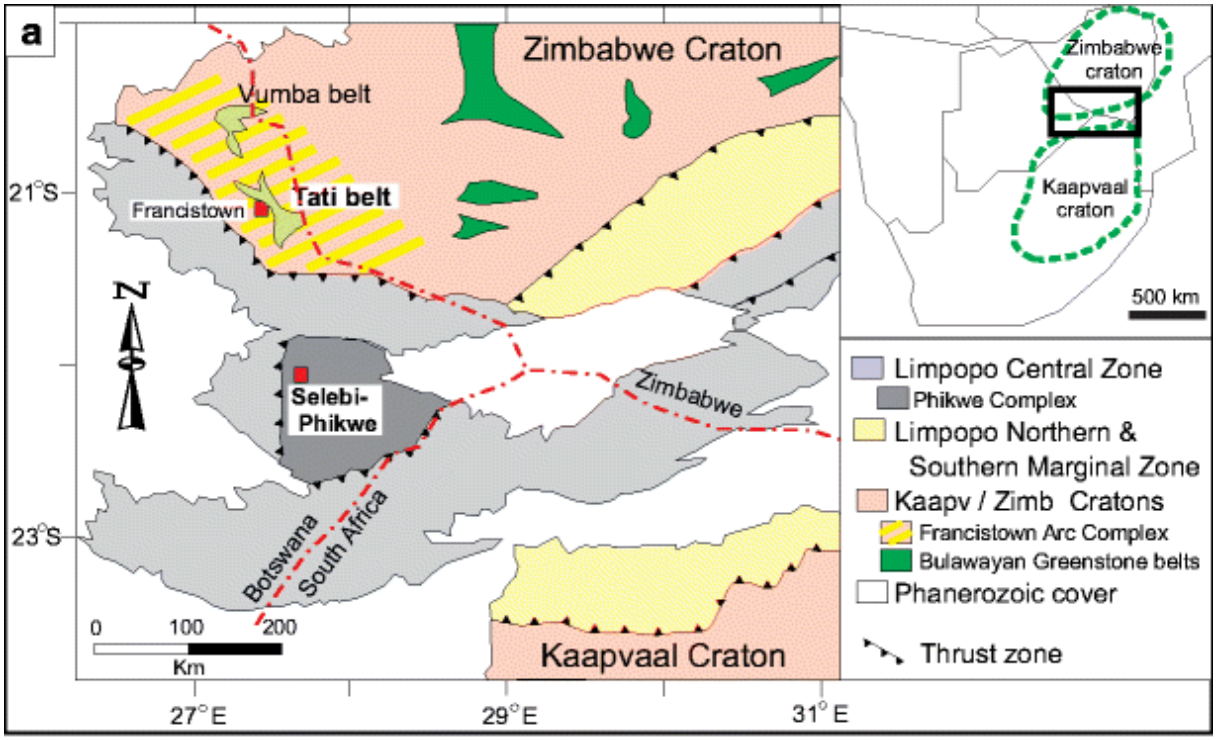


**Figure 2.4:** (a) Location of the Tati greenstone belt in Botswana. (b) Location of the Phoenix, Selkirk and Tekwane ore deposits. From: Maier *et al.* (2008).

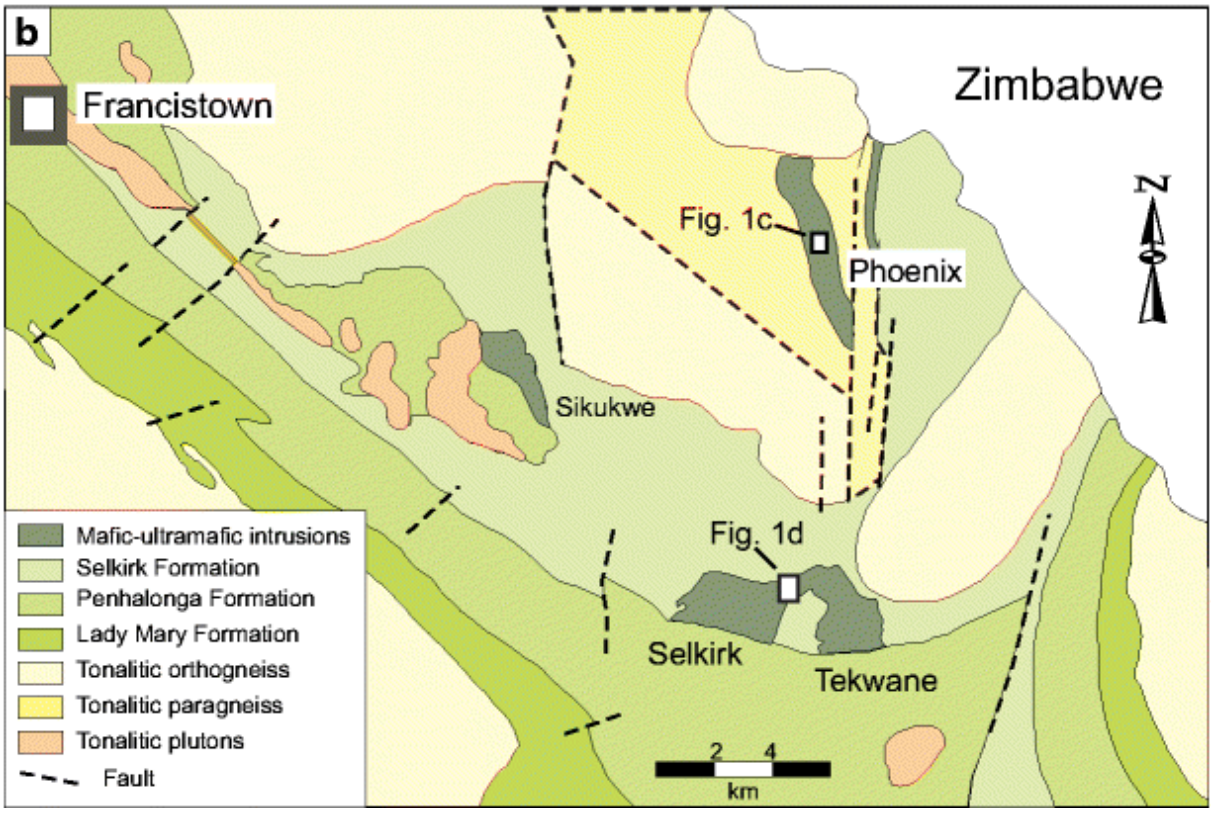


**Figure 2.4:** Continued.

### 2.1.4 Sudbury Igneous Complex, Canada

The Sudbury Igneous Complex, located in the Ontario Province of Canada is a Proterozoic geological feature well-known for its evidence of catastrophism, suggesting possible formation as a consequence of a meteorite impact (Rousell *et al.*, 2003). In mining and metallurgy, however, this deposit is well-known for its extensive nickel, copper and PGE reserves (1500 Mt at 1 % Ni, 1 % Cu, 1 g/t Pt, Pd; Farrow and Lightfoot, 2002). The Sudbury Igneous Complex is an oval shaped body 60 km long and 27 km wide as illustrated in figure 2.5. It is divided into an outer Main Mass and Sublayer with the surrounding Whitewater Group as basin in-fill (Naldrett and Kullerud, 1967; Farrow and Lightfoot, 2002). The northwest and southeast borders of the basin are more commonly known as the North and South Range, respectively. The terminology, Sudbury Igneous Complex is used here, but it should be mentioned that it is also referred to as Nickel Irruptive in some older literature e.g. Naldrett and Kullerud (1967). Rocks of the South Range are associated with the Proterozoic Huronian Supergroup sediments and volcanics whereas the North Range is associated with Archean gneisses (Keays and Lightfoot, 2004). The deposit can be further divided into the Main Mass, consisting of a lower norite, quartz gabbro and upper granophyre, and the Contact

Sublayer. The Contact Sublayer is an igneous breccia occurring discontinuously beneath the Norite and is in turn underlain by a metamorphic textured Footwall breccia.

Sulfide mineralisation in the Sudbury Igneous Complex has been recognised in four different environments as illustrated by figure 2.6. The first type of mineralisation is associated with the Contact Sublayer breccia. A second type occurs within the Footwall Breccia. A third type of mineralisation occurs in veins in the footwall. The last type of mineralisation is known as the Offset dykes and consists of sulfide mineralisation in quartz diorite dykes which may occur either as radial dykes extending away from the Complex, or as concentric dykes wrapped around the perimeter of the Complex (Farrow and Lightfoot, 2002; Keays and Lightfoot, 2004).

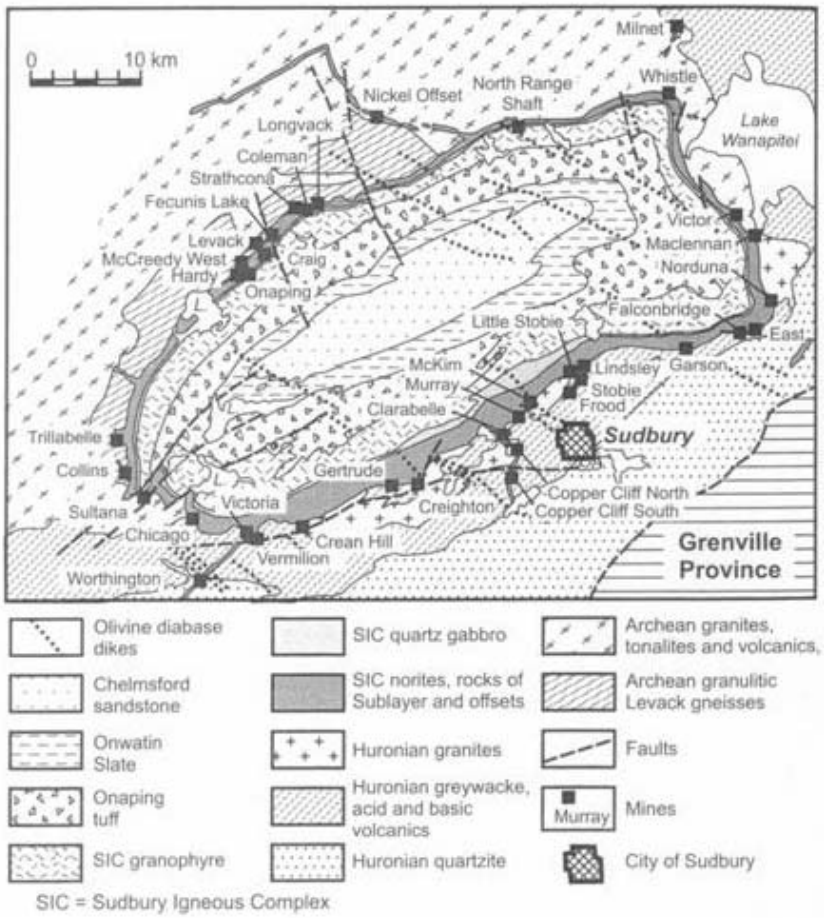


**Figure 2.5**: Geological map of the Sudbury Igneous Complex. From: Naldrett (2004).

The Gertrude pyrrhotite sample examined in this study is a typical Contact deposit occurring within the Footwall Breccia. The Gertrude site is marked by a distinct magnetic anomaly. The Gertrude mine was only recently reopened and is located just west of Creighton Mine in the South Range (Figure 2.5). The Gertrude ore body is tabular in shape and between 6 and 10 m in thickness with sulfides occurring as semi-massive, blebby and sometimes disseminated textures (E. Tremblay, Pers. Comm, 2007). The Contact type deposits typically have lower platinum group element grades relative to the Offset dyke type deposits. The Copper Cliff North (CCN) ore body examined in this study is a typical Offset dyke type deposit. The Copper Cliff Offset dyke extends for 7 km and strikes southwards from the South Range as shown in figure 2.5. It is subdivided into the North mine and South mine by the Creighton Fault. The ore body at Copper Cliff North mine is located within the centre of the dyke whereas, at Copper Cliff South mine, it is located at the edges of the dyke (Magyarosi *et al.*, 2002). Sulfide mineral textures present in the Copper Cliff ores include massive, semi-massive, blebby, net-textured and with rare disseminated sulfides (Rickard and Watkinson, 2001; Farrow and Lightfoot, 2002; Magyarosi *et al.*, 2002; Scott and Benn, 2002; Keays and Lightfoot, 2004).

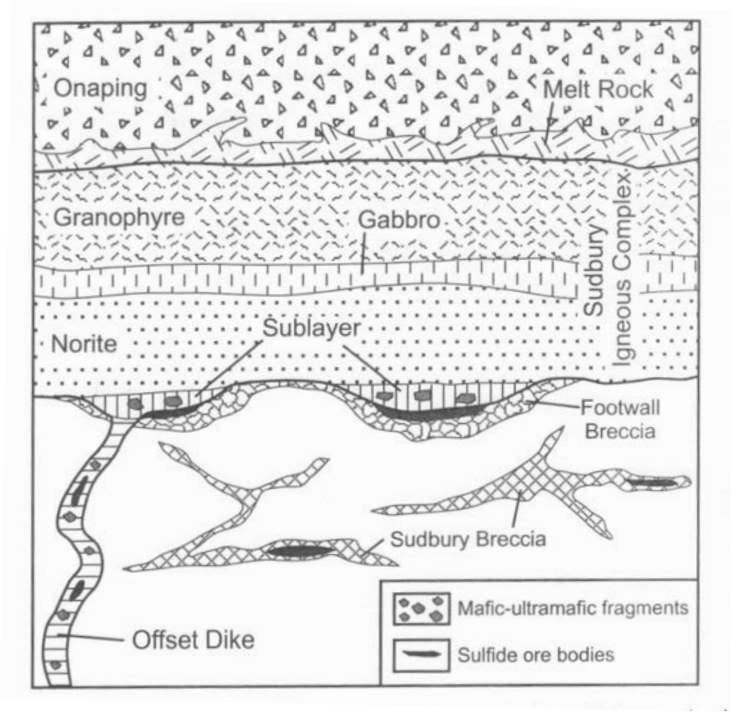


**Figure 2.6**: Vertical section showing the relationship between the Contact Sublayer and Offset dykes in the Sudbury structure. From: Naldrett (2004).

Dominant sulfides present within both Contact and Offset type deposits from mines of both the North and South Ranges are pyrrhotite, pentlandite, chalcopyrite, and minor sphalerite and magnetite displaying oxy-exsolution of ilmenite (Naldrett and Kullerud, 1967; Rickard and Watkinson, 2001; Farrow and Lightfoot, 2002; Magyarosi *et al.*, 2002; Keays and Lightfoot, 2004). The Offset dykes are generally more enriched in the platinum group elements than Contact deposits (Farrow and Lightfoot, 2002). Platinum group elements are mostly deported as discrete minerals with only minor elements in solid solution. Platinum group elements measured in solid solution in sulfides from the Contact type Strathcona deposit (Figure 2.5) include iridium, rhodium and ruthenium in pyrrhotite, whereas palladium was significantly enriched in pentlandite (Li *et al.*, 1993). The discrete platinum group minerals occurring in Sudbury ores are dominated by the tellurides (e.g. michenerite) and bismuth-tellurides (e.g. froodite) with distinct differences in platinum palladium mineral types between the North and South Ranges (e.g. sperrylite dominates in the South Range). Platinum group mineral sulfides are very rare, unlike the Bushveld Igneous Complex (Farrow and Lightfoot, 2002).

## 2.2 Pyrrhotite Mineralogy and Crystallography

### 2.2.1 Building blocks of pyrrhotite structures

The pyrrhotite group of minerals is based on the hexagonal structure of the mineral nickeline / niccolite (NiAs) and the nomenclature of the various pyrrhotite superstructures is based on the unit cell parameters of the NiAs structure (a =3.438Å, c = 5.880 Å; Wyckoff, 1963). Within this basic structure the metal atoms lie in a hexagonal lattice, whereas the non-metal atoms are positioned in a hexagonal close packed lattice. As shown in figure 2.7, nickel atoms are in octahedral coordination with the more electronegative arsenic atoms that are in trigonal prismatic coordination. One of the consequences of this structure is that the omission of metal atoms along certain crystallographic orientations is possible, thereby allowing the non-stoichiometry within the derivative pyrrhotite mineral group.

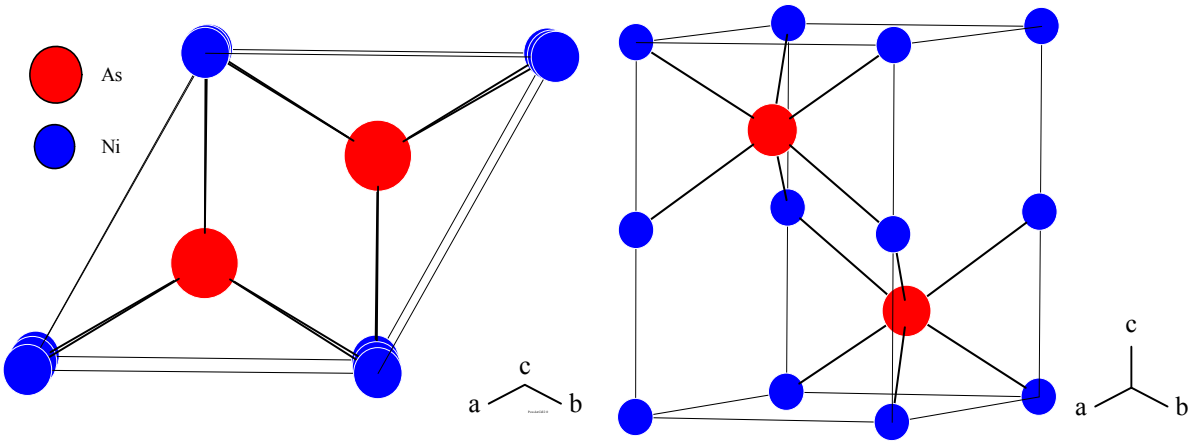


**Figure 2.7:** Illustration of the simple NiAs structure viewed in two orientations.

The pyrrhotite family consists of derivatives of the structure of the hexagonal NiAs subcell. These derivative structures are formed by extending the dimensions of the unit cell along the *c*-axis and are known as *superstructures*. These superstructures are non stoichiometric pyrrhotites varying in composition ($Fe_7S_8$ to $Fe_{11}S_{12}$), in crystal system, in mineral stability and in magnetic characteristics. These varying characteristics are essentially a function of the presence of metal cation vacancies in the pyrrhotite structure and the complexities associated with the stacking sequence of these vacancies, the repeat distance of the complete pattern and the direction of the vacancy layers within the superlattice. High temperature forms of

pyrrhotite are generally disordered and upon cooling, the iron site vacancies develop some order. Consequently, a number of pyrrhotite superstructures are developed such as those shown in table 2.2. In order to be able to describe these pyrrhotite superstructures, Wuensch (1963) introduced a nomenclature system whereby the superlattice dimensions are described according to the repeat of the NiAs unit cell either along the *a*-axis or *c*-axis. Accordingly a pyrrhotite with the structure and cell dimensions of NiAs is referred to as a 1C pyrrhotite, a pyrrhotite which has unit cell parameters of *c* equal to two times the dimension of *c* in the NiAs unit cell is known as 2C and corresponds to troilite, whereas 4C monoclinic pyrrhotite has unit cell parameters of *c* equal to four times the dimension of *c* in the NiAs unit cell.

**Table 2.2:** Summary of the different pyrrhotite varieties with some of their key physical attributes. See text for further description of the terminology used. Adapted from Posfai *et al.* (2000) and Fleet (2006).

| Type | Comp. | Structure | Magnetic Properties | Other names | Stability | Occurrence | Refs |
|---|---|---|---|---|---|---|---|
| 1C | FeS | Hex | pm | - | High temp phase | Synthetic | 1, 2 |
| 2C | FeS | Hex | afm | Troilite | $<147^0$C | Natural & lunar | 3-6 |
| NC | $Fe_9S_{10}$, $Fe_{10}S_{11}$, $Fe_{11}S_{12}$ | Hex, Ortho, Mon | afm | Non-magnetic, 5C, 6C, 11C, Intermediate pyrrhotite | $<209^0$C | Natural | 2-3, 6-7 |
| NA | $Fe_7S_8$ | Trig | afm | 2A, 3C | $< 262^0$C | Synthetic | 2, 8-10 |
| MC | | Hex? | afm | - | $< 315^0$C | Synthetic | 1, 2 |
| 4C | $Fe_7S_8$ | Mon | fm | Magnetic Pyrrhotite | $< 254^0$C | Natural | 3, 11-13 |
| - | $Fe_{7+X}S_8$ | Mon | afm | Anomalous Pyrrhotite | ? | Natural | 14 |

**Note:** pm – paramagnetic, afm – antiferromagnetic, fm - ferrimagnetic. [1] Nakazawa and Morimoto (1971) [2] Kissin and Scott (1982) [3] Morimoto *et al.* (1970) [4] Evans (1970) [5] Skala *et al.* (2006) [6] Fleet (2006) [7] Koto *et al.* (1975) [8] Francis and Craig (1976) [9] Nakano *et al.* (1979) [10] Keller-Besrest *et al.* (1982) [11] Bertaut (1953) [12] Tokonami *et al.* (1972) [13] Powell *et al.* (2004) [14] Clark (1966).

Following this nomenclature system, a number of pyrrhotite varieties or subgroups were identified based on some consideration of the stability of these phases within their experimental phase diagrams (Figure 2.8). A summary of the distinguishing physical properties of the pyrrhotite superstructures is given in table 2.2 along with the unit cell parameters and symmetry in table 2.3. The focus of this study however, will be on those pyrrhotite types that are naturally occurring (2C, NC, 4C) and are likely to be encountered in various mineral processing operations.

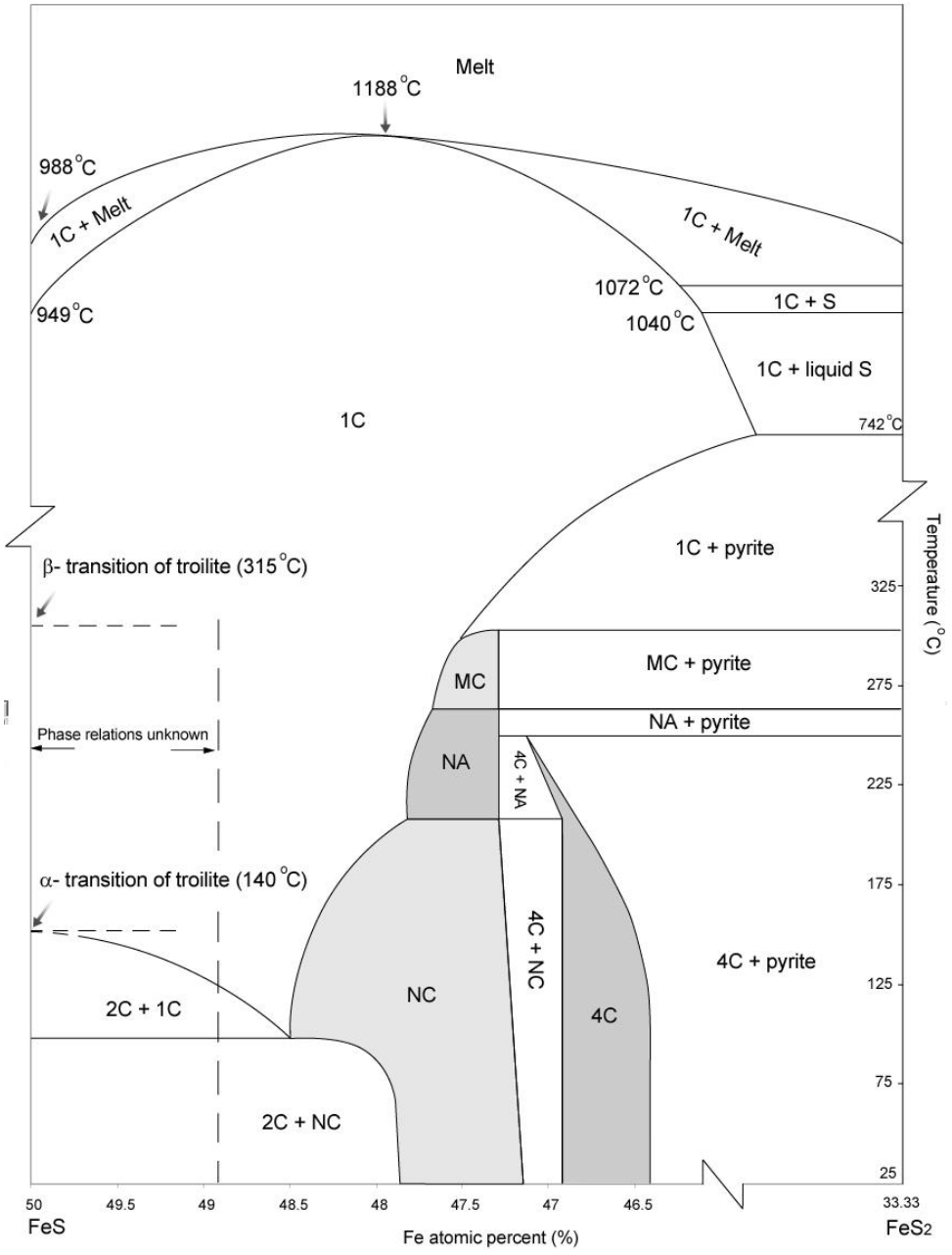


**Figure 2.8**: Phase diagram for the system FeS to $FeS_2$ representing stability fields of various pyrrhotite superstructures discussed in the text. From: Wang and Salveson (2005) and references therein.

**Table 2.3:** Summary of pyrrhotite superstructures and unit cell dimensions found in the literature.

| Type | Comp. | Structure | Symmetry | a (Å) | b (Å) | c (Å) | β | Location | Refs |
|---|---|---|---|---|---|---|---|---|---|
| Nickeline | NiAs | Hex | $P\bar{6}3mc$ | 3.602 | - | 5.009 | - | - | 1 |
| 2C | FeS | Hex | $P\bar{6}2c$ | 5.962 | - | 11.750 | - | Sea of Tranquility, Moon | 2 |
| 2C | FeS | Hex | $P\bar{6}2c$ | 5.965 | - | 11.757 | - | Etter Chondrite | 3 |
| 3C | $Fe_7S_8$ | Trig | $P3_1$ | 6.8673 | - | 17.062 | - | Synthetic | 4 |
| 3C | $Fe_7S_8$ | Trig | $P3_121$ | 6.8652 | - | 17.046 | - | Synthetic | 5 |
| 3C | $Fe_7S_8$ | Trig | $P3_121$ | 6.866 | - | 17.088 | - | Synthetic | 6 |
| 4C | $Fe_7S_8$ | Mon | F2/*d* | 11.902 | 6.859 | 22.787 | $90.26^0$ | Kisbanya, Romania | 7 |
| 4C | $Fe_7S_8$ | Mon | C2/c | 11.926 | 6.882 | 12.925 | $118.02^0$ | Synthetic | 8 |
| 5C* | $Fe_9S_{10}$ | Hex | - | 6.881 | - | 28.68 | - | Ore Knob, N. Carolina | 9 |
| 5C* | $Fe_9S_{10}$ | Hex | - | 6.88 | - | 28.7 | - | Outokumpu, Finland | 10 |
| 5C* | $Fe_9S_{10}$ | Ortho | C*ca | 6.8846 | 11.936 | 28.676 | - | Kishu, Japan | 11 |
| 6C* | $Fe_{11}S_{12}$ | Hex | - | 6.904 | - | 34.51 | - | Merensky Reef, RSA | 9 |
| 6C* | $Fe_{11}S_{12}$ | Mon, pseudo-ortho | F*d* or F2/*d* | 6.895 | 11.9536 | 34.518 | $90.00^0$ | Chigusa, Japan | 12 |
| 11C* | $Fe_{10}S_{11}$ | Ortho | Cmca or C2ca | 6.892 | 11.952 | 63.184 | - | Ongul, Antarctica | 10 |

* Indicates no structure solution presented in these references. [1] Wyckoff (1963) [2] Evans (1970) [3] Skala *et al.* (2006) [4] Fleet (1971) [5] Nakano *et al.* (1979) [6] Keller-Besrest *et al.* (1982) [7] Tokonami *et al.* (1972) [8] Powell *et al.* (2004) [9] Carpenter and Desborough (1964), [10] Morimoto *et al.* (1970), [11] Morimoto *et al.* (1975b), [12] Koto *et al.* (1975).

### 2.2.2 Metastable 1C pyrrhotite

The 1C pyrrhotite is an undifferentiated, high temperature form of pyrrhotite (Figure 2.8) with a disordered distribution of vacancies (Nakazawa and Morimoto, 1971; Kissin and Scott, 1982). It has a structure similar to the NiAs type of structure, based on a single repeat of the NiAs unit cell along the c-axis (Nakazawa and Morimoto, 1971). 1C pyrrhotite is paramagnetic in character. Due to its limited occurrence only at higher temperatures e.g. the experimental studies of Nakazawa and Morimoto (1971) and Kissin and Scott (1982), or in a

9 km deep borehole from the German Deep Continental Drilling program (Posfai *et al.*, 2000), it is unlikely to occur in natural ore deposits and will not be discussed further.

### 2.2.3 2C Troilite

Stoichiometric FeS is more commonly known as troilite for which the structure is shown in figure 2.9. It is hexagonal, falls into space group $P\bar{6}2c$, can be described as a =√3A, and c = 2C where A and C are dimensions of the NiAs subcell. All metal cation sites are filled in the pyrrhotite structure and therefore troilite has an ordered structure with no vacancies. The ideal stoichiometric troilite is comprised of equal atomic proportions of ferrous iron and sulfide sulfur, although the findings of Skinner *et al.* (2004) suggested the presence of minor amounts of ferric iron in the troilite structure. Unlike the ideal trigonal prismatic coordination of arsenic in the NiAs structure, the sulfur atoms are more distorted and may even verge upon a deformed tetragonal scalenohedron, whereas the coordination of iron atoms remains relatively close to octahedral (Figure 2.9; Skala *et al*., 2006).

Troilite is antiferromagnetic in character at temperatures less than $140^0$C at 1 bar, although it may undergo an α-magnetic phase transition, followed by a β phase transition at $315^0$C (Curie temperature) where it transforms into the disordered 1C subcell of the NiAs structure (Figure 2.8; Fleet, 2006). The question of whether troilite undergoes a structural change associated with the α-magnetic phase transition is debatable (Wang and Salveson, 2005; Fleet, 2006).

Troilite is generally formed in reducing environments where ferrous iron is stable. Extraterrestrial occurrences are strongly reducing environments and consequently, troilite is well-known for its presence in lunar samples or meteorites (Evans, 1970; Bullock *et al.*, 2005; Skala *et al.*, 2006). However, this does not preclude its presence in some terrestrial locations, as fine lamellar intergrowths with non-magnetic pyrrhotite e.g. Merensky Reef, South Africa (Liebenberg, 1970) or Voisey's Bay, Canada (Naldrett *et al.*, 2000).

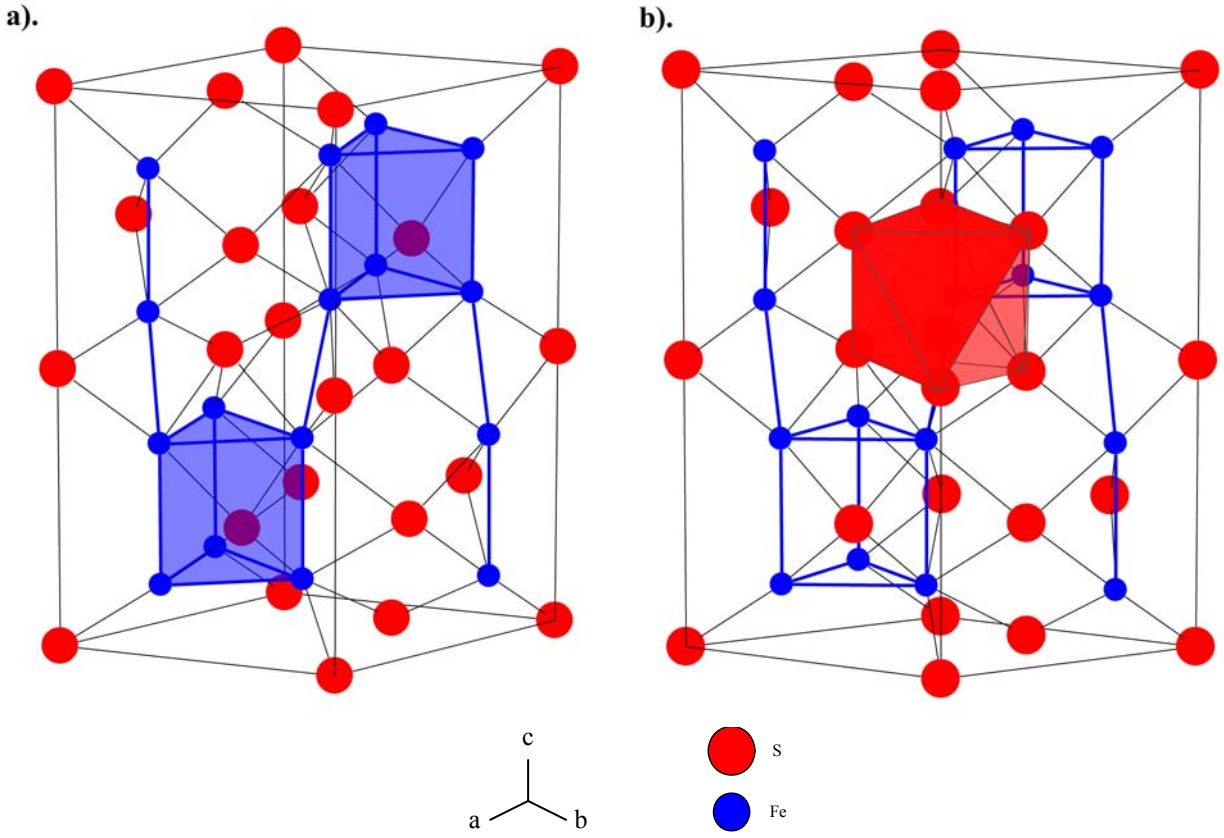


**Figure 2.9**: Illustration of the structure of lunar troilite. Blue lines represent Fe-Fe bonds, black lines represent iron sulfur bonds. The ideal coordination of sulfur in $SFe_6$ trigonal prisms is illustrated in (a) and coordination of iron in $FeS_6$ octahedra in (b). From: Evans (1970).

### 2.2.4 Metastable NA and MC pyrrhotites

Both the NA and MC pyrrhotite types are metastable existing in a relatively narrow temperature range between 209 and 308$^0$C (Figure 2.8; Kissin and Scott, 1982). The NA pyrrhotite is also sometimes known as 3C pyrrhotite due to the repeat distance of the *c*-axis representing three times that of the NiAs subcell (Francis and Craig, 1976). However, due to the presence of non-integral repeats along the *a*-axis of the NiAs unit cell, this pyrrhotite type is more correctly known as NA pyrrhotite (Nakazawa and Morimoto, 1971). The MC pyrrhotite is similar to NA pyrrhotite but with M non-integrally changing between 3 and 4 (Nakazawa and Morimoto, 1971). The NA and MC pyrrhotite superstructures represent a progressive ordering of vacancies with a decrease in temperature from the disordered 1C pyrrhotite. However, this still only represents a partial ordering of vacancies in comparison to the lower temperature 4C and NC structures where ordered vacancies exist (Keller-Besrest *et*

*al*., 1982; Makovicky, 2006). Due to the unlikely occurrence of these two pyrrhotite superstructures in natural ore deposits, they will not be discussed further.

### 2.2.5 Magnetic 4C pyrrhotite

The original monoclinic 4C pyrrhotite structure was proposed by Bertaut (1953) with unit cell parameters of a = 2√3A, b=2A, c = 4C where A and C represent the NiAs subcell dimensions. The 4C pyrrhotite superstructure is characterised by the distinct ordering of vacancy layers oriented along the *c*-axis. Individual vacancy containing layers are separated by completely filled metal cation layers in a sequence described as AFBFCFDF where A, B, C and D denote vacancy layers containing vacancies in the A, B, C, and D positions, and F, the completely filled iron layers as shown in figure 2.10. Within this structure a quarter of the iron atoms are absent and thus it has been proposed that charge balance is maintained by the presence of ferric iron in the pyrrhotite structure (Tokonami *et al*., 1972). Similarly to troilite, iron is in an octahedral coordination whereas sulfur is now in a combination of five fold and six fold coordination due to the presence of iron vacancies. More recent structure determinations of the 4C monoclinic pyrrhotite include that of Tokonami *et al.* (1972), although with the use of the unconventional space group F2/d that was originally used in the structure of Bertaut (1953). The unconventional unit cell was chosen to maintain an approximately orthogonal unit cell and to use nomenclature such that vacancy repeats are integral to the NiAs unit cell along the *c*-axis. Subsequently, Powell *et al.* (2004) determined the 4C structure with the use of powder neutron diffraction on a synthetic pyrrhotite sample and refined the structure in the C2/c space group. The relationship between the two space groups is shown in figure 2.11.

Monoclinic 4C pyrrhotite is ferrimagnetic and is therefore more commonly known as *magnetic pyrrhotite,* which is the choice of nomenclature for this study. The ideal composition of magnetic 4C pyrrhotite is $Fe_7S_8$ with a compositional range between 46.6 and 46.9 atomic % iron (Carpenter and Desborough, 1964). According to Bertaut (1953), the formula $Fe_7S_8$ can also be described as $Fe_2^{3+}Fe_5^{2+}S_8$ to account for the non-stoichiometry in the pyrrhotite structure. Bertaut (1953) also argued that the most stable energy configuration existed when the ferric iron cations were distributed over both the vacancy and full layers. According to the saturation magnetization from Powell *et al.* (2004) however, it is more likely that the ferric iron cations are restricted to the vacancy layers.

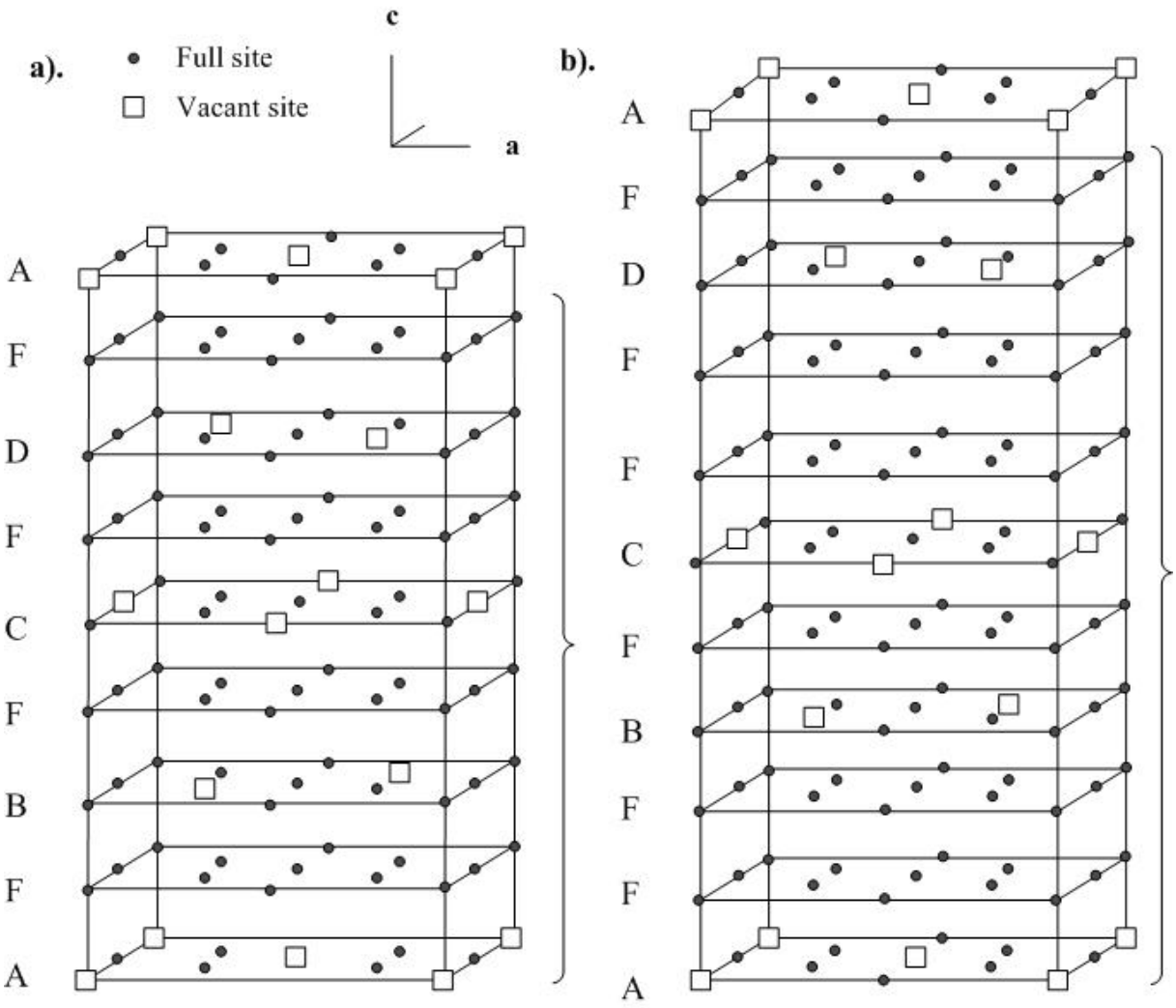


**Figure 2.10:** (a) Illustration of the vacancy structure in 4C magnetic pyrrhotite in the sequence AFBFCFDFA and based on the space group F2/d. (b) Illustration of the proposed vacancy structure for 5C pyrrhotite adapted from Vaughan *et al.* (1971). Sulfur sites are omitted for clarity.

However, the debate is still ongoing as to whether ferric iron even exists in the pyrrhotite structure. Mössbauer spectroscopy has not been a successful tool to recognise individual ferrous and ferric iron valence states in pyrrhotite due to the very rapid electron transfer, whereas both XANES and XPS have been successful. Pratt *et al.* (1994) used XPS on vacuum fractured monoclinic pyrrhotite to show the presence of both ferrous and ferric iron. Similarly, Mikhlin and Tomashevich (2005) showed the presence of ferric iron in monoclinic pyrrhotite using XANES. In contrast, Letard *et al.* (2007) used XMCD to study pyrrhotite and argued that only ferrous iron is present in pyrrhotite.

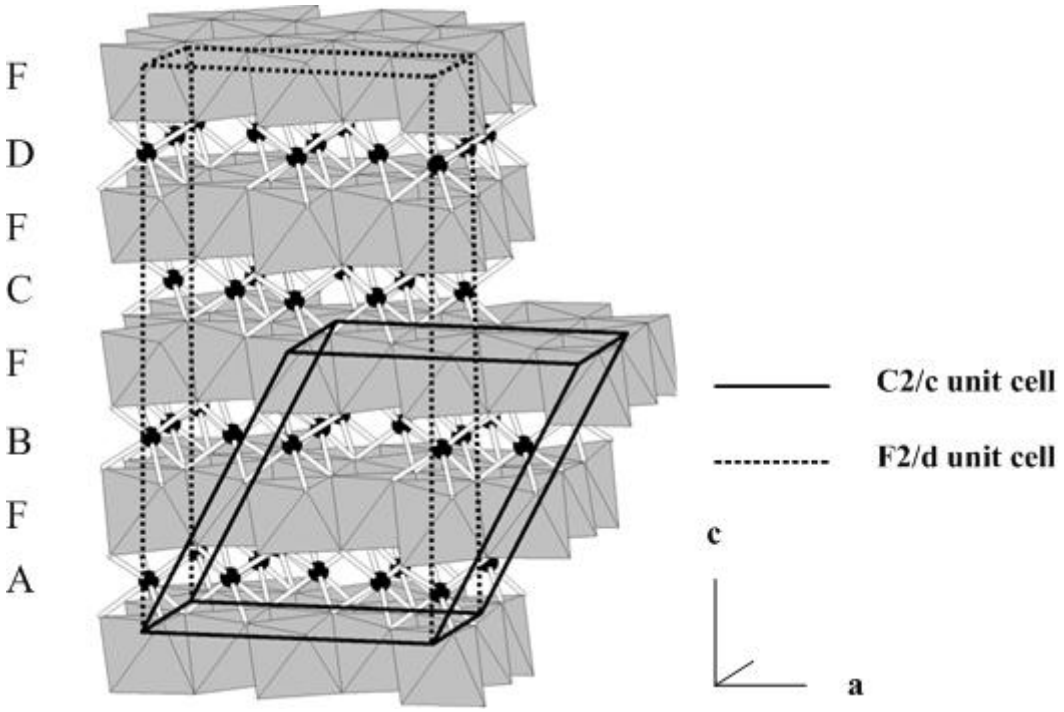


**Figure 2.11:** (a) Illustration of the relationship between the F2/d and C2/c space groups as used by Tokonami *et al.* (1972) and Powell *et al.* (2004), respectively, in describing the structure of magnetic 4C pyrrhotite. Iron sites are illustrated as solid circles in vacancy layers and as shaded octahedra in fully occupied layers. Adapted from: Powell *et al.* (2004).

According to the pyrrhotite phase relations shown in figure 2.8, magnetic 4C pyrrhotite is stable below $254^0$C (Kissin and Scott, 1982) and may co-exist with either NC pyrrhotite (more iron rich bulk compositions) or with pyrite (more sulfur rich compositions). The phase relations also suggest that the 4C monoclinic pyrrhotite is the lower temperature, more ordered form of pyrrhotite derived from NA pyrrhotite. Since primary magnetic 4C pyrrhotite and troilite are incompatible, it suggests that where magnetic pyrrhotite and troilite do co-exist, the role of secondary alteration or oxidation needs to be evaluated (Liebenberg, 1970; Lianxing and Vokes, 1996).

4C magnetic pyrrhotite is one of the most commonly documented pyrrhotite forms in natural terrestrial occurrences. Both Carpenter and Desborough (1964) as well as Arnold (1967) demonstrated the abundance of 4C pyrrhotite types in their respective studies of pyrrhotite from different geographic locations around the world. However, Arnold (1967) also showed that naturally occurring mixtures of 4C and NC pyrrhotite were far more frequent (73% of the samples analysed) and this has been verified by numerous other studies of pyrrhotite

occurrences (e.g. Naldrett and Kullerud, 1967; Liebenberg, 1970; Lianxing and Vokes, 1996; Posfai *et al.*, 2000).

An anomalous monoclinic pyrrhotite of composition $Fe_{7+x}S_8$ has also been described in the literature by Clark (1966). Anomalous pyrrhotite appears to be common in low-temperature sedimentary environments and is antiferromagnetic unlike normal monoclinic pyrrhotite that is ferrimagnetic.

### 2.2.6 Non-magnetic NC pyrrhotite

NC pyrrhotite, also known as intermediate or *non-magnetic* pyrrhotite consists of a series of pyrrhotite superstructures. These are generally grouped together for simplicity during phase relationship studies (e.g. Nakazawa and Morimoto, 1971) and are shown in tables 2.2 and 2.3. The value of N, representing the repeat distance of the *c*-axis dimension of the NiAs subcell may be both integral and non-integral, varying between 5 and 11. The integral NC superstructures of pyrrhotite can be linked to their ideal composition using the relationship of Morimoto *et al.* (1970) where: $Fe_{n-1}S_n$ (n>8). If *n* is even then the structure is *n*/2C (ie. 5C pyrrhotite with composition $Fe_9S_{10}$, 6C pyrrhotite with composition $Fe_{11}S_{12}$) or if *n* is odd then the structure is *n*C (ie 11C pyrrhotite with composition $Fe_{10}S_{11}$). Solid solutions between the compositions $Fe_9S_{10}$ to $Fe_{10}S_{11}$, and between $Fe_{10}S_{11}$ and $Fe_{11}S_{12}$ are considered to be metastable, although they may result in some of the non-integral or incommensurate periodicities of N identified in some studies (e.g. N = 5.38, 5.5, 5.7, 6.6, 10, 28; Pierce and Buseck, 1974; Morimoto *et al.*, 1975a; Posfai *et al.*, 2000).

The exact ordering of vacancies in the non-magnetic NC structure is rather complex and hence no complete crystal structure solutions exist in the literature. This does not preclude that some have postulated ideal vacancy distributions based on the 4C monoclinic structure (e.g. Vaughan *et al.*, 1971; Nakazawa and Morimoto, 1971; Posfai and Dodony, 1990). Since the absolute number of vacancies is theoretically fixed for the integral NC pyrrhotites, by inserting additional filled iron layers into the 4C structure, potential vacancy distributions can be proposed. Vaughan *et al.* (1971) proposed a structure alternating between one and two filled layers for the 5C pyrrhotite as shown in figure 2.10. For the 6C pyrrhotite Nakazawa and Morimoto (1971) suggested a vacancy layer at every third iron layer whereas Koto *et al.*

(1975) argued that the vacancy distribution for 6C pyrrhotite was probably not ideal and consisted of some half filled iron sites alternating with fully occupied iron sites.

As shown by table 2.3, the crystallography of the non-magnetic NC pyrrhotites is debatable with accounts of the 5C pyrrhotite described as hexagonal or orthorhombic, the 6C pyrrhotite described as hexagonal, monoclinic or pseudo-orthorhombic, and the 11C pyrrhotite as orthorhombic (Carpenter and Desborough, 1964; Morimoto *et al.*, 1970; Koto *et al.*, 1975; Morimoto *et al.*, 1975b). Since the apparent x-ray diffraction symmetry of the NC pyrrhotite subcell is hexagonal, non-magnetic pyrrhotite has been termed "hexagonal" in the past for ease of reference (Posfai *et al.*, 2000).

Similarly, to the representation of the magnetic 4C pyrrhotite structure as a mixture of both ferric and ferrous iron, the non-magnetic NC pyrrhotites can be represented as follows; $Fe_7^{2+}Fe_2^{3+}S_{10}^{2-}$, $Fe_8^{2+}Fe_2^{3+}S_{11}^{2-}$, $Fe_9^{2+}Fe_2^{3+}S_{12}^{2-}$. The absolute amount of ferric iron is constant in the NC pyrrhotite but the overall proportion varies such that the 5C pyrrhotite has more ferric iron than the 11C and so forth. Mikhlin and Tomashevich (2005) also showed the presence of ferric iron in the "hexagonal" pyrrhotite structure using XANES. The non-magnetic NC pyrrhotite is antiferromagnetic.

Non-magnetic NC pyrrhotite is stable at temperatures less than $209^0$C as shown by figure 2.8 and within this stability field, the type of NC superstructure formed is dependent upon both temperature and composition (Nakazawa and Morimoto, 1971). As to whether the non-integral NC pyrrhotite is metastable at ambient conditions or not, is a subject of debate in the literature, but this does not negate the observation that for some natural occurrences, the non-integral NC superstructures are far more abundant than integral NC superstructures (Morimoto *et al.*, 1970; Morimoto *et al.*, 1975b).

The iron content of the non-magnetic NC group of pyrrhotite superstructures at ambient conditions, has been found to vary between 47.0 and 48.0 atomic % iron (Carpenter and Desborough, 1964). The NC pyrrhotite can also coexist with 4C monoclinic pyrrhotite at more sulfur rich bulk compositions. However, for more iron rich bulk compositions with greater than 48 atomic % iron, troilite and NC pyrrhotite can coexist with one another (Figure 2.8). In natural occurrences, this has been observed as troilite exsolution lamellae from an NC pyrrhotite matrix (e.g. Gain and Mostert, 1982). Similarly, for more sulfur rich bulk

compositions, intergrowths of NC and 4C pyrrhotite are expected (e.g. Carpenter and Desborough, 1964; Naldrett and Kullerud, 1967; Lianxing and Vokes, 1996). However, the phase diagrams also suggest that there is a compositional stability field in which NC pyrrhotite exists by itself, which is borne out by descriptions of pure "hexagonal" pyrrhotite occurrences (Carpenter and Desborough, 1964; Arnold, 1967).

### 2.2.7 Relationship between pyrrhotite, pentlandite and the platinum group elements

*Relationship between pyrrhotite types*

In the past there have been many accounts describing the intergrowths between non-magnetic NC and magnetic 4C pyrrhotite. These have been performed using a variety of techniques in conjunction with optical microscopy such as the chromic acid etch and magnetic colloid method (e.g. Naldrett and Kullerud, 1967). In order for the description of pyrrhotite petrography in this study to be more meaningful, a summary of the types of intergrowth textures described in the literature is given along with the schematic of intergrowth textures in figure 2.12. This summary is based on the work of Lianxing and Vokes (1996), which characterised the textures of a variety of Norwegian pyrrhotites including those typical of magmatic nickel deposits.

Lianxing and Vokes (1996) classified the magnetic and non-magnetic pyrrhotite examined in their study into two groups; comprising "crystallographically controlled lamellar intergrowths" and "fissure controlled irregular intergrowths". The former were interpreted to represent textures controlled through primary ore forming processes involving pyrrhotite formation and annealing, whereas the latter were likely the result of secondary processes such as hydrothermal alteration (Desborough and Carpenter, 1965). There are several manifestations of the lamellar intergrowths of the crystallographically controlled magnetic pyrrhotite exsolved from non-magnetic pyrrhotite. All these manifestations are based on the interaction between multiple lamellae of magnetic pyrrhotite through processes such as annealing (Brady, 1987) and are summarised in figure 2.12. As shown in figure 2.12, the crystallographically controlled textures may consist of parallel lamellae of magnetic pyrrhotite hosted by non-magnetic pyrrhotite (a), thickness zonation (b), development of box work texture (c) or composite lamellae (d). The magnetic colloid may also highlight the

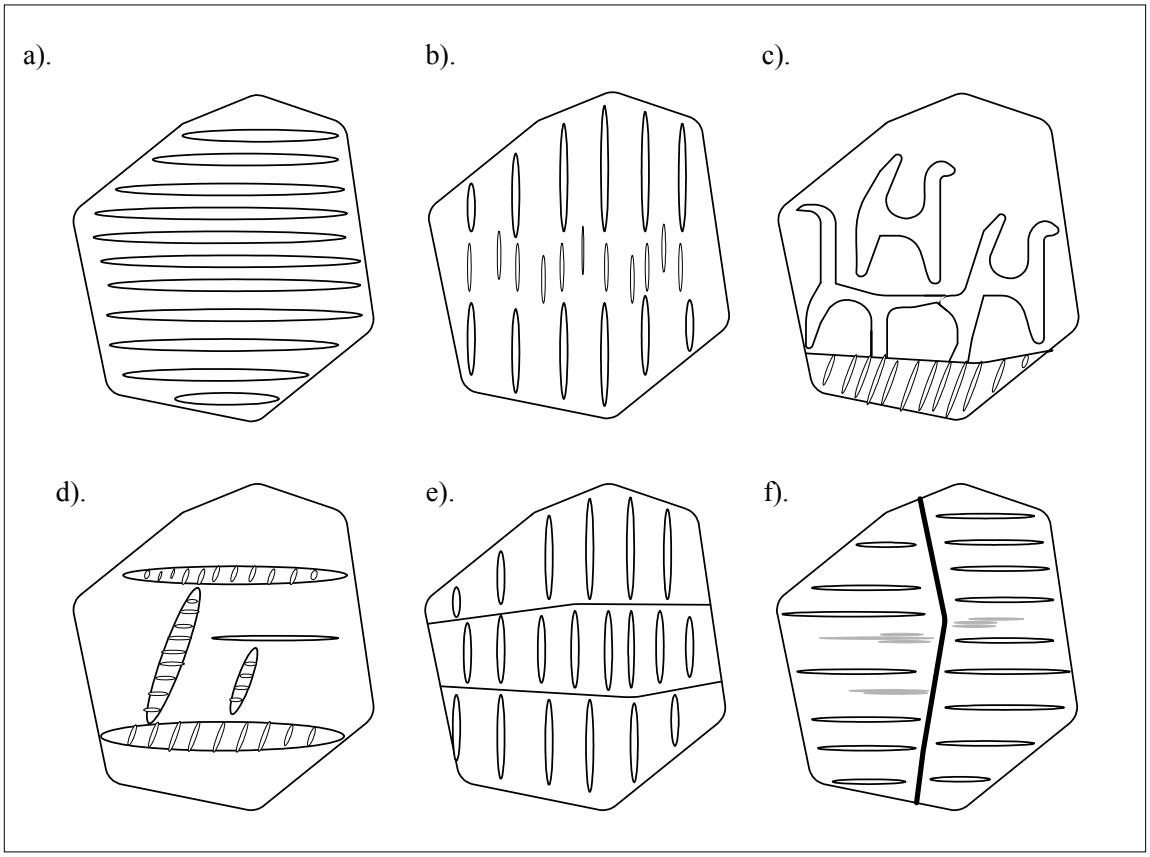


**Figure 2.12:** Graphical illustration of the types of crystallographically controlled intergrowths found in pyrrhotite. (a) Exsolution lamella of magnetic pyrrhotite hosted by non-magnetic pyrrhotite. (b) Thickness zonation of magnetic pyrrhotite lamellae hosted by non-magnetic pyrrhotite. (c) Box work textures of magnetic pyrrhotite hosted by non-magnetic pyrrhotite. (d) Composite lamellae of magnetic pyrrhotite hosted by non-magnetic pyrrhotite. (e) Magnetic domain walls in pyrrhotite. (f) Exsolution of pentlandite flames (grey) from fissure. Note that the orientation of the flames is parallel to the magnetic pyrrhotite exsolution lamellae. Adapted from photomicrographs in Lianxing and Vokes (1996) and Yamamoto *et al.* (1959).

location of magnetic domain walls (e). The second texture of "fissure controlled intergrowths" consists of irregular intergrowths of magnetic pyrrhotite blades and patches hosted along fissures and grain boundaries of non-magnetic pyrrhotite (Lianxing and Vokes, 1996).

*Relationship between pyrrhotite and pentlandite*

Due to the similarity in physical and chemical properties between iron and nickel cations in a thermo-chemical system, the behaviour of these two elements needs to be considered together. Practically, this means that the valuable nickel mineral, pentlandite, almost ubiquitously occurs with pyrrhotite, which has significant implications for mineral processing. Consequently, there has been much research in the past on understanding this

interrelationship in the Fe-Ni-S system. The work has generally focussed on the type example of the Sudbury magmatic sulfide deposit in Canada.

Pentlandite is classified as a metal sulfide with an excess of metal to sulfur. It is a solid solution between both iron and nickel with an ideal composition of $(FeNi)_9S_8$, is cubic in character and is based on a structure of metal-sulfur tetrahedra (Makovicky, 2006). Pyrrhotite and pentlandite both form from a high temperature immiscible Fe-Ni-S sulfide solid solution, more commonly know as the monosulfide solid solution or *MSS*. According to the phase diagram studies of Sugaki and Kitakaze (1998), at temperatures between 865 and $584^0$C a high form of pentlandite exsolves from the MSS. This high pentlandite has half the size of the unit cell of low temperature pentlandite. Upon further cooling to below $615^0$C, high pentlandite transforms into pentlandite *sensu stricto*. Textural forms of pentlandite which have been described for the Sudbury deposit include (Naldrett *et al.*, 1967; Naldrett and Kullerud, 1967; Kelly and Vaughan, 1983):

i). Blades of pentlandite along rims of pyrrhotite grain boundaries. The bladed texture tends to be replaced by a more granular pentlandite at triple junctions of pyrrhotite grain boundaries.
ii). Flame (lamellae-like) structures of pyrrhotite developed at grain boundaries or *en échelon* along fractures (Figure 2.12f).
iii). Flame structures of pentlandite hosted by a pyrrhotite matrix and unrelated to any structural defects.
iv). Occurrence of monoclinic pyrrhotite as rims around flame pentlandite.

These textural forms of pentlandite were recreated in the experimental studies of Kelly and Vaughan (1983) at $400^0$C and were subsequently explained through the following mechanisms. The key however, was the dependence of pentlandite texture on the metal / sulfur ratio and cooling rate of the *MSS* as shown in figure 2.13 During the formation of pentlandite, clusters of iron and nickel atoms agglomerate and nucleate from the *MSS*. Due to the free energy of the system, these clusters prefer to nucleate along zones of structural defects such as grain boundaries and fractures. Further nucleation results in the gradual formation of continuous rims of pentlandite blebs or grains along pyrrhotite grain boundaries (i). Continual nucleation, especially for bulk compositions with higher metal to sulfur ratios results in the formation of finer blades or flames on grain boundaries or *en échelon*

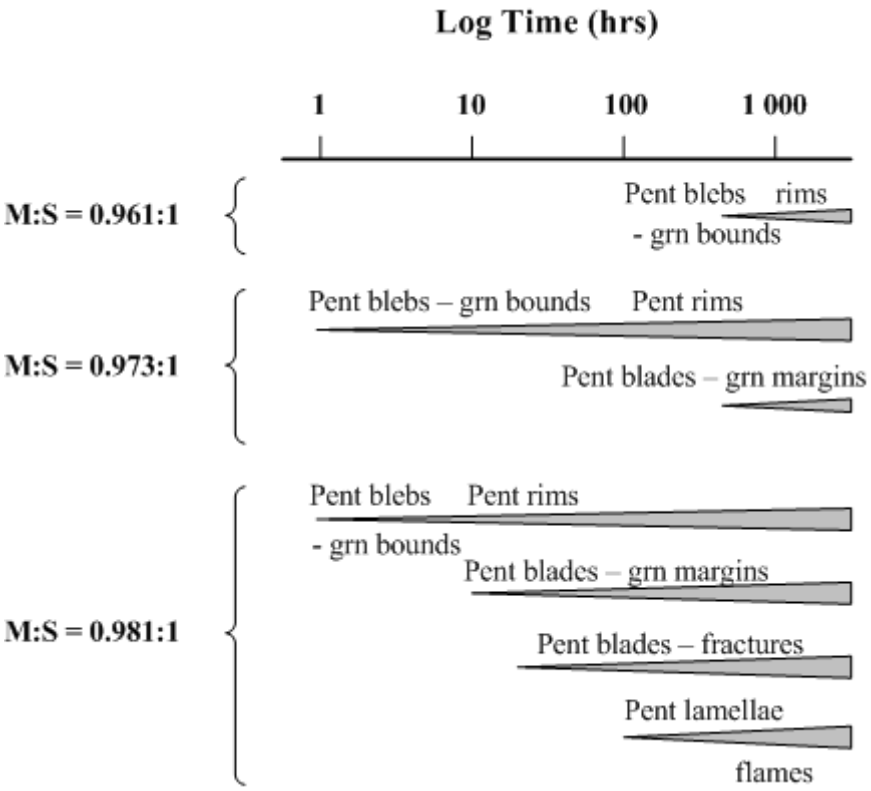


**Figure 2.13:** Relationship between the initial metal to sulfur ratio of the MSS and time in the formation of different pentlandite morphologies, based on an iron / nickel ratio of 5. "Grn bounds" represents pentlandite on grain boundaries, and "grn margins" represents the development of pentlandite on grain margins. From: Kelly and Vaughan (1983).

distribution along fractures (ii). With further cooling below ~240$^0$C, the diffusion rates decrease, and pentlandite nucleation is impaired, resulting in the formation of flames, unrelated to any defects. Crystallographic control may still exist resulting in the formation of these pentlandite flames in a direction perpendicular to the basal plane of the pyrrhotite (iii). Within these localised areas of flame pentlandite formation, the adjacent areas to the flames remain as nickel poor, sulfur rich sites causing the preferential formation of monoclinic pyrrhotite as rims to the flames (iv).

In addition to the formation of discrete pentlandite grains or flames, some residual nickel may occur in the pyrrhotite structure. Analyses of the residual concentration of nickel in "hexagonal" and monoclinic pyrrhotites from the Sudbury district, have shown that "hexagonal" pyrrhotites are more nickel rich (0.68 - 1.01 wt %) relative to the monoclinic pyrrhotite (0.35 - 0.5 wt %; Vaughan *et al.*, 1971; Batt, 1972).

*Relationship between pyrrhotite and the platinum group elements*

Some mention of the relationship between the platinum group elements and pyrrhotite should be made given that for some mineral processing operations, nickel is a by product of the beneficiation of the platinum group elements e.g. Merensky Reef, South Africa. This association is notable for magmatic sulfide deposits, although the Norilsk nickel deposits are also known to have measurable platinum group minerals (Cabri *et al.*, 2003). Experimentally derived partition coefficients show that the platinum group elements are more than 10 000 times more soluble in a sulfide liquid than the coexisiting basaltic liquid at high temperature (Crockett *et al.*, 1997). Upon cooling, the platinum group elements may remain in solid solution with minerals such as pentlandite or pyrrhotite. According to Ballhaus and Ulmer (1995), the 1C pyrrhotite structure can accommodate platinum and palladium in iron sites, but only when the occupied site is surrounded by 4 (Pd) or 5(Pt) vacancies in the crystal structure. Alternatively, discrete platinum group minerals may form through fractional crystallisation from the MSS.

### 2.2.8 Analytical methods for discrimination between pyrrhotite types

The need for an adequate methodology to be able to measure and quantify the textural relationship between magnetic and non-magnetic pyrrhotite types exists, since Arnold (1967) demonstrated that over 70 % of the pyrrhotite samples examined in his study were mixtures of "hexagonal" or non-magnetic pyrrhotite with monoclinic or magnetic pyrrhotite. These pyrrhotite types typically form a complex array of intergrowth textures such as those shown in figure 2.12. It is therefore apt in this process mineralogy study to review past methods as well as evaluate modern mineralogical analysis techniques which show potential for discrimination and quantification of the relationship between pyrrhotite types.

*Optical microscopy based methods*

The relationship between pyrrhotite types can be investigated based on differences in the optical and / or physical properties of magnetic and non-magnetic pyrrhotite using standard optical microscopy. In the study of Carpenter and Bailey (1973), troilite, "intermediate" and monoclinic pyrrhotite were differentiated entirely based on their inherent optical properties: reflectivity, tarnishing and angle of apparent rotation. It was shown that mineral structure had a greater influence on the optical properties (especially reflectivity) of pyrrhotite than

composition. Although Carpenter and Bailey (1973) were able to accurately distinguish between pyrrhotite types, the method used was highly specialised and appears not to have been used by their contemporaries.

Chromic acid etching techniques were more commonly used by others such as Ramdohr (1969), Graham (1969) and Naldrett *et al.* (1967) whereby etching caused one phase to be darker than the other. However, in some scenarios the non-magnetic pyrrhotite was the darker phase and magnetic pyrrhotite the lighter phase and in other cases, vice versa (Naldrett *et al*., 1967; Craig and Vaughan, 1981). An alternative method based on exploitation of the magnetic properties of ferrimagnetic monoclinic pyrrhotite has also been used. This has been known as "Bitter patterns" (Bitter, 1932), "powder patterns" (Zapletal, 1969) and more recently as the "magnetic colloid" method (Craig and Vaughan, 1981; Lianxing and Vokes, 1996). When the magnetic colloid method is used, magnetite particles suspended in a soapy solution aggregate in areas of the surface of the mineral where the greatest inhomogeneities exist in the magnetic field (Zapletal, 1969).

The strength of the magnetic colloid method is that once the colloid has been made and pyrrhotite samples prepared as polished ore mounts, it is a relatively quick, easy and inexpensive task to discriminate between pyrrhotite types. The inherent weaknesses in this method are that the observer needs to have some training in ore petrography in order to interpret the data. The response of pyrrhotite to the acid etch or colloid may also differ within an occurrence due to the varying surface reactivity of grains in varying orientations (Graham, 1969; Zapletal, 1972). In order to quantify the relative proportions of pyrrhotite types, methods such as point counting, which is subject to human error or image analysis would have to be used.

*Crystallographic based methods*

The primary means for the identification of pyrrhotite types is based upon their crystallographic properties. A number of fundamental analytical techniques have been used in the past in order to discriminate between pyrrhotite types and these include single crystal and precession camera x-ray methods as well as HRTEM (Morimoto *et al.*, 1970; Pierce and Buseck, 1974). Traditionally when single crystal x-ray information is examined, two types of information are obtained:

i) Geometry of all major spots or reflections derived from the interaction of the x-ray beam with the pyrrhotite single crystal
ii) Intensity of all major spots or reflections derived from the interaction of the x-ray beam with the pyrrhotite single crystal

By analysis of the geometry of all the major spots or reflections of the crystal, information on crystal lattice parameters and crystal symmetry is obtained. Once the crystal lattice parameters are known, the pyrrhotite superstructure can be deduced based on the length of the *c*-axis. The arrangement and number of weak spots derived from the superstructure reflections can also be used to confirm the pyrrhotite superstructure.

By analysis of the intensity of all the major spots or reflections of the crystal, the exact position of iron and sulfur atoms, as well as the position of vacant sites in the pyrrhotite crystal can also theoretically be determined. Due to the complexity of the pyrrhotite structure with respect to the ordering of vacancies as well as the lack of suitable pyrrhotite single crystals, complete structure solutions of pyrrhotite are quite limited. As shown in table 2.3, the majority of crystal structure solutions which exist are based on the analysis of synthetic specimens. To date, no complete crystal structure solution exists for non-magnetic NC pyrrhotite.

Single crystal x-ray diffraction (XRD) is however, too specialised for the routine measurement of pyrrhotite and is limited to single crystals. Consequently, powder x-ray diffraction methods are preferred, particularly since they are more representative of the bulk sample. The method described by Graham (1969) is based on the relative ratios of the characteristic pyrrhotite peaks in a powder x-ray diffractogram. This appears to have been the accepted method for many years in the nickel processing industry (e.g. A. Kerr, Pers. Comm. 2008). This method is based upon the differences in intensity between characteristic pyrrhotite peaks; magnetic pyrrhotite has a doublet at d = 2.066 and 2.056 Å, whereas non-magnetic pyrrhotite has a singlet at 2.066 Å, and troilite has a singlet at d = 2.094 Å as shown in figure 2.14. Comparison of the ratios of these characteristic pyrrhotite peaks with an external calibration curve, allows one to calculate the relative proportions of each pyrrhotite phase. More recently with the advent of XRD software using the Rietveld method for phase quantification based on the refinement of crystal structures using information obtained from an entire diffractogram as opposed to the characteristic pyrrhotite

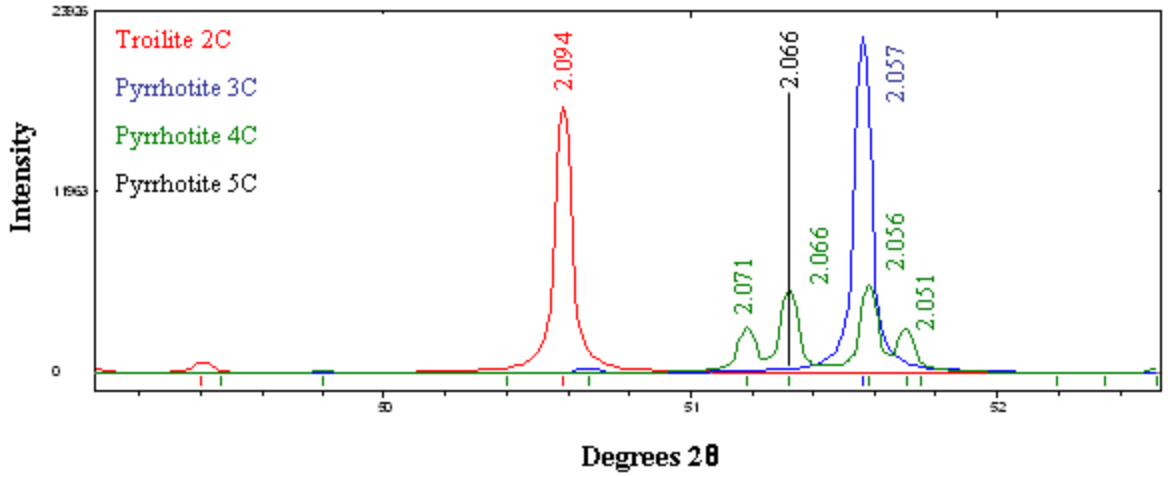


**Figure 2.14:** Comparison of the characteristic powder diffraction peaks of synthetic 3C hexagonal pyrrhotite, synthetic 4C magnetic, monoclinic pyrrhotite and natural 2C troilite based on the structures of Keller-Besrest *et al.* (1982), Powell *et al.* (2004) and Skala *et al.* (2006). The characteristic peak of 5C non-magnetic pyrrhotite based on the d-spacing of Carpenter and Desborough (1964) is also shown.

peaks, the relative proportions of the two pyrrhotite phases can in theory, be routinely determined in an unknown sample (Young, 1995; Raudsepp *et al.*, 2002; De Villiers and Verryn, 2008).

Strengths associated with the measurement and quantification of pyrrhotite in mixed samples with the powder XRD method are that both the sample preparation and measurement times are relatively quick and the cost of the analysis is moderate. Powder XRD methods are likely to be more statistically representative of the whole if samples are prepared following accepted sampling practice. However, the Rietveld method is based on upon the availability of appropriate crystal structure information. As shown in table 2.3, no complete crystal structure solution exists for non-magnetic NC pyrrhotite which is a significant short fall for the technique. Assuming the presence of suitable pyrrhotite crystal structures however, quantitative determination of the relative proportions of pyrrhotite types is restricted by the detection limits of the technique (~ 5 wt %). This may exclude the use of quantitative XRD for analysis of low grade ore deposits unless some upgrading of the sulfide component has been made.

*Electron beam based methods*

Electron beam based methods used for the differentiation of pyrrhotite forms may essentially be divided into those based upon the precise measurement of chemical composition or through the measurement of the average atomic number of the pyrrhotite sample based on its back scattered electron (BSE) signal. The electron microprobe (EMP) is ideal for spot analysis of the exact chemical composition of pyrrhotite which can be added to a dataset of magnetic and non-magnetic pyrrhotite compositions. However, proper calibration and standardisation is of the utmost importance to ensure the ability to be able to distinguish between the subtle differences in iron and sulfur contents. Since the EMP is a fairly specialised instrument, it is more appropriate to evaluate the potential contribution of a scanning electron microscope (SEM) for routine analysis of pyrrhotite types.

The SEM is an ideal instrument for using the BSE signal as a means to discriminate between pyrrhotite types. The BSE grey level of non-magnetic $Fe_9S_{10}$ pyrrhotite is ~ 43.33 and is only just a little higher than magnetic $Fe_7S_8$ pyrrhotite, where the BSE grey level is ~ 43.16. Using this subtle difference in the BSE grey level, one can theoretically differentiate between magnetic and non-magnetic pyrrhotite phases under ideal imaging conditions. Zapletal (1969) performed a thorough study comparing pyrrhotite textures obtained using a SEM with those from the magnetic colloid and chemical etch techniques. In general, good correlation was determined between all the methods, but it was observed that the BSE signal was also subject to the effects of crystal orientation. To date, discrimination of pyrrhotite types based on their BSE signal appears not to have been developed for routine use.

With the advent of modern automated mineralogical techniques based on the scanning electron microscope such as the QEMSCAN or MLA, there is potential to develop a technique for analysis of magnetic and non-magnetic pyrrhotite. This could be routinely applied on metallurgical samples and provide rapid, automated quantitative mineralogical analysis between pyrrhotite types. The use of QEMSCAN or MLA is considered a prospective method for the discrimination between pyrrhotite phases and is accordingly further developed in this study (Section 3.3).

## 2.3 Electrochemical Properties of Pyrrhotite

The sulfide minerals are known to be prone to anodic oxidation coupled with the cathodic reduction of oxygen in the presence of air or water. Unlike many other sulfides such as pyrite, pentlandite and chalcopyrite which are semi-conductors, pyrrhotite is a metallic conductor. The ease with which the different sulfide minerals are prone to oxidation can be determined by a comparison of the rest potentials or open circuit potential, which is the equilibrium potential of the mineral at zero electric current as shown in table 2.4. Understanding the mechanism and factors that affect pyrrhotite oxidation is of importance to interpreting its flotation behaviour, given that the surface species formed on pyrrhotite by the oxidation reaction influences its hydrophobicity and consequent flotation characteristics.

**Table 2.4:** Rest potential of selected sulfide minerals given as volts versus SHE. From: Kwong *et al.* (2003) and references therein.

| Mineral | Formula | Rest Potential (V vs SHE) |
|---|---|---|
| Pyrite | $FeS_2$ | 0.63 |
| Chalcopyrite | $CuFeS_2$ | 0.52 |
| Chalcocite | $Cu_2S$ | 0.44 |
| Covellite | CuS | 0.42 |
| Galena | PbS | 0.28 |
| Sphalerite | ZnS | -0.24 |
| Pyrrhotite | $Fe_{(1-x)}S$ | -0.28 |

Rest potential measurements of selected minerals sometimes differ slightly from one publication to the next, not only due to the differences in measurement conditions, but also due to differences in the mineralogy of these minerals. For example, the rest potential of pyrrhotite obtained by Buswell and Nicol (2002) at different points in a Merensky plant varied between 0.20 and 0.29 V. Variations in pyrite rest potential have also been reported. For example, Tao *et al.* (2003) used chronoamperometry measurements on natural pyrite samples to show that the stable potential of pyrite varied according to its derivation. Similarly, Lehner *et al.* (2007) examined the influence of arsenic, cobalt and nickel impurities on the reactivity of synthetically doped pyrite and showed that the composition of pyrite influenced

its reactivity. These differences were ascribed to impurities or surface defects and the effect they may have on changing the nature of the pyrite between an *n-type* semiconductor (donor defects) to a *p-type* semiconductor (acceptor defects). The variation between *n-type* and *p-type* semiconducting behaviour in pyrite may correlate with its metal / sulfur ratio. Since the metal / sulfur ratio and trace element composition of pyrrhotite is variable (e.g. Carpenter and Desborough, 1964; Arnold, 1967), differences in the conducting nature of the different pyrrhotites may be expected. Although Theodossiou (1965) examined the behaviour of pyrrhotite and found a change from *n-type* to *p-type* with increasing temperature for the specimen analysed, little detail is given on the exact mineralogy of the sample used.

### 2.3.1 Pyrrhotite Oxidation Reactions

One of the additional features about pyrrhotite which gives it a unique character is that it exhibits both oxidative and non-oxidative dissolution (Thomas *et al.*, 2000). Oxidative dissolution which is typical of pyrite is often known as acid producing (Equation I), whereas non-oxidative dissolution which is typical of troilite is acid consuming (Equation II; Thomas *et al.*, 2003).

$$FeS_2 + 8H_2O \rightarrow Fe^{2+} + 2SO_4^{2-} + 16H^+ \quad \text{(I)}$$

$$FeS + 2H^+ \rightarrow Fe^{2+} + H_2S \quad \text{(II)}$$

In the presence of oxidising agents such as oxygen or ferric iron that are likely to be fairly abundant in the flotation system, oxidative dissolution would be favoured (Thomas *et al.*, 2003) and therefore only this reaction will be focussed on. The oxidation of pyrrhotite by oxygen may then proceed as given below (Hamilton and Woods, 1984):

$$FeS_{1.13} \rightarrow Fe^{2+} + 1.13S^0 + 2e^- \quad \text{(III)}$$

$$FeS_{1.13} + 4.52\ H_2O \rightarrow Fe^{2+} + 1.13SO_4^{2-} + 9.04H^+ + 8.78e^- \quad \text{(IV)}$$

Given that ferric iron is likely to be a stable reaction product at alkaline conditions, the reactions can be represented as follows:

$$FeS_{1.13} + 3H_2O \rightarrow Fe(OH)_3 + 1.13S^0 + 3H^+ + 3e^- \quad (V)$$

$$FeS_{1.13} + 7.52\ H_2O \rightarrow Fe(OH)_3 + 1.13SO_4^{2-} + 12.04H^+ + 9.78e^- \quad (VI)$$

Hamilton and Woods (1981) showed that $SO_4^{2-}$ production as shown in equations IV and VI was favoured when the reaction was taken to higher potentials. The sulphoxy species ($S_xO_y^{2-}$) has also been reported as an intermediate of the pyrrhotite oxidation reaction (Steger and Desjardins, 1978; Almeida and Giannetti, 2003).

The oxidation of pyrrhotite may also take place with ferric iron as the oxidant as shown by equation VII (Belzile *et al.*, 2004):

$$Fe_{1-x}S + (8-2x)\ Fe^{3+} + 4H_2O \rightarrow (9-3x)\ Fe^{2+} + SO_4^{2-} + 8H^+ \quad (VII)$$

### 2.3.2 Mechanism of Pyrrhotite Oxidation

Since the early studies of Steger and Desjardins (1978) and Steger (1982) that determined the identity of the oxidation products of pyrrhotite using chemical extractive methods, much understanding has been gained of the oxidation reaction and change in the surface structure of pyrrhotite using spectroscopy techniques such as AES and XPS (e.g. Buckley and Woods, 1985; Jones *et al.*, 1992; Pratt *et al.*, 1994; Mycroft *et al.*, 1995; Legrand *et al.*, 2005a). This has led to some consensus regarding the nature of the pyrrhotite surface structure upon oxidation. All of the abovementioned authors identified the presence of ferric oxyhydroxides at the surface of pyrrhotite overlying another surface zone depleted in iron that may contain disulfides or polysulfides. Using AES, both Mycroft *et al.* (1995) and Pratt *et al.* (1994) determined the depth profiles for iron and sulfur from which a schematic illustration of the oxidation reaction can be shown as illustrated in figure 2.15. The outermost layer comprised of ferric oxyhydroxides is ~ 5 Å in thickness, underlain by a layer of composition $FeS_2$ which Jones *et al.* (1992) suggested has a disordered pyrite type structure. This is in turn underlain by a mixture of $Fe_2S_3$ and $Fe_7S_8$. The oxidised surface zone of pyrrhotite is only ~ 35 Å in thickness, below which the bulk unreacted pyrrhotite occurs (Pratt *et al.*, 1994; Mycroft *et al.*, 1995).

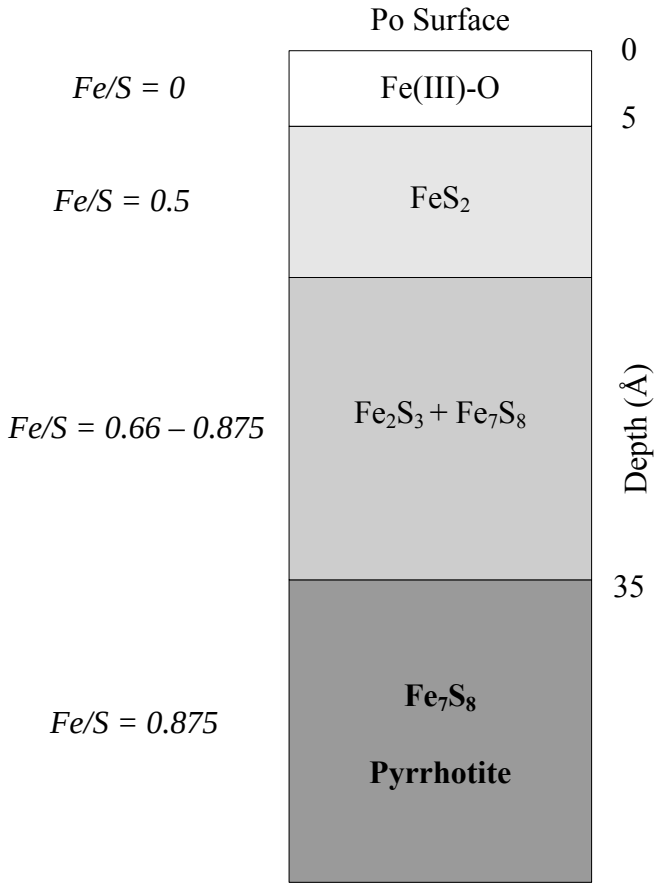


**Figure 2.15:** Schematic of a cross section through the surface of pyrrhotite during oxidation. Adapted from Mycroft *et al.* (1995).

Based on the species identified with XPS and the AES depth profiling, Pratt *et al.* (1994) proposed the following mechanism for the pyrrhotite oxidation reaction. They suggested that at no time during the oxidation reaction does oxygen significantly diffuse into the sulfide layer and neither does sulfur diffuse to the oxyhydroxide layer. The only movement during the reaction is by the transfer of electrons from the crystal lattice and the diffusion of iron towards the surface ferric oxyhydroxide layer. Pratt *et al.* (1994) proposed that the most reactive sites for oxygen reduction were associated with the ferric iron – sulfur bonds and the vacancies in the pyrrhotite crystal lattice. Vacancies are likely to facilitate electron transfer as well as the diffusion of iron through the lattice resulting in the conversion of the $Fe^{3+}$-S bonds to $Fe^{3+}$-O bonds and subsequent ferric oxyhydroxide formation. The formation of the ferric oxyhydroxide layer was observed to decrease over time since it is controlled by the supply of oxygen from the atmosphere, water to the mineral, the rate of diffusion of iron from the underlying sulfur rich layer, and the rate of electron transfer from ferrous iron reduction. The

last two factors are essentially the rate determining steps and may be responsible for the "passivation" of the pyrrhotite surface (Pratt *et al.*, 1994).

Various authors have described the effect of passivation of the pyrrhotite surface by the formation of a layer which prohibits further contact of the pyrrhotite surface with oxygen. This has also been known as an amorphous, non-equilibrium layer which is depleted in iron and may be referred to as the NL layer (Mikhlin *et al.*, 2002). Passivation of the pyrrhotite surface was argued as the mechanism responsible for the decrease in pyrrhotite oxidation at alkaline conditions (Hamilton and Woods, 1981), the interference with collector or activator adsorption mechanisms (Buswell *et al.*, 2002; Gerson and Jasieniak, 2008) and as a potential means of controlling acid mine drainage (Cruz *et al.*, 2005).

In the study of Legrand *et al.* (2005a) that investigated the oxidation reaction of coexisting pentlandite and pyrrhotite, both minerals were observed to form a thin surface layer of ferric oxyhydroxide overlying a metal deficient sublayer. Comparison of the time taken to produce the ferric oxyhydroxide overlayer of similar thickness for pentlandite and pyrrhotite demonstrated that that oxidation reaction was far more rapid for pyrrhotite (5 minutes) relative to pentlandite (30 minutes; Legrand *et al.*, 2005a).

### 2.3.3 Factors affecting Pyrrhotite Oxidation

*Oxygen*

Since the oxidation reaction of pyrrhotite is dependent on the presence of oxygen as an oxidising agent, it is expected that a correlation between oxidation rate and the availability of oxygen exists. This correlation was quantified by Lehmann *et al.* (2000) who examined the oxidative dissolution of pyrrhotite by cyanide. Lehmann *et al.* (2000) found that the rate constant of the dissolution reaction showed a progressive increase in magnitude correlating with sparging the solution with nitrogen, air or oxygen. Legrand *et al.* (2005b) similarly examined the influence of the dissolved oxygen concentration on pyrrhotite by investigating the change in the thickness of the ferric oxyhydroxide surface formed during oxidation with XPS. It was shown that as the dissolved oxygen concentration increased, so too did the thickness of the ferric oxyhydroxide surface layer. Spira and Rosenblum (1974) similarly showed an increase in oxygen demand according to whether the pyrrhotite slurry was sparged

with air or pure oxygen. Equation IV is also dependent upon the presence of water and in the early work of Steger (1982), the effect of relative humidity on the oxidation of pyrrhotite was examined. It was shown that the amount of iron and sulfate released by the oxidation reaction positively correlated with an increase in the relative humidity illustrating the dependency of the oxidation reaction on the water or moisture content. Steger (1982) also showed that the oxidised surface changed colour from orange-brown, blue-purple, blue-green back to orange-brown corresponding with the increasing amount of ferric hydroxide produced by the reaction.

*Ferric Iron*

As shown in equation VII, ferric iron also acts as an oxidising agent for the oxidation of pyrrhotite. Janzen (1996) examined the oxidation of pyrrhotite using ferric iron as the oxidising agent and showed that it followed a Langmuir type adsorption mechanism. The calculated rate constant was approximately ten times greater than that calculated for oxidation by oxygen, suggesting that ferric iron was a much faster oxidising agent than oxygen.

*pH*

The pH of the solution is known to affect both the nature of the oxidation products produced as well as the rate of the oxidation reaction. Janzen (1996) found an increase in the oxidation rate constant of pyrrhotite corresponding with an increase in pH, suggesting that the oxidation reaction takes place more rapidly in alkaline conditions. Spira and Rosenblum (1974) in their study on pyrrhotite also noted an increase in oxygen demand with increasing pH. Although Chirita *et al.* (2008) investigated the oxidation of troilite and not pyrrhotite, they similarly found an increase in the rate constant of the oxidation reaction when the experiment was performed at a higher pH. In contrast, Hamilton and Woods (1981) showed that the oxidation reaction was retarded at alkaline pH, most likely due to the passivation of the surface layer. The formation of the insoluble ferric hydroxide species is also favoured in alkaline conditions (Hamilton and Woods, 1984).

*Temperature*

Steger (1982) examined the oxidation of pyrrhotite under a variety of temperatures ranging from $28^0$C to $50^0$C and showed a corresponding increase in the amount of ferrous iron and sulfate produced with increasing temperature. Based on a model from the Arrhenius equation, Janzen (1996) also found an increase in the oxidation rate of pyrrhotite by 3-5 times for a $20^0$

temperature increase with oxygen as the oxidant and an increase by 2-11 times for a $30^0$ temperature increase with ferric iron as the oxidant. Similarly, for an increase in temperature from 25 to $40^0$C, both the monoclinic and "hexagonal" pyrrhotite examined in the oxidation dissolution study of Lehmann *et al.* (2000) showed a four fold increase in the rate constant.

*Crystal Structure*

In general, accounts in the literature relating pyrrhotite crystal structure to oxidation or its relative reactivity tend to show little agreement although more frequently suggest that magnetic monoclinic pyrrhotite is the more reactive phase. Janzen (1996) summarised the relevant literature as follows; that Vanyukov and Razumovskaya (1979; In Russian) suggested that the more sulfur rich phase (monoclinic pyrrhotite relative to troilite) had a higher oxidation rate. According to Janzen (1996), Yakhontova *et al.* (1983; In Russian) suggested that the greater amount of vacancies in monoclinic relative to "hexagonal" pyrrhotite allowed for easier electron transfer facilitating the oxidation reaction. In contrast, the study of Orlova *et al.* (1988; In Russian) suggested that "hexagonal" pyrrhotite was more easily oxidised than monoclinic pyrrhotite due to its lower activation energy. In the study of Janzen (1996) itself, no correlation between pyrrhotite crystal structure and oxidation rate was established. The study of Spira and Rosenblum (1974) that investigated the oxygen demand of various pyrrhotite ores, showed an increased oxygen demand for non-magnetic Noranda pyrrhotite relative to magnetic pyrrhotite. However, it was noted by Spira and Rosenblum (1974) that the non-magnetic pyrrhotite sample was probably troilite. More recently, Lehmann *et al.* (2000) determined larger rate constants for the oxidation of monoclinic relative to "hexagonal" pyrrhotite. The associated activation energy for the oxidation reaction was also lower for monoclinic pyrrhotite relative to "hexagonal" pyrrhotite (Lehmann *et al.*, 2000). Comparison of the amount of dissolved and EDTA extractable nickel, iron and sulfur ions from a pyrrhotite mineral slurry by Gerson and Jasieniak (2008) showed that the concentration of these species associated with the oxidation reaction was greater for monoclinic pyrrhotite relative to "hexagonal" pyrrhotite. This suggests that the monoclinic phase underwent more extensive oxidation than "hexagonal" pyrrhotite.

*Trace Element Content*

Similarly to the role of crystal structure and its effect on pyrrhotite oxidation, the effect of trace metal content on pyrrhotite oxidation is unclear. Kwong (1993) found a semi-quantitative correlation between trace metal content and oxidation rate for monoclinic

pyrrhotite. In his study, samples enriched in nickel and cobalt tended to oxidise slightly slower. When elements to the right of iron on the periodic table (Co, Ni) substitute for iron, they are likely to cause a positive effective charge because of donor defects (Janzen, 1996). The implication of a positive effective charge within the vicinity of nickel substitution sites would be to retard the movement of electrons, thereby inhibiting the oxidation process. In the study of Janzen (1996), no correlation between oxidation rate and trace metal content was found. However, it should be noted that Janzen (1996) compared a variety of pyrrhotite samples from different locations, of which only a quarter of the samples examined were associated with pentlandite which is the focus of this study.

Although the presence of dissolved oxygen in the pyrrhotite structure and its effect on pyrrhotite reactivity have not previously been rigorously evaluated, this does not negate that it may be of importance in influencing pyrrhotite oxidation. Magnetite has been described as an important accessory phase present in some massive sulfide ores (e.g. Sudbury; Naldrett and Kullerud, 1967). This is indicative of the presence of oxygen during the formation and cooling of the MSS. The relationship between iron, sulfur and oxygen during cooling and crystallisation of silicate melts, has in the past been extensively investigated (e.g. Kullerud, 1957; Naldrett, 1969; Shima and Naldrett, 1975). In addition to the relationship between pyrrhotite and magnetite, oxygen can also occur within the pyrrhotite structure. Graham and Mc Kenzie (1987) successfully detected oxygen in the pyrrhotite crystal structure using neutron microprobe techniques to a level of ~ 0.05 wt%. According to Graham *et al.* (1987), the magnetic properties of monoclinic pyrrhotite derived from different sources may be quite variable due to the relative degree of magnetite association, degree of oxidation and also presence of chemical impurities. Therefore the possibility exists, that the presence of oxygen in pyrrhotite may influence its reactivity.

*Galvanic Effects*

Due to the conductive or semi-conductive nature of the sulfide minerals, they can facilitate electron transfer when they come into contact with one another in a mineral slurry or solution (Ekmekci and Demirel, 1997). Under these circumstances, the mineral with the higher rest potential causes the cathodic reduction of oxygen at the mineral surface, whereas the mineral with the lower rest potential acts as the anode and is oxidised through a reaction such as that illustrated in figure 2.16. According to Rand (1977) the relative rest potentials of the sulfide

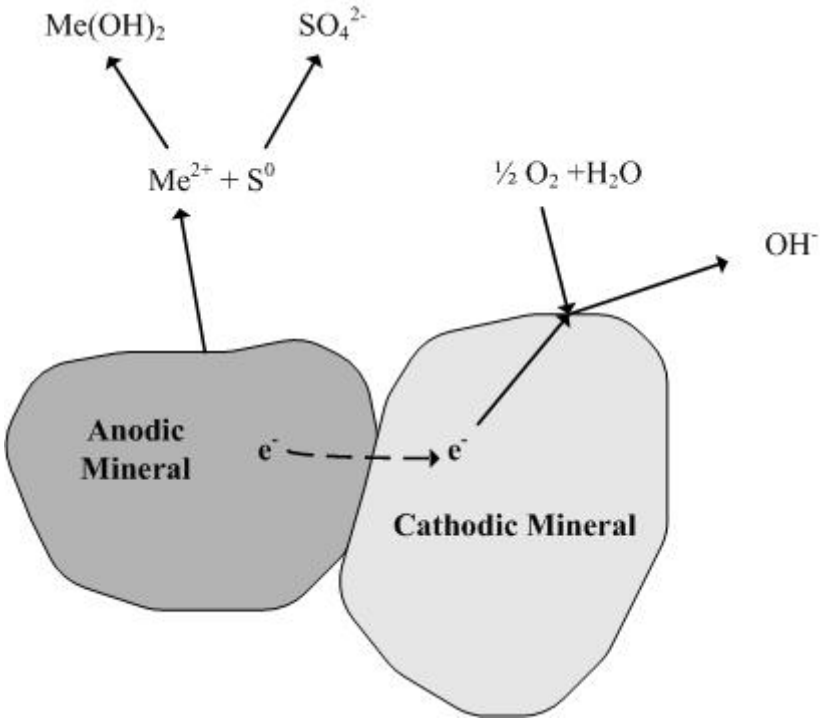


**Figure 2.16:** Schematic of the galvanic interaction between pyrrhotite (anode) and a more noble sulfide mineral such as pyrite or pentlandite (cathode). Adapted from: Ekmekci (2008).

minerals can be ranked as follows:

Pyrite > Pentlandite > Chalcopyrite > Arsenopyrite > Pyrrhotite > Galena

For pyrrhotite in nickel and platinum group element ore deposits, pentlandite is the more noble mineral with the higher rest potential and likely accelerates the oxidation of pyrrhotite. Pyrite may also occur in this mineral system and would have an even more severe effect on pyrrhotite due to its very noble character. Studies examining the galvanic interaction between pentlandite and pyrrhotite have tended to focus on how this interaction affects the adsorption of flotation reagents and its implications on flotation performance and not on pyrrhotite oxidation (e.g. Bozkurt *et al.*, 1998; Khan and Kelebek, 2004).

### 2.3.3 Electrochemical measurements of pyrrhotite

*Measurement of electrochemical reactions*

The measurement of pyrrhotite electrochemical reactions can be divided into two categories, based upon whether the measurement is taken using standard chemical probes (e.g. Dissolved oxygen, pH or ORP) or with the use of a working electrode. Measurements using standard probes are usually taken in mineral slurries or flotation cells, such as the measurement of the ORP or oxygen demand (e.g. Ekmekci et *al.*, 2003). The Magotteaux mill is one such device that not only allows for this type of measurement, but also allows one the ability to control the pulp chemistry (Greet *et al.*, 2004). Various authors such as Johnson and Munro (2008), Greet and Brown (2000) and Spira and Rosenblum (1974) have described the importance of quantifying the oxygen demand of different ore types with respect to their flotation performance. In the past, a variety of methodologies have been developed in order to do this, based upon the original method described by Spira and Rosenblum (1974). In general, a freshly ground mineral slurry is purged with air or oxygen and the decay of oxygen with time is measured and quantified (Spira and Rosenblum, 1974; Greet and Brown, 2000; S.H. He *et al.*, 2008). The methodology used to quantify oxygen uptake in this study is based upon that developed by Afrox (Afrox, 2008) and is described in more detail in Section 3.4.

Alternatively, electrochemical reactions can be measured with the use of a working electrode manufactured from pure mineral specimens. Measurements are made by either immersing the working electrode into a buffer solution or into a mineral slurry such as a flotation cell (e.g. Hamilton and Woods, 1981; Buswell and Nicol, 2002) in the presence of counter electrode (e.g. Pt) and a non-polarisable reference electrode (e.g. SHE, SCE or Ag/AgCl). Based on this experimental set up, a number of different electrochemical measurements can be made including rest potential, cyclic voltammetry, chronoamperometry and impedance spectroscopy. Further details of these measurement types can be found in Mendiratta (2000), Buswell and Nicol (2002) and Tao *et al.* (2003).

*Measurement of electrochemical reaction products*

In order to identify the reaction products on the pyrrhotite surface, a number of different measurements have been used. This includes in-situ XPS analysis where the binding energy of various ionic species (e.g. Fe *2p*) are measured and the peaks assigned to different bond types (e.g. $Fe^{2+}$-S, $Fe^{3+}$-S, $Fe^{3+}$-O). The use of ToF-SIMS allows the distribution of surface

species on particles to be examined with the use of in-situ chemical maps (e.g. distribution of $Fe(OH)^{+}$; Shackleton, 2003; Gerson and Jasieniak, 2008). Alternatively, spectroscopic studies including UV and FTIR techniques have been used to measure the reaction products of pyrrhotite with xanthate collectors (Fornasiero *et al.*, 1995; Bozkurt *et al.*, 1998). Lastly, one of the more popular techniques to measure electrochemical reaction products is EDTA dissolution. It is based on the ability of EDTA to dissolve soluble oxidation products which can be later analysed with standard chemical assay methods (Rumball and Richmond, 1996; Gerson and Jasienek, 2008).

## 2.4 Pyrrhotite Flotation

### 2.4.1 Principles of Flotation

Froth flotation is a physico-chemical process that harnesses the difference in surface properties using air bubbles in a flotation cell to separate valuable minerals from the gangue minerals in an ore. The theory of froth flotation has been extensively investigated and reviewed in the past (Sutherland and Wark, 1955; King, 1982; Wills and Napier-Munn, 2006) and so will not be expanded upon here. However, in order to manipulate the nature of the surface species of the valuable mineral (e.g. pyrrhotite with associated PGE and PGM, Merensky Reef) or gangue minerals (e.g. pyrrhotite in Ni ore, Sudbury) a variety of chemical reagents such as collectors, activators, depressants and modifiers are added. In general, the flotation system is affected by numerous parameters (Klimpel, 1984) including equipment (e.g. cell design, air flow), chemical (e.g. collector, activator, pH) and operational components (e.g. mineralogy, feed rate, particle size). In this study of pyrrhotite flotation, the focus is on pyrrhotite mineralogy and how it affects flotation performance. In order to do this, an understanding of the interaction of the pyrrhotite surface with chemical reagents is needed, with specific reference to xanthate collectors and copper activation.

### 2.4.2 Collectorless flotation of Pyrrhotite

In the past, there have been accounts of the collectorless, natural or self induced flotation of pyrrhotite (e.g. Heyes and Trahar, 1984; Hodgson and Agar, 1984). The mechanism by which this occurs has been heavily debated upon, although Heyes and Trahar (1984) suggested that pyrrhotite self flotation occurs through mild oxidation and the formation of elemental sulfur. Hodgson and Agar (1984) however, suggested that the formation of a stable $Fe(OH)S_2$ intermediate species renders pyrrhotite its hydrophobicity. Others have suggested that the formation of polysulfides and metal deficient sulfides as well as elemental sulfur from pyrrhotite oxidation may provide the necessary hydrophobicity to cause the natural flotation of pyrrhotite (Hamilton and Woods, 1981; Buckley and Woods, 1985; Legrand *et al.*, 2005a). General agreement however, exists that extensive oxidation of pyrrhotite is detrimental to its flotation performance due to the formation of the hydrophilic ferric hydroxide species through a reaction such as that given in equations III-V (e.g. Rao and Finch, 1991; Kelebek, 1993).

Since the solubility of the ferric hydroxide species is considerably lower at a higher pH, so it is observed that the natural floatability of pyrrhotite decreases with increasing pH. Miller *et al.* (2005) have similarly shown a decrease in the contact angle of pyrrhotite with increasing pH illustrating the increase in the hydrophilic character of pyrrhotite to more alkaline conditions.

### 2.4.3 Flotation with Xanthate Collectors

In most mineral processing operations, chemical reagents are added to enhance the hydrophobicity of the valuable minerals. Although there is a suite of thiol collectors available for use in flotation (Adkins and Pearse, 1992), only the xanthate group is used in this study. Some commonly occurring xanthates including sodium isobutyl xanthate (SIBX) and sodium normal propyl xanthate (SNPX) are illustrated in figure 2.17. The xanthate collectors occur in varying chain lengths, and it well-known that an increase in chain length is associated with a lower solubility product and hence increase in hydrophobicity (M.C. Fuerstenau, 1982). The trade off however, is that an increase in collector chain length is normally associated with a decrease in selectivity (e.g. Mbonambi, 2009).

Collector bonding to the sulfide mineral is generally accepted to be via an electrochemical reaction, where M is the metal, X is xanthate and $X_2$ is dixanthogen:

$$MS + X^- \rightarrow MX + S + e^- \qquad \text{(VIII)}$$

$$MS + 2X^- \rightarrow MX_2 + S + 2e^- \qquad \text{(IX)}$$

The metal xanthate may in turn be oxidised to the dixanthogen species (Equation IX) depending on the rest potential of the mineral relative to that of the xanthate oxidation reaction. Harris and Finkelstein (1977) showed differences in the rate of oxygen consumption of different chain length collectors due to differences in collector oxidation rate. FTIR and UV spectroscopic studies have suggested that dixanthogen tends to be the more commonly occurring collector species on pyrrhotite under standard oxidising conditions and is the species responsible for rendering pyrrhotite its hydrophobicity during flotation (Allison *et al.*, 1972; Fornasiero *et al.*, 1995; Bozkurt *et al.*, 1998). Fornasiero *et al.* (1995) showed that the

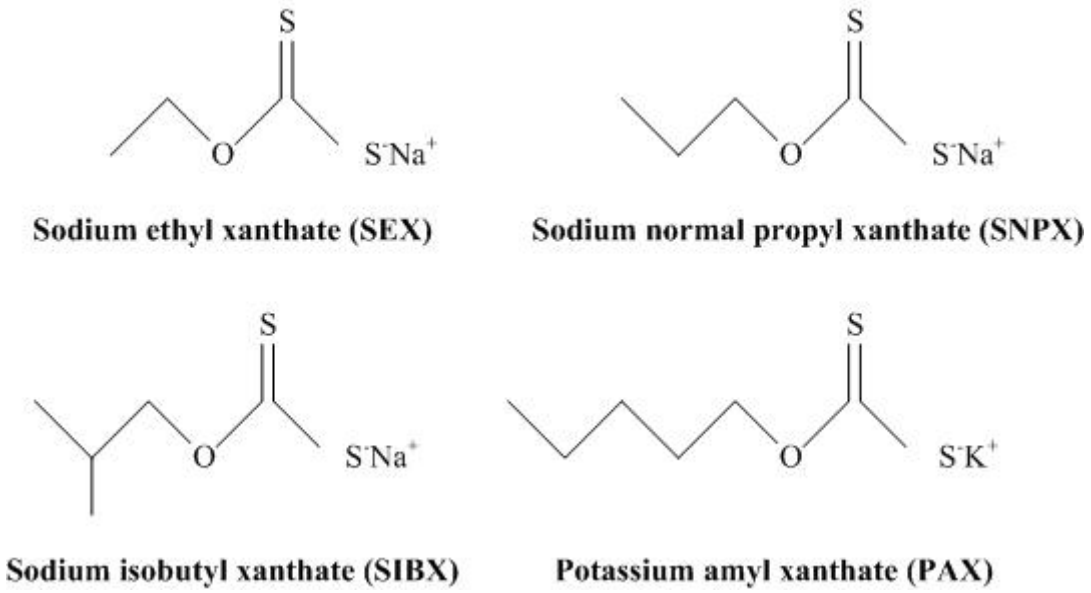


**Figure 2.17:** Structure of some commonly occurring xanthate collectors used in flotation, including SNPX and SIBX which are used in this study.

xanthate adsorption rate and consequent dixanthogen formation were dependent on pH, and decrease with an increase in pH of the mineral solution. The stability of the xanthate and dixanthogen species is also dependent on solution pH (M.C. Fuerstenau, 1982).

Leppinen (1990) showed some discrepancy when comparing flotation recovery with xanthate adsorption on pyrrhotite throughout the pH range. Even though the maximum xanthate adsorption was at pH 5.5, two peaks in pyrrhotite flotation recovery were observed. The first peak was at pH 3 and then a second minor peak at pH 8 was observed, even though xanthate adsorption was effectively at a minimum at pH 8. The majority of flotation studies however, show that pyrrhotite flotation in the presence of thiol collectors is poor at alkaline conditions and is progressively inhibited as the pH is increased (e.g. Rao and Finch, 1991; Kalahdoozan, 1996; M.F. He *et al.*, 2008). The reason for the reduction in pyrrhotite flotation with increasing pH is described by the Barsky relationship where $[X^-]/[OH^-] = K$ (Kelebek *et al.*, 2007) in that the presence of excess hydroxide anions in solution interferes with xanthate adsorption.

It is known that some degree of oxidation is necessary for both the collectorless and the collector induced flotation of pyrrhotite (Heyes and Trahar, 1984; Kelebek *et al.*, 2007). For collector induced flotation, the presence of oxygen is required for the oxidation of xanthate to

dixanthogen, which is the collector species that renders pyrrhotite its hydrophobicity. The presence of additional minerals to the pyrrhotite system can however, interfere with xanthate adsorption. Bozkurt *et al.* (1998) measured open circuit potentials for both pyrrhotite and pentlandite as single mineral systems and found pentlandite to have a higher potential than pyrrhotite (~100 versus ~ 60 mV SCE, respectively). In the presence of xanthate however, the potentials were reversed and the equilibrium potential of pentlandite was considerably lower than before (-55 mV SCE), whereas for pyrrhotite it was only slightly reduced (40 mV SCE). These results were interpreted by Bozkurt *et al.* (1998) to suggest the establishment of a galvanic interaction, characterised by the anodic oxidation of xanthate on pentlandite and the cathodic reduction of oxygen on pyrrhotite. Consequently, pyrrhotite flotation would suffer due to the enhanced floatability of pentlandite.

S.H. He *et al.* (2008) also considered the effect of a galvanic interaction when trying to account for the differences in pyrrhotite and pentlandite flotation between the scavenger cleaner feed (non-magnetic) and magnetic pyrrhotite concentrate streams treating Sudbury ore at the Clarabelle Mill. One of the mechanisms proposed for the enhanced recovery of pentlandite in the magnetic concentrate stream was the greater abundance of pyrrhotite in the magnetic concentrate stream (59.8 %) relative to the scavenger cleaner feed (25.6 %). If preferential oxidation of pyrrhotite occurred, then oxidation of pentlandite and the consequent reduction in pentlandite floatability would have been prevented.

Pyrite is also more noble than pyrrhotite (Rand, 1977) and it would be anticipated that the preferential oxidation of pyrrhotite and reduction in its floatability would occur relative to pyrite, similarly to the reaction between pentlandite and pyrrhotite as described by S.H. He *et al.* (2008). However, the study of Nakazawa and Iwasaki (1995) showed an enhancement in pyrrhotite flotation recovery when in contact with pyrite.

An additional variable responsible for causing galvanic interactions with pyrrhotite during flotation is that of the grinding media in milling, whether it is mild steel, high chromium steel or ceramic media. In general, steel grinding media have lower rest potentials than pyrrhotite and are oxidised during grinding thus preventing the oxidation of the sulfide minerals themselves. Adam and Iwasaki (1984) observed a reduction in pyrrhotite flotation according to whether the ore was prepared using stainless steel, mild steel, zinc or magnesium grinding media. They suggested that passivation of the pyrrhotite surface occurred by the formation a

ferric hydroxide surface layer due to the disassociation and release of ferrous iron from pyrrhotite. Kirjavinen *et al.* (2002) however, argued that the iron particles adhered to the sulfides were derived from the grinding media. The presence of these particles resulted in poor xanthate adsorption and sulfide flotation but only for the first few minutes of flotation. Once relaxation took place, pentlandite and pyrrhotite experienced some mild oxidation and the floatability was restored. An improvement in pentlandite and pyrrhotite flotation was also observed following grinding in ceramic media relative to steel media (Kirjavinen *et al.*, 2002).

Kirjavinen *et al.* (2002) further investigated the effect of ions derived from the process water on pyrrhotite flotation. The presence of both $Ca^{2+}$ and $S_2O_3^{2-}$ ions served to improve pyrrhotite floatability although not to the same extent as pentlandite. Hodgson and Agar (1989) also investigated the effect of ions in the process water on pyrrhotite flotation and concluded that the presence of $Ca^{2+}$ increased the required dosage of xanthate to cause hydrophobicity due to the competitive adsorption of $Ca^{2+}$ for xanthate with the mineral surface. In the study of Rao and Finch (1991) on xanthate adsorption, it was observed that the presence of $Ca^{2+}$ ions was only beneficial to pyrrhotite recovery at pH 8.4 with nitrogen as the flotation gas. For the other conditions tested (air, pH 6), negligible difference in pyrrhotite recovery was obtained for tests with and without the presence of $Ca^{2+}$ ions. Rao and Finch (1991) suggested that under these conditions (pH 8.4, $N_2$, 300 ppm $Ca^{2+}$), the formation of $Ca(OH)^+$ as a surface species would have helped to enhance xanthate adsorption.

The results comparing magnetic and non-magnetic pyrrhotite flotation performance in the presence of xanthate collectors tend to have been quite mixed. According to Iwasaki (1988), it was noted by Harada (1967; In Japanese) that samples of freshly ground monoclinic pyrrhotite were more floatable than “hexagonal” pyrrhotite although the reverse occurred on more oxidised samples. Kalahdoozan (1996) compared the flotation response of synthetic monoclinic, natural monoclinic (magnetic) and synthetic “hexagonal” (non-magnetic) pyrrhotite at a variety of different conditions. The flotation results obtained by Kalahdoozan (1996) were consistent with the results of the adsorption studies. Both sets of results showed synthetic monoclinic pyrrhotite was more floatable at a pH between 7 and 8.5, whereas synthetic “hexagonal” pyrrhotite was more floatable at a pH greater than 10. The natural monoclinic pyrrhotite sample was however, the most floatable for the entire pH range tested. In this study there was no comparison with a natural “hexagonal” pyrrhotite sample, and all

microflotation tests were performed with nitrogen as the flotation gas and may therefore not be entirely representative of the processing of a real ore.

More recently, M.F. He *et al.* (2008) examined the effect of crystallography on pyrrhotite flotation although the focus was on pyrrhotite derived from the Mengzi lead zinc ore in China. Using monoclinic and "hexagonal" pyrrhotite derived from this ore, the flotation performance of pyrrhotite was compared with sodium butyl xanthate, sodium diethyl dithiocarbamate and butyl dithiophosphate. For both pyrrhotite types examined, the maximum flotation recovery was obtained at ~ pH 7. For the pH range tested (4-13), monoclinic pyrrhotite was more floatable than "hexagonal" pyrrhotite.

It does not appear that the role of trace metal content has been investigated with respect to pyrrhotite flotation performance, although Chanturia *et al.* (2004) examined the difference in flotation response of nickel rich, cobalt rich and iron rich pentlandite. Since pyrrhotite and pentlandite are both monosulfides containing similar elements, a comparison can be made. Nickel rich pentlandite exhibited the best flotation performance followed by cobalt rich pentlandite, whereas iron rich pentlandite was the least floatable. Chanturia *et al.* (2004) suggested that differences in the open circuit potential resulting in the preferential formation of hydrophobic elemental sulfur species or preferential xanthate adsorption on the nickel rich pyrrhotite could be responsible for the differences observed in flotation performance.

### 2.4.4 Activation of Pyrrhotite

In order to improve the efficiency of the adsorption of thiol collectors to sulfide minerals during flotation, an activator is used. Activators typically include metal cations such as copper, lead, silver, cadmium, mercury, nickel and iron, although activation with copper appears to have been the most widely studied and reviewed (D.W. Fuerstenau, 1982; Finkelstein, 1997; Chandra and Gerson, 2009). These studies have tended to focus on the classical activation mechanism, shown here for sphalerite as follows:

$$Cu^{2+} + ZnS \rightarrow CuS + Zn^{2+} \qquad (X)$$

The reaction has been argued to take place by a direct ion exchange mechanism of cupric copper for $Zn^{2+}$ followed by the rapid reduction of cupric copper to cuprous copper and the formation of a hydrophobic CuS or covellite like surface. With the subsequent addition of xanthate collector, a hydrophobic copper-xanthate species is likely to form. Copper activation is heavily influenced by the pH of the solution due to the solubility of the different copper species. At alkaline pH, the copper added to the system may precipitate as a hydrophilic copper hydroxide type species which can potentially react with the collector causing inadvertent activation of gangue minerals (e.g. Nagaraj and Brinen, 1996; Malysiak *et al.*, 2002).

Early studies of the copper activation mechanism for pyrrhotite suggested one similar to sphalerite (Nicol, 1984), although more recently it has been proposed that the copper activation of pyrrhotite is not through direct ion exchange but rather an ion adsorption mechanism similar to that for pyrite (Gerson and Jasieniak, 2008). Using ARXPS, SIMS and chemical analysis, Weisener and Gerson (2000) suggested that pyrite activation occurs through direct adsorption of cupric copper onto the pyrite surface followed by in-situ reduction of cupric copper to cuprous copper. At no point during the reaction do the copper ions migrate into the bulk of the pyrite, but they rather remain as a monolayer on the pyrite surface. Following the reduction of cupric copper, an overlayer of $Cu(OH)_2$ formed when the reaction occurred at alkaline conditions. Similarly, Gerson and Jasieniak (2008), demonstrated an ion adsorption mechanism for pyrrhotite activation. They showed the presence of both cuprous and cupric ions on the pyrrhotite surface and that the $Cu^{1+}$ / $Cu^{2+}$ ratio showed a progressive decrease with increasing oxidation of the pyrrhotite.

Since the majority of mineral processing operations operate within an alkaline pH, the activation of pyrrhotite by copper during flotation at these conditions is of key interest. In the study of Nicol (1984), copper activation only served to improve pyrrhotite flotation recovery at pH 5, whereas at pH 8, there was no improvement in pyrrhotite floatability. Similarly, Miller *et al.* (2005) showed no difference in pyrrhotite contact angle at alkaline conditions with or without copper activation. However, numerous other authors including Leppinen, (1990), Senior *et al.* (1995), Kalahdoozan (1996) and Wiese *et al.* (2007) have shown an improvement in pyrrhotite floatability with copper activation conditions at alkaline pH. Leppinen (1990) showed that the maximum pyrrhotite recovery was obtained at pH 8, even though the accompanying adsorption tests showed very low xanthate adsorption at this pH.

The discrepancy in these results relating to copper activation may be related to the nature of the pyrrhotite sample in terms of its degree of oxidation or crystallography. In the work of Wiese *et al.* (2005) which compared the flotation performance of pyrrhotite from different mines of the Merensky Reef, it was shown that the effect of copper activation was quite different between the ores. For one of the ores, the addition of copper caused relatively little improvement in pyrrhotite recovery whereas for the other ore, there was 50 % improvement in pyrrhotite recovery with copper activation.

In the study of Kalahdoozan (1996) that compared the flotation and adsorption characteristics of monoclinic and "hexagonal" pyrrhotite, all samples examined at pH 10 showed some improvement in floatability with copper activation. At this pH, the natural monoclinic pyrrhotite sample was the most floatable whereas the synthetic monoclinic pyrrhotite sample examined was the most sensitive to changes in collector concentration. More recently, M.F. He *et al.* (2008) examined the flotation response of monoclinic and "hexagonal" pyrrhotites for a variety of thiol collectors at different pH conditions with and without copper activation. Their results showed that the monoclinic pyrrhotite was more sensitive to copper addition than "hexagonal" pyrrhotite.

Although Gerson and Jasieniak (2008) did not evaluate the flotation response of pyrrhotite subsequent to copper activation, their study compared the effect of surface oxidation on both monoclinic and "hexagonal" pyrrhotite at pH 9. The ToF-SIMS analyses in their study showed that with increasing the conditioning time during sample preparation, there was an associated increase in the degree of oxidation on the pyrrhotite surface. Monoclinic pyrrhotite was shown to be more severely oxidised than "hexagonal" pyrrhotite under the conditions studied. It was also shown that oxidation of the mineral surface prior to copper activation could prove to be detrimental for subsequent copper activation. Following the copper activation of pyrrhotite, the mineral surface was stabilised and less likely to be prone to further oxidation.

In addition to copper causing activation of pyrrhotite, Yoon *et al.* (1995) as well as Xu and Wilson (2000) attributed the flotation of pyrrhotite and decrease in pyrrhotite – pentlandite selectivity at the Clarabelle Mill in Sudbury to the inadvertent activation by nickel ions. Yoon *et al.* (1995) detected both nickel and copper ions on the surface of pyrrhotite using LIMS. Xu and Wilson (2000) showed a change in the concentration of nickel ions in the process water

between seasons corresponding to differences in element solubility with temperature change. Increased nickel contents during winter were argued to cause inadvertent flotation of pyrrhotite and the resultant decrease in flotation selectivity.

### 2.4.5 Pyrrhotite Rejection

In the past there have been numerous strategies which have been investigated in laboratory scale tests for the rejection of pyrrhotite in order to cause selective flotation of pentlandite over pyrrhotite in nickel processing operations (Wells *et al.*, 1997). These strategies include:

(i) Pyrrhotite rejection with magnetic separation
(ii) Pyrrhotite depression with oxygen in flotation
(iii) Pyrrhotite depression with nitrogen in flotation
(iv) Pyrrhotite depression with cyanide in flotation
(v) Pyrrhotite depression with chelating agents in flotation
(vi) Pyrrhotite depression with polymeric depressants in flotation

Although not all of these strategies have been implemented in plant scale processing operations, each of these strategies will in turn be briefly discussed, since some of them will likely influence the flotation behaviour of pyrrhotite.

*Pyrrhotite rejection by magnetic separation*

One of the first measures that was implemented by the Sudbury nickel processing operations following their policy decision to reject pyrrhotite was the incorporation of a magnetic circuit (Wells *et al.*, 1997). By installing drum magnetic separators, the magnetic monoclinic pyrrhotite could be separated from the bulk ore and then processed separately as illustrated by the flow sheet shown in figure 2.18 of the Clarabelle Mill in Sudbury. The advantage of this mechanism is that it allows the operation to produce both a high sulfur (magnetic pyrrhotite) and low sulfur (silicate mineral) tails which can be disposed of appropriately (Lawson *et al.*, 2005). Within the magnetic separation circuit however, selectivity between pentlandite and pyrrhotite in flotation still needs to be maintained and therefore additional measures for pyrrhotite depression are needed.

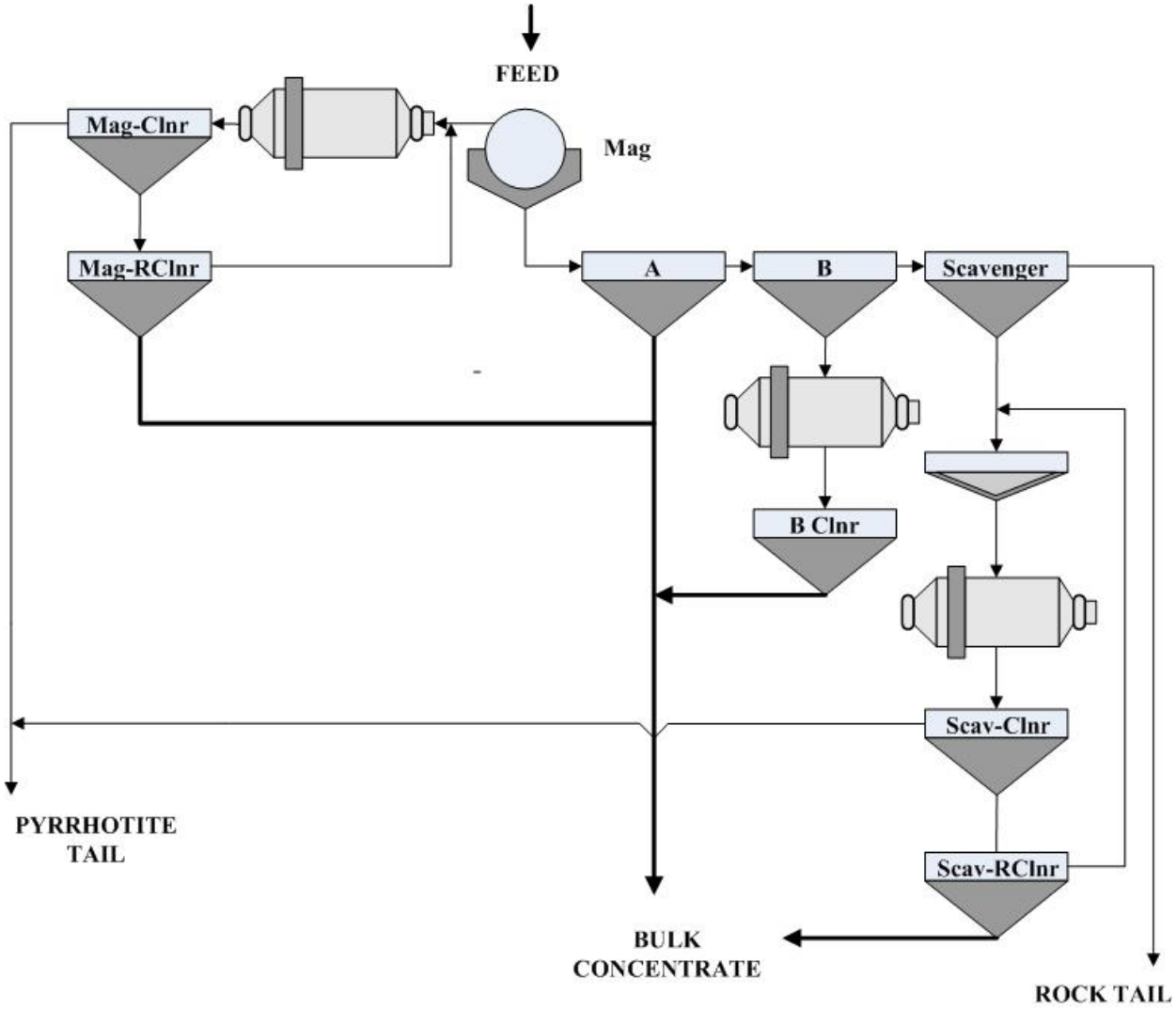


**Figure 2.18:** Flow sheet of the Clarabelle Mill in Sudbury, Canada, which incorporates both magnetic and non-magnetic circuits, where pyrrhotite rejection is targeted. Adapted from: Lawson *et al*. (2005).

*Oxygen depression in flotation*

Literature related to the use of oxygen as a pyrrhotite depressant shows contradictory results and this may possibly be resolved by understanding the degree of oxidation. Kelebek (1993) suggested that mild oxidation of pyrrhotite promoted the amount of surface sites available for xanthate adsorption, the production of elemental sulfur and the oxidation of xanthate to dixanthogen. This would account for the good flotation response of pyrrhotite in the stockpiled sulfide ore examined by Kelebek *et al.* (2007). It was suggested that during the stock piling, the pyrrhotite experienced some degree of mild oxidation. However, after extensive oxidation or aeration, the formation of the hydrophilic ferric hydroxides was promoted resulting in the depression of pyrrhotite during flotation. Kelebek (1993) showed a

consistent decrease in pyrrhotite recovery in batch flotation tests with increasing oxidation time of the pyrrhotite prior to flotation.

*Nitrogen depression in flotation*

The use of nitrogen for potential control during flotation as a means for pyrrhotite depression was investigated by Khan and Kelebek (2004). In the electrochemical study of Khan and Kelebek (2004), a comparison was made of the rest potentials of pyrrhotite and pentlandite with that of the potential for the xanthate to dixanthogen transformation under oxygenated and deoxygenated conditions. On the basis that the formation of dixanthogen was essential for pyrrhotite flotation but not pentlandite flotation, a strategy was proposed. By controlling the potential of the flotation system to avoid the oxidation of xanthate to dixanthogen, the flotation of pyrrhotite would be inhibited and so selective pentlandite flotation was likely (Cheng *et al.*, 1994; Khan and Kelebek, 2004).

*Cyanide depression in flotation*

Kalahdoozan (1996) investigated the use of sodium cyanide as a pyrrhotite depressant at alkaline pH. The exact mechanism by which cyanide causes pyrrhotite depression is unclear, although numerous suggestions including the formation of metal cyanide complexes and the decomposition of adsorbed dixanthogen have been proposed (Prestidge *et al.*, 1993). Although the use of cyanide as a depressant showed promise in laboratory scale test work (Kalahdoozan, 1996), it has not been implemented on industrial processing operations due to the associated environmental concerns with the handling and treatment of this hazardous chemical (Wells *et al.*, 1997).

*Depression with amines*

The current methodology used for pyrrhotite depression in the Sudbury ores is with the use of the chelating agents, DETA or TETA in conjunction with sodium metabisulfite (Lawson *et al.*, 2005). Kelebek and Tukel (1999) showed that use of TETA alone or use of sodium metabisulfite by itself showed little depressing effect on pyrrhotite, but when the two reagents were used in conjunction with one another, effective pyrrhotite depression was achieved. LIMS analysis in the study of Yoon *et al.* (1995), showed both nickel and copper ions on the pyrrhotite surface in the flotation concentrate that were most likely derived from the process water and which inadvertently activated the pyrrhotite. It has been argued that both DETA and TETA are able to form stable complexes or chelates with these heavy metal ions that

prevent the inadvertent activation of pyrrhotite (Kelebek *et al.*, 2005). The addition of sulfite in conjunction with TETA has been proposed to assist in maintaining low redox potentials and thereby inhibit the formation of hydrophobic sulfur species (Kelebek *et al.*, 2005).

*Depression with polymeric depressants in flotation*

For some of the platinum deposits in South Africa, there is no association of pyrrhotite with the platinum group minerals and only the pentlandite and chalcopyrite are of interest. In the flotation of these ores, polymeric depressants are used to reduce the floatable silicate gangue minerals such as talc (Wiese *et al.*, 2005). In order to investigate whether these same polymeric depressants could perform an additional role in promoting the selective flotation of pentlandite, Mbonambi (2009) conducted microflotation tests on pentlandite and pyrrhotite. Mbonambi (2009) showed that the combination of a guar depressant with SNPX at high pH could cause some depression of pyrrhotite for selective pentlandite flotation.

### 2.4.6 Comparison of plant operating strategies for pyrrhotite flotation and rejection

In flotation operations where pyrrhotite recovery is targeted for its association with the platinum group minerals and elements, pyrrhotite is recovered through a bulk sulfide float (e.g. Merensky Reef). These operations generally use an MF2 (mill-float, mill-float) circuit configuration comprising fine grinding in the regrind stage to optimise the liberation of the fine grained platinum group minerals. Thiol collectors are normally used to recover the sulfides chalcopyrite, pentlandite and pyrrhotite. Copper sulfate is used as an activator to enhance the recovery of the slower floating pyrrhotite in some operations (Miller *et al.*, 2005; Vos, 2006). Polymeric depressants such as carboxymethylcellulose (CMC) or guar gum are also used to depress the naturally floating gangue minerals present in the ore and bulk flotation occurs at the natural pH of the ore, which is ~ 9 (Wiese *et al.*, 2005).

Following the move in the early 1980's to target pyrrhotite rejection due to high sulfur dioxide emissions in the smelters treating Sudbury ores and its detrimental effect on the environment, these operations have had to implement numerous steps to optimise pyrrhotite rejection while still maintaining selectivity between pyrrhotite and pentlandite (Pietrobon and Grano, 2001). These Sudbury operations now use two circuits as illustrated in figure 2.18; a magnetic circuit for treating magnetic monoclinic pyrrhotite and non-magnetic circuit for

treating "hexagonal" pyrrhotite, pentlandite and chalcopyrite (Wells *et al.*, 1997; Lawson *et al.*, 2005). In order to maintain selectivity between pentlandite and pyrrhotite during flotation numerous reagent schemes have been tried and tested on these plants including the use of cyanide, nitrogen and oxygen (Wells *et al.*, 1997). The preferred reagent scheme which is currently used on these operations as pyrrhotite depressants are the amines DETA or TETA in conjunction with sodium sulfite (Lawson *et al.*, 2005). Flotation normally occurs around pH 9.2 for the Sudbury ore and progressively drops through the circuit down to ~ 8 (Kelebek *et al*., 2007). At Nkomati Nickel in South Africa, a proprietary depressant comprised of a modified polyacrylamide blend of sulfite and sulfate is used as their preferred pyrrhotite depressant.

## 2.5 Process Mineralogy

Process Mineralogy, a subdivision of the field of geometallurgy (Hoal, 2008; Walters, 2008), is the application of mineralogy to the mineral processing industry (Petruk, 2000). The earliest accounts of process mineralogy in practice extend back to Irving (1906), Gaudin (1939) and Stillwell and Edwards (1945). Consequently, it has been reviewed several times in the past e.g. Petruk (2000), Baum *et al*. (2006). Due to the comprehensive nature of the account of Henley (1983), this review will be focussed upon here. Henley (1983) described how mineralogy can be applied right through the fields of exploration and drilling, preliminary metallurgical testing, pilot plant testing, plant design and engineering, plant construction and commissioning as well as during plant operation. The ultimate goal is to develop a predictive model of mineral processing performance from the understanding of the variation of the mineralogy through the flow sheet. In order to achieve this goal, scientific knowledge and techniques are drawn from a number of disciplines including geology, mineralogy, mathematics, sampling statistics, physics, chemistry and engineering (Henley, 1983; Lotter *et al.*, 2002).

Henley (1983) illustrated the need for information on the identity of the minerals present in the ore sample, relative proportions of each phase, mineral composition, liberation characteristics of both valuable and gangue minerals as well as element deportment for the feed, concentrates and tail samples. A variety of analytical methods for determining mineral abundances (grain counting, point counting, gross counting, area counting, image analysis), mineral composition (optical methods, XRD, EMP and proportional dissolution) and mineral liberation (point counting, area counting, image analysis, density separation, and selective dissolution) were reviewed. More recently, the development of key analytical instruments such as QXRD with Rietveld refinement, x-ray computed tomography (X-ray CT), as well as the automated SEM instrumentation, QEMSCAN and MLA have to some degree, made the acquisition of mineralogical data considerably faster, more detailed and statistically representative (Raudsepp *et al.*, 2002; Gu, 2003; Fandrich *et al.*, 2007; Gottlieb, 2008). The focus of much of the literature on process mineralogy has been on the application of these techniques to mineral processing in the form of case studies, as well as use of this information to enhance the models that describe the breakage, liberation and separation processes (e.g. Wightman *et al.*, 2008). Several case studies on process mineralogy are reviewed below.

Several QEMSCAN based case studies have been published by Lotter and his co-workers such as Lotter *et al.* (2002), Baum *et al.* (2006) and Charland *et al.* (2006). The case study of Charland *et al.* (2006) however, is a key example that shows the integration of process mineralogy from plant design to commissioning for the Montcalm nickel copper concentrator in Ontario, Canada. During the prefeasibility and feasibility studies of the Montcalm ore, several geometallurgical end-members were defined by examination of drill core samples based on ore geology, microscopy and QEMSCAN analysis. Disseminated, net-textured and massive sulfide textures were defined as geometallurgical end members and the grinding and flotation characteristics of each of these end members determined. The recognition of potential problematic minerals; presence of pyrite in very variable amounts (effect on pH during flotation), presence of both granular and flame pentlandite (flame pentlandite likely to remain locked unless ultra fine grinding was used) as well as fine grained disseminated chalcopyrite were noted. These mineralogical factors were in turn taken into consideration during plant design. Subsequent bench mark surveys following plant start up were also described and the nature of the losses of locked pentlandite and chalcopyrite to the tails were evaluated by QEMSCAN. Based on the plant survey, it was recommended that some optimisation of the primary grinding circuit was needed to reduce the proportion of fines, a regrind stage was needed to liberate locked chalcopyrite and pentlandite, and further electrochemical control of the pulp chemistry was needed to optimise the rejection of pyrrhotite.

Bojcevski *et al.* (1998) similarly determined the metallurgical performance of different textural types of ore, but the study was focused on the division of the George Fisher lead zinc ore in Australia into a variety of meso and microtextures. The mesotextures identified varied between massive galena, massive sphalerite and galena, massive sphalerite, massive pyrite, banded galena and sphalerite, banded sphalerite and banded pyrite. The metallurgical characteristics in terms of ore feed grade, grindability, proportion of naturally floating material, mineral liberation and flotation were in turn assessed. Based on this information and that gained from the ore microtextures, textural modelling could be conducted so that the performance of any combination of ore types could be predicted. The benefits gained by such an approach during feasibility and production stages were in turn noted by Bojcevski *et al.* (1998). Bojcevski *et al.* (1998) also highlighted the need for interaction between geologists, mining engineers and metallurgists in order to improve overall operating performance.

On similar principles, Johnson and Munro (2008) presented guidelines on how to assign different domains of an ore body based on their metallurgical performance. Physical and chemical properties of the ore which needed to be taken into consideration included the identity of the valuable and gangue minerals, mineral grain size, associations and degree of liberation, and the flotation response as determined by a variety of tests. The oxygen demand, as well as the degree of oxidation of the slurry after grinding were noted as important parameters that also needed consideration, especially if the ore contained significant proportions of pyrrhotite or pyrite.

Process mineralogy has been of particular use to the platinum industry due to the large variation in mineralogy, very low grade of the ores and the ease with which the automated SEM instrumentation (QEMSCAN, MLA) are able to locate the platinum group minerals based on their BSE intensity (Brown and Dinham, 2006; Fandrich *et al.*, 2007). Schouwstra *et al.* (2000) also showed the large variation in mineralogy in terms of the different proportion of platinum group alloys, arsenides, sulfides, tellurides present from one Merensky Reef mine to another. Similarly, the association of these platinum group minerals with the base metal sulfides, silicates and chromite was quite variable. Based on this specific type of information, improved understanding of the grinding, liberation and flotation response of these different platinum group minerals could be employed in order to optimise metallurgical performance (Schouwstra *et al.*, 2000; Nel *et al.*, 2005; Shackleton *et al.*, 2007). Although not focused on the platinum group minerals but rather on the base metal sulfides, Brough (2008) characterised the mineralogy of the Normal, Pothole (P2) and Transitional (NP2) Merensky Reef types. The influence of the geology and mineralogy (base metal sulfide grain size, mode of occurrence, liberation, association etc) on the metallurgical performance of the different ore types was shown. Brough (2008) showed that the plagioclase rich NP2 reef type had the best metallurgical performance in terms of potential mill throughput, base metal sulfide liberation, recovery and amount of floatable gangue.

Nel *et al.* (2005) also used process mineralogy in evaluating the effects of regrind circuit configuration, but with the focus on the expansion project of the UG2 circuit at the Impala Concentrator. Since lower platinum group mineral recovery was achieved than targeted, the project was carried out to examine the effect of a change from a closed to open circuit configuration. It was subsequently shown with the use of QEMSCAN that the change in regrind circuit configuration improved the liberation of the platinum group minerals in the

regrind product. Becker *et al.* (2008) also investigated platinum group mineral liberation in the UG2 ore, but with the focus on quantifying the influence of classification with the 3 product cyclone. It was demonstrated that the 3 product cyclone provided a more efficient means of classification of the dual density UG2 ore than conventional cyclones based on the composition and degree of liberation of the flotation feed as determined by MLA.

## 2.6 Critical Review of the Literature

### 2.6.1 Pyrrhotite Mineralogy

Although a significant body of research that was developed over the last 40 years has positively contributed towards the general understanding of the details of pyrrhotite mineralogy (e.g. Nakazawa and Morimoto, 1971; Francis and Craig, 1976; Kissin and Scott, 1982; Powell *et al.*, 2004; Fleet, 2006), the majority of the research has focused on the use of synthetic samples in order to understand pyrrhotite phase relations and determine pyrrhotite crystal structures. Synthetic samples were not only used for experimental phase relation studies due to the nature of the experiments, but also due to the lack of suitable natural pyrrhotite single crystals for structure determination. Similarly, although the compositional variation and nature of the mineral association between natural pyrrhotite samples from a variety of deposits have been examined in the past (e.g. Carpenter and Desborough, 1964; Arnold, 1967), this was based on the d-spacing method of Arnold and Reichen (1962) and not by direct measurement of the composition. In addition, little research has focused on understanding the compositional variation of pyrrhotite within any single ore deposit. Therefore, the application of the fundamental understanding and use of compositional and crystallographic information based on synthetic pyrrhotite are of limited relevance to process mineralogy where natural ores are focused upon.

### 2.6.2 Pyrrhotite Reactivity

There appears to be a good understanding of the electrochemistry of pyrrhotite in terms of oxidation reactions and the mechanism of oxidation based on the work of Rand (1977), Hamilton and Woods (1981), Pratt *et al.* (1994) and Mycroft *et al.* (1995) to name but a few researchers. However, the accounts with respect to the role of crystallography and trace element content on pyrrhotite oxidation are in conflict (e.g. Kwong, 1993; Janzen, 1996; Gerson and Jasieniak, 2008). Similarly, the presence of ferric iron in the pyrrhotite structure is debatable (Pratt *et al.*, 1994; Mikhlin and Tomashevich, 2005; Letard *et al.*, 2007), even though it may act as an oxidising agent during pyrrhotite oxidation and be a factor responsible for the variation in oxidation rates between pyrrhotite types. In general, little attention was paid to the mineralogy of the pyrrhotite samples upon which the experimental work was

performed and therefore comparison of the results from different studies is difficult. Studies comparing oxidation rates of magnetic and non-magnetic pyrrhotite have used pyrrhotite samples derived from many different localities (e.g. pyrrhotite from nickel copper ore deposits, lead zinc ore deposits or even synthetic pyrrhotite) without consideration that the provenance of pyrrhotite may influence its oxidation.

### 2.6.3 Pyrrhotite Flotation

A similar situation to pyrrhotite reactivity occurs with respect to the understanding of pyrrhotite flotation; a reasonable understanding exists with regard to the mechanism and species which lend pyrrhotite its floatability (e.g. Allison *et al.*, 1972; Heyes and Trahar, 1984; Hodgson and Agar, 1984; Buckley and Woods, 1985; Fornasiero *et al.*, 1995; Bozkurt *et al.*, 1998), but the accounts comparing the floatability of the different pyrrhotite types are in conflict (e.g. Kalahdoozan, 1996; M.F. He *et al.*, 2008). Since little attention was generally paid to the mineralogy of the pyrrhotite samples used in flotation tests, a comparison of the results from these different accounts is not easy. In addition, experimental work from these literature accounts was based on pyrrhotite samples derived from natural nickel copper ores, lead zinc ores and on synthetic pyrrhotite. The role of mineral chemistry (including trace metal substitution) and mineral association and its effect on flotation performance were not considered in these studies.

### 2.6.4 Approach of this Thesis

Sections 2.6.1 to 2.6.3 have shown the limitations in the existing literature on pyrrhotite mineralogy, reactivity and flotation performance whereas Section 2.5 has shown the value which process mineralogy can add to mineral processing based on a through understanding of the variation of the mineralogy of an ore. On this basis, a platform is set for the contribution of this piece of research on pyrrhotite flotation that aims to develop the relationship between pyrrhotite mineralogy and flotation performance.

A thorough characterisation of the mineralogy of pyrrhotite from natural nickel and platinum group element ore deposits will contribute to the fundamental understanding of pyrrhotite

mineralogy. The characterisation of natural pyrrhotite using modern analysis methods (e.g. EMP, QXRD, Automated SEM) will also be a notable advance for process mineralogy.

A suitably designed experimental program to explore pyrrhotite reactivity and flotation based on a set of naturally occurring pyrrhotite samples for which the mineralogy has been thoroughly characterised, will provide a unique data set with which to develop the relationship between pyrrhotite mineralogy and flotation. By focussing on naturally occurring pyrrhotite from a single type of ore deposit, additional mineralogical variables associated with ore deposit type that could create further confusion are constrained. Therefore, experimental information on pyrrhotite reactivity and flotation will be of the nature that is amenable to allow only the key mineralogical factors that influence pyrrhotite flotation to be identified.

By using an integrated approach towards the interpretation of pyrrhotite reactivity and flotation performance, an understanding of the mineralogical factors which affect pyrrhotite flotation performance will be gained. Based on this critical review of the literature, the key questions from Chapter 1 are presented again:

(i) Hoes does the mineral association, mineral chemistry and crystallography vary between magnetic and non-magnetic pyrrhotite?

(ii) How does ore deposit formation affect the mineralogy of pyrrhotite?

(iii) How does the reactivity of magnetic and non-magnetic pyrrhotite differ? Can these differences be accounted for in terms of the:
a) crystallography
b) mineral chemistry
c) mineral association of pyrrhotite?

(iv) How does the flotation performance of magnetic and non-magnetic pyrrhotite differ? Can these differences be accounted for in terms of the:
a) crystallography
b) mineral chemistry
c) mineral association of pyrrhotite?

# Chapter 3

# SAMPLING AND ANALYTICAL METHODS

---

## 3.1 Pyrrhotite sampling

Pyrrhotite samples have been sourced from a variety of magmatic sulfide deposits in order to satisfy several criteria. The first of which is that the pyrrhotite deposits are of some economic relevance either due to the presence of the nickel hosted in pentlandite or due to the presence of the platinum group elements and platinum group minerals in these ore deposits. It was also desirable to obtain pyrrhotite samples where solely magnetic, solely non-magnetic and mixtures of magnetic and non-magnetic pyrrhotite were present. The capability to produce high grade pyrrhotite samples for mineral reactivity and microflotation tests was also a criteria in the selection of pyrrhotite samples for study.

### 3.1.1 Merensky Reef

Pyrrhotite samples were sourced from the Merensky Reef located at Impala Platinum Mines, near Rustenburg, South Africa. Two samples were used, namely samples *IMP-1* as shown in figure 3.1 and sample *IMP-2*, both of which represented cross sections through the basal portions of the Merensky Reef.

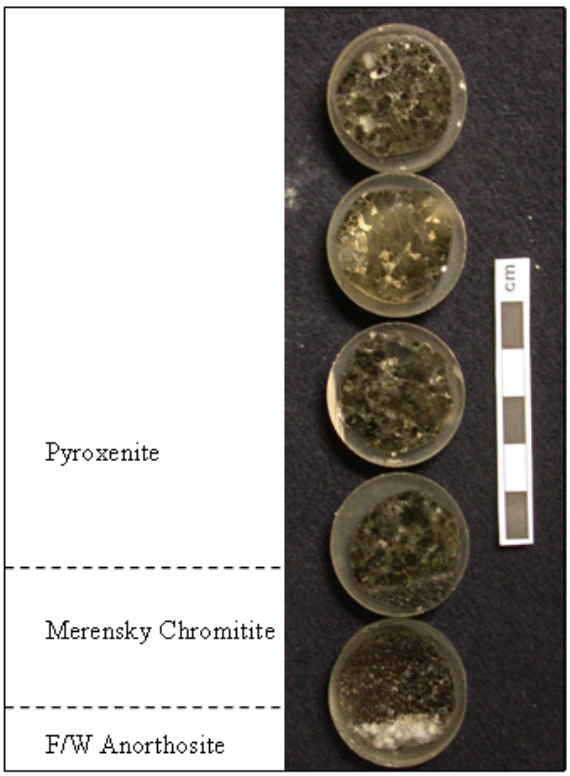


**Figure 3.1:** Photograph of the ore mounts from the Merensky Reef sample *IMP-1* used for pyrrhotite characterisation. F/W refers to the footwall.

### 3.1.2 Nkomati

Pyrrhotite samples were sourced from the Nkomati Nickel mine, Uitkomst Complex, near Barberton in South Africa from the massive sulfide body (MSB) and main mineralized zone (MMZ) of the mine by Nkomati personnel. Samples were extracted from the mine in January 2008 and the same sample batch was used for pyrrhotite characterisation, mineral reactivity and microflotation test work. Hand specimens of the samples used are shown in figure 3.2a, b.

### 3.1.3 Phoenix

Pyrrhotite samples were sourced from the Phoenix ore body at Tati Nickel mine near Francistown, Botswana. Massive sulfide samples occurring as veins in the host rock were accordingly hand picked from the Phoenix open pit. Samples were extracted from the mine in 2005 and the same sample batch was used for pyrrhotite characterisation, microflotation and


**Figure 3.2:** Photographs of the pyrrhotite samples used from (a) Nkomati MSB, (b) Nkomati MMZ (sample *MMZ-1*), (c) Phoenix, (d) Sudbury CCN, (e) Sudbury Gertrude and (f) Sudbury Gertrude West. The scale bars shown represent 5cm. Field of view for (d) and (e) is ~ 30cm. Photographs (d) and (e) courtesy of Vale INCO.

mineral reactivity test work. A photograph of a hand specimen representative of the Phoenix pyrrhotite used is shown in figure 3.2c.

### 3.1.4 Sudbury Copper Cliff North

Pyrrhotite samples were sourced from the Copper Cliff North mine, Sudbury Igneous Complex in Ontario, Canada by VALE Inco personnel from level 2400 of the 100 ore body at Copper Cliff North. Pyrrhotite from the 100 ore body is known to be unique in that it tends to be more than 90% non-magnetic whereas for the other ore bodies, the magnetic phase dominates (A. Kerr, Pers. Comm., 2007). Samples for pyrrhotite characterisation and microflotation tests were sourced from the mine in 2006 (Figure 3.2d), whereas the sample used for oxygen uptake tests was sourced from the mine in 2008. The sulfide grade for both samples was similar although the latter sample tended to be slightly more chalcopyrite rich.

### 3.1.5 Sudbury Gertrude and Gertrude West

Pyrrhotite samples for characterisation from the Gertrude mine, Sudbury Igneous Complex in Ontario, Canada were sourced by VALE Inco personnel from the Gertrude open pit mine in 2006. These samples were used for pyrrhotite characterisation and microflotation tests (Figure 3.2e). Since very poor recovery was obtained in microflotation tests for the original Gertrude pyrrhotite sample, a new sample was sourced in 2008 (Figure 3.2f). The new sample however, was derived from the Gertrude West ore body located 200 m west of the Gertrude mine. Initial mineral characterisation of the Gertrude West sample showed its mineralogical similarity to the original Gertrude sample in terms of petrography and mineral chemistry, and so the Gertrude West sample was then used in subsequent mineral reactivity and microflotation tests.

## 3.2 Mineralogical Characterisation

### 3.2.1 Optical Microscopy

Petrography of pyrrhotite samples was performed using a standard Zeiss petrographic microscope. Determination of magnetic and non-magnetic phases was performed with the use of a magnetic colloid (see associated photomicrographs in Section 4.2). The colloid was prepared by making a mixture of $FeCl_2$ and $FeCl_3$ particles to create an insoluble black magnetite precipitate which was stored in a soapy solution of sodium oleate as described by Craig and Vaughan (1981). Droplets of wet colloid were placed over the surface of the ore mount, the magnetic particles given a few seconds to interact with the pyrrhotite before the sample was viewed under the microscope and the image captured using a digital camera before the colloid dried on the sample. After use the colloid was wiped off the ore mount. Intergrowth textures and patterns highlighted by the colloid were observed to be the same for any particular sample when repeated immediately, or even several months later.

### 3.2.2 Powder X-ray Diffraction

Powder X-ray diffraction was used for the routine determination of mineralogy in ore samples on a Panalytical X'Pert Pro diffractometer with XCelerator detector housed at the University of Pretoria. Samples were run with automatic divergence slits using cobalt Kα radiation as the x-ray source. Samples were run from 5 to $90^0$ 2θ using a step size of $0.001^0$. Samples run in order to confirm the crystallography were prepared by hand picking pyrrhotite grains from a crushed sample and mounted on a low background plate. Samples prepared for phase quantification, were taken from the microfloat feed sample or oxygen uptake sample, and subsampled with a Fritsch rotary sample divider. These samples were further subsampled using a Quantachrome microriffler. The final aliquot was micronized in ethanol using a McCrone micronizer. Phase quantification was carried out using the BGMN Autoquan Rietveld refinement software.

Phase quantification with the Autoquan Rietveld software was used to determine the proportion of sulfides for both oxygen uptake and microflotation feed samples so that

**Table 3.1:** Summary table of the mineralogy of samples used in oxygen uptake and microflotation tests. The proportion of pyrrhotite (po), pentlandite (pent), chalcopyrite (ccp), pyrite (py) as well as the total amount of base metal sulfides (BMS) and other minerals (mostly silicates) is also given in wt % as determined by QXRD using the Autoquan software. The associated 2σ standard deviation of the Rietveld refinement is also shown. Samples used for MLA characterisation are also distinguished.

| **Sample Details** | **Phoenix** Mag Po | | **Nkomati** Mixed Po | | **Sudbury CCN** Non-mag Po | | **Sudbury Gertrude** Mag Po | | **Sudbury Gertrude West** Mag Po | |
|---|---|---|---|---|---|---|---|---|---|---|
| **Test** | $O_2$ | Float | $O_2$ | Float | $O_2$ | Float | $O_2$ | Float | $O_2$ | Float |
| **MLA** | X | - | X | X | - | X | - | - | X | X |
| **Po** | - | 88.6 | 85.9 | 85.9 | 62.1 | 68.7 | - | 63.0 | 86.8 | 86.8 |
| *2σ* | - | *(0.24)* | *(0.32)* | *(0.32)* | *(1.18)* | *(2.00)* | - | *(0.66)* | *(1.58)* | *(1.58)* |
| **Pent** | - | 11.3 | 6.27 | 6.27 | 6.12 | 6.88 | - | 5.48 | 9.53 | 9.53 |
| *2σ* | - | *(0.24)* | *(0.20)* | *(0.20)* | *(0.30)* | *(0.34)* | - | *(0.11)* | *(0.28)* | *(0.28)* |
| **Ccp** | - | 0.13 | - | - | 3.50 | - | - | - | - | - |
| *2σ* | - | *(0.13)* | - | - | *(0.16)* | - | - | - | - | - |
| **Pyrite** | - | - | - | - | - | - | - | 1.12 | - | - |
| *2σ* | - | - | - | - | - | - | - | *(0.13)* | - | - |
| **Other** | - | 0.00 | 6.86 | 6.86 | 28.3 | 11.4 | - | 30.4 | 4.77 | 4.77 |
| **BMS** | - | *100* | *92.2* | *92.2* | *71.7* | *75.6* | - | *69.6* | *96.3* | *96.3* |

collector and activator dosages could be accordingly calculated based on the total amount of base metal sulfides in the feed sample as shown in table 3.1.

### 3.2.3 Single Crystal X-ray Diffraction

Single crystal x-ray diffraction was used in order to determine unit cell dimensions of pyrrhotite crystals. Pyrrhotite single crystals from Sudbury CCN and the Impala Merensky (sample *IMP-1*) were measured on the diffractometer at the University of Pretoria whereas the Phoenix pyrrhotite sample was run on the diffractometer at the University of Cape Town. It was not possible to obtain single crystals suitable for x-ray diffraction for the remaining pyrrhotite localities.

The Phoenix pyrrhotite single crystal was mounted on a nylon loop suspended in oil and run on a Nonius Kappa CCD instrument at the University of Cape Town. The diffractometer was run at 50kV and 30mA for x-ray generation to produce monochromated molybdenum Kα

radiation with a graphite crystal monochromator. The analysis of pyrrhotite was performed at room temperature.

The Sudbury CCN and Impala Merensky (sample *IMP-1*) pyrrhotite single crystals were mounted on a glass fibre and run on a Siemens P4 diffractometer with Bruker SMART 1K CCD detector at the University of Pretoria. The diffractometer was run at 50kV and 30mA for X-ray generation to produce monochromated molybdenum Kα radiation with a graphite crystal monochromator. The analysis of pyrrhotite was performed at room temperature.

### 3.2.4 Electron Microprobe Analysis

Pyrrhotite compositions were analysed from several polished ore mounts derived from each locality on a Jeol JXA 8100 Superprobe housed at the Department of Geological Sciences, University of Cape Town. Pyrrhotite samples were analysed using an accelerating voltage of 25 kV and probe current of 20 nA. Iron and sulfur standardisation was performed on a meteoritic troilite standard from the Smithsonian Institution whereas nickel, copper and cobalt were calibrated against pure metal standards. Counting times for peak and background were 10 and 5 seconds, respectively. The relative instrument detection limits and standard deviations for measurements are given in table 3.2. A synthetic troilite specimen was also made by fusion of analytical grade iron and sulfur in an evacuated silica glass tube. The sample was placed in a furnace for 2 days at $400^0$C and then a further 2 days at $800^0$C prior to cooling, upon which the silica tube was manually fractured and the resulting troilite prepared into an ore mount for optical microscopy and microprobe calibration verification. The prepared ratio of Fe/S in the silica glass tube was such that the system was suitably iron saturated to ensure no non-stoichiometry or formation of pyrrhotite. This is reflected in the optical photomicrograph shown in figure 3.3 which displays zones of native iron indicating the reducing environment during troilite formation. The measured atomic iron / sulfur ratio of the synthetic troilite was 0.996 ± 0.01 (2σ) ensuring that the calibration procedure of the electron microprobe (EMP) based on the meteoritic troilite was suitable. The complete pyrrhotite mineral chemistry dataset is given in Appendix A1.

**Table 3.2:** Lower limit of detection (LLD) and 2-sigma standard deviation on pyrrhotite measurements using EMP operating conditions as described above.

| Element | LLD (wt%) | 2σ (wt%) |
|---|---|---|
| Ni | 0.028 | *(0.002)* |
| Cu | 0.031 | *(< 0.001)* |
| Co | 0.032 | *(< 0.001)* |
| Fe | 0.041 | *(0.118)* |
| S | 0.032 | *(0.108)* |

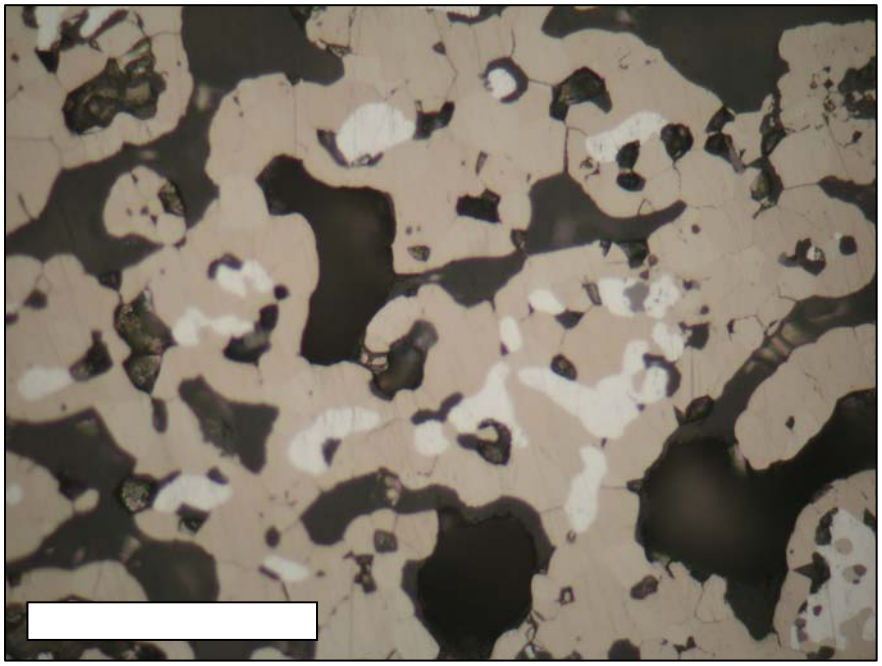

**Figure 3.3**: Reflected light photomicrograph of the synthetic troilite made for verification of the EMP standardisation. The pale cream phase is the troilite interrupted with occasional zones of bright white native iron. Scale bar represents 100 µm.

### 3.2.5 Automated SEM

Preliminary work in preparing a method for mapping magnetic and non-magnetic pyrrhotite was performed on a QEMSCAN® EVO50 located at Intellection, Brisbane in September 2006. Further developmental work in optimising the experimental routine was performed by Intellection in 2007 and the results of both sets of work are presented here (Section 3.3). Further details of the exact experimental conditions used can be found in Botha and Butcher (2008).

Mineralogical characterisation of microflotation feed samples by MLA was performed by Vale INCO Technical services in Sheridan Park, Toronto. The MLA consisted of a JEOL 6400 SEM fitted with two energy dispersive EDAX Si(Li) spectrometers with digital pulse processors. Measurements were run at 20 kV with counting times of 32 ms per pixel using the GXMAP routine in order to determine the relative proportion of all mineral phases present which are shown in table 3.3. All particles containing pentlandite, pyrrhotite, chalcopyrite and pyrite were individually mapped by the MLA. The liberation characteristics of pyrrhotite and pentlandite were also determined and are given in Appendix C1.

**Table 3.3:** Composition of pyrrhotite samples as determined by MLA and used for the experimental test work programme. See table 3.1 for specific details regarding samples used for oxygen uptake or microflotation tests.

| Mineral (wt %) | Phoenix<br>Magnetic Po | Nkomati MSB<br>Mixed Po | Sudbury CCN<br>Non-magnetic Po | Sudbury Gert West<br>Magnetic Po |
|---|---|---|---|---|
| **Pyrrhotite** | 81.8 | 83.8 | 75.4 | 85.2 |
| **Pentlandite** | 16.9 | 6.61 | 7.87 | 8.21 |
| **Chalcopyrite** | 0.22 | 2.92 | 0.66 | 0.21 |
| **Pyrite** | 0.54 | 0.86 | 0.00 | 0.30 |
| **Other Sulphides** | 0.00 | 0.01 | 0.00 | 0.00 |
| **Olivine** | 0.07 | 0.05 | 0.35 | 0.14 |
| **Orthopyroxene** | 0.00 | 0.00 | 0.40 | 0.54 |
| **Clinopyroxene** | 0.01 | 0.00 | 0.00 | 0.00 |
| **Amphibole** | 0.06 | 0.06 | 3.36 | 0.92 |
| **Talc** | 0.00 | 0.00 | 0.00 | 0.00 |
| **Serpentine** | 0.00 | 0.00 | 0.00 | 0.00 |
| **Chlorite** | 0.02 | 0.03 | 0.20 | 0.89 |
| **Biotite** | 0.01 | 0.01 | 1.61 | 0.58 |
| **Plagioclase** | 0.00 | 0.07 | 6.42 | 1.14 |
| **Quartz** | 0.03 | 0.01 | 2.27 | 0.74 |
| **Calcite** | 0.00 | 0.01 | 0.02 | 0.00 |
| **Magnetite** | 0.19 | 5.49 | 1.11 | 0.61 |
| **Other oxides** | 0.01 | 0.01 | 0.26 | 0.30 |
| **Other** | 0.09 | 0.07 | 0.04 | 0.18 |
| | | | | |
| **Total BMS** | *99.5* | *94.2* | *84.0* | *94.0* |
| ***Total*** | *100* | *100* | *100* | *100* |

## 3.3 Development of methodology for discrimination of pyrrhotite types

The overall approach used in order to review the methods for quantitative pyrrhotite analysis was considered in two phases. The first of which was to ensure that the Rietveld method in conjunction with powder XRD was able to successfully quantify the proportions of magnetic and non-magnetic pyrrhotite in mixed pyrrhotite samples. The aim of the second phase was to develop a method and prescribed operating parameters for phase quantification of magnetic and non-magnetic pyrrhotite using an automated SEM (e.g. QEMSCAN, MLA). It should be noted that the advantages of utilising an automated SEM is that the relative proportions, as well as the textural relationships between pyrrhotite phases can be quantified.

### 3.3.1 Analysis of pyrrhotite types using QXRD

Based on the characterisation of the Phoenix and Sudbury CCN pyrrhotite as pure (< 5 % of a second coexisting pyrrhotite phase) magnetic and non-magnetic pyrrhotite end-members, respectively (see Chapter 4), these two pyrrhotite samples were selected for powder XRD analysis to review the capability of the Rietveld method in order to quantify the relative proportions of pyrrhotite in a mixed sample. Successful phase quantification in QXRD is based upon the input of reference crystal structural information which is similar in character (e.g. crystallographic superstructure, composition, natural versus synthetic, phase stability) to the sample being analysed. The C2/c 4C pyrrhotite crystal structure of Powell *et al.* (2004) was used as the reference structure for Phoenix pyrrhotite, and the 5C pyrrhotite crystal structure from De Villiers *et al.* (Submitted) was used as the reference for Sudbury CCN pyrrhotite. The reference crystal structure of the C2 4C structure from sample *IMP-1* was also used (De Villiers *et al*., In Prep.).

A calibration curve was made by mixing the Phoenix magnetic pyrrhotite and Sudbury CCN non-magnetic pyrrhotite in carefully weighed out proportions such that the sample contained 0, 30, 50, 70 and 100 % magnetic pyrrhotite, respectively. Phase quantification to determine the relative proportions of magnetic 4C and non-magnetic 5C pyrrhotite was not successfully achieved using the Autoquan software since the user is unable to specify which parameters are refined. However, successful quantification was achieved using the Topas software and the diffractogram from the refinement is shown in figure 3.4. The key elements to the

successful determination of the relative proportions of magnetic and non-magnetic pyrrhotite in a mixture of pyrrhotite types, was based on the simultaneous refinement of all the samples. It was also necessary to constrain the crystallite size and unit cell parameters of the different pyrrhotite phases to be equal to one another for all the samples analysed. The final calibration curve comparing the actual and calculated proportions of magnetic C2/c 4C and non-magnetic 5C pyrrhotite in the calibration curve is shown in figure 3.5 where it is evident that the refinement works well for mixtures of pyrrhotite types, but slightly underestimates the proportion of pure magnetic C2/c 4C pyrrhotite.

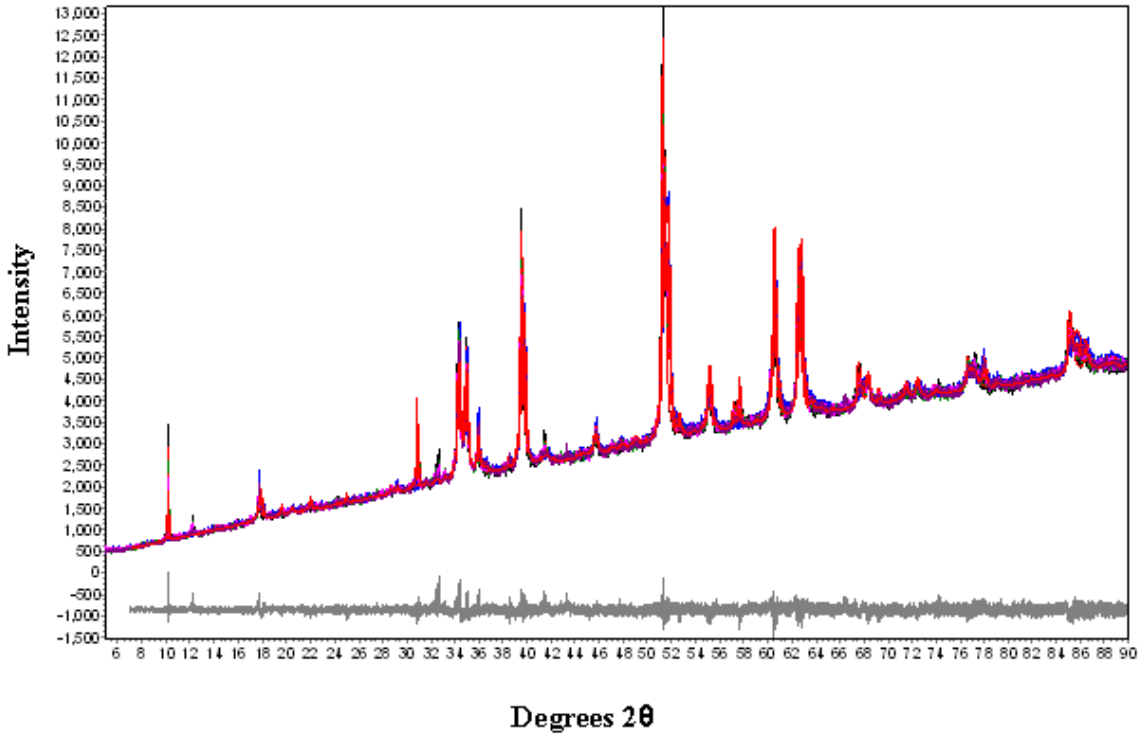


**Figure 3.4:** Diffractogram showing the results of the simultaneous Rietveld refinement of all the samples in the pyrrhotite calibration curve using Topas. The red line represents the calculated diffractogram, blue line represents the measured diffractogram and the grey line indicates the residual.

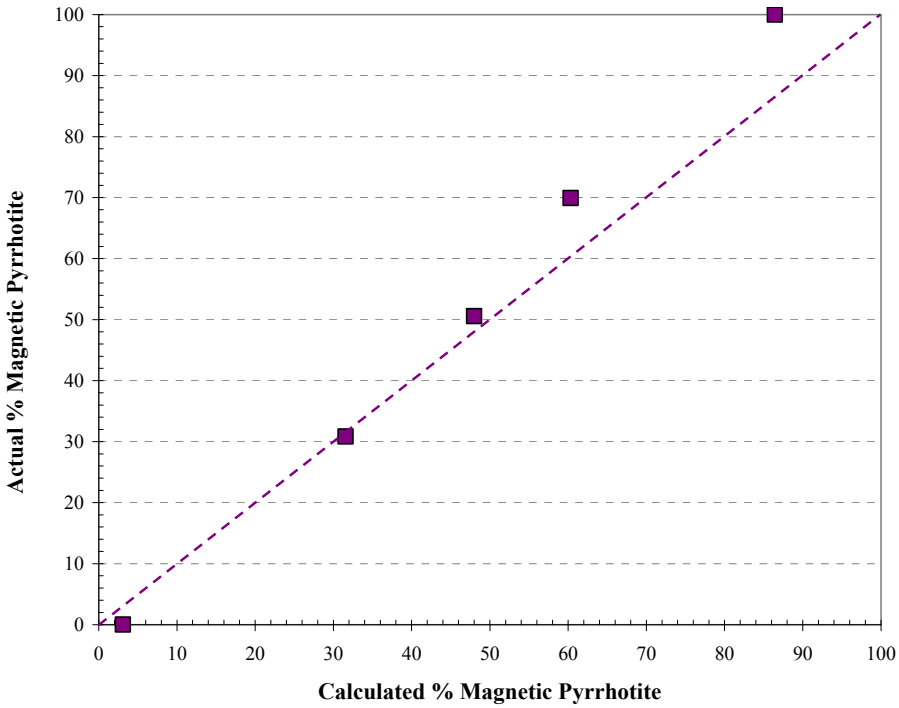


**Figure 3.5**: The calibration curve obtained for pyrrhotite phase quantification using the Topas Rietveld QXRD software. The proportion of magnetic *C2/c* 4C pyrrhotite is shown.

### 3.3.2 Analysis of pyrrhotite types using QEMSCAN

Nkomati MSB mixed pyrrhotite samples were initially viewed using only the BSE functionality of QEMSCAN under routine operating conditions in order to establish the relationship between magnetic and non-magnetic pyrrhotite. This test established two critical factors, the first of which was that the x-ray spectra of the different pyrrhotite phases captured by the energy dispersive detectors was unable to discriminate between the phases based entirely on composition. The second factor established was that the BSE grey level contrast between magnetic (~ 43.16) and non-magnetic pyrrhotite (~ 43.33) viewed using routine operating conditions was too subtle to reliably be used as a means to discriminate between pyrrhotite types (Figure 3.6 a, b), especially since it was subject to secondary effects such as polishing scratches. This prompted a series of developmental stages relating to the capture of the BSE signal by the QEMSCAN operating software and customised calibration settings of the QEMSCAN system in order to create a specialised routine for pyrrhotite mapping.

After numerous iterations and developments in brightness and contrast settings, as well as developments relating to the method in which the instrument obtained the BSE image were performed (Botha and Butcher, 2008), the QEMSCAN was able to successfully discriminate

between pyrrhotite types (Figure 3.6 c, d). Further work in order to perform a thorough data validation programme utilising optical microscopy, QXRD and EBSD in order to confirm the results shown in figure 3.6 is recommended before this is used as a standard procedure. It is however noted even with further validation and development of the QEMSCAN procedure, several limitations will still exist with this technology. This includes those features that affect the BSE signal, such as crystal orientation or anistropism and surface polishing (Section 2.2.8) as well as the likelihood of long measurement times to improve precision.

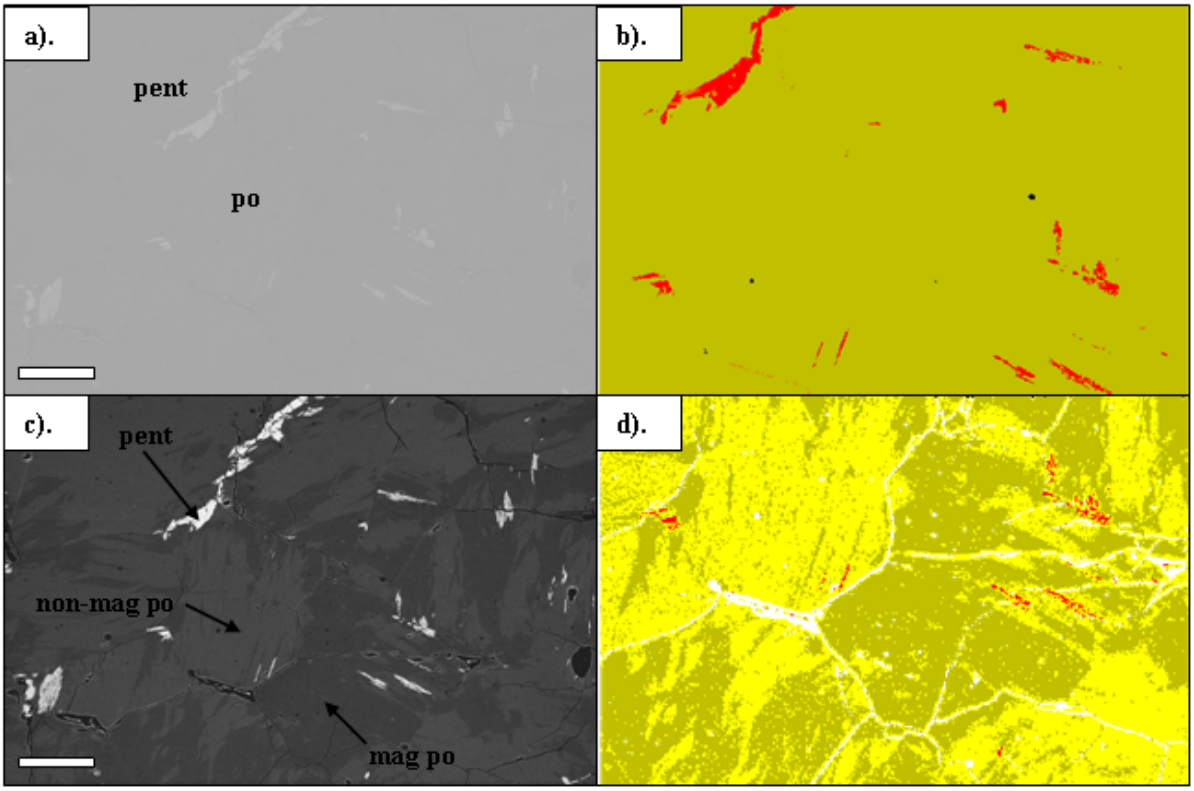


**Figure 3.6**: Summary of the BSE images (a, c) and the respective QEMSCAN false colour images (b, d) of Nkomati MSB pyrrhotite during the development of the pyrrhotite mapping technique. (a, b) show pyrrhotite under routine conditions whereas (c, d) show intergrown magnetic and non-magnetic pyrrhotite using adjusted SEM brightness and contrast settings in addition to specialised operating and calibration conditions. Colours used in the false colour QEMSCAN images are as follows: red – pentlandite, yellow – non-magnetic pyrrhotite, mustard – magnetic pyrrhotite. Scale bar represents 200 µm.

## 3.4 Pyrrhotite Reactivity

The reactivity of pyrrhotite samples was measured using a combination of both electrochemical measurements with pyrrhotite electrodes and determination of the oxygen uptake of pyrrhotite in mineral slurry. Both the open circuit potential and cyclic voltammetry measurements were performed at Haceteppe University in Turkey (Ekmekci *et al.*, Submitted), whereas oxygen uptake measurements were performed at the University of Cape Town.

### 3.4.1 Electrode Preparation

Working electrodes of the pyrrhotite samples in this study were manufactured by mounting a ~ 2 x 2 mm slice of pyrrhotite into an epoxy resin. Contact with the electrode was made by plating one side of the pyrrhotite surface with copper. A copper wire held in a glass casing was then attached to the copper plate. The electrodes were polished after every run with 500 grit SiC paper for 1 minute after which any residual particulate matter was removed in an ultrasonic bath. In order to confirm the purity of the mineral electrodes, BSE images and elemental maps of the electrodes were taken on an EVO 50 SEM with Bruker AXS XFlash 3001 Energy dispersive detectors at Hacettepe University. The annotated BSE images of the pyrrhotite working electrodes shown in figure 3.7 illustrate that the electrodes were slightly contaminated by minerals such as pentlandite, chalcopyrite, pyrite and magnetite. Figure 3.7 shows that pyrrhotite was however, always the dominant phase and since the focus of this study is on real ore samples, the electrodes were used as is.

### 3.4.2 Open Circuit Potential

Following preparation of the electrode as described in section 3.4.1, open circuit potential measurements were performed on the various pyrrhotite samples to determine the state of surface oxidation. An electrochemical cell containing the working electrode, reference electrode (calomel) and counter electrode (Pt wire) was set up in a 50 ml buffer solution. Open circuit potential measurements were performed at either pH 7 or 10 with buffer solution composition of 0.025M $KH_2PO_4$ + 0.025M $Na_2HPO_4$, or 0.025M $Na_2B_4O_7.10H_20$ + 0.1M

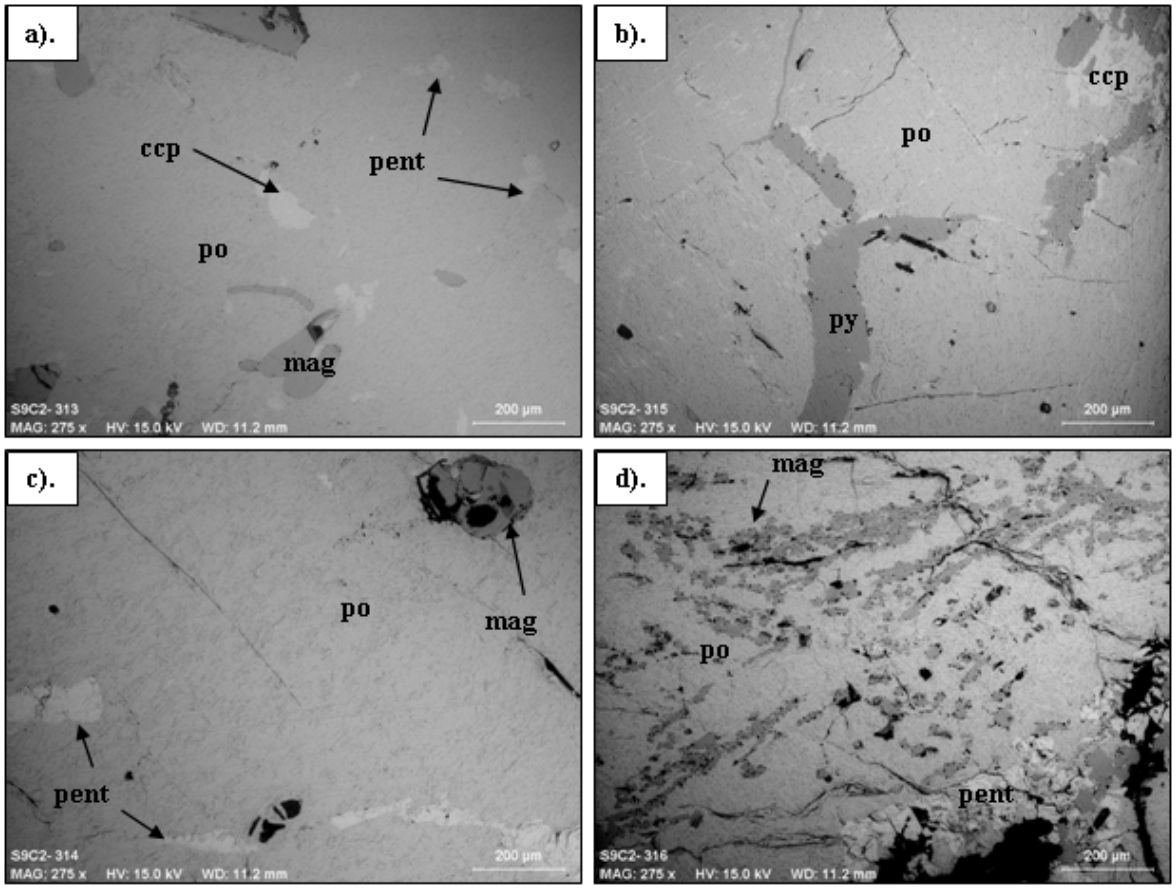


**Figure 3.7:** SEM BSE images of the pyrrhotite working electrodes used for electrochemical measurements. The contaminant minerals in the electrodes are shown. Images are shown for (a) Nkomati MSB mixed pyrrhotite (b) Phoenix magnetic pyrrhotite (c) Sudbury CCN non-magnetic pyrrhotite and (d) Sudbury Gertrude West magnetic pyrrhotite. Photograph courtesy of E. Bagci Tekes.

NaOH, respectively. Measurements were performed in deoxygenated solutions prepared by purging nitrogen gas through the solution prior to each experiment. Measurements were taken after 10 minutes to allow stabilisation of the potential. The solution was stirred continuously throughout the duration of the experiment. After each run, the surface of the electrode was repolished to prevent any poisoning of the electrode. Measurements were performed in triplicate. The raw data from open circuit potential measurements are presented in Appendix B1.

### 3.4.3. Cyclic Voltammetry

Cyclic voltammetry was used as an additional technique to compare the electrochemical characteristics of the different pyrrhotite samples examined in this study. The same electrode used in the open circuit potential measurements (Section 3.4.2) was used in the electrochemical cell illustrated in figure 3.8. The electrochemical cell was purged with nitrogen for 15 minutes at which point the clean electrode was transferred into the cell. Measurements were performed with a Gamry Instruments model PCl4/750 Potentiostat at a scanning rate of 20 mV per second. Scanning was initiated at open circuit potential and gradually taken to more negative potentials in order to remove any oxidised species formed on the electrode surface during polishing. The measured current was then converted to a current density based on the real surface area of the individual electrodes given in table 3.4, determined using a roughness factor of ~ 7. After each run, the surface of the electrode was repolished to prevent any poisoning of the electrode. All measurements were performed in duplicate. The complete set of cyclic voltammetry results is given in Appendix B2.

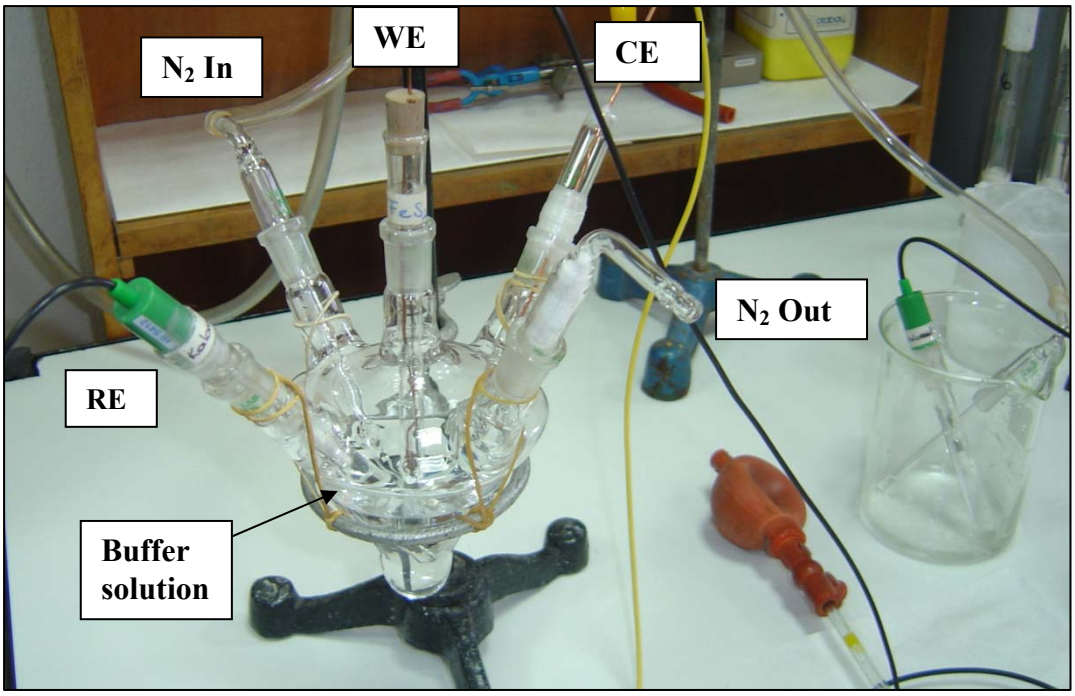


**Figure 3.8:** Photograph of the cell used for electrochemical measurements. The working pyrrhotite electrode (WE), reference electrode (RE) and counter electrode (CE) are annotated. Photograph courtesy of E. Bagci Tekes.

**Table 3.4:** Real surface area of the different pyrrhotite electrodes used for cyclic voltammetry.

| Pyrrhotite | Mineralogy | Surface Area (cm2) |
|---|---|---|
| Nkomati MSB | Mixed | 1.225 |
| Phoenix | Magnetic | 2.065 |
| Sudbury CCN | Non-magnetic | 1.505 |
| Sudbury Gertrude West | Magnetic | 1.750 |

### 3.4.4 Oxygen Uptake

An additional measurement used to compare the reactivity of different pyrrhotite samples was based on the rate of oxygen uptake of a pyrrhotite slurry through pyrrhotite oxidation. Using methodology developed by Afrox (Afrox, 2008), oxygen uptake factors were determined. The method is based upon the measurement of the rate of dissolved oxygen decay of a pyrrhotite slurry once the sample had been sparged with a controlled amount of pure oxygen. A schematic of the apparatus used for the oxygen uptake is illustrated in figure 3.9 and which consists of a dissolved oxygen probe connected to a TPS meter, in turn connected to a PDA computer.

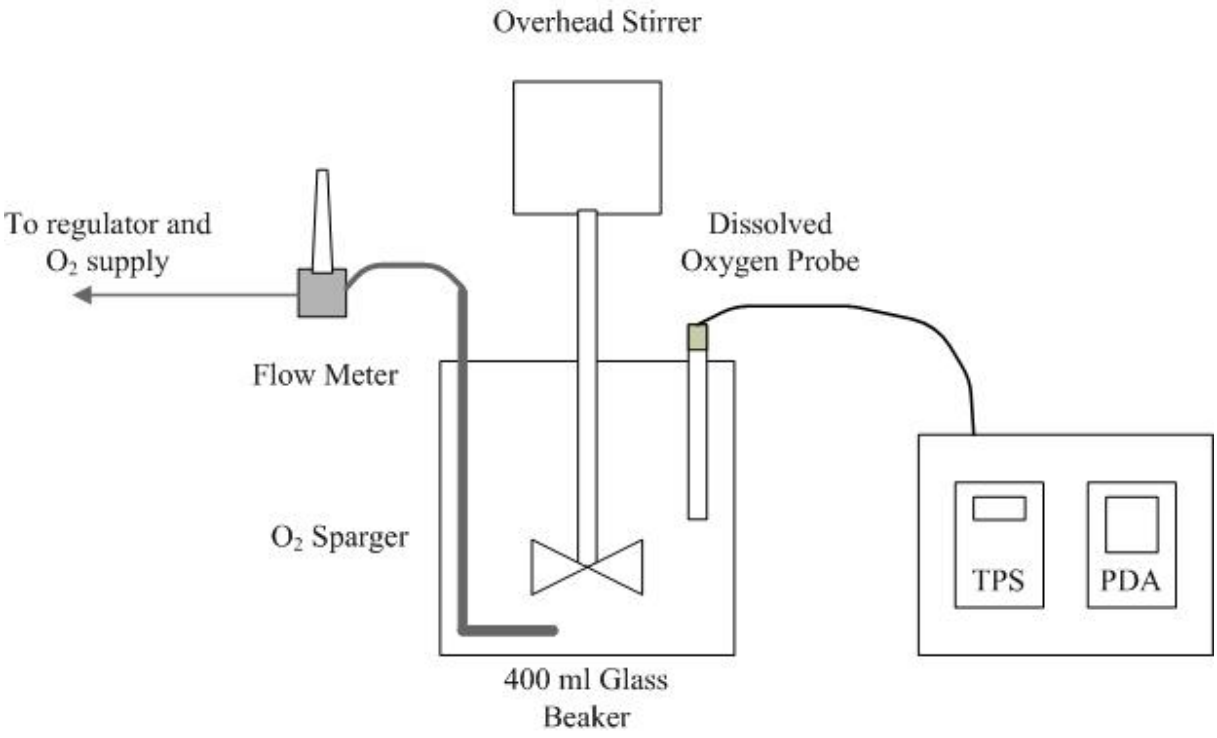


**Figure 3.9**: Diagram of the apparatus used for dissolved oxygen uptake measurements.

Pyrrhotite samples for oxygen uptake tests were prepared by crushing lumps of massive pyrrhotite with a jaw crusher and then dry milling with a Sieb mill. Samples were dry screened to the desired size fraction of 53 to 106 µm and then split and packaged into representative aliquots of ~ 80 g using a Fritsch rotary sample divider and stored in a freezer until needed. Where necessary, the pyrrhotite was upgraded by either hand picking out chips of silicate minerals from the jaw crush (Sudbury CCN), or removing excess chalcopyrite from the milled sample with a hand magnet (Sudbury CCN, Nkomati MSB).

At the start of the oxygen uptake tests, individual sample aliquots were ultrasonicated in distilled water to disaggregate any fine particles. The pyrrhotite was then wet screened at 53 µm with 3.33 x $10^{-3}$ M calcium water ($10^{-2}$ ionic strength) and transferred into a 400 ml beaker for the oxygen uptake tests. Surface area measurements of pyrrhotite samples after ultrasonication were obtained using the Brunauer Emmet and Teller (BET) technique with nitrogen adsorption to check the equivalence of samples (Table 3.5). The pyrrhotite sample was made into a slurry using 300 ml of 3.33 x $10^{-3}$ M calcium water ($10^{-2}$ ionic strength) at the desired pH to produce a slurry of ~ 25 % solids by weight. The mineral sample was then agitated with an overhead stirrer, dosed and conditioned with depressant, activator ($CuSO_4$) and collector respectively according to the specifications in table 3.6. Collector dosage was determined according to the proportion of BMS in the oxygen uptake sample as measured by QXRD and as shown in table 3.1. A collector dosage of 4.0 x $10^{-5}$ M was used for a sample containing ~ 100 % BMS (see Appendix B3). Activator dosage was based on a 0.4:1.0 ratio of copper to xanthate. This ratio was selected to ensure an excess of xanthate and minimise the formation of copper hydroxides. Collectors were supplied by SENMIN, Sty 504 guar from Chemquest and $CuSO_4.5H_2O$ from Merck. The sample was then modified to the desired pH with the use of NaOH or $HNO_3$ prior to the dissolved oxygen uptake measurements.

**Table 3.5**: BET surface area measurements of mineral samples used for oxygen uptake tests.

| Pyrrhotite | Mineralogy | Surface Area ($m^2.g^{-1}$) |
|---|---|---|
| Phoenix | Magnetic | 0.33 |
| Sudbury CCN | Non-magnetic | 0.22 |
| Sudbury Gertrude West | Magnetic | 0.32 |
| Nkomati MSB | Mixed magnetic and non-magnetic | 0.23 |

The dissolved oxygen content of the sample was then measured with a YSI 5739 DO probe fitted with YSI high speed membrane (1 s response) connected to a TPS WP-91 dissolved oxygen meter. Data from the TPS meter were extracted using a PDA computer. The pyrrhotite slurry was sparged with medical oxygen for 10 seconds at a flow rate of 1.15 $L.min^{-1}$ and controlled using a Sierra Smart Trak flow meter provided by Process Kinetics. Dissolved oxygen measurements were taken every 2 seconds for 2-3 minutes to measure the decay of the dissolved oxygen by the pyrrhotite slurry. The associated oxygen uptake factor was then calculated according to the methodology shown in Appendix B4. Due to considerable mass of pyrrhotite required in the correct size fraction for each test (~ 80 g in 53-106 µm) analyses were not performed in duplicate. Based on previous work by Becker *et al.* (2005) however, it is known that the repeatability is fair (see Appendix B4) and relative errors are ~ 10% on the calculated oxygen uptake factor. The complete set of oxygen uptake results is given in Appendix B5.

**Table 3.6:** Summary of the procedure used for oxygen uptake experiments.

| Activity | Conditions | Time (min) |
|---|---|---|
| Retrieval of sample from freezer | ~ 80g pyrrhotite sample (53-106 µm) | - |
| Ultrasonification | 400 ml Distilled Water | 5 |
| Wet screening | Synthetic water @ desired pH, $10^{-2}$ ionic strength $Ca^{2+}$ | - |
| Transferral into beaker | Sample stirring at point of depressant addition | - |
| Depressant addition | Sty 504 @ 10ppm | 5 |
| Activator addition* | $CuSO_4$ @ 1.6 X $10^{-4}$M | 2 |
| Collector addition* | Xanthate (SIBX or SNPX) @ 4.0 X $10^{-4}$M | 2 |
| pH modification | NaOH | - |
| DO measurement | - | - |
| $O_2$ Introduction | $O_2$ sparging at 1.15L.$min^{-1}$ | 10 sec |
| DO measurement | - | 3 |

* Reagents are given for a sample containing 100% BMS.

## 3.5 Pyrrhotite Microflotation

### 3.5.1 Microflotation tests

Microflotation tests were conducted using the UCT microfloat cell illustrated in figure 3.10 and developed by Bradshaw and O' Connor (1996). The microfloat cell consists of a 365 ml columnar glass cell with launder. Synthetic air is injected into the base of the cell with a Hamilton syringe that produces a single bubble stream. Hydrophobic particles attached to these bubbles rise to the top of the cell where the bubbles burst when they hit a glass cone, and the hydrophobic particles fall into the launder to be collected as concentrates.

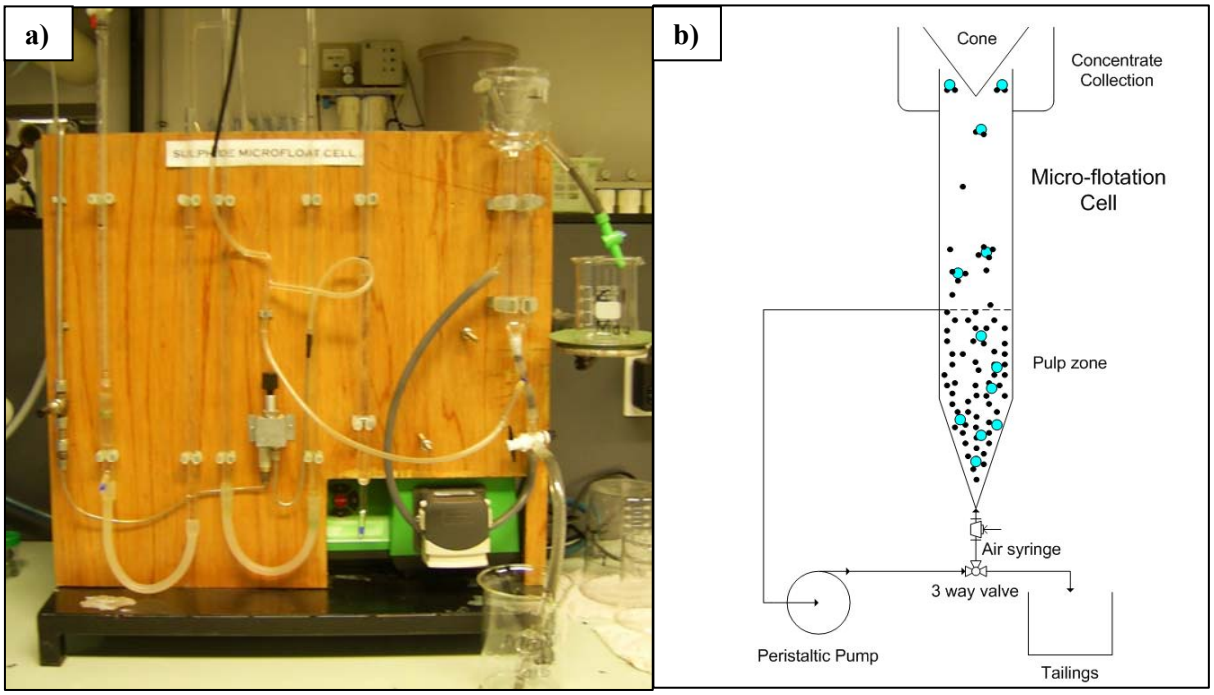


**Figure 3.10:** (a) Photograph and (b) diagram of the microflotation cell used for the tests in this study. From: Mbonambi (2009).

Microfloat tests were carried out using pyrrhotite which was prepared with a Sieb mill and then dry screened to the desired size fraction of 53 to 106 µm. Since the microflotation tests were only performed on high grade pyrrhotite samples, the Merensky Reef pyrrhotite samples were excluded from this set of test work. Pyrrhotite samples were stored in a freezer until needed for the microfloat test work programme. Surface area measurements of pyrrhotite samples prior to ultrasonication were obtained using the Brunauer Emmet and Teller

technique with nitrogen adsorption to check the equivalence of samples (Table 3.6). The morphology of the pyrrhotite microfloat samples was also examined using a Leica LEO Stereoscan S440 Scanning Electron Microscope at the University of Cape Town. Selected images of the pyrrhotite particles are shown in figure 3.11. Samples were examined both prior to and post ultrasonification to examine whether there were any significant differences in particle morphology of the pyrrhotite specimens examined.

**Table 3.7**: BET surface area measurements of mineral samples used for microflotation tests.

| Pyrrhotite | Mineralogy | Surface Area ($m^2.g^{-1}$) |
|---|---|---|
| Phoenix | Magnetic | 0.13 |
| Sudbury CCN | Non-magnetic | 0.23 |
| Sudbury Gertrude | Magnetic | 0.35 |
| Sudbury Gertrude West | Magnetic | 0.17 |
| Nkomati MSB | Mixed magnetic and non-magnetic | 0.13 |

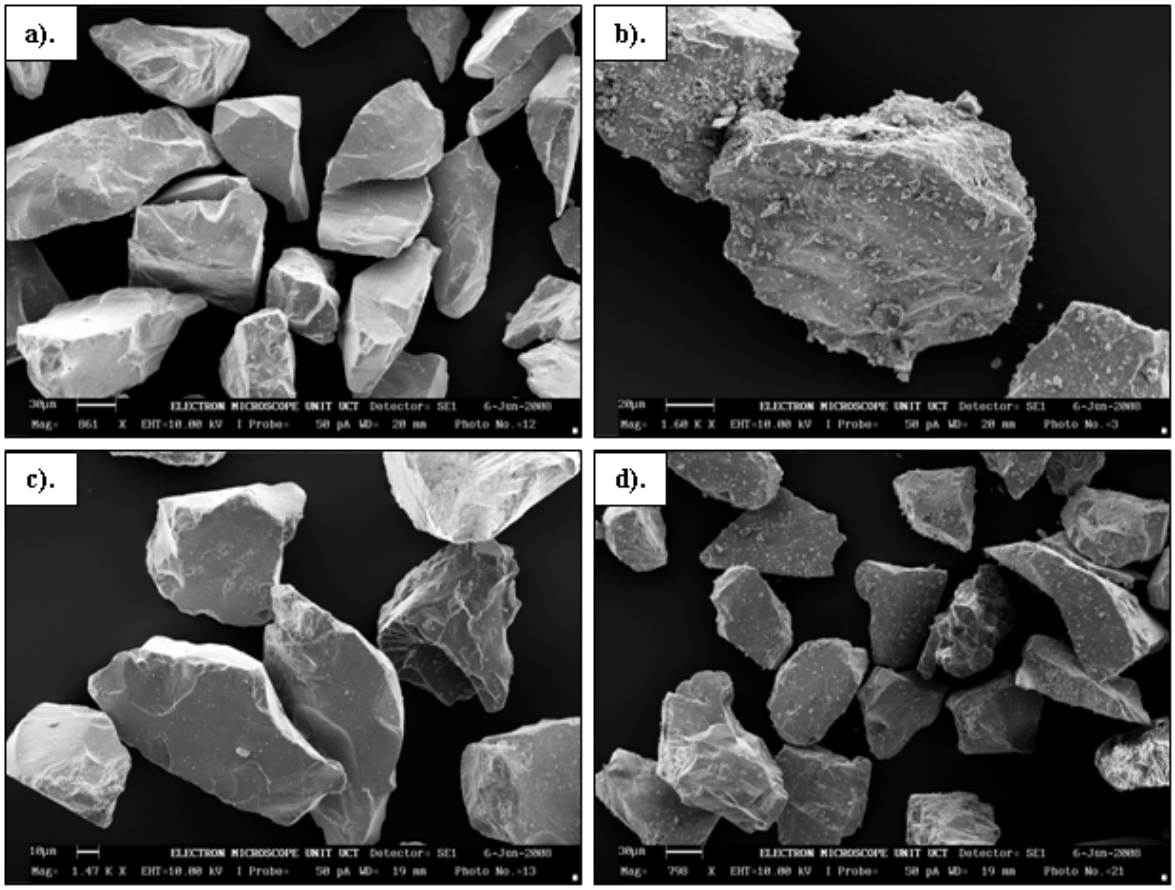


**Figure 3.11**: SEM images of ultrasonicated pyrrhotite particles used for microflotation tests. Images are shown for (a) Nkomati MSB mixed pyrrhotite, (b) Phoenix magnetic pyrrhotite, (c) Sudbury CCN non-magnetic pyrrhotite and (d) Sudbury Gertrude magnetic pyrrhotite.

2g of pyrrhotite was then carefully weighed out and ultrasonicated in distilled water for 5 minutes in order to detach fine material most likely derived from the oxidation of pyrrhotite. Following ultrasonification the sample was wet screened at 53 µm to remove the fines and transferred into the conditioning vessel with 3.33 x $10^{-3}$M calcium water ($10^{-2}$ ionic strength). The mineral sample was then agitated and dosed with depressant, activator (copper) and collector (SIBX, SNPX), respectively according to the specifications in Table 3.8. Collector dosage was determined according to the proportion of sulfide in the flotation feed sample as measured by QXRD (Table 3.1). Activator dosage was based on a 0.4:1.0 ratio of copper to xanthate. This ratio was selected to ensure an excess of xanthate and minimise the formation of copper hydroxides. Collectors were supplied by SENMIN, Sty 504 guar from Chemquest and $CuSO_4.5H_2O$ from Merck. The sample was then modified to the desired pH with the use of NaOH or $HNO_3$ and transferred into the microflotation cell. The exact reagent dosages used for each pyrrhotite sample are given in Appendix C2.

**Table 3.8:** Summary of the procedure used for microflotation tests.

| Activity | Conditions | Time (min) |
|---|---|---|
| Sample weighing | 2g pyrrhotite sample (53-106µm) | - |
| Ultrasonification | 80 ml Distilled Water | 5 |
| Wet screening | Synthetic water @ desired pH, $10^{-2}$ ionic strength $Ca^{2+}$ | - |
| Transferral into beaker | Sample stirring at point of depressant addition | - |
| Depressant addition | Sty 504 @ 10ppm | 5 |
| Activator addition* | $CuSO_4$ @ 0.4 X $10^{-5}$M | 2 |
| Collector addition* | Xanthate (SIBX or SNPX) @ 1.0 X $10^{-5}$M | 2 |
| pH modification | NaOH or $HNO_3$ | - |
| Transferral into microfloat cell | 100rpm pump speed, 7ml.min$^{-1}$ synthetic air flow | - |
| Conc 1 Collection | - | 2 |
| Conc 2 Collection | - | 3 |
| Conc 3 Collection | - | 5 |
| Conc 4 Collection | - | 5 |

* Reagent are given for a sample containing 100 % BMS

Flotation was initiated with the insertion of a Hamilton syringe needle into the base of the float cell at a flow rate of 7 ml.min$^{-1}$ using synthetic air. The mineral sample was kept in

suspension by a peristaltic pump operating at 100 rpm. Mineral concentrates were collected after 2, 5, 10 and 15 minutes of flotation, carefully filtered and dried for further analysis. Recoveries were calculated either on the basis of total mass or calculated pyrrhotite from the chemical assay. All microflotation tests were conducted in duplicate. The complete set of flotation results is given in Appendix C3.

### 3.5.2 Analysis of Flotation Performance

Where sufficient pyrrhotite mass was available from the microflotation tests, samples were selected for chemical assay. Microflotation test concentrate and tails were measured for iron, nickel and copper using Atomic Absorption Spectroscopy (AA) and sulfur using a LECO Sulfur Analyser.

Samples for AA were prepared by the digestion of a carefully measured amount of pyrrhotite (between 0.05 and 0.1 g) in a mixture HF, $HNO_3$, $HClO_4$ and HCl using the acid digestion procedure as given in Brough (2008). Concentrations were measured on a Varian Spectra AA at the University of Cape Town. Sulfur analyses performed prior to July 2008 were measured on a LECO 423 Sulfur Analyser and after July 2008 on a S632 Leco Sulfur Analyser housed at the University of Cape Town. Where iron, nickel and sulfur assays were available for all material obtained from microflotation tests, the pyrrhotite recovery was calculated. Pyrrhotite recovery was based on the assumption that all nickel was hosted in pentlandite, all copper in chalcopyrite. Therefore, once the amount of pentlandite and chalcopyrite were known, the amount of sulfur unaccounted for was assumed to be hosted by pyrrhotite and the proportion of pyrrhotite was accordingly calculated for $Fe_7S_8$ or $Fe_9S_{10}$. The method was unable to account for the proportion of solid solution nickel hosted by pyrrhotite or the presence of pyrite but within the limitations of this study, is the best possible method for calculating pyrrhotite recovery.

# Chapter 4

# PYRRHOTITE MINERALOGY

---

## 4.1 Introduction

As described in Chapter 2, a general understanding of the details of pyrrhotite mineralogy already exists, but the majority of the research was focussed on the use of synthetic samples in order to understand pyrrhotite phase relations and determine pyrrhotite crystal structures (Section 2.6.1). Similarly, although the compositional variation and nature of the mineral association between natural samples from a variety of ore deposits have been examined in the past, this was based on the d-spacing method of Arnold and Reichen (1962) and not on direct chemical methods. Therefore the use of mineralogical information based on natural samples using modern mineralogical analysis techniques is of key interest within the field of process mineralogy. In order to be able to develop the relationship between pyrrhotite mineralogy and flotation performance, a thorough characterisation of the mineralogy of pyrrhotite from selected nickel and platinum group element ore deposits is needed. Consequently, the aim of this chapter is *explore and compare the mineralogy in terms of the mineral association, crystallography and mineral chemistry of magnetic and non-magnetic pyrrhotite*. The results of the petrographic, crystallographic and mineral chemistry studies of the various pyrrhotite samples are therefore presented in this chapter. The complete mineral chemistry data set is presented in Appendix A.

## 4.2 Petrography

Measurement of the relative proportions of non-magnetic and magnetic pyrrhotite in this study using the magnetic colloid method is subject to the interpretation of the textures enhanced by the colloid itself. It is known that particles of the magnetic colloid preferentially adhere to zones where the greatest inhomogeneities exist in the magnetic field and correspond to the occurrence of ferrimagnetic (magnetic) pyrrhotite (Zapletal, 1969). On application of the magnetic colloid onto non-magnetic pyrrhotite or pentlandite, the magnetic colloid particles showed no evidence of preferential attachment and simply hovered homogeneously over the entire ore sample. On repeated application of the magnetic colloid onto a ferrimagnetic pyrrhotite sample, it was found that the exact same textures were enhanced as on the previous occasion. According to Yamamoto *et al.* (1959), only when an external magnetic field is applied to the same sample, do the patterns in the magnetic domains shift slightly, although the boundary between non-magnetic and magnetic phases remains unaltered. In the study of Zapletal (1972), a comparison was made of intergrowths between pyrrhotite phases enhanced by the magnetic colloid method and acid etch technique, the results of which indicated a good correlation. Based on this evidence, the magnetic colloid method was the preferred method used in this study.

### 4.2.1 Merensky Reef Pyrrhotite

Pyrrhotite samples from the Merensky Reef at Impala Platinum Mine used for mineral characterisation in this study originated from two cross sections through the Merensky Reef. Both of these cross sections sampled the norite footwall, the Merensky chromitite and the overlying pyroxenite giving a reasonable approximation of the variation in lithology within the Merensky Reef in order to examine pyrrhotite mineralogy in detail (Figure 3.1). In hand, specimen the two samples differed most notably in the coarser-grained, more pegmatoidal textured pyroxenite overlying the Merensky chromitite in sample *IMP-1*, relative to sample *IMP-2*.

*Overview of sulfide mineralogy*

Sulfide mineralization within the Merensky reef samples examined was recognised in three textural settings as follows:

i) Large multi-mineralic sulfide blebs or domains
ii) Smaller mono-mineralic sulfide blebs
iii) Disseminated sulfides

The first texture comprising multi-mineralic sulfide blebs consisted of irregularly shaped domains of sulfides interstitial to the coarser grained, cumulus orthopyroxene. These sulfide blebs could be up to several millimetres in size and were comprised of the minerals pyrrhotite, pentlandite and chalcopyrite. These sulfide blebs were variable in texture and commonly consisted of a core of pyrrhotite surrounded by a rim of granular pentlandite and chalcopyrite (Figure 4.1a, b). Alternatively, equigranular mosaic textured domains were also recognised.

The second sulfide texture observed consisted of fine grained sulfide blebs (50 µm), that were still interstitial to the coarse grained silicates but the sulfide blebs were mono-mineralic; with pyrrhotite as the predominant mineral type (Figure 4.1c). The third typical sulfide texture observed within the samples analysed in this study consisted of very fine-grained disseminated sulfides (< 5 µm) which could be hosted by the silicate minerals themselves, or were sometimes restricted to cleavage planes and fracture zones within the silicates. Most of the discrete disseminated sulfide grains were chalcopyrite and were likely to be secondary in origin. The occasional fine-grained (50 µm) sulfide was also observed locked within chromite and was probably encapsulated during chromite annealing.

*Pyrrhotite*

Pyrrhotite was the most abundant sulfide mineral in the Merensky Reef samples analysed and typically occurred as the host phase of other minerals due to the formation of the other base metal sulfide minerals from the MSS (Figure 4.1a, b). Within these large multi-mineralic blebs, pyrrhotite generally consisted of a single large pyrrhotite grain in the core up to a few hundred microns in size, whereas the smaller sulfide blebs consisted of multiple pyrrhotite grains showing well-developed anisotropism. On occasion, it was possible to observe fine lamellar twinning within pyrrhotite.

Treatment of the Merensky samples with the magnetic colloid showed that magnetic pyrrhotite was restricted to sample *IMP-1* (Figure 4.1d, e). Pyrrhotite in sample *IMP-1* consisted of more than ~ 95% magnetic pyrrhotite. The magnetic colloid highlighted a texture

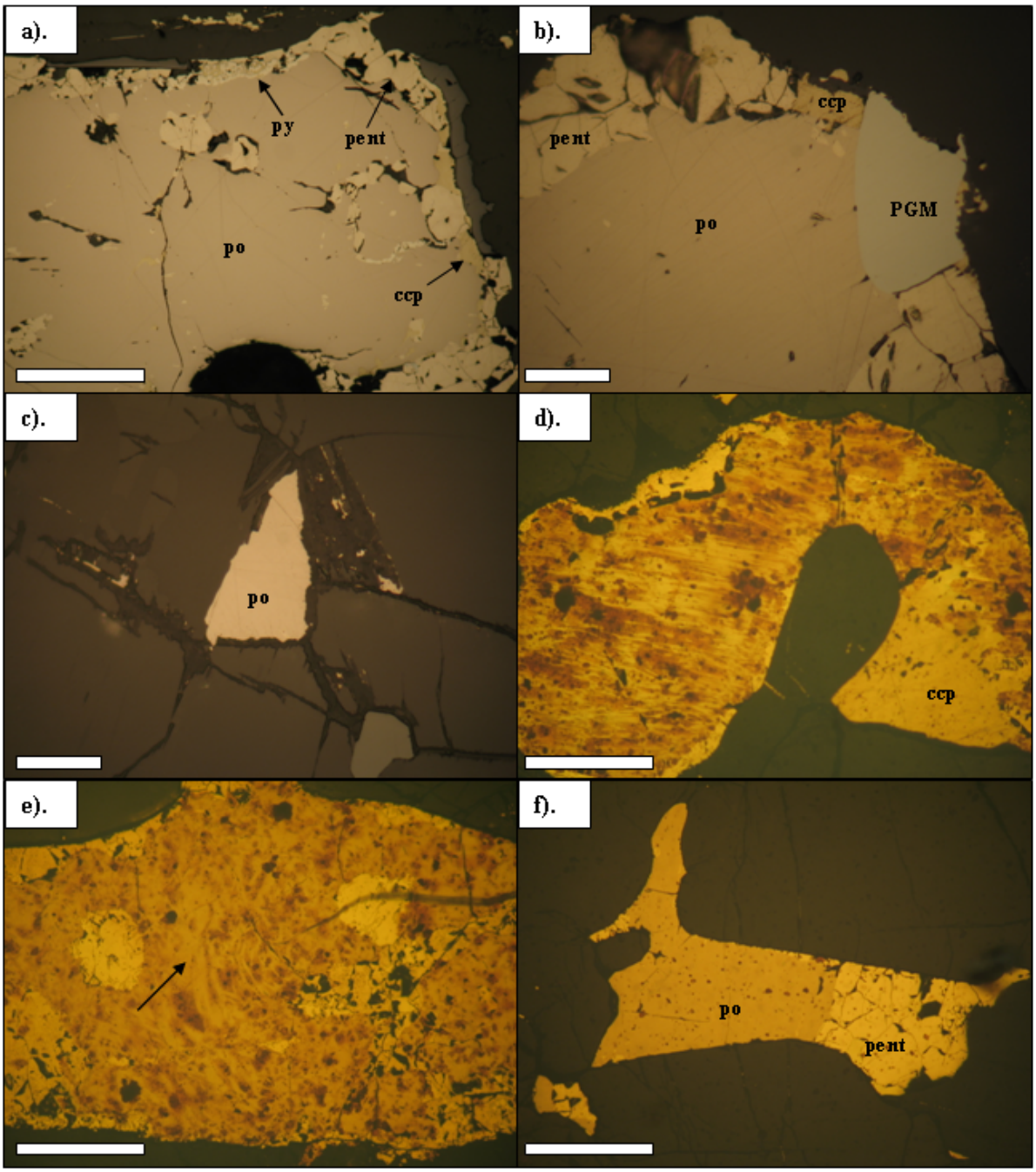


**Figure 4.1**: Photomicrographs of Impala Merensky Reef pyrrhotite shown in RPL. (a) Multi-mineralic sulfide domain texture consisting of granular pentlandite and chalcopyrite surrounding a core of pyrrhotite. (b) Discrete PGM hosted by a multi-mineralic sulfide domain. (c) Mono-mineralic sulfide bleb consisting of pyrrhotite. (d, e) Magnetic colloid treatment shows sample *IMP-1* consists of almost entirely magnetic pyrrhotite. The arrow in (e) highlights a zone of magnetic pyrrhotite with limited colloid coverage. (f) Magnetic colloid treatment shows non-magnetic pyrrhotite in sample *IMP-2*. Scale bar represents 500 µm for (a, d-f) and 50 µm for (b and c).

of multiple, closely spaced lamellae of magnetic pyrrhotite between 5 and 10 µm in thickness. These lamellae were typically tapered and narrowed towards a point before a new lamella commenced; a feature known as growth zonation (see also Figure 2.12). The length of these individual lamellae varied between 30 and 200 µm in size with the longer length lamellae restricted to larger pyrrhotite grains. In some circumstances the coverage of the colloid on the magnetic pyrrhotite was not entirely homogeneous, a feature which is more likely due to the magnetic domain structure of the pyrrhotite rather than the presence of non-magnetic pyrrhotite (Figure 4.1e).

Non-magnetic pyrrhotite on the other hand was restricted to sample *IMP-2* which was generally more pristine in character (Figure 4.1f). Exsolved troilite hosted by pyrrhotite was also observed in sample *IMP-2*. The troilite occurred as minor exsolution flames with a distinct "zig-zag" like pattern and were generally less than 5 µm in width (Figure 4.2). The direction of troilite exsolution was noted to be parallel to flame pentlandite exsolution, indicating the crystallographic control during exsolution.

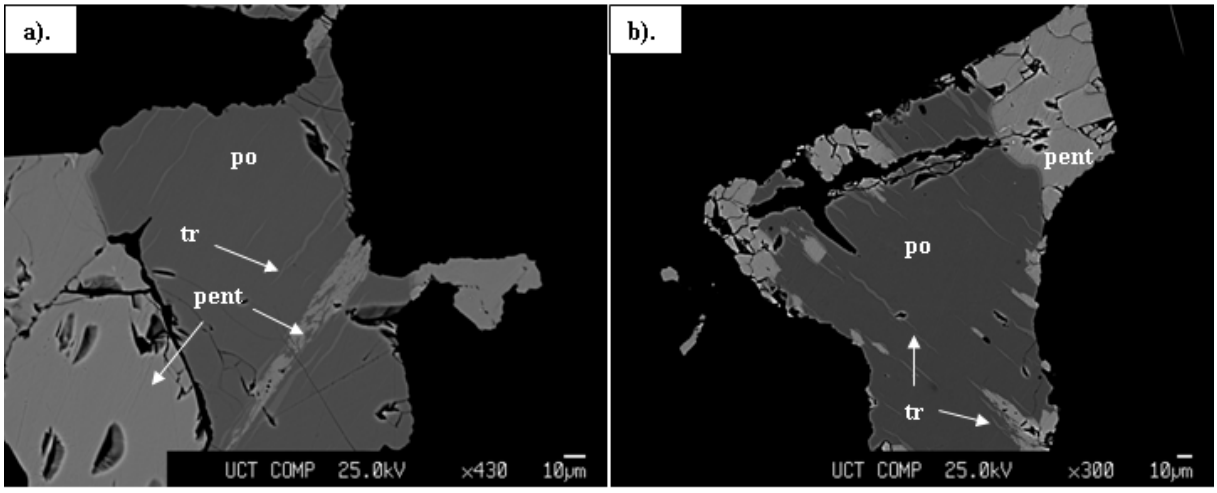


**Figure 4.2:** Back scattered electron (BSE) images of non-magnetic pyrrhotite in Merensky Reef sample *IMP-2* with exsolution of troilite (medium grey) and pentlandite (light grey). Exsolution lamellae of both troilite and pentlandite are crystallographically controlled.

*Pentlandite*

Pentlandite typically occurred in two textural occurrences in the Merensky Reef samples, as granular and flame pentlandite. Granular pentlandite was by far the more abundant and only the occasional pentlandite flame was observed. Granular pentlandite occurring along the

boundaries of the multi-mineralic sulfide blebs was typically subhedral in shape (Figure 4.1a, b), varying in size between 20 and 150 µm, whereas pentlandite occurring in the equigranular mosaic textured aggregates of sulfides was between 30 and 40 µm in size. Both pentlandite occurrences exhibited typical triangular pits as cleavage. The mosaic textured aggregates of pentlandite appeared to tarnish relatively rapidly, and consisted of very fine grained inclusions (these were too fine grained to accurately determine the composition with EMP). The mosaic textured, "altered" pentlandite pyrrhotite aggregates were restricted to sample *IMP-1*. Altered pentlandite was not observed in sample *IMP-2*.

Occasional pentlandite flames were observed but it should be mentioned that they were by no means the dominant pentlandite texture within the Merensky samples analysed here. Pentlandite flames were generally 5 µm in width and up to 50 µm in length and hosted by pyrrhotite. Most zones of pentlandite flames were fairly simple in texture, consisting of less than five discrete flames, oriented parallel to one another.

*Other Minerals*

Chalcopyrite was common within both the multi-mineralic sulfide blebs interstitial to silicates and as disseminated sulfides hosted by silicates. Within the multi-mineralic sulfide blebs granular chalcopyrite was noted to occur on the boundaries of the sulfide blebs in association with granular pentlandite (Figure 4.1a, b). Occasional pyrite was also recognised and was restricted to the sample *IMP-1* and occurred in association with the "altered pentlandite". Relict textures of large cubic pyrite grains (up to 200 µm in size) also occurred, although they appeared to have suffered from extensive resorption. Rare platinum group minerals were observed within the Merensky Reef sulfides and noted for their occurrence in association with the sulfides (generally hosted within the sulfide blebs). Although only larger euhedral PGMs (up to 100 µm in size, Figure 4.1b) were observed in this study, this is not thought to be representative in that many of the smaller fine-grained and very fine-grained PGMs were more than likely overlooked.

### 4.2.2 Nkomati Pyrrhotite

*Overview of sulfide mineralogy*

Pyrrhotite samples used for characterisation in this study were sourced from both the Massive Sulfide Body (MSB) and the Main Mineralized Zone (MMZ). Pyrrhotite was the dominant sulfide for both the MSB and MMZ. Selected photomicrographs of pyrrhotite from the MSB and MMZ are shown in figures 4.3 and 4.4, respectively. Four different manifestations of sulfide mineralisation were noted:

(i) Massive sulfide
(ii) Large multi-mineralic sulfide blebs or domains
(iii) Net textured sulfides
(iv) Disseminated sulfides

The MSB was dominated by massive sulphide (texture i), whereas textures (ii) to (iv) were more common within the two MMZ samples analysed (sample *MMZ-1*, *MMZ-4*). Sample *MMZ-1* tended to be the more pristine sample with less sulfide mineralisation which was confined to the development of discrete multi-mineralic sulfide blebs (up to several mm in size and dominated by pyrrhotite; Figure 4.4a) with occasional disseminated sulfides hosted by silicates. Sulfide mineralisation in sample *MMZ-4* however, suggested more interaction of the sulfide melt with the silicate minerals. Mineralisation in sample *MMZ-4* occurred as both domains of massive sulfide and net textured sulfides hosting silicate minerals (Figure 4.4b). These net textured domains appeared to be the result of the resorption of the primary silicate minerals and consequent formation of acicular tremolite and secondary alteration minerals (e.g. serpentine) surrounding a sulfide core of fine-grained pyrrhotite and pentlandite (Figure 4.4b). The abundance of tremolite in sample *MMZ-4* produced very irregular boundaries between the silicate and sulfide phase due to its acicular nature.

**Nkomati MSB Pyrrhotite**

*Pyrrhotite*

Pyrrhotite was the dominant sulfide in the MSB ore and generally occurred as subhedral shaped grains between 200 and 1000 µm in size, with an average of ~ 400 µm (Figure 4.3a).

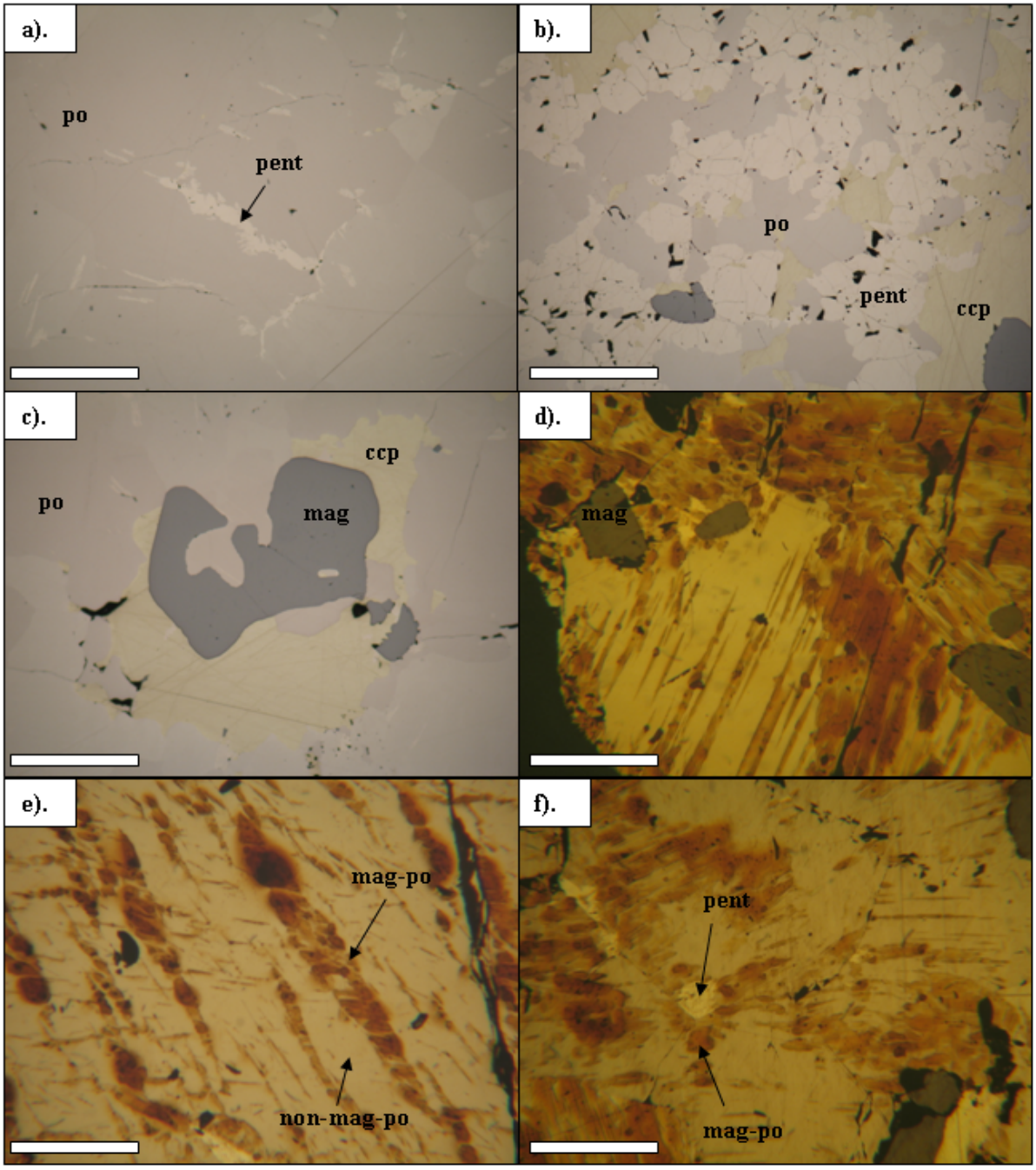


**Figure 4.3:** Photomicrographs of the Nkomati MSB shown in RPL. (a) Coarse-grained pyrrhotite hosting flame pentlandite inclusions. (b) Aggregate of granular pentlandite intergrown with pyrrhotite and chalcopyrite. (c) Irregular shaped inclusion of magnetite and chalcopyrite hosted by pyrrhotite. (d) Magnetic colloid treatment shows lamellae of magnetic pyrrhotite hosted by non-magnetic pyrrhotite. (e) Magnetic colloid treatment shows composite lamellae of magnetic pyrrhotite hosted by non-magnetic pyrrhotite. (f) Magnetic colloid treatment shows magnetic pyrrhotite rims surrounding flame pentlandite. Scale bar represents 200 µm.

Pyrrhotite grains in contact with other sulfides e.g. pentlandite, could however have more irregular shaped grain boundaries (Figure 4.3b, c). Since pyrrhotite formed from the host MSS (Section 2.2.7) in the Nkomati MSB ore, it contained multiple inclusions of pentlandite, chalcopyrite and also magnetite similar to those shown in figures 4.3 b and c.

Application of the magnetic colloid to the Nkomati MSB pyrrhotite, revealed complex intergrowths of magnetic and non-magnetic pyrrhotite similar to the textures described from the literature (see Figure 2.12). Magnetic pyrrhotite generally occurred as elongate lamellae that were hosted by the non-magnetic phase. Individual magnetic pyrrhotite lamellae could extend up to 50 µm in length. Examples of composite lamellae, thickness zonation, box work textures and formation of magnetic pyrrhotite rims surrounding flame pentlandite were all observed although only photomicrographs of selected intergrowth textures are shown in figure 4.3 e-f. Similar intergrowths of magnetic and non-magnetic pyrrhotite were obtained from the BSE and QEMSCAN images of the Nkomati pyrrhotite in section 3.3 (Figure 3.6).

*Pentlandite*

Photomicrographs of both the granular and flame pentlandite varieties present in the Nkomati MSB pyrrhotite are shown in figures 4.3a and b. Subhedral granular pentlandite was observed on pyrrhotite grain boundaries and varied between 50 and 150 µm in size. Aggregations of granular pentlandite were sometimes associated with irregular shaped chalcopyrite grains. Exsolved flame pentlandite was relatively abundant along pyrrhotite grain boundaries and fractures. Individual flames were typically 5 µm wide and 30 µm in length and some very intricate feather-like textures were observed. Individual pentlandite flames were also mantled by magnetic pyrrhotite as shown in figure 4.3f. Pentlandite appeared to be relatively unaltered and the violarite described by van Zyl (1996) was not noted here.

*Other Minerals*

Chalcopyrite and pyrite were both relatively common in the Nkomati MSB pyrrhotite. Chalcopyrite grains were typically irregular in shape and associated with aggregations of granular pentlandite or magnetite (Figure 4.3b, c). Pyrite grains were euhedral with a well developed cubic habit and varied in size by several orders of magnitude (e.g. from 50 to 5000 µm). Magnetite was also relatively abundant and formed anhedral grains which varied from rounded to elongate (Figure 4.3c). Variable degrees of ilmenite exsolution forming very fine

grained exsolution lamellae less than 10 µm in size and hosted by magnetite were also observed.

**Nkomati MMZ Pyrrhotite**

*Pyrrhotite*

The occurrence of pyrrhotite in the two Nkomati MMZ samples was quite distinct from one another although both contained large sulfide blebs with pyrrhotite occurring as the dominant host phase from the MSS (Figure 4.4a-d). In sample *MMZ-1* pyrrhotite occurred in discrete sulfide blebs and individual grains that were up to 1 mm in size. Pyrrhotite in both samples appeared to show a very distinct parting developed parallel to the direction of flame pentlandite exsolution, but closer examination revealed the "parting" was in fact very fine-grained elongate rod-like inclusions of magnetite (30 µm in length, 2 µm in width; Figure 4.4c). The fine-grained magnetite inclusions suggest that the MSS must have contained some dissolved oxygen upon cooling and crystallisation of pyrrhotite. These magnetite inclusions were more common in sample *MMZ-1* than *MMZ-4*, whereas the occurrence of magnetite as larger anhedral grains (up to 200 µm in size) hosted by pyrrhotite was restricted to sample *MMZ-4* (Figure 4.4d). The individual grain size of pyrrhotite in sample *MMZ-4* was also slightly smaller (100-200 µm) relative to sample *MMZ-1*.

Treatment of pyrrhotite with the magnetic colloid revealed that sample *MMZ-1* was entirely magnetic (Figure 4.4e), whereas sample *MMZ-4* consisted of inter-grown magnetic and non-magnetic pyrrhotite (Figure 4.4f) more similar to the pyrrhotite from the MSB (Figure 4.3d-f). Individual lamellae of magnetic pyrrhotite in sample *MMZ-1* were up to 100 µm in length and 10 µm in width. These lamellae were always parallel to one another within a grain and also showed thickness zonation (see also Figure 2.12). Magnetic pyrrhotite lamellae in sample *MMZ-4* tended to be smaller (50 µm in length, < 10 µm in width) and sparser and typically hosted by the non-magnetic phase (Figure 4.4f). Concentrations of magnetic pyrrhotite were also observed on pyrrhotite grain boundaries. The relative proportion of magnetic to non-magnetic pyrrhotite in sample *MMZ-4* tended to be quite variable with some domains dominated by magnetic pyrrhotite and vice versa.

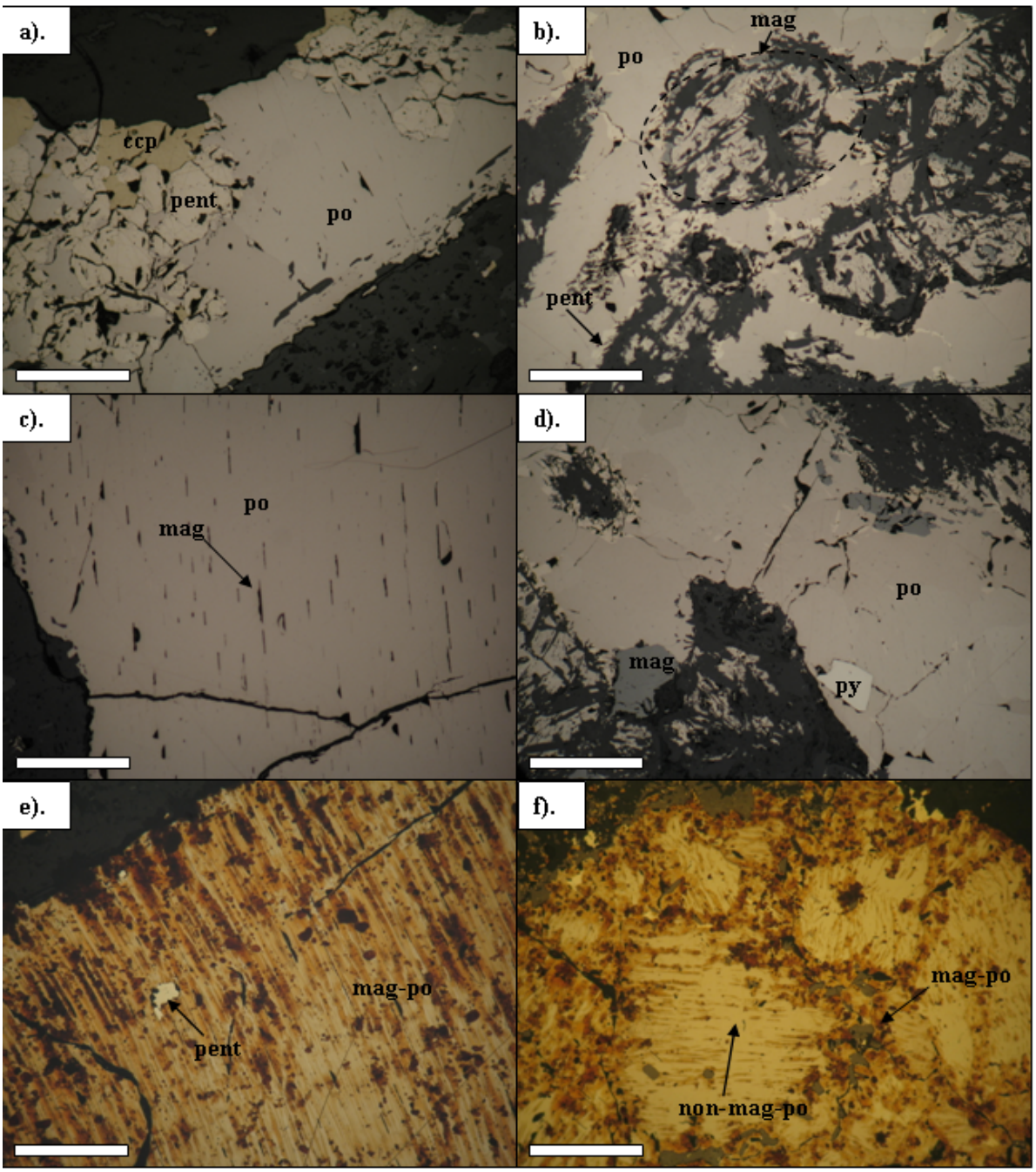


**Figure 4.4:** Photomicrographs of the Nkomati Main Mineralised Zone (MMZ) pyrrhotite shown in RPL. (a) Typical sulfide bleb of chalcopyrite and pentlandite with pyrrhotite as the host phase in sample *MMZ-1*. (b) Net textured sulfide intergrown with acicular tremolite from sample *MMZ-4*. See marked ellipse highlighting the outline of a relict silicate. (c) Very fine-grained magnetite inclusions hosted by pyrrhotite in sample *MMZ-1*. (d) Net texture pyrrhotite with anhedral magnetite and subhedral pyrite in sample *MMZ-1*. (e) Magnetic colloid treatment shows sample *MMZ-1* is entirely magnetic pyrrhotite. Note the thickness zonation evident in the magnetic pyrrhotite lamellae. (f) Magnetic colloid treatment shows intergrowths of both magnetic and non-magnetic pyrrhotite in sample *MMZ-4.* Scale bar represents 200µm.

*Pentlandite*

Pentlandite commonly occurred as granular pentlandite that was developed along the margins of the multi-mineralic sulfide domains and net textured sulfide blebs (Figure 4.4a, b). Individual grains were ~ 200 µm in size and showed well-developed octahedral cleavage. Granular pentlandite tended to have an irregular pock marked texture which was previously described by van Zyl (1996) as due to the development of very fine-grained violarite inclusions. Pentlandite flames up to 30 µm in length and less than 5 µm in width also occurred, but were fairly sparse in both MMZ samples.

*Other Minerals*

Chalcopyrite was noted in both samples of MMZ ore examined and occurred as large euhedral grains (300 µm) associated with the boundary of the large sulfide domains (Figure 4.4a) and also as very fine-grained monomineralic inclusions (< 50 µm) hosted by the silicate minerals. Pyrite was recognised in both occurrences of pyrrhotite examined in the MMZ ore, but was more common for sample *MMZ-4* where it occurred as medium-grained euhedral to subhedral grains hosted by pyrrhotite (Figure 4.4d). Pyrite in sample *MMZ-1* more commonly occurred as fine-grained lenses less than 10 µm in width forming partial rims to the sulfide domains. Magnetite was also recognised in two different morphologies. The first of which was discrete magnetite grains and the second, very fine-grained inclusions in pyrrhotite forming parallel rods situated in the same direction as the pentlandite flame exsolution suggesting that their formation was crystallographically controlled (Figure 4.4c). Both occurrences of magnetite were recognised in sample *MMZ-4*, whereas in *MMZ-1* only the very fine-grained magnetite was recognised. Some oxy-exsolution of ilmenite from magnetite was recognised in the larger anhedral magnetite grains from pyrrhotite sample *MMZ-4*.

### 4.2.3 Phoenix Pyrrhotite

Pyrrhotite samples sourced from the Phoenix ore deposit in this study were generally massive in nature although they contained some irregular shaped, millimetre sized silicate inclusions. Sulfide minerals hosted by the silicate inclusions tended to be fairly resorbed (Figure 4.5a). The Phoenix ore was fairly heavily fractured and dominated by pyrrhotite as the host sulfide with abundant flame pentlandite, lesser chalcopyrite and pyrite.

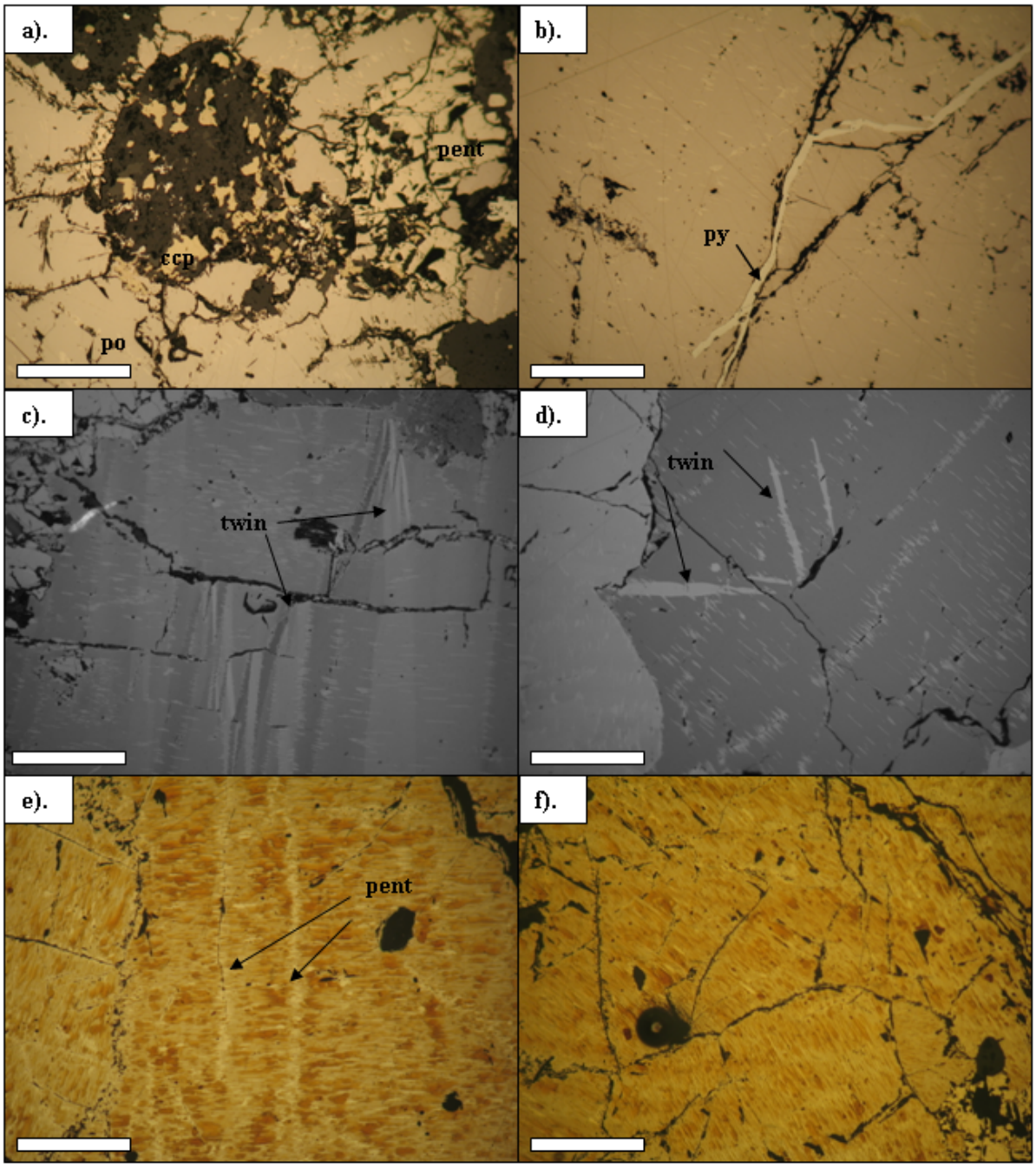


**Figure 4.5:** Photomicrographs of the Phoenix massive sulfide ore shown in RPL and XPRL (c, d). (a) Silicate inclusion hosted by the massive sulfide. Note the resorbed nature of the pyrrhotite hosting the silicate inclusion. (b) Pyrite vein hosted by pyrrhotite, which in turn hosts multiple flame pentlandite lamellae. (c, d) Twinning in pyrrhotite. Feathered textures belong to the flame pentlandite lamellae. (e, f) Magnetic colloid treatment shows Phoenix pyrrhotite is magnetic. Note the exsolution of flame pentlandite parallel from a fracture, coincident to the direction of magnetic pyrrhotite lamellae in (e). Scale bar represents 200 µm.

*Pyrrhotite*

Pyrrhotite occurred as large, well-developed grains up to a few millimetres in size although grain boundaries were marked by extensive fracturing (Figure 4.5a, b). The grains showed limited variation in size in the massive sulfide ore whereas for pyrrhotite hosted by silicate inclusions, individual grains were as small as 100 µm. Pyrrhotite grains hosted by silicate inclusions showed extensive resorption on grain boundaries (Figure 4.5a). Occasional twinning was also visible as discrete elongate lamellae up to 200 µm long and 30 µm wide from which pentlandite flame exsolution occurred (Figure 4.5 c, d, see also Figure 2.12).

Use of the magnetic colloid method illustrated that Phoenix pyrrhotite was entirely magnetic with no evidence of the non-magnetic pyrrhotite phase (Figure 4.5e, f). Individual magnetic pyrrhotite lamellae highlighted by the use of the colloid were always parallel to one another within a single grain. Sometimes the magnetic pyrrhotite lamellae were truncated by a perpendicularly running feature (e.g. twin boundary, grain boundary or fracture) from which abundant pentlandite flame exsolution occurred, parallel to the direction of the magnetic pyrrhotite lamellae (Figure 4.5e).

*Pentlandite*

Pentlandite commonly occurred in two textural settings, with the third only occurring occasionally. Pentlandite in the Phoenix deposit was encountered as large mosaic textured, granular pentlandite domains up to several millimetres in size. Individual grains of granular pentlandite were 100 to 200 µm in size, and showed parting as well as well-developed triangular pits indicative of their cubic cleavage (Figure 4.5a). The second and far more common occurrence of pentlandite was exsolved flame pentlandite lamellae hosted by pyrrhotite (Figure 4.5b). These “featherlike” flames, less than 5 µm in width but up to 30 µm in length were always parallel to one another, confirming the crystallographic control during the exsolution process. Pentlandite flames were recognised as exsolution lamellae from pyrrhotite grain boundaries, fractures and twin planes. Granular pentlandite was subtly more yellow than the cream flame pentlandite. A third and more minor occurrence of pentlandite consisted of granular pentlandite veins linking mosaic textured pentlandite domains to one another across the ore sample and which typically occurred in association with pyrite.

*Other Minerals*

Chalcopyrite was generally fairly sparse in the massive samples examined and where observed, occurred in association with granular pentlandite domains or pyrite veins. Some coarse grained chalcopyrite was however, recognised within the silicate inclusions. Unlike pyrrhotite hosted by the silicate inclusions, the chalcopyrite showed no indication of extensive resorption. Pyrite commonly occurred as irregular shaped veins cross cutting the pyrrhotite (Figure 4.5b). These veins varied in width between 20 and 60 µm and appeared to show no distinct grain boundaries. Within the pyrite veins, occasional inclusions hosting very fine grained anhedral sphalerite (< 10 µm) were also observed. Pyrite hosted by the silicate inclusions was very dissimilar to that in the massive sulfide, since euhedral pyrite cubes (50 µm) were recognised in conjunction with other finer grained resorbed spherules of pyrite.

### 4.2.4 Sudbury Pyrrhotite

*Overview of sulfide mineralogy*

Sulfide mineralization from the Copper Cliff North (Figure 4.6), and Gertrude and Gertrude West pyrrhotite samples (Figure 4.7, 4.8) from Sudbury examined in this study occurred in two textural settings as follows:

i) Massive sulfide to semi-massive sulfides
ii) Disseminated sulfides

The first texture comprising massive sulfide was the dominant texture in the Copper Cliff North and Gertrude West ores (Figure 4.7a), whereas the Gertrude pyrrhotite tended to be massive to semi-massive. All three ores contained silicate inclusions of several millimetres in size and which hosted disseminated sulfides. The disseminated sulfides were mostly comprised of pyrrhotite although occasional chalcopyrite was present. Pyrrhotite hosted by silicate inclusions was generally irregular in shape and varied in size from 50 µm (Copper Cliff North) to 200 µm (Gertrude).

**Sudbury Copper Cliff North (CCN) Pyrrhotite**

*Pyrrhotite*

Pyrrhotite occurred in three textural forms within the massive sulfide ore. The first consisted of coarse-grained, well-developed euhedral pyrrhotite grains up to 2 mm in size showing perpendicular partings (Figure 4.6a). The second textural form consisted of medium-grained aggregations of pyrrhotite grains on the order of 200 µm in size. The third textural form occurred as finely disseminated pyrrhotite grains hosted by silicate inclusions. Examination of coarse-grained pyrrhotite showed that the seemingly homogeneous pyrrhotite showed the development of several varieties of twinning including discrete lamellae (up to 200 µm in length and 50 µm in width) and also more irregular shaped twins (Figure 4.6b).

Pyrrhotite was dominated by the non-magnetic phase with occasional magnetic pyrrhotite lamellae (< 5 %) present at the grain boundaries of pentlandite in all the textural forms of its occurrence (Figure 4.6c, d). Although the morphology of the magnetic pyrrhotite was not always well defined by the colloid, some discrete lamellae 20-30 µm radiating from the pentlandite grain boundaries could be recognised.

*Pentlandite*

Pentlandite occurred in three textural relationships in the Sudbury CCN pyrrhotite. The first and most common textural relationship consisted of granular pentlandite showing well-developed octahedral cleavage. This granular pentlandite had a distinctive brecciated appearance and consisted of many individual grains (up 250 µm in size) forming a pentlandite aggregate several millimetres in size. The second textural occurrence comprised granular pentlandite "veins" on pyrrhotite grain boundaries (Figure 4.6a, d), with individual pentlandite grains between 50 and 100 µm in size. Occasional chalcopyrite grains 10-20 µm in size were associated with the pentlandite veins. The third textural occurrence of pentlandite was caused by pentlandite exsolution from the granular veins, resulting in the formation of finely developed flames of pentlandite that extended in excess of 30 µm away from pentlandite granular veins. Pentlandite flames which exsolved from fractures and grain boundaries within the pyrrhotite MSS were generally rather rare, although when present were noted to display intricate feather-like textures and were free from fracturing unlike vein and granular pentlandite.

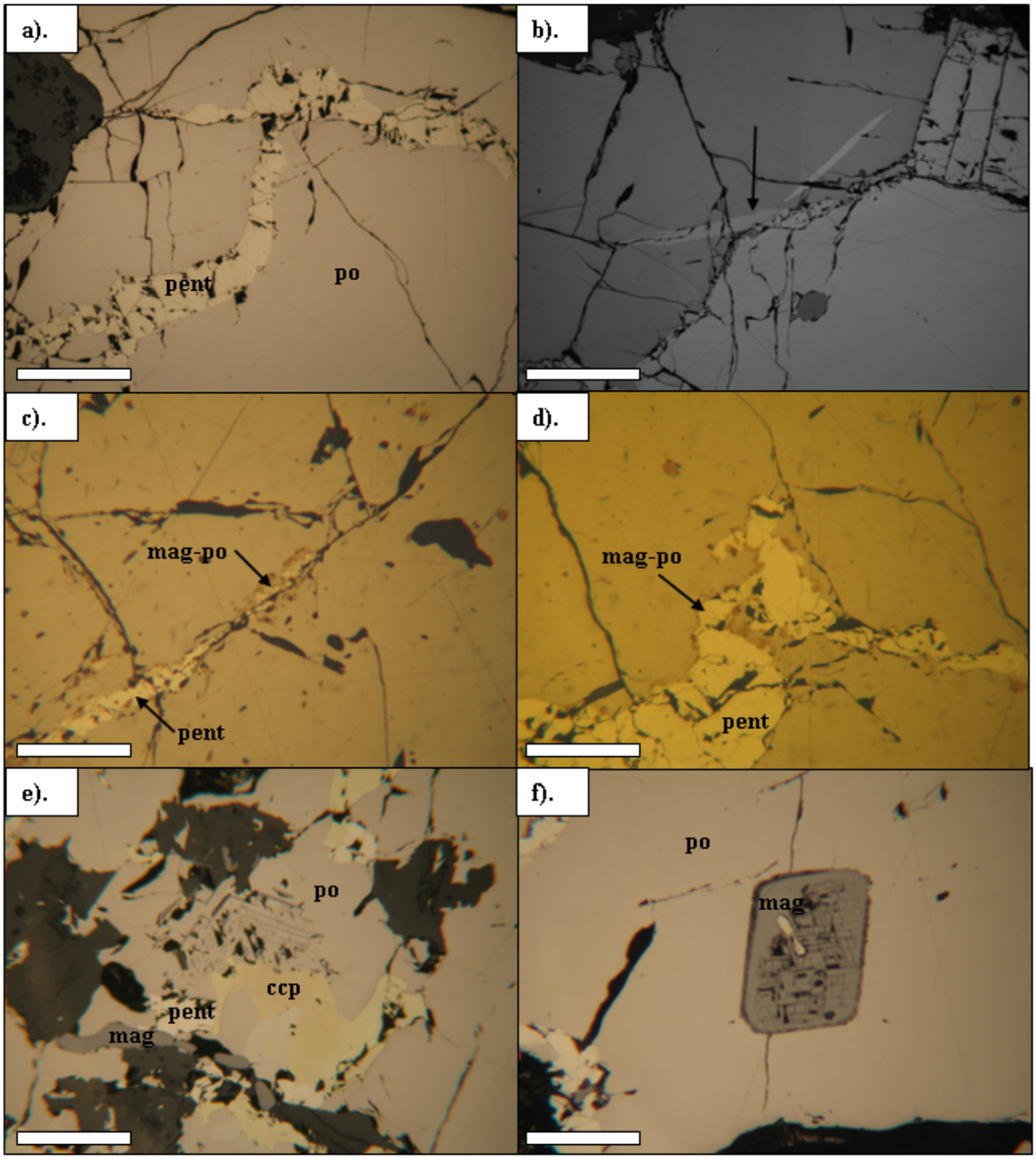


**Figure 4.6:** Photomicrographs of Sudbury Copper Cliff North ore shown in RPL and XPRL (b). (a) Massive sulfide texture with pyrrhotite as the host phase. Pyrrhotite grain boundaries are intersected by veins of granular pentlandite. (b) Twinning in pyrrhotite, shown in XPL. (c) Magnetic colloid treatment shows non-magnetic pyrrhotite hosting a vein of fine-grained pentlandite mantled by a thin rim of magnetic pyrrhotite. (d) Magnetic colloid treatment shows non-magnetic pyrrhotite hosting granular pentlandite mantled by a thin rim of magnetic pyrrhotite. (e) Intergrowth of magnetite, pentlandite, chalcopyrite and pyrrhotite. (f) Euhedral titanomagnetite grain with cross cutting exsolved lamellae of ilmenite. The titanomagnetite grain is also mantled by ilmenite. Scale bar represents 200 µm for all photomicrographs.

*Other Minerals*

Chalcopyrite occurred as individual chalcopyrite grains up to 50 µm in size that were hosted by both pentlandite and pyrrhotite (Figure 4.6e). The chalcopyrite grains were recognised in association with granular pentlandite veins and also the more brecciated granular pentlandite domains. Where chalcopyrite occurred in association with granular pentlandite domains, the individual grains were as large as 400 µm.

Individual magnetite grains were fairly variable in their shape occurring as well developed euhedral crystals with octahedral cleavage (400-500 µm) to extensively resorbed grains consisting of multiple magnetite lamellae (Figure 4.6e, f). Magnetite grains showed octahedrally exsolved lamellae of ilmenite up to 100 µm in length and less than 5 µm in width, orientated at $120^0$ to each other (Figure 4.6f). The abundant oxy-exsolution of ilmenite from magnetite here suggested that was relatively titaniferous in composition. These magnetite grains were sometimes rimmed by a combination of ilmenite and another dark mineral which Naldrett and Kullerud (1967) suggested was hercynite.

No pyrite was recognised in any of the Copper Cliff North pyrrhotite samples examined here even though a thorough search was made for it. Occasional small euhedral grains hosted by pyrrhotite with high reflectivity were also observed and may represent one of the accessory phases such as the sulphoarsenides or platinum group minerals recognised in other studies of the Sudbury ores (e.g. Naldrett and Kullerud, 1967; Magyarosi *et al.*, 2002; Szentpéteri *et al.*, 2002).

**Sudbury Gertrude and Gertrude West Pyrrhotite**

*Pyrrhotite*

The overall occurrence of pyrrhotite in the Gertrude and Gertrude West samples was similar to Copper Cliff North pyrrhotite, consisting of coarse-grained, medium-grained and fine-grained pyrrhotite occurrences (Figure 4.7, 4.8). The fine-grained pyrrhotite occurrences were more common in the Gertrude sample given its semi-massive nature (Figure 4.7a). These fine-grained pyrrhotite silicate intergrowths generally consisted of fine-grained (30 µm) euhedral crystal growths and formed the gradational boundary between the silicate inclusions and sulfide matrix (Figure 4.7a).

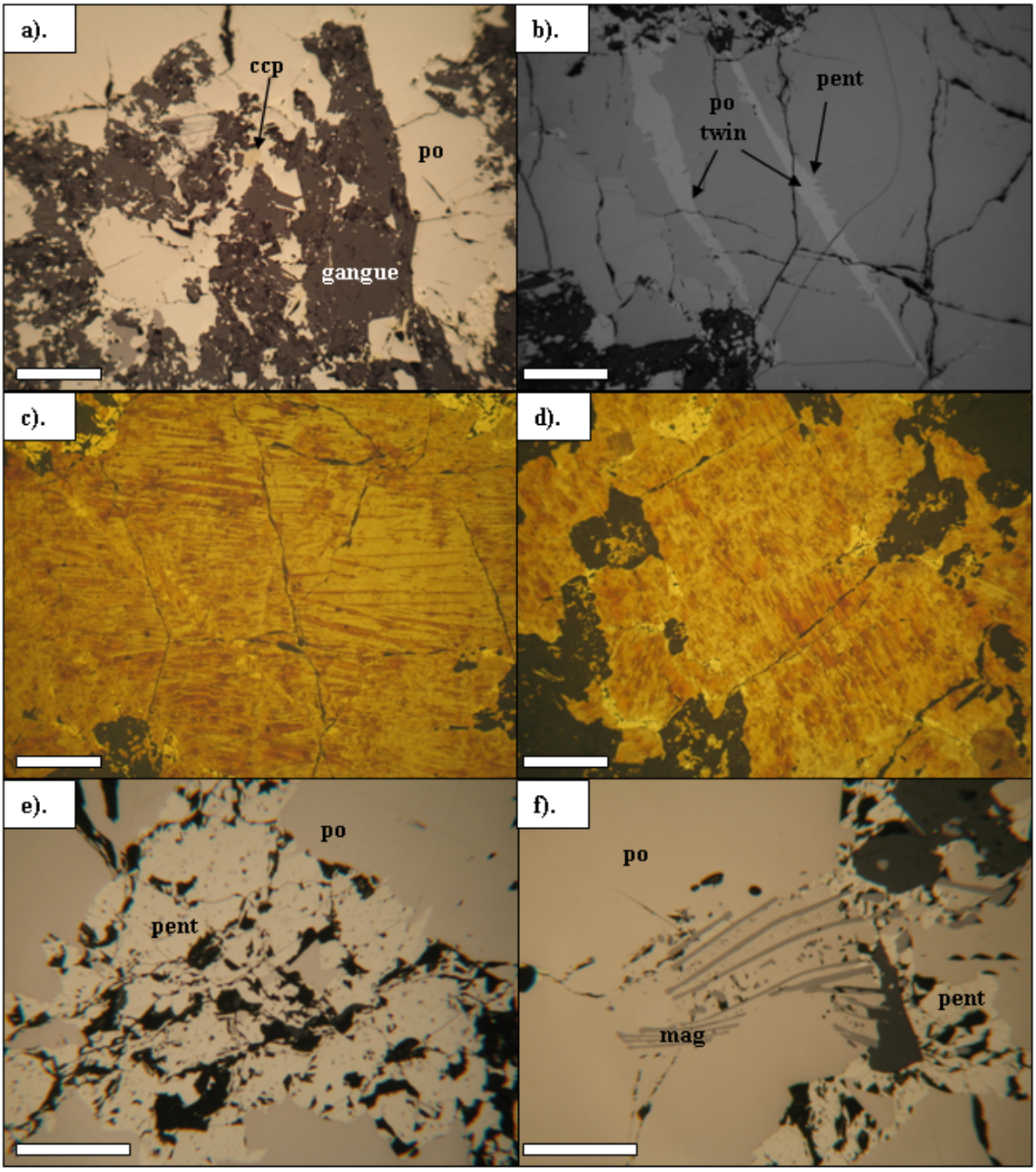


**Figure 4.7**: Photomicrographs of Sudbury Gertrude pyrrhotite shown in RPL and XPRL (b). (a) Irregular shaped boundaries between semi-massive sulfides and silicate inclusions. (b) Twinning in coarse grained pyrrhotite shown in XPL. Note the flame pentlandite exsolved from the twin boundaries. (c ,d) Magnetic colloid treatment shows Gertrude pyrrhotite is almost entirely magnetic pyrrhotite. (e) Granular pentlandite domains with characteristic "pockmarked" texture due to very fine-grained pyrite inclusions. (f) Extensively resorbed titanomagnetite hosted by pyrrhotite. Scale bar represents 200 µm in (e, f) and 500 µm for the rest.

Gertrude West pyrrhotite was characterised by a well-developed parting (Figure 4.8a), which although present in the Gertrude pyrrhotite was not as well defined. Other internal features recognised in the Gertrude and Gertrude West pyrrhotite samples included the abundance of twinning and exsolution of flame pentlandite from pyrrhotite twin boundaries (Figure 4.7b). Some of the lamellar twins were observed to cross cut grain boundaries and were up to 2 mm in length.

Both the Gertrude and Gertrude West pyrrhotite samples were dominated by the magnetic pyrrhotite phase that showed multiple lamellae with distinctive thickness zonation features (Figure 4.7c, d; 4.8b, c). Other textural features noted with the magnetic colloid included composite lamellae (multiple generations of lamellae located at $60^0$ to one another) and box work textures (see Figure 2.12). In some areas, the magnetic colloid did not appear to cover all the pyrrhotite, suggesting that a minor component of non-magnetic pyrrhotite could exist (Figure 4.7c).

*Pentlandite*

The occurrence of pentlandite in the Gertrude and Gertrude West ores was similar to Copper Cliff North ore since pentlandite occurred in brecciated granular pentlandite domains, granular pentlandite veins and as flame pentlandite. The only notable difference in pentlandite between the ores was the occurrence of a “pockmarked” texture in the granular pentlandite domains and veins (Figure 4.7e, 4.8d), whereas the flame pentlandite was free from this alteration. Closer examination of the pockmarks revealed very fine grained, subhedral pyrite inclusions less than 10 μm in size that were confirmed with EMP analysis.

*Other Minerals*

Chalcopyrite was fairly sparse in the Gertrude and Gertrude West pyrrhotite samples and where present occurred as irregular shaped blebs in association with granular pentlandite domains or veins. The chalcopyrite was fairly dark yellow in colour possibly due to the presence of very fine grained anisotropic lathes (< 10 μm) which could possibly represent cubanite. Chalcopyrite was also recognised inter-grown with silicate gangue (Figure 4.7a).

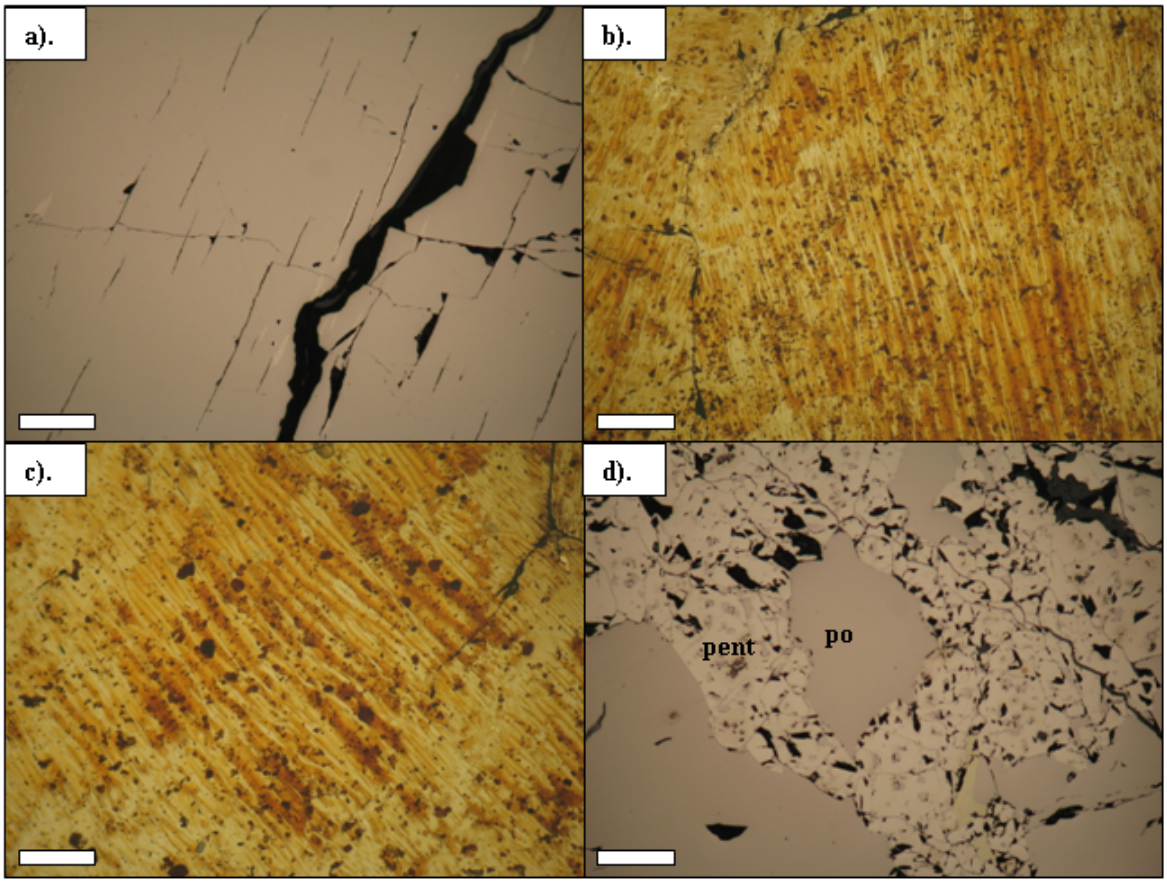


**Figure 4.8**: Photomicrographs of Sudbury Gertrude West pyrrhotite shown in RPL. (a) Parting developed in coarse-grained pyrrhotite. (b, c) Magnetic colloid treatment shows Gertrude West pyrrhotite is entirely magnetic. (d) Granular pentlandite domains with characteristic "pockmarked" texture caused by very fine-grained pyrite inclusions. Scale bar represents 200 µm.

Titanomagnetite in association with lamellae of ilmenite exsolved by oxy-exsolution were common. Titanomagnetite occurred as anhedral grains 50 to 100 µm in size or as extensively resorbed lamellae of titanomagnetite hosted by pyrrhotite (Figure 4.7f). No discrete ilmenite grains were observed.

Occasional small euhedral grains hosted by pyrrhotite with high reflectivity were also observed and could represent one of the accessory phases such as the sulphoarsenides or platinum group minerals recognised in other studies of the Sudbury ores (e.g. Naldrett and Kullerud, 1967; Magyarosi *et al.*, 2002; Szentpéteri *et al.*, 2002).

## 4.3 Crystallography

In order to investigate the crystallographic properties of the pyrrhotite samples from nickel and platinum group element ore deposits forming part of this study, pyrrhotite single crystal specimens were analysed by single crystal x-ray diffraction (Section 3.2.3). The aim of the crystallographic studies was primarily to determine the crystallography and unit cell dimensions (Section 1.4) from which the pyrrhotite superstructure could be deduced. The results obtained from the single crystal XRD of the pyrrhotite crystals are shown in table 4.1 along with selected pyrrhotite cell dimensions from the literature. The selection of pyrrhotite single crystals with well-developed crystallinity and without any evidence of twinning was limited to the Impala Merensky Reef (sample *IMP-1*), Phoenix and Sudbury CCN pyrrhotite samples. The complete structure solutions for the Impala Merensky Reef pyrrhotite (sample *IMP-1*) and the Sudbury CCN pyrrhotite can be found in De Villiers *et al.* (In Prep) and De Villiers *et al.* (Submitted).

**Table 4.1:** Summary of the cell parameters obtained for pyrrhotite single crystals in this study (Impala Merensky Reef sample *IMP-1*, Phoenix, Sudbury CCN pyrrhotite). Comparative cell dimensions from the literature are also shown. [1] This study [2] De Villiers *et al.* (In Prep) [3] Tokonami *et al.* (1972) [4] Powell *et al.* (2004) [5] De Villiers *et al.* (Submitted) [6]Morimoto *et al.* (1975b).

| **Type** | 4C Magnetic | 4C Magnetic | 4C Magnetic | 4C Magnetic | 5C Non-mag | 5C Non-mag |
|---|---|---|---|---|---|---|
| **Composition** | $Fe_7S_8$ | $Fe_7S_8$ | $Fe_7S_8$ | $Fe_7S_8$ | $Fe_9S_{10}$ | $Fe_9S_{10}$ |
| **Crystallography** | Monoclinic | Monoclinic | Monoclinic | Monoclinic | Ortho. | Ortho. |
| **Symmetry** | C2 | - | F2/d | C2/c | Cmca | C*ca |
| **a (Å)** | 11.890 | 11.866 | 11.902 | 11.926 | 6.893 | 6.885 |
| **b (Å)** | 6.872 | 6.851 | 6.859 | 6.882 | 11.939 | 11.936 |
| **c (Å)** | 22.785 | 22.710 | 22.787 | 12.925 | 28.673 | 28.676 |
| **β** | $90.12^0$ | $90.08^0$ | $90.26^0$ | $118.02^0$ | - | - |
| **Location** | Impala Merensky | Tati Phoenix | Kisbanya, Romania | Synthetic | Sudbury CCN | Kishu, Japan |
| **References** | 1, 2 | 1 | 3 | 4 | 1, 5 | 6 |

### 4.3.1 Merensky Reef Pyrrhotite

Use of the magnetic colloid on pyrrhotite samples in Section 4.2 showed that the Impala Merensky Reef sample *IMP-1* pyrrhotite was magnetic. According to the cell dimensions obtained by single crystal x-ray diffraction as shown in table 4.1, the length of the c-axis for the Merensky pyrrhotite was 22.785 Å, which is approximately four times the length of the NiAs unit cell (5.880 Å; Wyckoff, 1963). Therefore, the Merensky pyrrhotite can be classified as 4C magnetic pyrrhotite. The single crystal x-ray diffraction showed monoclinic symmetry in space group C2 for sample *IMP-1*. Table 4.1 also shows that the cell dimensions obtained for the Merensky pyrrhotite were in good agreement with the 4C pyrrhotite analysed by Tokonami *et al.* (1972) using the unconventional F2/d space group (Figure 2.9).

According to the preliminary crystal structure solution obtained by De Villiers *et al.* (In Prep), the theoretical composition of sample *IMP-1* was $Fe_{6.83}S_8$, and which is slightly more iron deficient than the stoichiometric composition $Fe_7S_8$ used by Tokonami *et al.* (1972) and Powell *et al.* (2004). This deviation from the ideal composition is most likely due to the non-stoichiometry which is invariably present in natural pyrrhotite samples.

It is apparent from the powder XRD diffractogram shown in figure 4.9a that the Impala Merensky sample *IMP-1* pyrrhotite showed the characteristic doublet for magnetic, monoclinic 4C pyrrhotite similar to that described in Section 2.2.8 and shown in figure 2.14. The d-spacing obtained for the characteristic monoclinic pyrrhotite doublet was ~ 2.052 and 2.062 Å respectively, which shows reasonable correlation to the ideal spacing derived from the structure of Powell *et al.* (2004) of 2.056 and 2.066 Å.

### 4.3.2 Phoenix Pyrrhotite

Use of the magnetic colloid in Section 4.2 on the Phoenix pyrrhotite showed that it was magnetic and therefore most likely 4C monoclinic pyrrhotite. Single crystal XRD of the Phoenix pyrrhotite sample showed monoclinic symmetry and that the length of the c-axis was 22.710 Å (Table 4.1). This is similar to that obtained for both the Impala Merensky Reef sample *IMP-1* pyrrhotite and the Tokonami *et al.* (1972) pyrrhotite, and confirms that the Phoenix pyrrhotite was monoclinic 4C pyrrhotite. The space group could not be

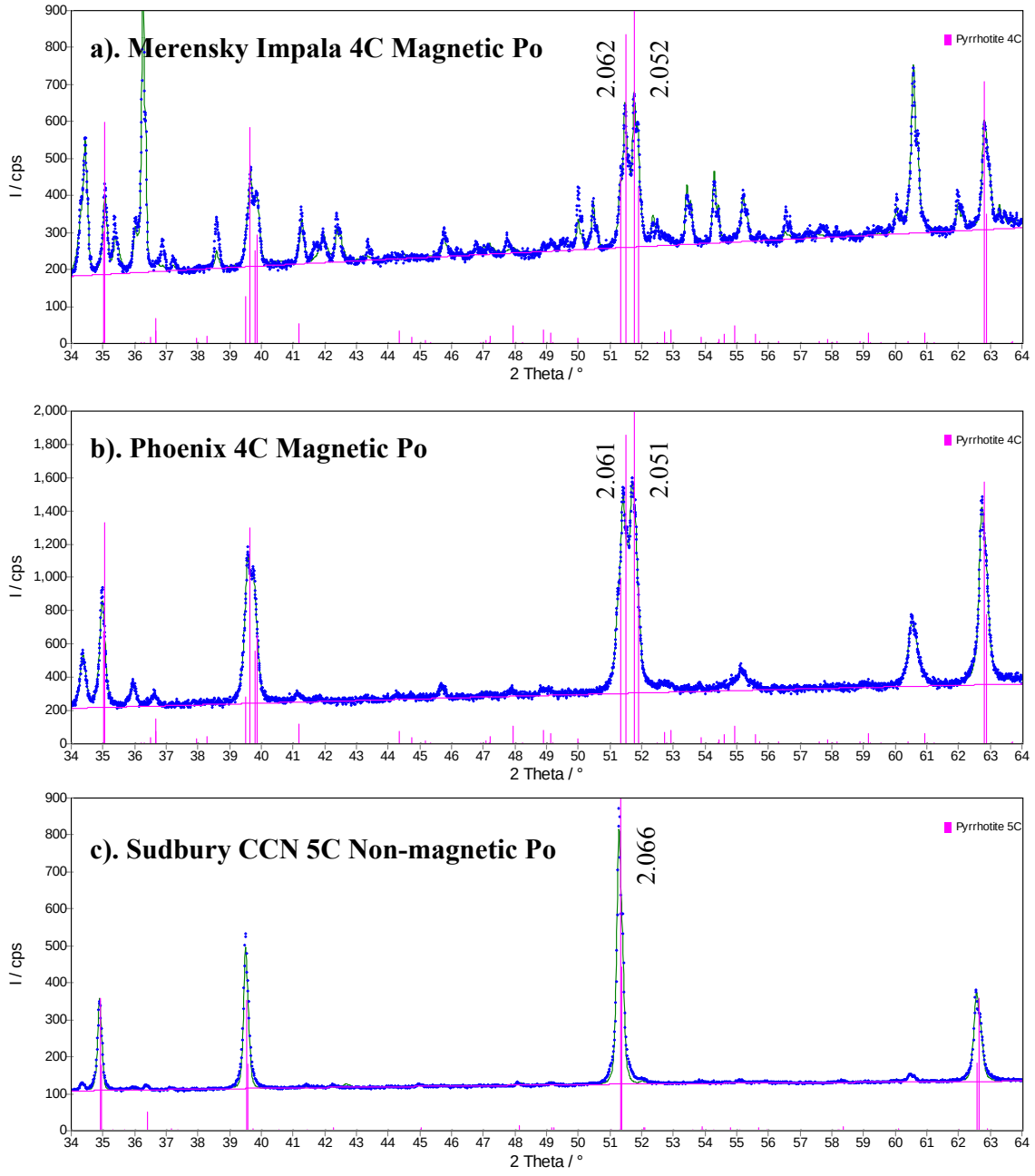


**Figure 4.9:** Diffractograms from powder XRD analysis of (a) Impala Merensky Reef sample *IMP-1* 4C magnetic pyrrhotite (b) Phoenix 4C magnetic and (c) Sudbury CCN 5C non-magnetic pyrrhotite samples. The peak positions calculated from the reference structures for magnetic pyrrhotite from Powell *et al.* (2004) and non-magnetic pyrrhotite from De Villiers *et al.*(Submitted) are shown in pink, whereas the measured diffractogram is shown in blue. d-spacings of characteristic peaks are given in Å.

unequivocally determined, most likely as a consequence of the poor crystallinity of the specimen analysed. However, since another suitable single crystal could not be found for complete structure analysis, the cell dimensions obtained here are accepted as sufficient evidence to confirm that the Phoenix pyrrhotite is 4C monoclinic pyrrhotite.

The powder XRD diffractogram of the Phoenix magnetic pyrrhotite in figure 4.9b also shows the characteristic doublet for monoclinic 4C pyrrhotite similar to that described in Section 2.2.8 and shown in figure 2.14. The d-spacing obtained for the characteristic monoclinic pyrrhotite doublet was ~ 2.051 and 2.061 Å respectively, and which showed reasonable correlation to the ideal spacing derived from the structure of Powell *et al.* (2004) of 2.056 and 2.066 Å.

### 4.3.3 Sudbury Pyrrhotite

Preliminary mineralogical characterisation of the Sudbury CCN pyrrhotite showed that it was non-magnetic (Section 4.3) and therefore based on the literature review from Section 2.2, is most likely naturally occurring, NC pyrrhotite. The single crystal XRD results given in table 4.1 show that the c-axis was 28.673 Å in length. This is approximately five times the length of the NiAs unit cell (5.880 Å; Wyckoff, 1963), and hence the Sudbury CCN pyrrhotite was classified as 5C pyrrhotite. The classification of the Sudbury CCN pyrrhotite as 5C pyrrhotite is in agreement with that proposed by Vaughan *et al.* (1971) on their powder diffraction study of pyrrhotite from the Strathcona mine in Sudbury. The cell dimensions for the Sudbury CCN pyrrhotite obtained from single crystal XRD and given in table 4.1 were also similar to that obtained by Morimoto *et al.* (1975b) for 5C pyrrhotite from Kishu mine in Japan. Similarly to the pyrrhotite examined by Morimoto *et al.* (1975b), the Sudbury CCN pyrrhotite displayed orthorhombic symmetry. It should be noted that this is contrary to the common classification of non-magnetic pyrrhotite as “hexagonal” due to the apparent x-ray diffraction symmetry and hexagonal crystal habit (Posfai *et al.*, 2000).

The complete crystal structure of the Sudbury CCN 5C pyrrhotite was subsequently solved by De Villiers *et al.* (Submitted) and will be briefly discussed here. The structure of the Sudbury CCN pyrrhotite is based on sulfur atoms in a hexagonal close packed lattice octahedrally

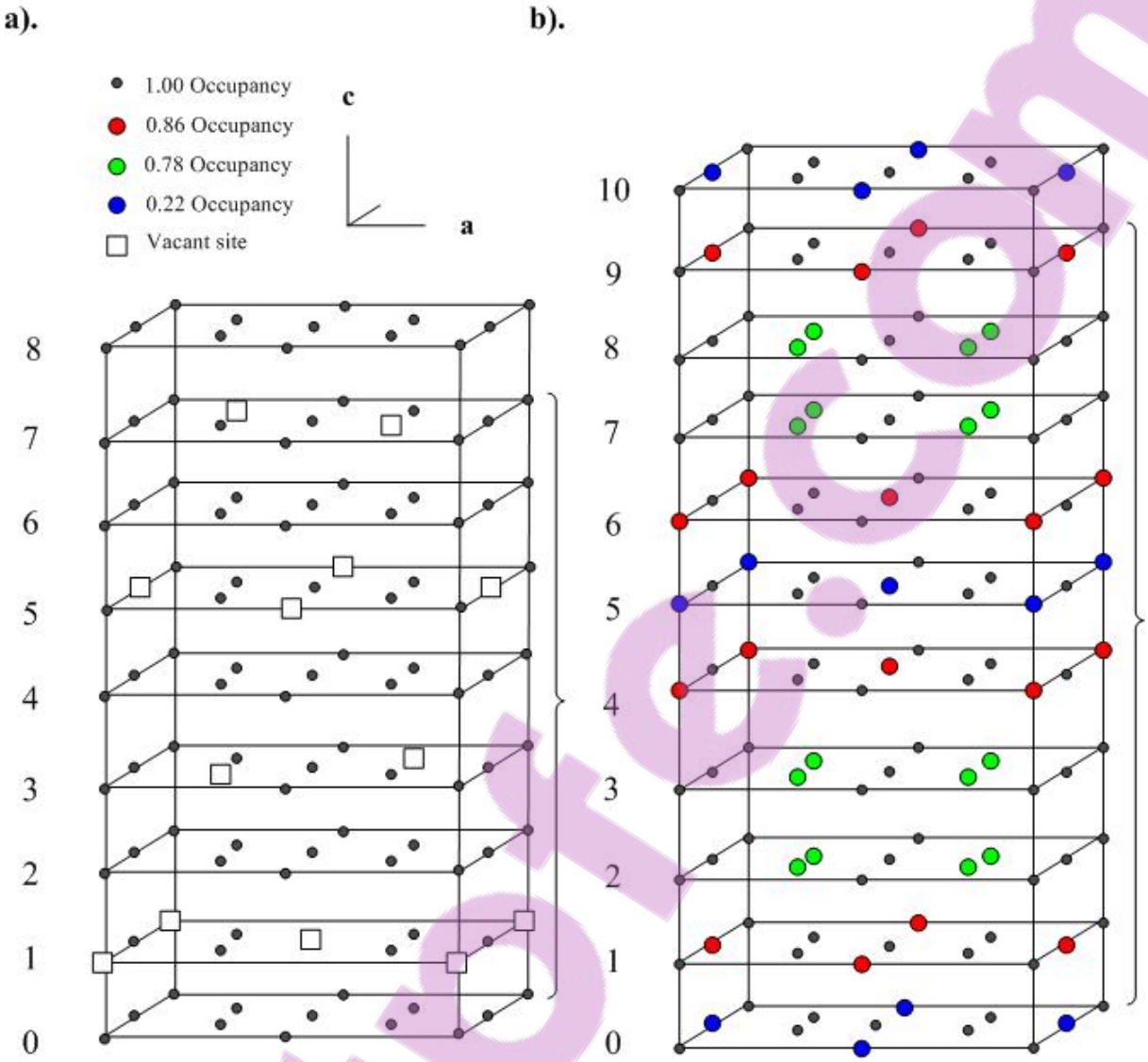


**Figure 4.10:** Illustration of the vacancy distribution of (a) magnetic 4C pyrrhotite from the structure given in Tokonami *et al.* (1972) and (b) non-magnetic Sudbury CCN 5C pyrrhotite from the structure given in De Villiers *et al.* (Submitted). Sulfur sites are omitted for clarity. Layer 0 represents the origin and the brackets indicate a complete unit cell.

coordinated around the metal atoms. These arrays form a series of layers that are vertically stacked on top of one another as shown in figure 4.10. One of key contributions from De Villiers *et al.* (Submitted) is that unlike the 4C pyrrhotite structures of Tokonami *et al.* (1972) and Powell *et al.* (2004), the 5C pyrrhotite structure contains partially filled iron sites as opposed to completely vacant irons sites. These partially filled iron sites are distributed throughout the entire pyrrhotite structure such that no single layer of the structure is fully

occupied. Rather, every layer consists of a series of partially filled iron sites and hence, the annotation "…FAFBFCFD…" where F denotes a fully occupied layer, and A to D vacancy containing layers (Figure 2.8), and which was used in Section 2.2.5 is not applicable here. Consequently, individual layers are described numerically in figure 4.10. The comparison of the pyrrhotite structures in figure 4.10 is based upon the unconventional F2/d unit cell by Tokonami *et al.* (1972), but which is used since it facilitates comparison of the vacancy ordering.

The vacancy distribution of the 5C Sudbury CCN pyrrhotite illustrated in figure 4.10 shows that in addition to the fully occupied iron sites, layer 1 is comprised of four partially filled iron sites with an occupancy of 0.86. This is overlain by layers 2 and 3 which have four partially filled iron sites with an occupancy of 0.78. This is in turn overlain by layers 4, 5 and 6 whereby the partially occupied sites fall in the same positions, although with an occupancy of 0.86, 0.22 and 0.86, respectively. Layers 7 and 8 are a repeat of layers 2 and 3. Layer 9 is a repeat of layer 1. Layer 10 is repeat of layer 9, although the vacancy of the partially occupied sites is 0.22 instead of 0.86. Based on this ordering of iron site occupancies, the formula for the Sudbury CCN single crystal analysed was $Fe_{8.961}Ni_{0.117}Cu_{0.001}S_{10}$ (De Villiers *et al.*, Submitted).

Some correlation however, exists between the position of the partially filled sites of the 5C pyrrhotite and the vacant sites in the 4C pyrrhotite structure (Figure 4.10). The distribution of partially filled iron sites for the 5C pyrrhotite in layers 1, 9 and 10 is similar to the vacant sites in layer 5 of the 4C pyrrhotite. Similarly, the distribution of the partially filled iron sites for the 5C pyrrhotite in layers 4, 5, and 6 is similar to the vacant sites in layer 1 of the 4C pyrrhotite.

The average occupancy for each layer was calculated on the basis that the occupancy of a layer without any vacant sites is 1 and the occupancy of a layer with 2 vacant sites is 0.75. Based on the monoclinic 4C pyrrhotite structure of Tokonami *et al.* (1972) and Powell *et al.* (2004), an occupancy of 0.75 was obtained for the vacancy layers. This results in a saw tooth pattern when the occupancy is described according to the layer number as in figure 4.11. Similarly, the occupancy of 5C pyrrhotite can be calculated to be 0.968 in layers 1, 4, 6 and 9; 0.893 in layers 2, 3, 7 and 8; and 0.817 in layers 5 and 10. Unlike the saw tooth pattern

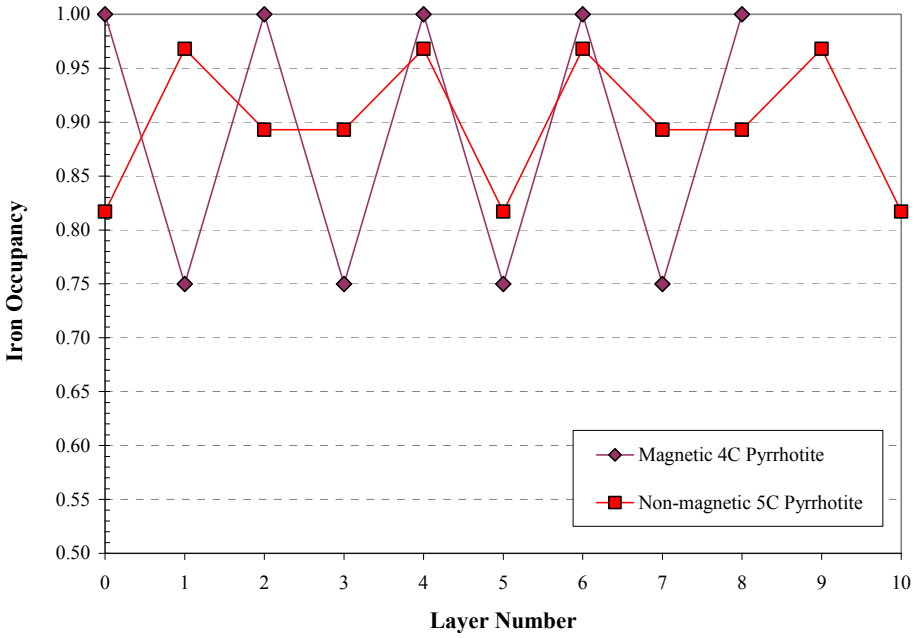


**Figure 4.11:** Occupancy of iron in the different layers of Sudbury CCN non-magnetic 5C pyrrhotite compared to magnetic 4C pyrrhotite based on the crystal structures from De Villiers *et al.*(Submitted) and Tokonami *et al* .(1972), respectively.

observed for 4C pyrrhotite that varied periodically between alternate layers in figure 4.11, the periodicity for 5C pyrrhotite occurred every five layers.

Based upon the structure obtained from the 5C Sudbury CCN pyrrhotite by De Villiers *et al*, (Submitted), the lines forming the characteristic powder diffraction pattern for 5C pyrrhotite could be calculated. These were compared with the actual powder diffraction pattern obtained for the Sudbury CCN pyrrhotite in figure 4.9c where it is evident that there is good agreement. Figure 4.9c also shows that the powder XRD pattern of the Sudbury CCN pyrrhotite contains a characteristic singlet at d = 2.066 Å. This is similar to the observed and calculated d-spacing for 5C pyrrhotite from Vaughan *et al.* (1971) as well as Carpenter and Desborough (1964).

## 4.4 Mineral Chemistry

Previous studies on pyrrhotite mineral chemistry have indirectly derived the chemical composition of the pyrrhotite based on the d-spacing of the 102 reflection following the method developed by Arnold and Reichen (1962). Few have examined the inter- and intra-pyrrhotite compositional variation in mineral chemistry for pyrrhotite from various localities and compared it to the ideal composition of $Fe_7S_8$ (60.4 wt % Fe), $Fe_9S_{10}$ (61.1 wt % Fe), $Fe_{10}S_{11}$ (61.3 wt % Fe) and $Fe_{11}S_{12}$ (61.5 wt % Fe). As such, the following dataset presented here can be considered to be unique in its content, especially since it is based on actual mineral chemistry as opposed to inferred mineral chemistry. The mineral chemistry of pyrrhotite is described first according to locality, then the combined compositions of magnetic and non-magnetic pyrrhotite are compared for the entire pyrrhotite dataset. Individual pyrrhotite analyses are reported in Appendix A.

### 4.4.1 Merensky Reef Pyrrhotite

Chemical analyses of the Impala Merensky Reef pyrrhotite are illustrated in figure 4.12 where analyses from both samples *IMP-1* and *IMP-2* are shown. The petrographic studies (Section 4.2) showed that sample *IMP-1* consisted of entirely magnetic pyrrhotite, whereas *IMP-2* was comprised of intergrown non-magnetic pyrrhotite and troilite.

Iron contents for all Merensky Reef pyrrhotite occurrences varied between 58.7 and 61.9 wt % with the most iron poor compositions occurring for the magnetic pyrrhotite (Figure 4.12a). The most iron rich pyrrhotite was the non-magnetic Merensky Reef pyrrhotite sample *IMP-2*, although the troilite coexisting with this pyrrhotite was even more iron rich (up to 63.1 wt % Fe; Figure 4.12). Accordingly, the most sulfur rich pyrrhotite was the magnetic Merensky Reef sample *IMP-1* (40.2 wt %) and the most sulfur poor pyrrhotite was the non-magnetic Merensky Reef pyrrhotite (37.4 wt %). The measured sulfur contents of troilite were however, even more depleted in sulfur (36.2 wt %).

Three distinct clusters are apparent when the nickel content of the Impala Merensky Reef pyrrhotite is evaluated as shown in figure 4.12b. Merensky Reef troilite was the most nickel

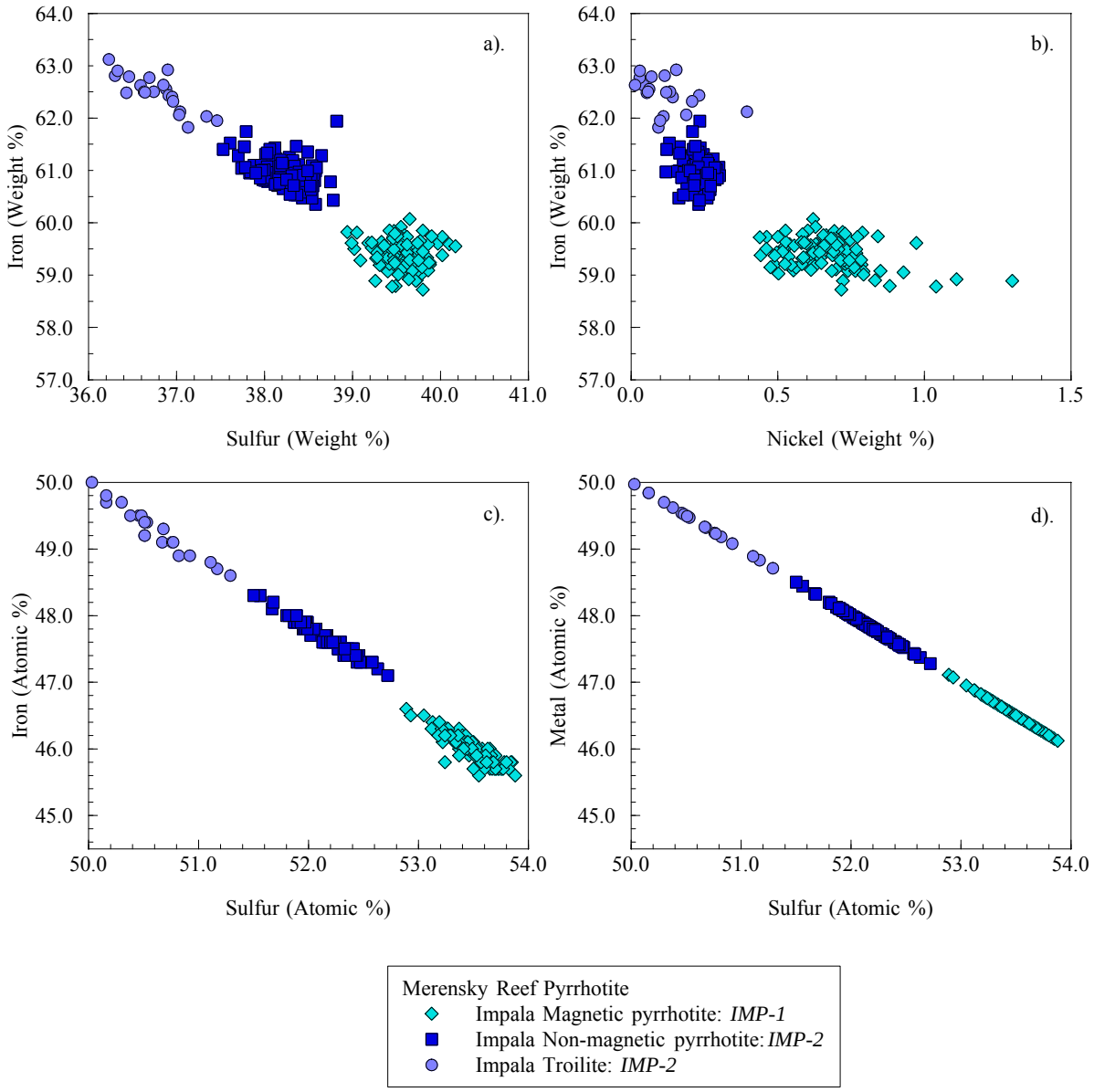


**Figure 4.12:** Mineral chemistry of Merensky Reef magnetic and non-magnetic pyrrhotite shown as both weight % (a, b) and atomic % (c, d).

poor occurrence (< 0.23 wt % Ni) and the coexisting non-magnetic pyrrhotite in sample *IMP-2* was only slightly more nickel rich (0.11 - 0.30 wt %). Magnetic Merensky Reef pyrrhotite sample *IMP-1* however, was significantly the most nickel rich pyrrhotite of the occurrences investigated here (0.44 – 1.30 wt % Ni).

Atomic iron contents for Impala Merensky Reef troilite varied between 48.6 and 50.0 atomic %, and sulfur varied between 50.0 and 51.3 atomic % (Figure 4.12c). It is noted that the

troilite composition was somewhat more iron poor than would be expected for stoichiometric FeS (~ 50% atomic Fe, 50% atomic S), but it is recognised that this was most likely due to contamination from the coexisting non-magnetic pyrrhotite because of the analytical difficulties associated with analysing such fine grained minerals (< 5 µm). The coexisting non-magnetic pyrrhotite sample *IMP-2*, however, varied between 47.1 and 48.3 % atomic iron, and between 51.4 and 52.7 % atomic sulfur. Magnetic pyrrhotite sample *IMP-1* was distinctly more iron poor (45.5 – 46.6 atomic %) and sulfur rich (52.9 – 53.9 atomic %) than the non-magnetic pyrrhotite.

When the atomic iron is graphed against the atomic sulfur composition of the Merensky Reef pyrrhotite occurrences, a fairly linear, negative correlation is observed (Figure 4.12c), although there is some scatter in terms of atomic iron compositions. When the entire element suite analysed is shown as atomic metal (Fe + Ni + Cu + Co) versus sulfur as in figure 4.12d, it is apparent that this scatter was compensated for by the additional metal cations. However, the compensation was almost entirely due to the nickel composition since the contribution of cobalt and copper to the pyrrhotite chemistry was virtually negligible (Appendix A).

In order to determine the ideal or theoretical composition of the different Merensky Reef pyrrhotite samples, the metal to sulfur ratios were calculated and then the ratio normalised to different ideal sulfur proportions. When normalised to 8 sulfur atoms, the metal / sulfur ratio could be used to examine the variation for a pyrrhotite of ideal composition $Fe_7S_8$. When normalised to 10 sulfur atoms, the metal / sulfur ratio could be used to examine the variation of pyrrhotite for an ideal composition of $Fe_9S_{10}$ and so forth. The ratios of all the Merensky pyrrhotite occurrences were subsequently examined to determine their ideal composition and the normalised ratio closest to n (for $Fe_{n-1}S_n$ where $n \geq 8$) selected as the ideal. None of the metal / sulfur ratios obtained corresponded to a composition of $Fe_{10}S_{11}$.

By following such a strategy to determine the ideal composition of Impala Merensky Reef pyrrhotite, the compositional variation in terms of the distribution could be examined and the data illustrated in histogram format. It is apparent from the histogram for magnetic Merensky Reef pyrrhotite shown in figure 4.13a that sample *IMP-1* has an ideal composition close to $Fe_7S_8$. The histogram of the metal / sulfur ratios for magnetic pyrrhotite tends to show a Gaussian distribution and it is noted that the peak of the histogram corresponded with a composition between 6.95 and 7.00 metal cations (34 occurrences) per 8 sulfur anions. The

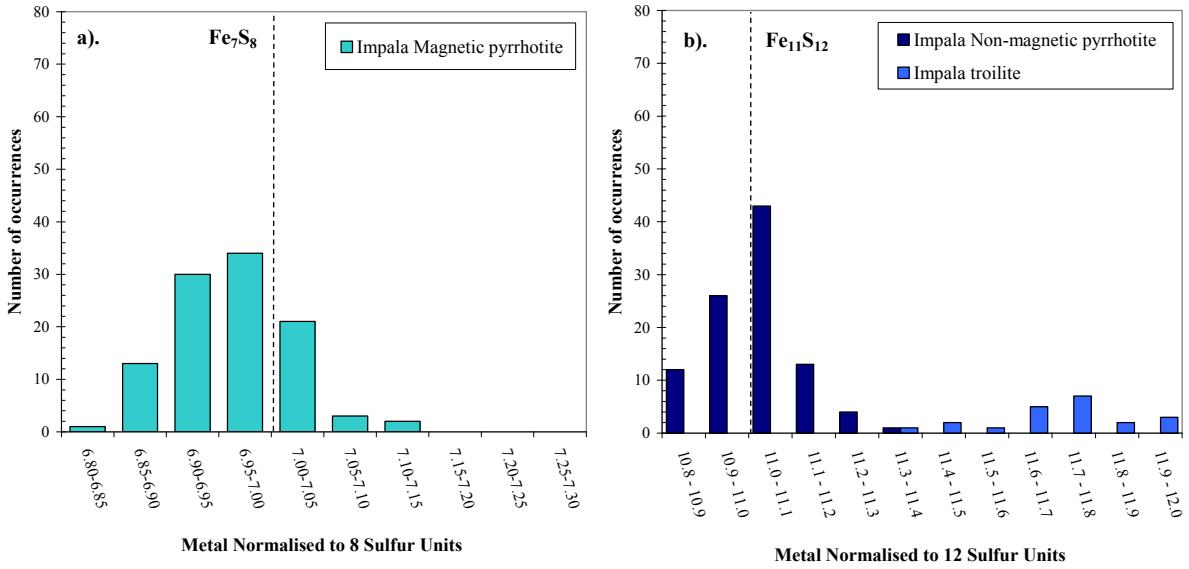


**Figure 4.13:** Histogram of metal / sulfur ratios normalised to differing sulfur contents for Merensky Reef magnetic (a) and non-magnetic (b) pyrrhotite.

ideal composition obtained for non-magnetic Impala Merensky Reef pyrrhotite sample *IMP-2* (Figure 4.13b) was close to $Fe_{11}S_{12}$ and the most commonly occurring composition was actually slightly more iron rich (43 occurrences in the 11.0 – 11.1 bin) than the ideal.

Based on the mineral chemistry, magnetic pyrrhotite from sample *IMP-1* was classified as $Fe_7S_8$ which is in agreement with the assignment of sample *IMP-1* pyrrhotite as 4C monoclinic pyrrhotite from the crystallographic studies (Table 4.1). Given that the non-magnetic pyrrhotite is naturally occurring and not synthetic, it could also be assumed that the pyrrhotite falls into the NC superstructure (Table 2.2). From the mineral chemistry, the composition of the non-magnetic pyrrhotite in sample *IMP-2* was determined to be $Fe_{11}S_{12}$. The NC superstructure of pyrrhotite could be linked to its ideal composition using the relationship of Morimoto *et al.* (1970) whereby $Fe_{n-1}S_n$ ($n > 8$). If *n* is even, then the structure is *n*/2C and therefore pyrrhotite from sample *IMP-2* was classified as 6C pyrrhotite. It is also noted that the 6C pyrrhotite from sample *IMP-2* was intergrown with 2C troilite.

Although only 4C magnetic and 6C non-magnetic pyrrhotite were identified in the Merensky Reef samples examined in this study, this is probably not the only occurrence of pyrrhotite in the Merensky Reef. According to Liebenberg (1970), intergrown magnetic and non-magnetic

pyrrhotite are common. Further sampling of pyrrhotite from the Merensky Reef is therefore recommended, in order to confirm the observations of Liebenberg (1970).

### 4.4.2 Nkomati Pyrrhotite

Iron and sulfur contents of non-magnetic Nkomati pyrrhotite from both the MMZ and MSB illustrated in figure 4.14a are almost identical in composition to each other, and varied from 59.4 to 60.7 wt % iron and between 38.4 and 39.3 wt % sulfur. In contrast, the magnetic pyrrhotite occurrences from the MSB and MMZ show some disparity. Magnetic pyrrhotite from sample *MMZ-4* is compositionally similar to magnetic pyrrhotite from the MSB, both of which were noted to occur in conjunction with non-magnetic pyrrhotite. Magnetic pyrrhotite sample *MMZ-1* from the MMZ however, does not coexist with any other pyrrhotite type and it is this pyrrhotite which is compositionally much more iron poor (58.4 -59.3 wt % Fe) than the other Nkomati magnetic pyrrhotite occurrences (59.1 – 60.2 wt % Fe). In terms of sulfur content, no difference was observed between sample *MMZ-1* and the other magnetic MSB and MMZ (sample *MMZ-4*) pyrrhotite occurrences (39.0 – 39.9 wt % S).

The difference in iron content between the different Nkomati magnetic pyrrhotite occurrences is similarly manifested by the differences in nickel content shown in figure 4.14b. Magnetic MSB and MMZ pyrrhotite (sample *MMZ-4)* coexisting with non-magnetic pyrrhotite was generally more nickel poor (0.26 – 0.67 wt % Ni) than the coexisting non-magnetic MSB and MMZ pyrrhotite (0.55 – 0.90 wt % Ni). Magnetic pyrrhotite sample *MMZ-1* was distinctly more nickel rich (0.66 – 1.20 wt % Ni) than the other pyrrhotite occurrences.

Once the atomic iron and sulfur compositions of the Nkomati pyrrhotite occurrences were calculated it is apparent from figure 4.14c that the different pyrrhotite occurrences have distinctive compositional signatures. Non-magnetic pyrrhotite from both the MSB and MMZ was distinctly more iron rich and sulfur poor than the coexisting magnetic pyrrhotite (46.3 - 47.2 atomic % Fe, 52.3 – 53.1 atomic % S). Although magnetic pyrrhotite sample *MMZ-1* was almost identical in sulfur composition (53.1 – 53.9 atomic % S) to magnetic pyrrhotite

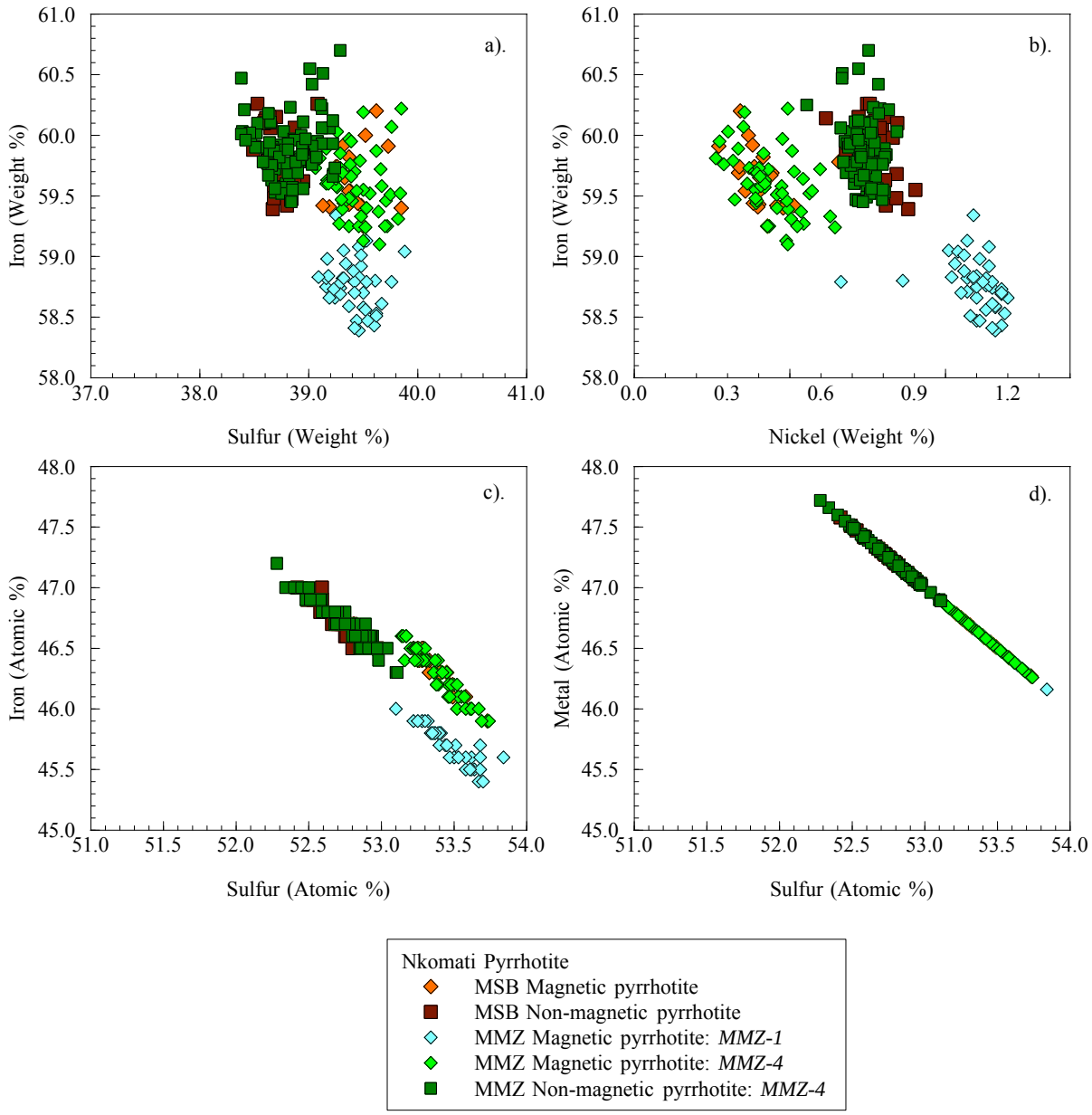


**Figure 4.14**: Mineral chemistry of Nkomati MSB and MMZ magnetic and non-magnetic pyrrhotite shown as both weight % (a, b) and atomic % (c, d).

sample *MMZ-4* and MSB pyrrhotite, the iron content was quite different (45.4 – 46.0 atomic % Fe). These differences in iron content between the magnetic pyrrhotite occurrences were compensated for by the solid solution substitution of nickel for iron. Therefore, the graph of atomic metal versus atomic sulfur shown in figure 4.14d displays an almost perfect negative correlation for all the Nkomati pyrrhotite occurrences.

Given that all the magnetic pyrrhotite occurrences from Nkomati, including sample *MMZ-1* are similar in composition in terms of their atomic metal composition, the mineral chemistry data could be grouped together and a histogram of the distribution of their metal / sulfur ratios compared. The histogram in figure 4.15a shows that magnetic pyrrhotite from Nkomati has an ideal composition close to $Fe_7S_8$. Although the most commonly occurring metal / sulfur ratio is 7.00 – 7.05 per 8 sulfur units for the MSB (11 occurrences) and 6.90 – 6.95 per 8 sulfur units for the MMZ (38 occurrences), it is not clear whether they are statistically different or if the difference is due to the small number of Nkomati MSB magnetic pyrrhotite samples analysed. However, for non-magnetic Nkomati pyrrhotite from both the MMZ and MSB, the histogram is similar with an ideal composition close to $Fe_9S_{10}$ (Figure 4.15b). The most commonly occurring metal / sulfur ratio was 8.90 – 8.95 per 10 sulfur units (43 occurrences in total).

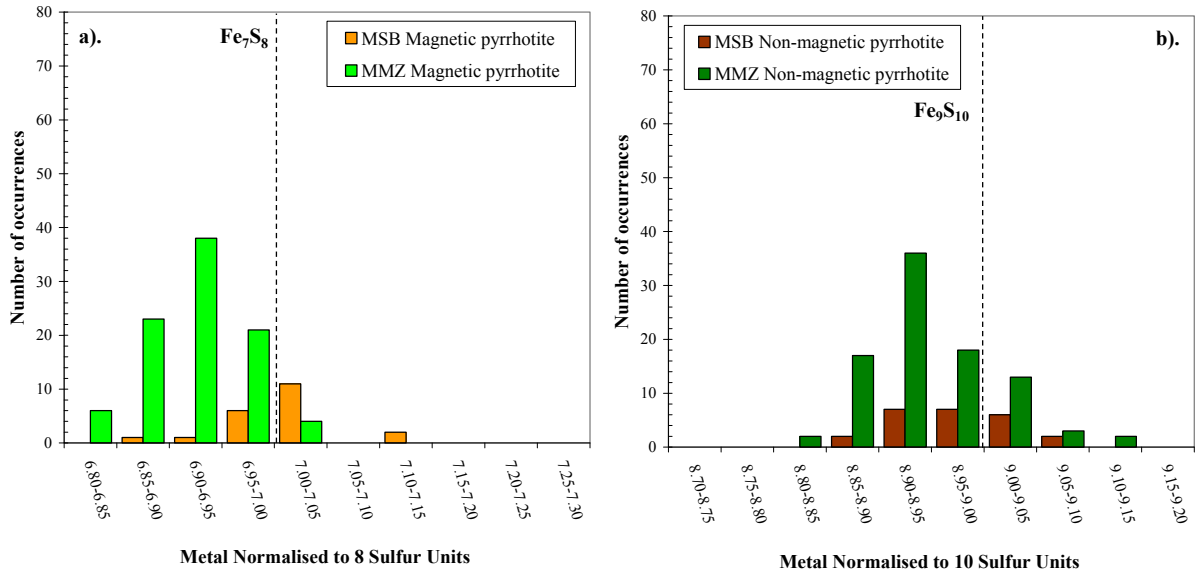


**Figure 4.15**: Histogram of metal / sulfur ratios normalised to differing sulfur contents for Nkomati magnetic (a) and non-magnetic (b) pyrrhotite.

Based on the mineral chemistry, magnetic $Fe_7S_8$ and non-magnetic $Fe_9S_{10}$ were identified for the Nkomati pyrrhotite. According to the relationship of Morimoto *et al.* (1970) this corresponds to 4C and 5C pyrrhotite, respectively. It is probable that 5C pyrrhotite observed in the Nkomati MSB and MMZ samples is also orthorhombic, similar to the 5C Sudbury CCN

pyrrhotite sample examined in the crystallographic studies (Section 4.3; De Villiers *et al.*, Submitted).

### 4.4.3 Phoenix Pyrrhotite

Pyrrhotite from the Phoenix nickel deposit occurred as magnetic pyrrhotite without any coexisting non-magnetic phase. The variation in mineral chemistry of the Phoenix pyrrhotite occurrence is illustrated in figure 4.16. From figure 4.16a, it is evident that Phoenix pyrrhotite shows a broad range in iron composition (57.3 – 60. 0 wt % Fe), but only a relatively narrow range in sulfur content (38.6 – 40.1 wt % S). Similarly to iron in the Phoenix pyrrhotite, nickel also shows a broad range in composition and varied from 0.53 to 2.43 wt % (Figure 4.16b) and which substitutes for iron via solid solution substitution. On the whole, the Phoenix pyrrhotite was relatively enriched in nickel since not only could the nickel budget in the system be accounted for by solid solution nickel but there was also abundant nickel hosted in flame pentlandite. Pyrrhotite from the Phoenix deposit is in fact actively recovered at Tati Nickel mine due to its high solid solution nickel content and abundant pentlandite flames.

The atomic iron content of Phoenix pyrrhotite shown in figure 4.16c displays a broad variation (44.0- 46.5 atomic % Fe), whereas the variation in atomic sulfur is narrow (52.5 – 53.9 atomic % S). Once the contribution from solid solution nickel was accounted for in terms of atomic metal (46.1 – 47.5 atomic % metal), an almost straight and negative correlation occurred between atomic metal and sulfur for the Phoenix pyrrhotite (Figure 4.16d).

Given the very iron deficient nature and the magnetic character of the Phoenix pyrrhotite (Section 4.2), it is likely to have an ideal composition of $Fe_7S_8$. When the metal / sulfur ratio of Phoenix pyrrhotite was normalised to 8 sulfur atoms, then it is apparent that the most commonly occurring compositions were in the 6.95 – 7.00, 7.00 – 7.05 and 7.05 – 7.10 bins of the histogram illustrated in figure 4.17 (43 occurrences for each bin).

The mineralogical studies of the Phoenix pyrrhotite have therefore shown that it is representative of the archetypal monoclinic 4C pyrrhotite since it was magnetic in character (Section 4.2), showed 4C unit cell dimensions, showed monoclinic symmetry (Section 4.3) and had an ideal composition close to $Fe_7S_8$.

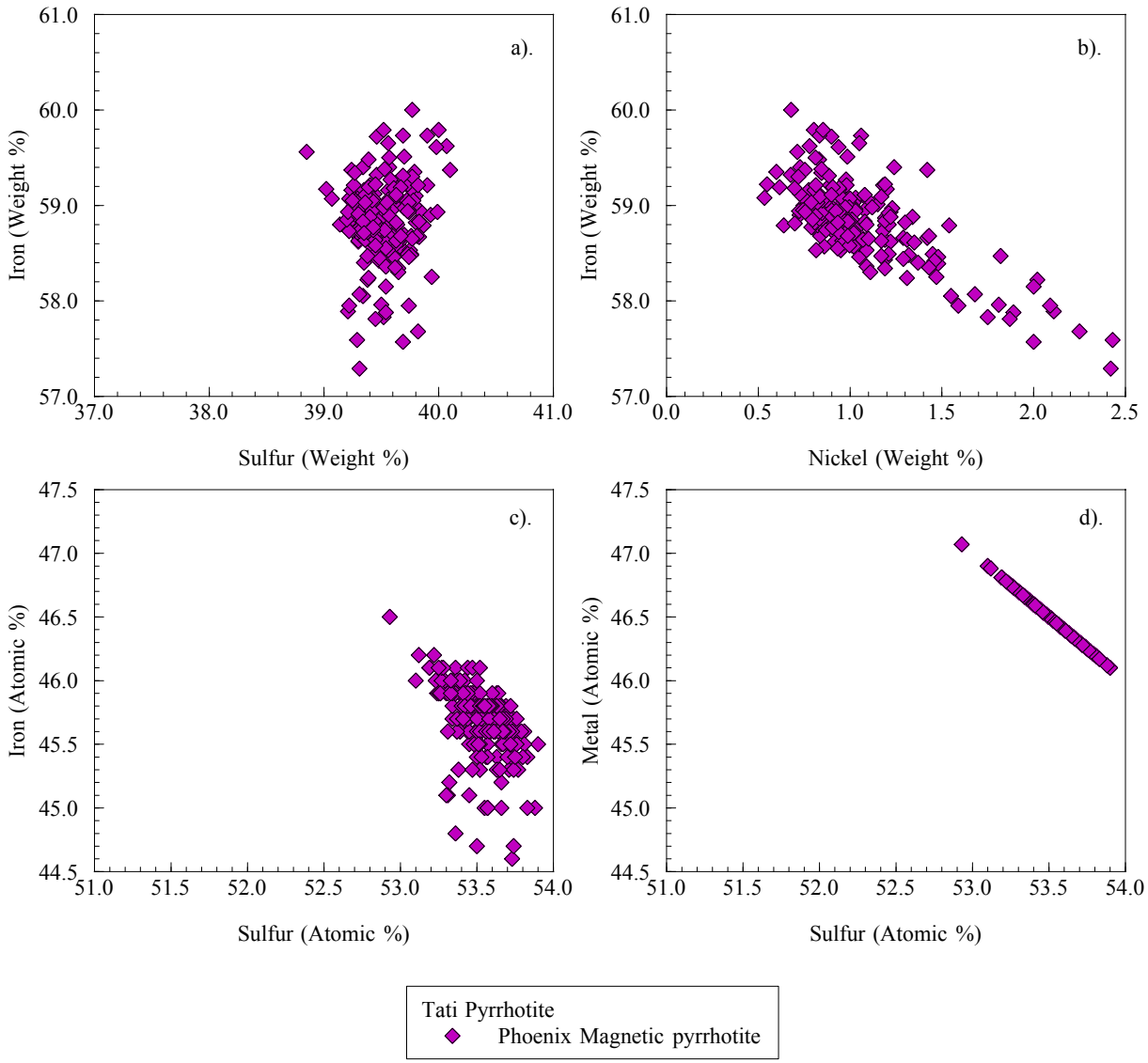


**Figure 4.16**: Mineral chemistry of Phoenix magnetic pyrrhotite shown as both weight % (a, b) and atomic % (c, d).

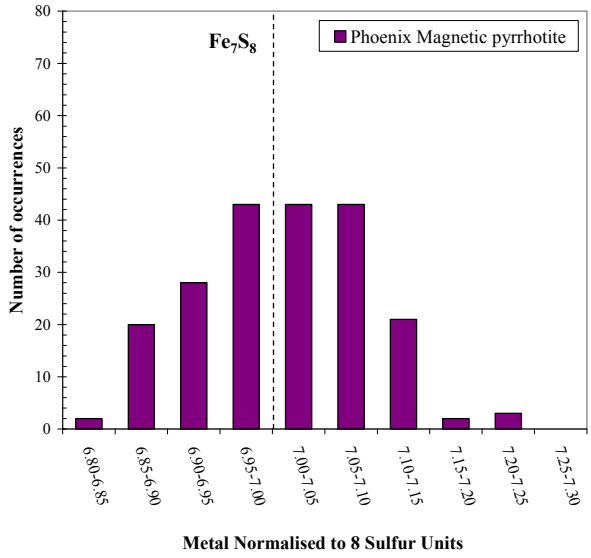


**Figure 4.17**: Histogram of metal / sulfur ratios normalised to eight sulfur units for Phoenix magnetic pyrrhotite.

### 4.4.4 Sudbury Pyrrhotite

The petrographic studies showed that both the Sudbury non-magnetic CCN and magnetic Gertrude, Gertrude West pyrrhotite samples were dominated by a single pyrrhotite phase, although very minor proportions of a coexisting secondary phase were recognised on occasion, e.g. magnetic pyrrhotite rims surrounding flame pentlandite in Sudbury CCN pyrrhotite (Figure 4.6c, d). However, for simplicity, the mineral chemistry of each of the pyrrhotite samples is evaluated and interpreted as discrete pyrrhotite occurrences. The variation in mineral chemistry of the Sudbury pyrrhotite occurrences is shown in figure 4.18. The composition of non-magnetic CCN pyrrhotite varied in iron from 59.2 to 60.9 wt % and between 38.2 and 39.5 wt % sulfur (Figure 4.18a). Magnetic Gertrude pyrrhotite was distinctly more iron poor (58.5 – 59.7 wt % Fe) and sulfur rich (38.9 - 40.3 wt % S) than CCN non-magnetic pyrrhotite. Iron and sulfur contents of Gertrude West pyrrhotite (58.4 - 59.8 wt % Fe, 39.2 - 40.1 wt % S) fell into similar compositional fields as Gertrude pyrrhotite. Little difference was observed between the nickel content of the three pyrrhotite localities (Figure 4.18b), although it does appear that the magnetic Gertrude / Gertrude West pyrrhotite were slightly more nickel rich (0.27 – 1.04 wt % Ni) than CCN pyrrhotite (0.40 – 0.98 wt % Ni).

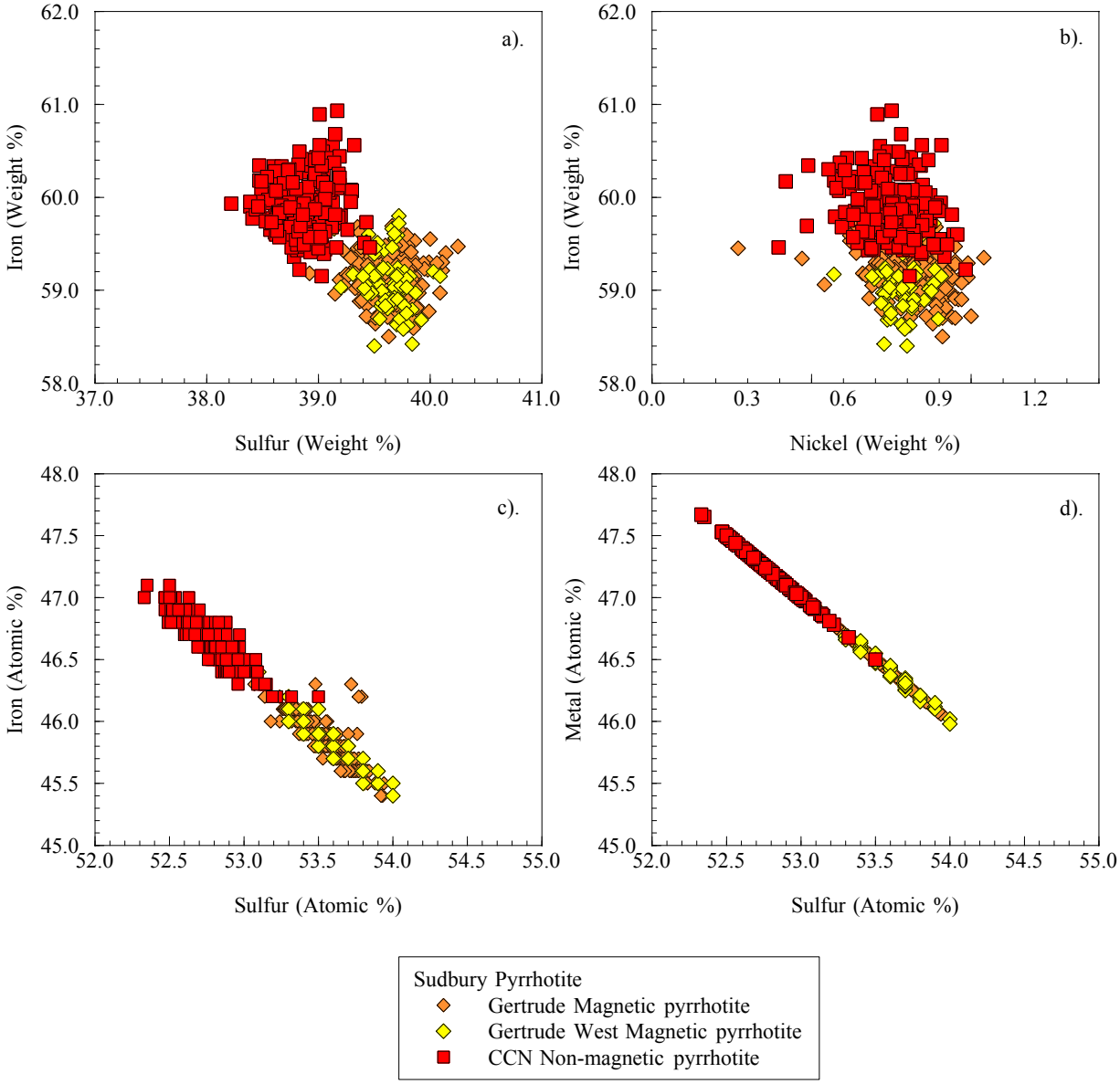


**Figure 4.18**: Mineral chemistry of Sudbury magnetic Gertrude, Gertrude West and non-magnetic CCN pyrrhotite shown as both weight % (a, b) and atomic % (c, d).

Similarly to the pyrrhotite compositions shown in weight percent, the atomic compositions shown in figure 4.18c for the Sudbury CCN non-magnetic pyrrhotite were more iron rich (46.2 – 47.1 atomic % Fe) and sulfur poor (52.3 – 53.5 atomic % S) than the magnetic Gertrude pyrrhotite (45.4 – 46.3 atomic % Fe, 53.1 – 53.9 atomic % S). The magnetic Gertrude West pyrrhotite showed almost identical atomic iron and sulfur contents to the Gertrude pyrrhotite, confirming their similar origin. Once the additional metal cations were accounted in terms of the contribution of nickel, copper and cobalt as shown in figure 4.18d,

then it is evident that the non-magnetic CCN pyrrhotite varied in atomic metal from 46.5 to 47.7 atomic %, and the magnetic Gertrude / Gertrude West pyrrhotite between 46.0 and 46.9 atomic %.

Due to the iron poor character of the magnetic Gertrude pyrrhotite, the metal / sulfur ratios were normalised to 8 sulfur units according to the ideal composition of magnetic pyrrhotite, $Fe_7S_8$. It is evident from figure 4.19a that the most frequently occurring metal / sulfur ratio for both Gertrude and Gertrude West magnetic pyrrhotite was between 6.85 and 7.00 Within analytical error this was interpreted to represent a composition close to $Fe_7S_8$. Gertrude and Gertrude West pyrrhotite were therefore interpreted to represent the archetypal magnetic, monoclinic 4C pyrrhotite. The metal / sulfur ratios corresponding to the non-magnetic CCN pyrrhotite were normalised to 10 sulfur units, as per the ideal composition $Fe_9S_{10}$ (Figure 4.19b). This was consistent with the assignment of Sudbury CCN non-magnetic pyrrhotite as 5C orthorhombic pyrrhotite in the crystallographic studies (Section 4.3). The most frequently occurring metal / sulfur ratio for CCN pyrrhotite was 8.90 – 8.95 per 10 sulfur units (56 occurrences).

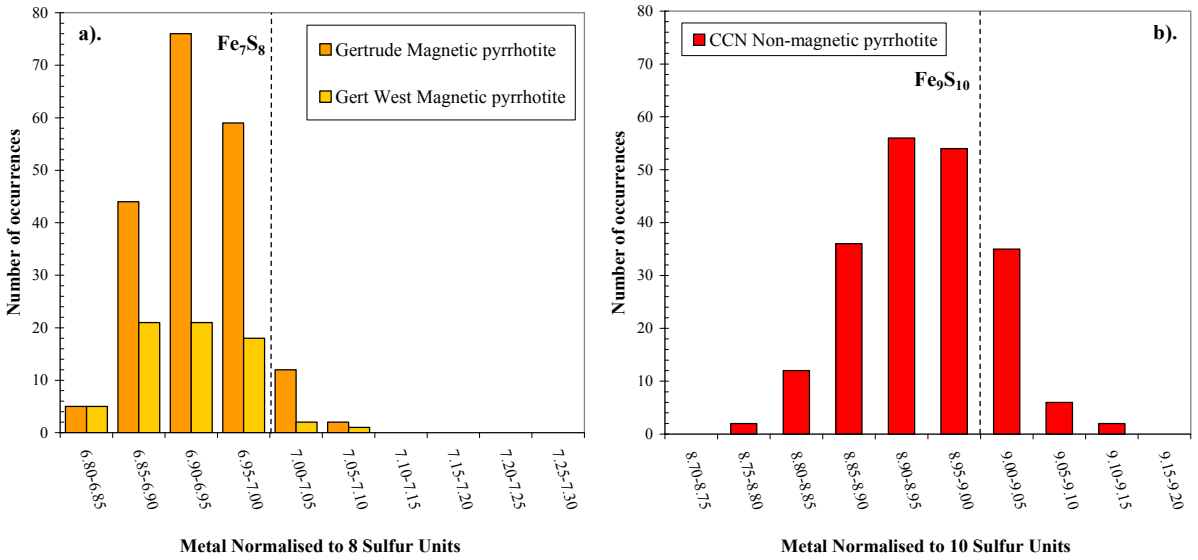


**Figure 4.19**: Histogram of metal / sulfur ratios normalised to differing sulfur contents for Sudbury magnetic (a) and non-magnetic (b) pyrrhotite.

## 4.5 Comparison of the Mineral Chemistry of Pyrrhotite Samples

A number of pyrrhotite samples from well-known nickel and platinum group element ore deposits have been characterised in terms of their petrography, crystallography and mineral chemistry. This includes pyrrhotite from magmatic sulfide deposits in South Africa (Merensky Reef, Nkomati) and Canada (Sudbury: Copper Cliff North and Gertrude mines) and from the Tati greenstone belt in Botswana (Phoenix). It is now relevant to compare the compositions of pyrrhotite from these locations in order to develop some general relationships between the pyrrhotite types and explore the compositional variation between the different samples.

Comparison of the iron and nickel contents as illustrated in figure 4.20 showed that a continuum almost exists in terms of the variation in composition of pyrrhotite as a mineral. All non-magnetic pyrrhotite occurrences examined varied in iron between 59.2 and 61.9 wt % and with the more iron rich compositions corresponding to the Impala Merensky Reef 6C $Fe_{11}S_{12}$ pyrrhotite. It is noted that the very iron rich $Fe_{11}S_{12}$ pyrrhotite contained by far the lowest solid solution nickel content (0.30 wt % Ni) and coexisted with 2C troilite (Section 4.2), whereas the nickel content of all the other non-magnetic pyrrhotite occurrences (ie. 5C $Fe_9S_{10}$) varied between 0.40 and 0.98 wt % (Sudbury CCN, Nkomati MSB and MMZ). The range of nickel contents in non-magnetic $Fe_9S_{10}$ pyrrhotite from this study is significantly broader than the range given by Batt (1972) for non-magnetic Sudbury pyrrhotite and shown in figure 4.20. This may be attributed to the difference in the size of the data sets from this study (> 400 grains) and from the study of Batt (1972; 45 grains). No significant difference in nickel content occurred between non-magnetic pyrrhotite 5C $Fe_9S_{10}$ pyrrhotite which exists as the sole pyrrhotite phase (Sudbury CCN pyrrhotite) or non-magnetic pyrrhotite that coexisted with magnetic 4C $Fe_7S_8$ pyrrhotite (Non-magnetic Nkomati MSB, MMZ sample *MMZ-4*).

Nickel contents of the more iron poor magnetic 4C $Fe_7S_8$ pyrrhotite showed a very broad variation from 0.26 to 2.43 wt % nickel. Once again, the variation in nickel contents of magnetic pyrrhotite shown in figure 4.20 are significantly greater than the range given for Sudbury magnetic pyrrhotite by Batt (1972). Only magnetic pyrrhotite that coexists with non-magnetic pyrrhotite (Nkomati MSB and MMZ sample *MMZ-4*) showed some similarity in

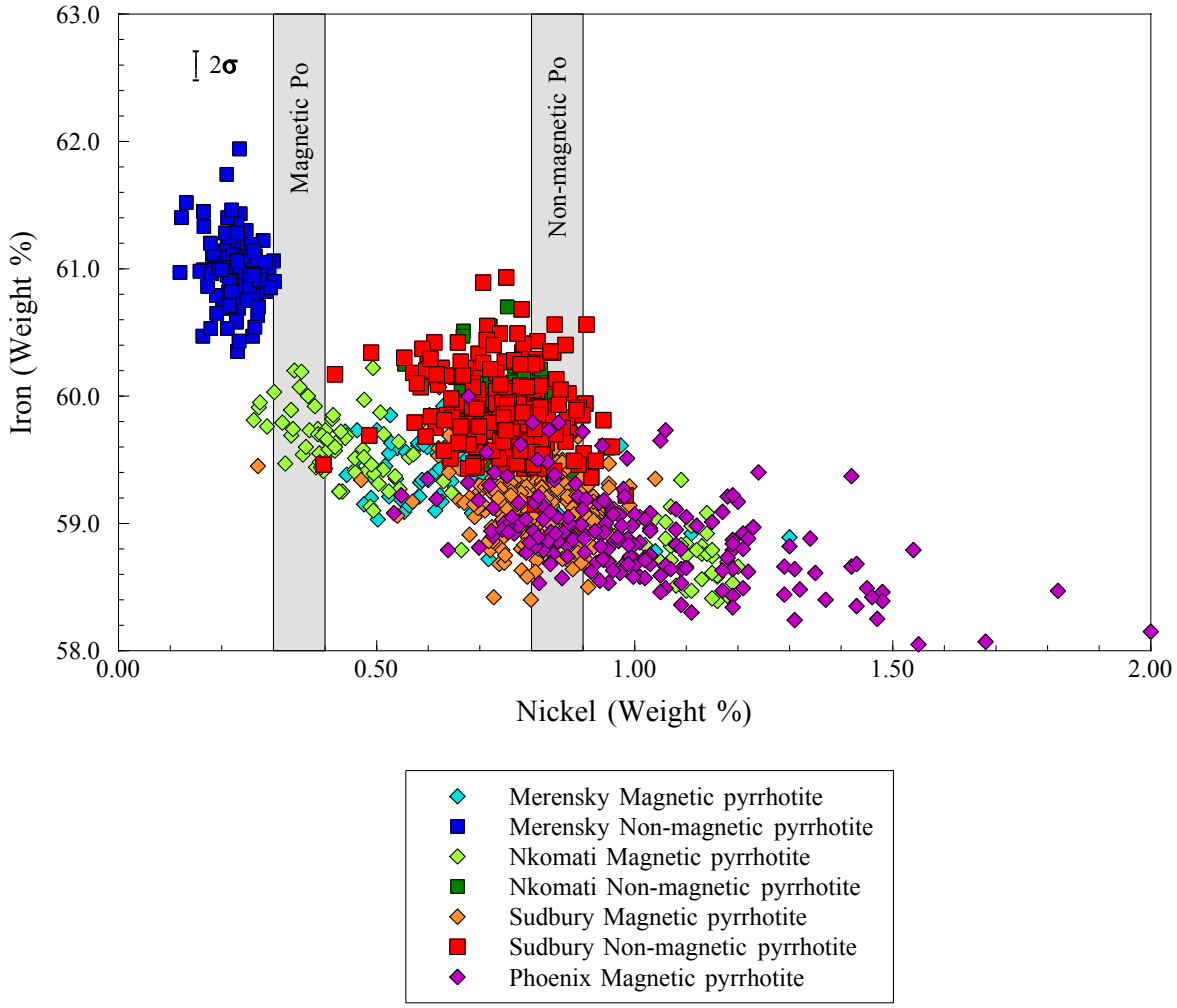


**Figure 4.20**: Comparison of the wt % iron versus nickel for all magnetic and non-magnetic pyrrhotite occurrences examined in this study. The 2σ standard deviation for iron is shown, whereas the 2σ standard deviation for nickel is too small for representation. The grey bars represent nickel contents for Sudbury pyrrhotite as given by Batt (1972).

nickel content to the values given by Batt (1972), which would be expected given that that the samples examined by Batt (1972) contained intergrown magnetic and non-magnetic pyrrhotite. Under these circumstances, the magnetic pyrrhotite had lower solid solution nickel than the coexisiting non-magnetic pyrrhotite which is in agreement with Batt (1972). The highest solid solution nickel contents for all the pyrrhotite samples in this study were measured for magnetic pyrrhotite that does not coexist with any other pyrrhotite phase (Sudbury Gertrude, Phoenix, Nkomati MMZ sample *MMZ-1*). The Phoenix magnetic pyrrhotite sample however, was notably the most enriched in solid solution nickel of all the pyrrhotite occurrences examined. This confirms that the mineral chemistry of pyrrhotite seems to be correlated with the mineral association.

Atomic iron and sulfur contents for all magnetic and non-magnetic pyrrhotite samples examined and shown in figure 4.21a similarly showed a continuum in terms of the variation in their composition. Non-magnetic pyrrhotite varied between 46.2 and 48.3 atomic % iron and 51.4 and 53.5 atomic % sulfur whereas magnetic pyrrhotite varied between 44.6 and 46.6 atomic % iron and 52.9 and 54.0 atomic % sulfur. Given the degree of overlap in terms of atomic iron or sulfur contents, consideration of both parameters is needed on an x-y diagram to recognise discreet compositional fields of pyrrhotite. On this basis, three groupings in pyrrhotite composition corresponding to magnetic 4C $Fe_7S_8$, non-magnetic 5C $Fe_9S_{10}$ and non-magnetic 6C $Fe_{11}S_{12}$ can be recognised in figure 4.21a.

For a given sulfur content it also evident that the variation in atomic iron for non-magnetic 6C $Fe_{11}S_{12}$ (~ 0.2 atomic % Fe) was less than for non-magnetic 5C $Fe_9S_{10}$ (~ 0.3 atomic % Fe), and which was even less than for magnetic 4C $Fe_7S_8$ (~ 0.8 atomic % Fe). This variation in atomic iron was compensated for by other metal cations (i.e. nickel) and when illustrated as the variation of atomic metal versus sulfur in figure 4.21b, an almost perfect negative correlation is observed. The continuum in terms of atomic sulfur contents indicates that the pyrrhotite structure as a whole must be sufficiently flexible that it can accommodate virtually any sulfur content between 51.4 and 53.9 atomic % sulfur.

This continuum observed in terms of pyrrhotite compositional variation was also manifested in the atomic metal / sulfur ratio of pyrrhotite shown in figure 4.22. Pyrrhotite compositions with the lowest metal / sulfur ratio corresponded to the magnetic pyrrhotite occurrences examined in this study, namely the Nkomati MSB and MMZ, Merensky Reef, Phoenix and Sudbury Gertrude and Gertrude West pyrrhotite samples. The variation in metal / sulfur ratio was observed to be broader (Atomic Metal / Sulfur = 0.851 – 0.889) than the ideal for pyrrhotite of composition 4C $Fe_7S_8$ (Atomic Metal / Sulfur = 0.875). Non-magnetic pyrrhotite of ideal composition 5C $Fe_9S_{10}$ (Sudbury CCN, Nkomati MSB and MMZ) also showed a significantly broader atomic metal / sulfur ratio (0.869 – 0.913) than the ideal (Atomic Metal / Sulfur = 0.900). The highest atomic metal / sulfur ratios occurred for the very iron rich Impala Merensky Reef pyrrhotite (Atomic Metal / Sulfur = 0.897 – 0.942) of ideal composition 6C $Fe_{11}S_{12}$ (Atomic Metal / Sulfur ratio = 0.917).

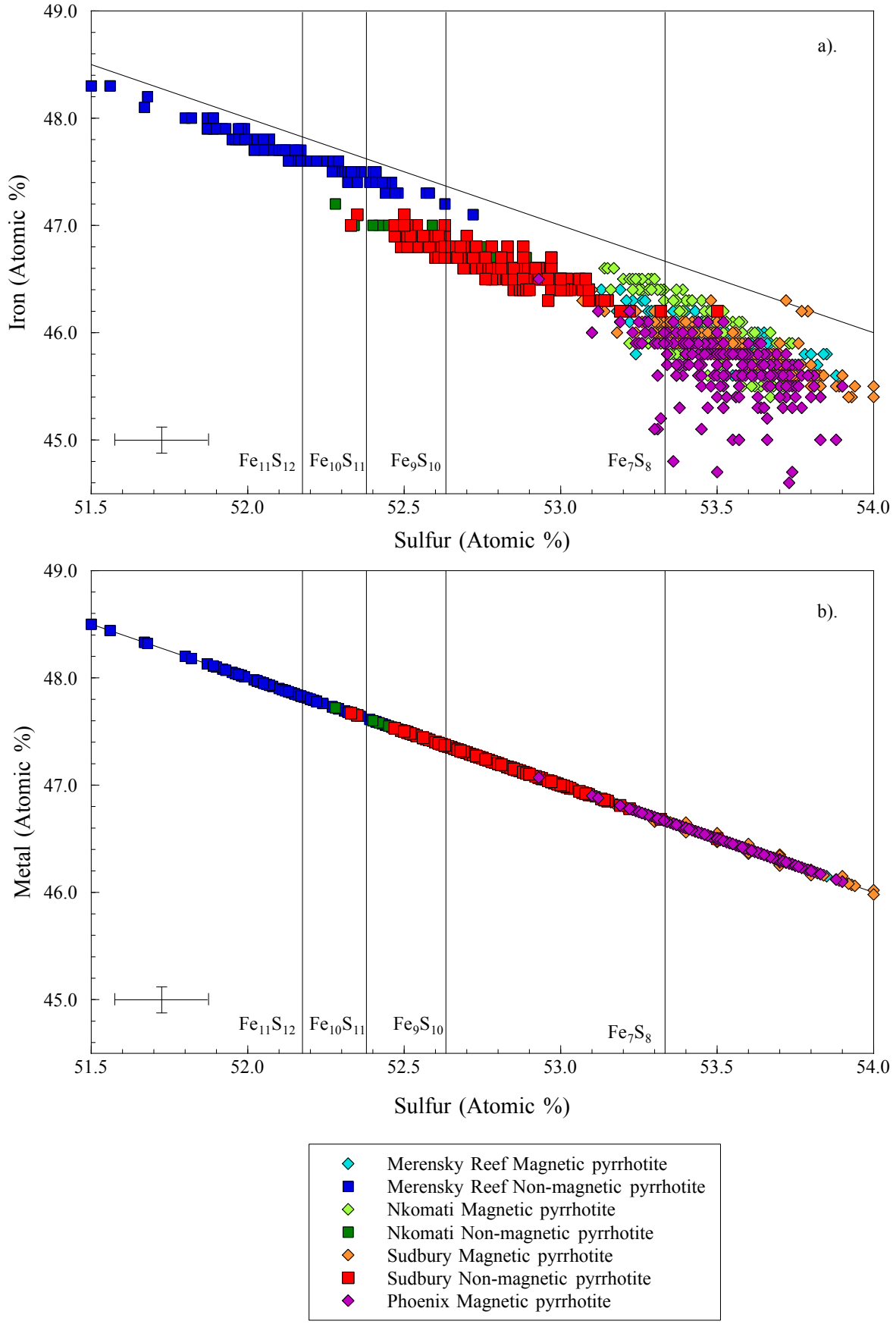


**Figure 4.21:** Comparison of the atomic % iron (a) and metal (b) versus sulfur for all magnetic and non-magnetic pyrrhotite occurrences examined in this study. The 2σ standard deviation is also shown.

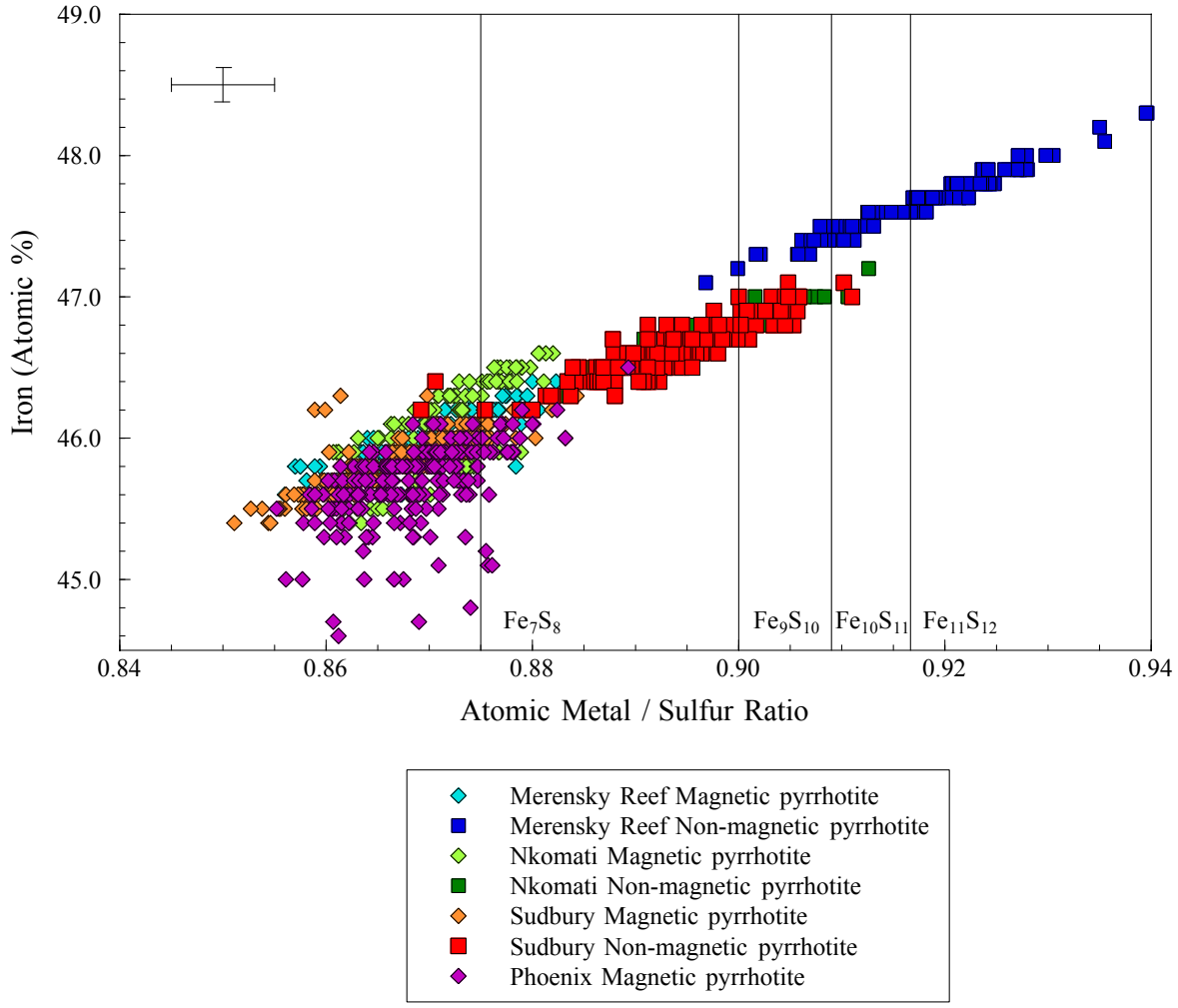


**Figure 4.22**: Comparison of the atomic % iron versus metal to sulfur ratio for all magnetic and non-magnetic pyrrhotite occurrences examined in this study. The 2σ standard deviation is also shown.

## 4.7 Key Findings

Key features noted with respect to the mineralogy of pyrrhotite from selected nickel and platinum group element ore deposits were as follows:

Pyrrhotite was the most common sulfide mineral in all of the occurrences examined and with sulfide mineralisation occurring in a variety of textures from massive, semi-massive, net-textured to disseminated. Pyrrhotite was generally fairly coarse-grained, showed well-developed anisotropism, occasional twinning and intergrowth textures to other sulphide minerals characteristic of crystallisation from the MSS. Pentlandite showed a strong association to pyrrhotite and occurred in both granular and flame pentlandite form. Other minerals present in the samples examined included chalcopyrite, pyrite and magnetite in varying proportions.

Application of the magnetic colloid to the pyrrhotite samples revealed the presence of samples that consisted of solely magnetic pyrrhotite, solely non-magnetic pyrrhotite, and intergrowths of magnetic and non-magnetic pyrrhotite. A variety of intergrowth textures between magnetic and non-magnetic pyrrhotite phases that included magnetic pyrrhotite lamellae hosted by non-magnetic pyrrhotite, thickness zonation, box work textures, composite lamellae and magnetic pyrrhotite rims surrounding crystallographically controlled flame pentlandite exsolution were all noted. Very fine grained troilite lamellae intergrown with non-magnetic pyrrhotite were also recognised in the Merensky Reef pyrrhotite sample.

The crystallographic studies showed that both the magnetic Impala Merensky sample *IMP-1* and Phoenix pyrrhotite samples were monoclinic 4C pyrrhotite whereas the non-magnetic Sudbury CCN pyrrhotite was orthorhombic 5C pyrrhotite. The crystal structure solution of the Sudbury CCN pyrrhotite was shown to consist of a series of iron layers that were vertically stacked. Each layer consisted of a series of fully occupied as well as partially occupied iron sites in contrast to the classic structure of 4C pyrrhotite that is comprised of a series of alternating fully occupied layers with vacancy containing layers.

The composition of magnetic pyrrhotite was shown to be more sulfur rich (52.9 - 54.0 atomic % S) and iron deficient (44.6 - 46.6 atomic % Fe) than non-magnetic pyrrhotite (51.4 and 53.5 atomic % S; 46.2 - 48.3 atomic % Fe). Three compositional groups of pyrrhotite were observed correlating to magnetic 4C $Fe_7S_8$, non-magnetic 5C $Fe_9S_{10}$ and non-magnetic 6C $Fe_{11}S_{12}$. Non-magnetic 6C $Fe_{11}S_{12}$ pyrrhotite was intergrown with 2C FeS.

Nickel was determined to be the main trace element impurity in the pyrrhotite structure. Non-magnetic 6C $Fe_{11}S_{12}$ pyrrhotite was less nickel rich (0.22 ± 0.07 wt %) relative to non-magnetic 5C $Fe_9S_{10}$ pyrrhotite (0.75 ± 0.19 wt %). Magnetic 4C $Fe_7S_8$ pyrrhotite coexisting with non-magnetic 5C $Fe_9S_{10}$ pyrrhotite typically had a lower nickel content (0.43 ± 0.18 wt %) than the non-magnetic phase (0.75 ± 0.10 wt %). The highest solid solution nickel contents were obtained for magnetic pyrrhotite with no coexisting non-magnetic phase (> 0.82 wt %).

# Chapter 5

# PYRRHOTITE REACTIVITY

---

## 5.1 Introduction

As described in Chapter 2, pyrrhotite is a highly reactive sulfide mineral that is prone to oxidation. Severe oxidation of pyrrhotite and subsequent formation of hydrophilic iron hydroxides will have a detrimental effect on flotation performance. Since the accounts in the literature with respect to the role of mineralogy on pyrrhotite oxidation are in conflict (Section 2.3.3), it is necessary to characterise the differences in the reactivity of magnetic and non-magnetic pyrrhotite on a set of pyrrhotite samples for which the mineralogy is already well-known (Chapter 4). Therefore the aim of this chapter is to "*explore and compare the reactivity of magnetic and non-magnetic pyrrhotite*". In order to do this, a series of electrochemical measurements comprising open circuit potential and cyclic voltammetry, as well as determination of the oxygen uptake of a pyrrhotite slurry have been performed; the results of which are presented in this chapter. Due to the nature of the experiments, reactivity measurements were only performed on the high grade pyrrhotite samples: Nkomati mixed pyrrhotite, Phoenix magnetic pyrrhotite, Sudbury CCN non-magnetic pyrrhotite and Sudbury Gertrude West magnetic pyrrhotite. The complete set of results from this chapter is presented in Appendix B.

## 5.2 Open Circuit Potential

Open circuit or rest potential measurements were used to investigate differences in surface oxidation between the different mineral electrodes. The open circuit potential describes the mixed potential between the anodic oxidation of pyrrhotite and the cathodic reduction of oxygen at the surface of pyrrhotite. Since the oxidation rate is influenced by the presence of the hydroxide species, it is expected that differences will be observed for different pH conditions (Section 2.3.3) and different ore samples. Results of the open circuit potential measurements for the Nkomati MSB mixed pyrrhotite, Phoenix magnetic pyrrhotite, Sudbury CCN non-magnetic pyrrhotite and Sudbury Gertrude West magnetic pyrrhotite samples are shown at pH 7 and pH 10 in figures 5.1 and 5.2, respectively.

### 5.2.1 Comparison of the Open Circuit Potentials of Pyrrhotite Samples

The open circuit potential of the Sudbury CCN non-magnetic pyrrhotite was the highest (170 mV) of the pyrrhotite samples investigated at pH 7 (Figure 5.1). Sudbury Gertrude West magnetic pyrrhotite and Nkomati MSB mixed pyrrhotite had slightly lower and similar open circuit potentials (~ 140 mV). The open circuit potential of the Phoenix magnetic pyrrhotite was the lowest at pH 7 (117 mV). The results at pH 10 were quite different to pH 7, possibly due to differences in rates of electrochemical reactions at the different pH values. At pH 10, the open circuit potential of Gertrude West magnetic pyrrhotite (116 mV) was significantly greater than the other pyrrhotite samples for which the open circuit potential was less than 44 mV (Figure 5.2). The lowest open circuit potential measurement was obtained for Sudbury CCN non-magnetic pyrrhotite (15 mV).

Since the differences between the open circuit potential measurements of the different electrodes at pH 7 were not as significant as they were at pH 10, it is under these conditions that any inferences relating to differences in pyrrhotite reactivity are drawn. Consequently, it can be inferred that at pH 10, the Sudbury Gertrude West pyrrhotite sample was the most oxidised and had the greatest proportion of ferric hydroxide species on the electrode surface in comparison to the other pyrrhotite samples. In contrast, the Sudbury CCN non-magnetic pyrrhotite sample was the least oxidised as evidenced by the very low open circuit potential obtained at pH 10 (15 mV; Figure 5.2).

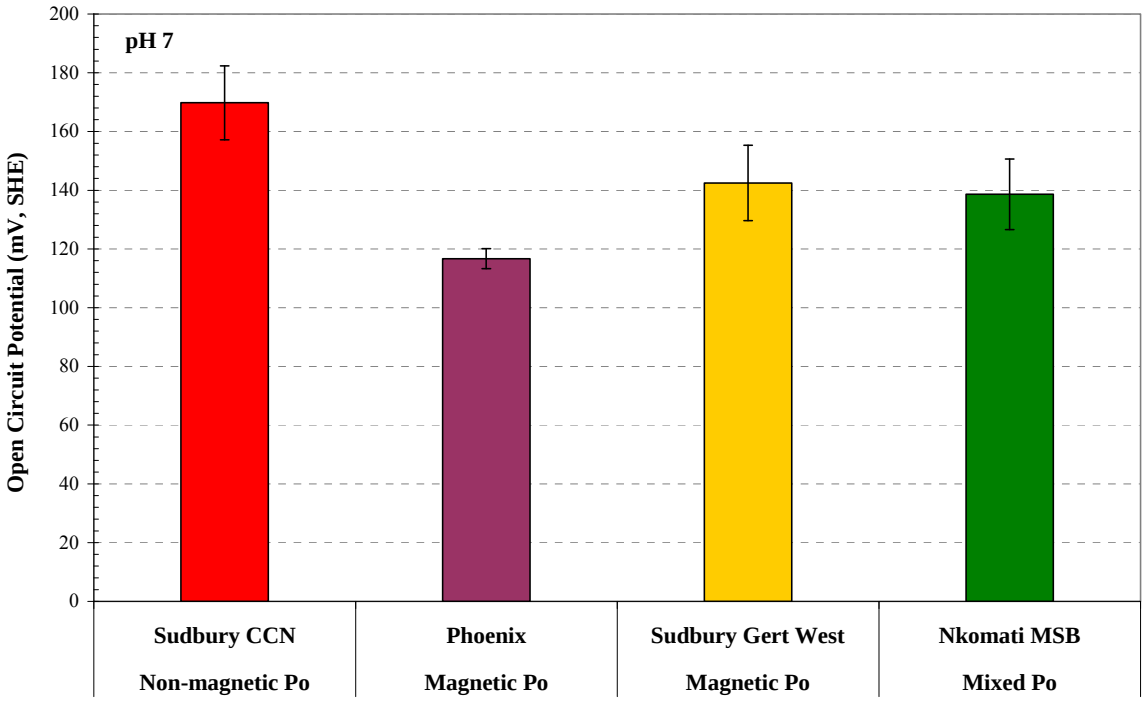


**Figure 5.1:** Open circuit potential for pyrrhotite samples at pH 7. The 2σ standard deviation is also shown.

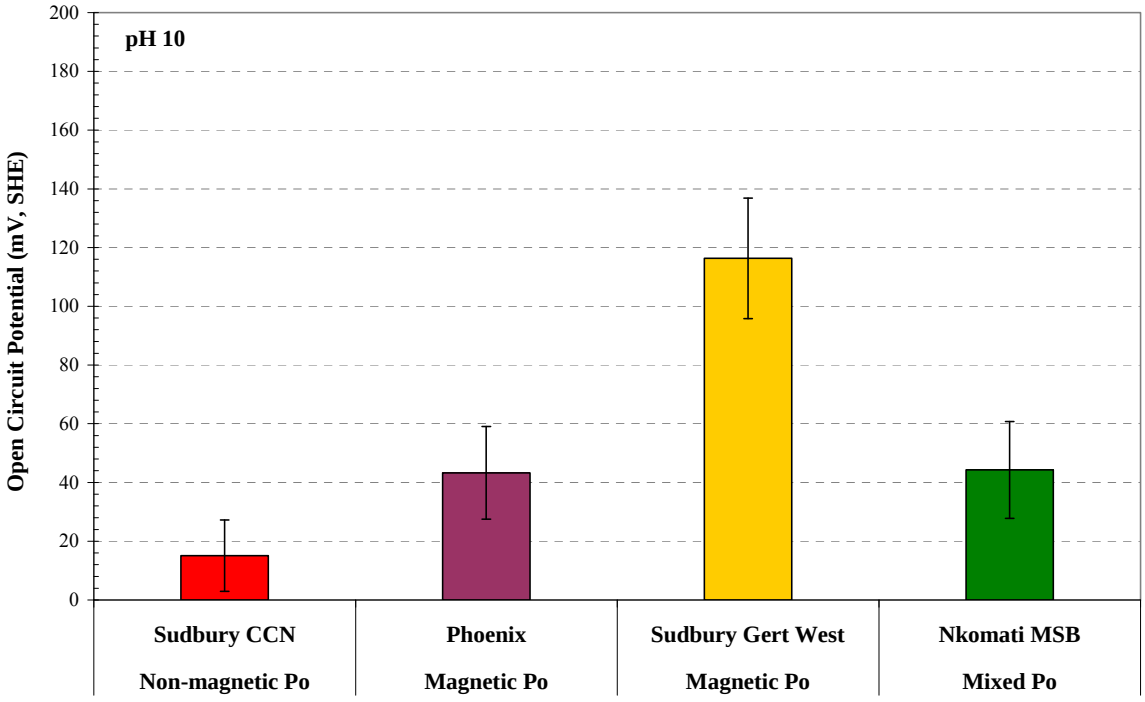


**Figure 5.2:** Open circuit potential for pyrrhotite samples at pH 10. The 2σ standard deviation is also shown.

## 5.3 Cyclic Voltammetry

Cyclic voltammetry was used to investigate differences in the surface reactions of the different pyrrhotite samples by varying the potential of the pyrrhotite electrode through several anodic and cathodic sweeps. Cyclic voltammetry was performed on electrodes of the Nkomati MSB mixed pyrrhotite, Phoenix magnetic pyrrhotite, Sudbury CCN non-magnetic pyrrhotite and Sudbury Gertrude West magnetic pyrrhotite at both pH 7 and 10. The cyclic voltammograms showed similar shapes to those obtained in other studies of pyrrhotite that were accounted for by typical pyrrhotite REDOX reactions found in the literature (e.g. Hamilton and Woods, 1984; Buswell and Nicol, 2002) and similar to those given in Section 2.3.1.

### 5.3.1 Nkomati MSB Pyrrhotite

The cyclic voltammogram of Nkomati MSB mixed pyrrhotite at pH 7 in figure 5.3 shows that for the first two sweeps from -800 to -300 mV, and -800 to -100 mV, there were no significant anodic or cathodic peaks. Only when the potential was increased to + 100 mV for the third scan, was an anodic peak at ~ 100 mV recognised (A1). A second anodic peak formed only when the potential was further increased from + 500 to + 700 mV, and which is annotated as A2 in figure 5.3. Three cathodic peaks were recognised and which were the most well developed for the scan from – 800 to + 700 mV, at ~ -100 mV (C1), ~ -300 (C2) and ~ -500 mV (C3), respectively. For the potential sweep from -800 to +700 mV, the maximum anodic current density achieved for reaction A1 was 34 $\mu A.cm^{-2}$, and a maximum cathodic current density of - 48 $\mu A.cm^{-2}$ for reaction C3.

Similarly to the results obtained at pH 7, the first anodic peak A1 was recognised on the potential sweep at pH 10 from -800 to +100 mV, followed by a second anodic peak A2 as shown in figure 5.4. On the return scan from the -800 to + 300 mV sweep, the cathodic peaks C1 and C2 were recognised at ~ -300 and -500 mV, respectively. In addition, a third anodic peak was recognised at ~ -200 mV when the upper limit of the sweep was increased to +500 mV. For the potential sweep from -800 to +700 mV, the maximum current density achieved for reaction A1 was 78 $\mu A.cm^{-2}$, and a maximum cathodic current density of -125 $\mu A.cm^{-2}$ for reaction C2.

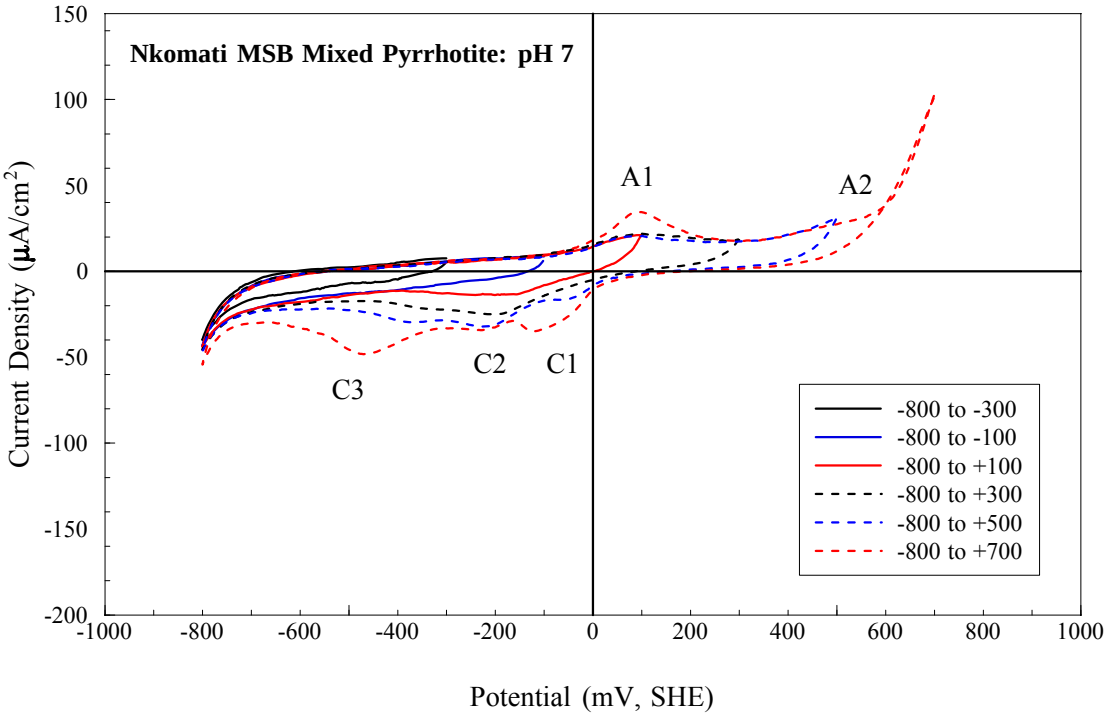


**Figure 5.3:** Cyclic voltammogram of Nkomati MSB mixed pyrrhotite at pH 7 for different anodic switching potentials.

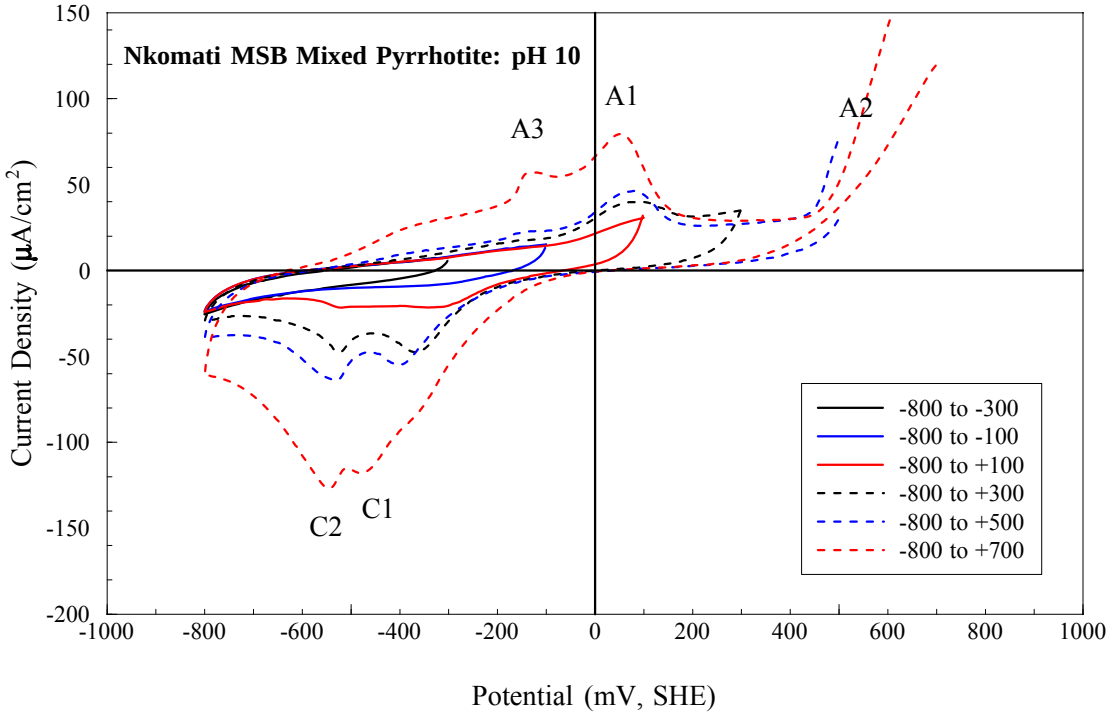


**Figure 5.4:** Cyclic voltammogram of Nkomati MSB mixed pyrrhotite at pH 10 for different anodic switching potentials.

### 5.3.2 Phoenix Pyrrhotite

Similarly to the behaviour of the Nkomati MSB mixed pyrrhotite electrode at pH 7, the Phoenix magnetic pyrrhotite showed an anodic reaction A1 when the upper limit of the potential sweep was increased to +100 mV as shown in figure 5.5. The corresponding cathodic reaction C1 was noted at ~ -100 mV. At greater positive potentials, a second anodic peak was recognised at ~ 600 mV. The cathodic reactions C2 and C3 were also noted at ~ -300 and - 500 mV, respectively.

The effect of an increase in pH from 7 to 10 as shown in figures 5.5 and 5.6, respectively, was to influence the reaction rates. For the anodic reaction A1 at pH 7, the maximum current density obtained for the Phoenix magnetic pyrrhotite was 53 $\mu A.cm^{-2}$, whereas at pH 10 the current density increased to 110 $\mu A.cm^{-2}$. A third anodic reaction A3 was also noted at ~ -200 mV when the upper limit of the potential was further increased. The cathodic reactions C1 and C2 were particularly prominent for the largest potential sweeps (-800 to + 700 mV) where the current density reached a maximum cathodic current density of almost - 200 $\mu A.cm^{-2}$.

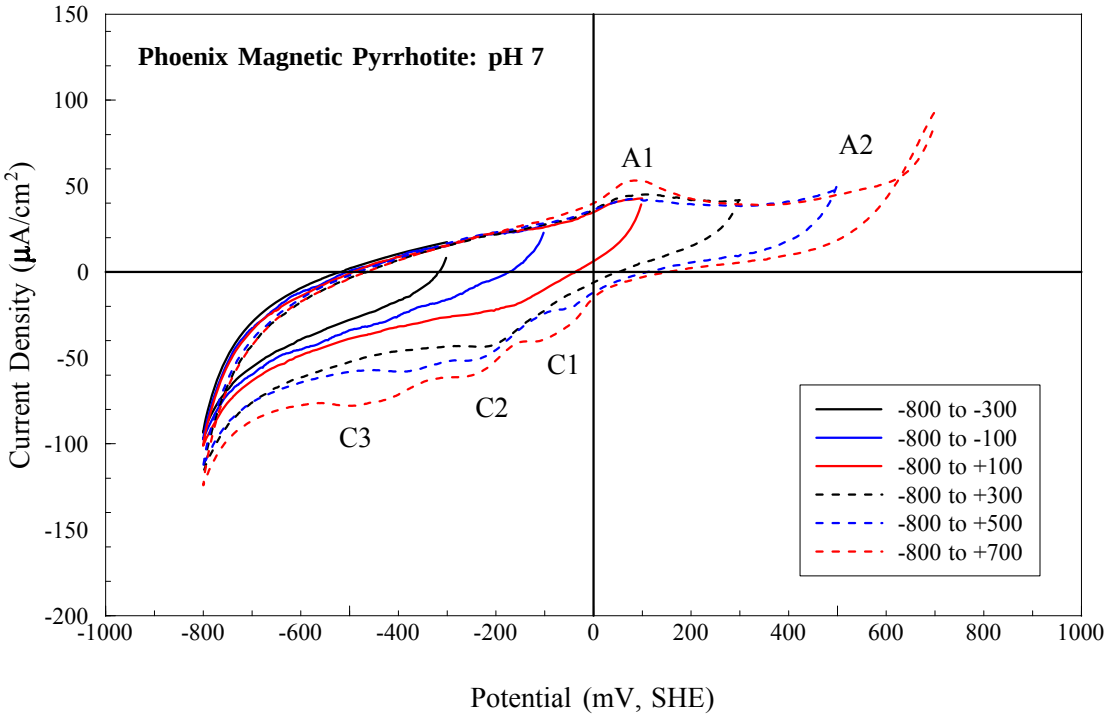


**Figure 5.5:** Cyclic voltammogram of Phoenix magnetic pyrrhotite at pH 7 for different anodic switching potentials.

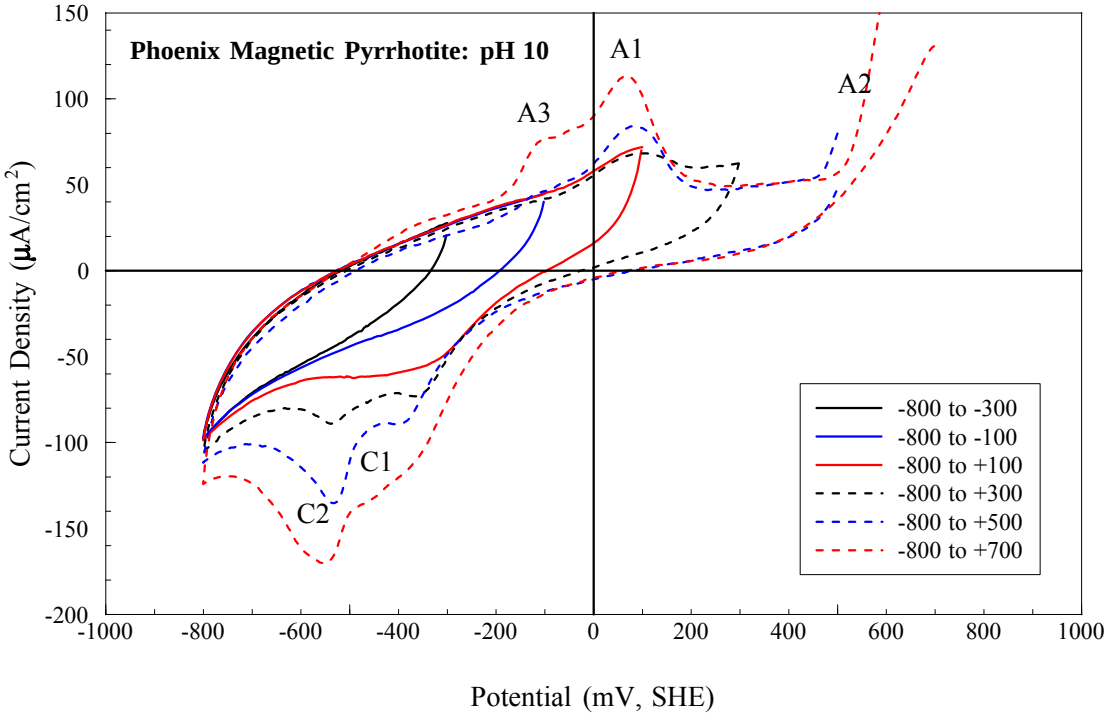


**Figure 5.6:** Cyclic voltammogram of Phoenix magnetic pyrrhotite at pH 10 for different anodic switching potentials.

### 5.3.3 Sudbury CCN Pyrrhotite

It is notable that the current density for all anodic and cathodic cycles was relatively small in the cyclic voltammetry studies of the Sudbury CCN non-magnetic pyrrhotite at pH 7 and pH 10 (Figures 5.7, 5.8). This suggests that the Sudbury CCN non-magnetic pyrrhotite was not particularly reactive towards oxidation and reduction even when the potential was increased to very oxidising conditions (> + 500 mV). However, similarly to the cyclic voltammograms from the Nkomati and Phoenix pyrrhotite electrodes, two anodic (A1, A2) and three cathodic (C1, C2, C3) peaks were recognised at pH 7.

The cyclic voltammogram for Sudbury CCN at pH 10 shown in figure 5.8 however, only shows two anodic peaks, A1 and A2. Even when the upper limit of the potential for the sweep was increased to + 700 mV, no additional anodic peaks were recognised. Two minor cathodic peaks C1 and C2 were recognised at ~ -300 and -500 mV, respectively.

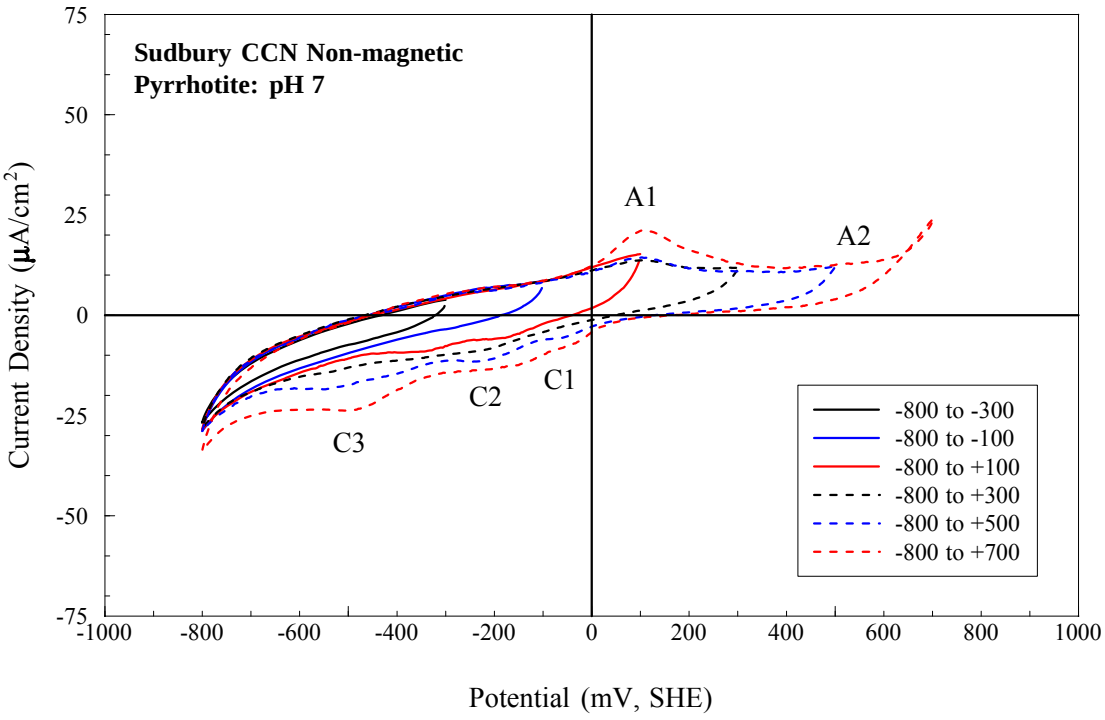


**Figure 5.7:** Cyclic voltammogram of Sudbury CCN non-magnetic pyrrhotite at pH 7 for different anodic switching potentials.

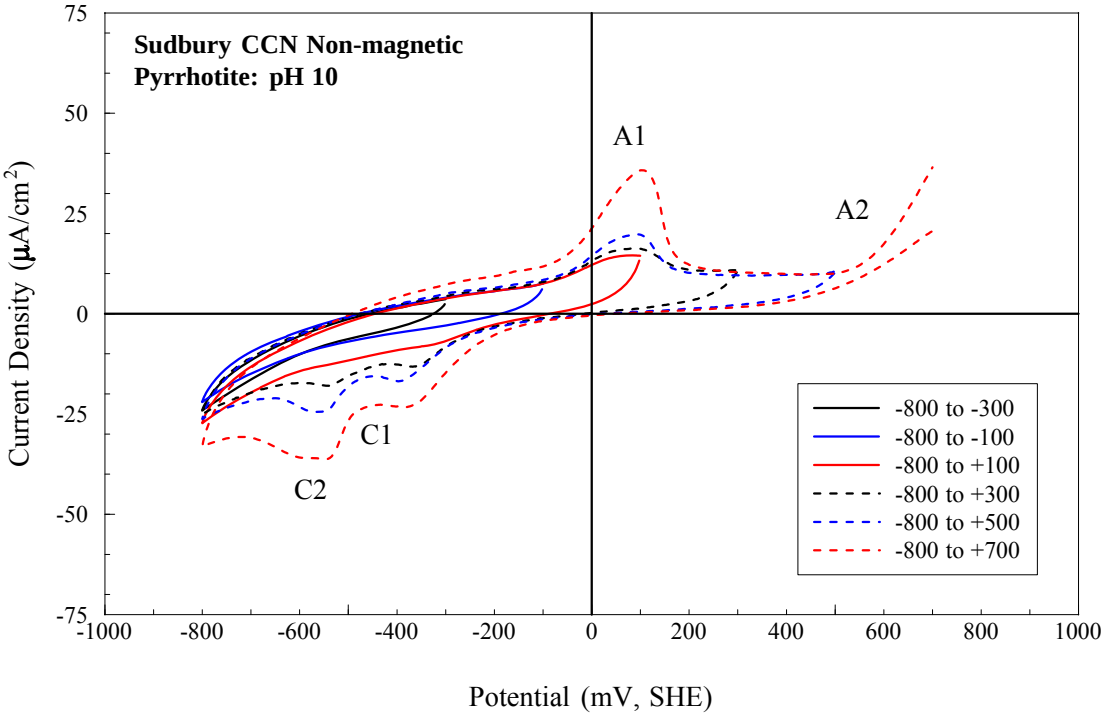


**Figure 5.8:** Cyclic voltammogram of Sudbury CCN non-magnetic pyrrhotite at pH 10 for different anodic switching potentials.

### 5.3.4 Sudbury Gertrude West Pyrrhotite

The cyclic voltammograms for the Sudbury Gertrude West magnetic pyrrhotite shown in figures 5.9 and 5.10 for pH 7 and 10, respectively, show well developed anodic and cathodic peaks. This is due to the intensity of the current associated with the electrochemical reactions that took place at the surface of the Gertrude West pyrrhotite electrode. At pH 7, two anodic peaks (A1, A2) and three cathodic peaks (C1, C2, C3) were recognised. For the potential sweeps associated with the most oxidising potentials, the current density associated with reaction A2 exceeded 75 $\mu A.cm^{-2}$. The current density associated with the most intense cathodic reaction C3, was less than -100 $\mu A.cm^{-2}$.

The current density associated with these electrochemical reactions was even more intense at pH 10 for the Sudbury Gertrude West magnetic pyrrhotite as shown in figure 5.10. Similarly to the Phoenix and Nkomati pyrrhotite samples, three anodic peaks (A1, A2 and A3) and two cathodic peaks (C2, C2) were recognised. For the potential sweeps associated with the most oxidising potentials, the current density associated with reaction A2 exceeded 250 $\mu A.cm^{-2}$. The current density associated with the most intense cathodic reaction C2, was less than -200 $\mu A.cm^{-2}$.

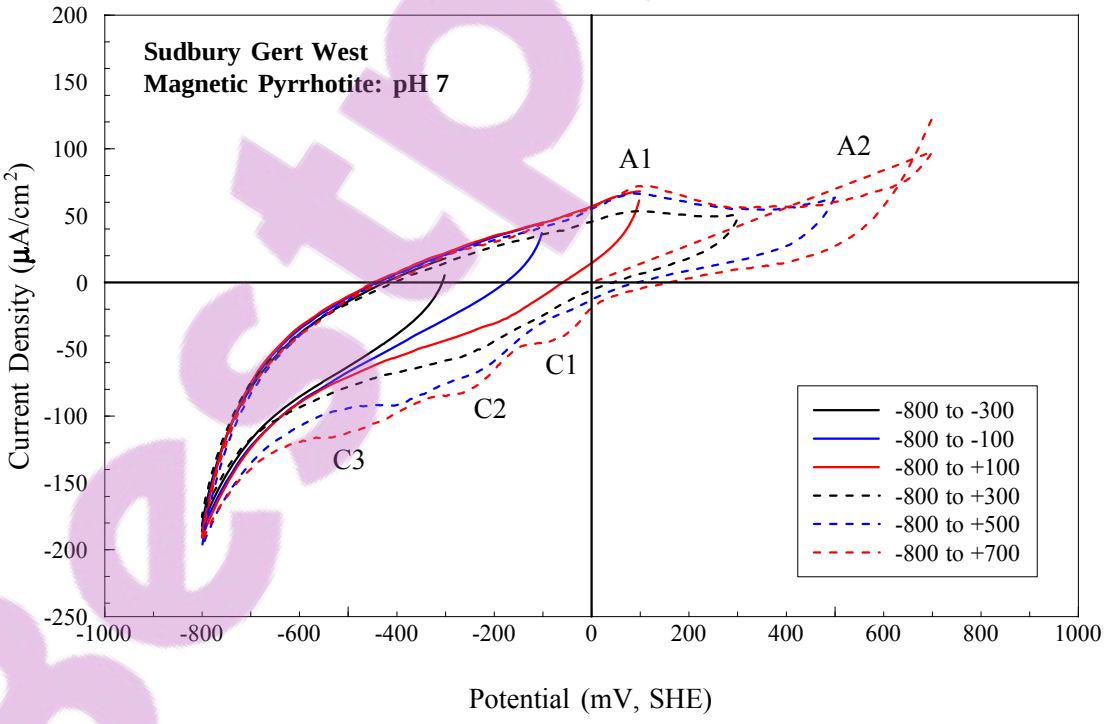


**Figure 5.9:** Cyclic voltammogram of Sudbury Gertrude West magnetic pyrrhotite at pH 7 for different anodic switching potentials.

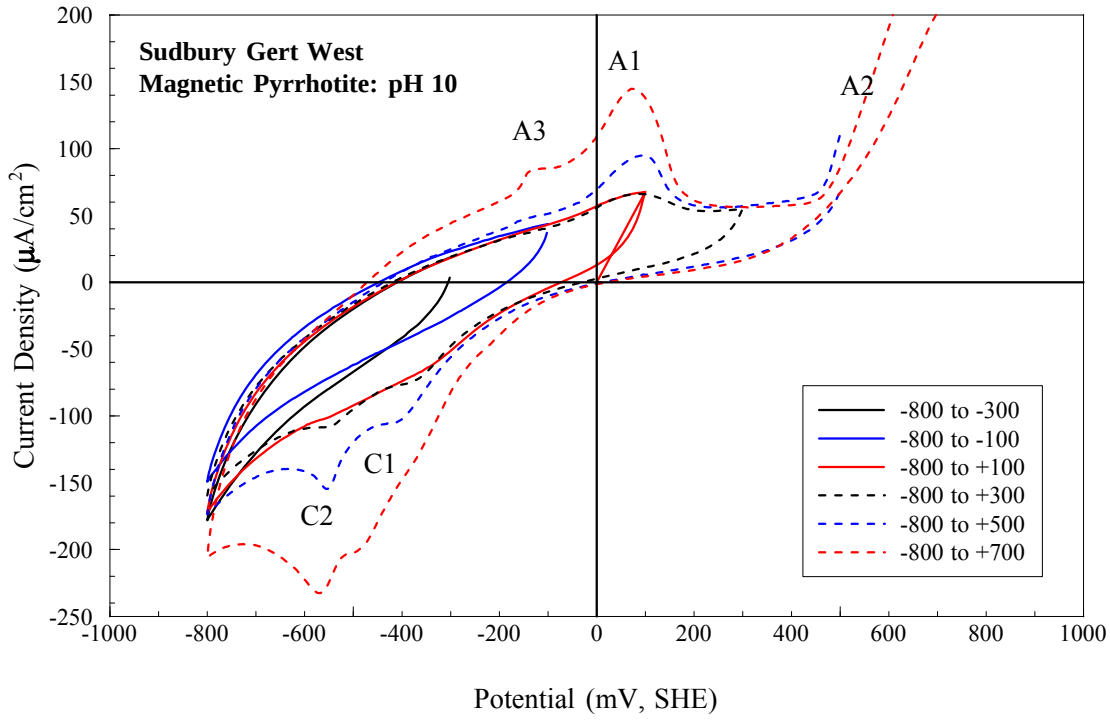


**Figure 5.10:** Cyclic voltammogram of Sudbury Gertrude West magnetic pyrrhotite at pH 10 for different anodic switching potentials.

### 5.3.5 Comparison of the Cyclic Voltammetry of Pyrrhotite Samples

In order to compare the reactivity of the different pyrrhotite samples, the cyclic voltammogram obtained for each pyrrhotite sample corresponding to the sweep from -800 to +700mV is shown in figures 5.11 and 5.12 for pH 7 and 10, respectively. Comparison of the voltammograms for the pyrrhotite samples examined at pH 7 shows that each of the pyrrhotite samples showed two anodic and three cathodic peaks at similar potentials. In general, the current density was greater at the higher pH due to the increase in reaction rates associated with the increase in hydroxide ion concentration. At pH 10, it is also evident that the Nkomati mixed pyrrhotite, Phoenix magnetic pyrrhotite and Sudbury Gertrude West magnetic pyrrhottie electrodes showed three anodic peaks whereas Sudbury CCN non-magnetic pyrrhotite only showed two. The anodic reaction A3 did not occur for the Sudbury CCN non-magnetic pyrrhotite at pH 10, which could be directly related to differences in pyrrhotite reactivity.

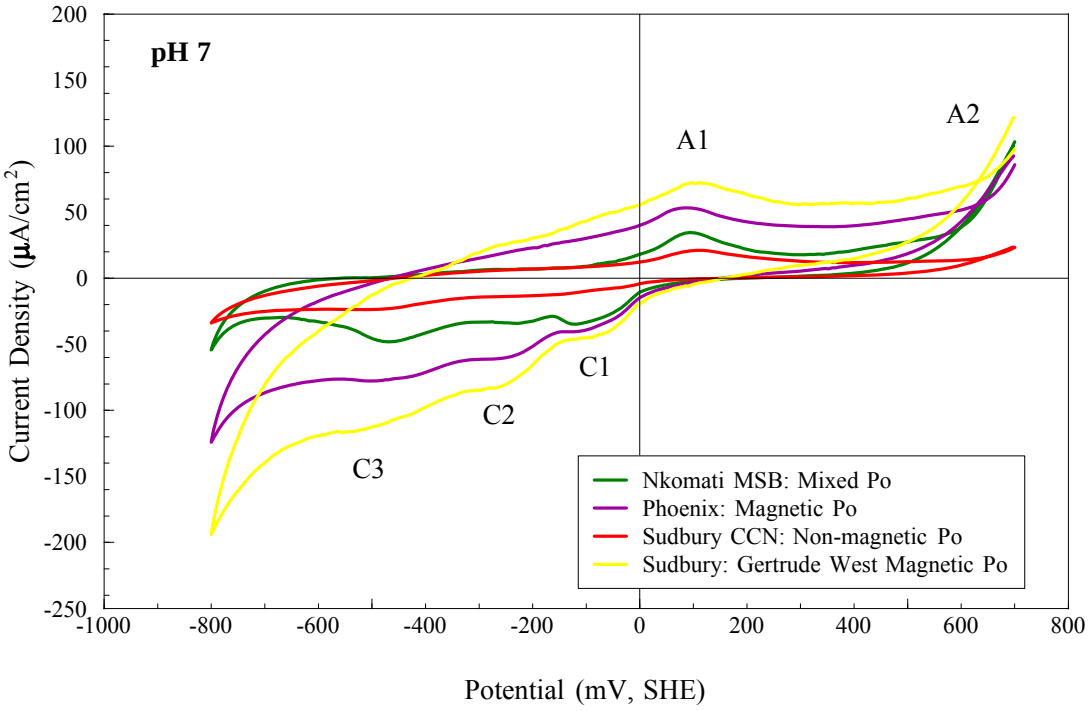


**Figure 5.11:** Comparison of the cyclic voltammograms obtained for the different pyrrhotite samples at pH 7 for the sweep from -800 to +700 mV.

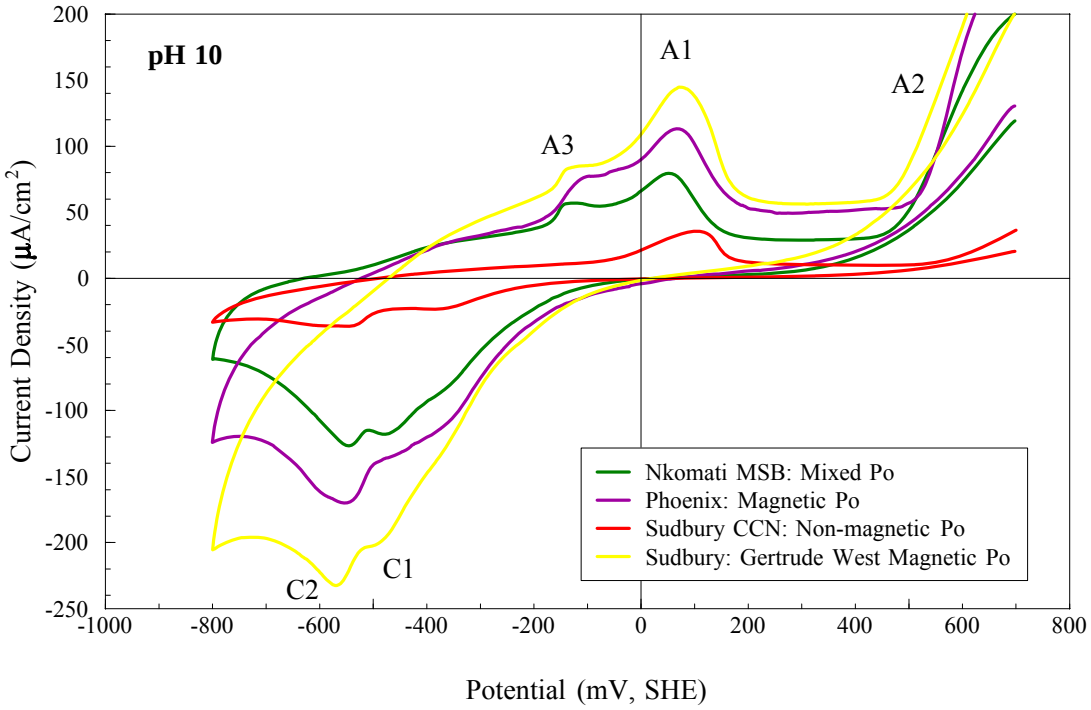


**Figure 5.12:** Comparison of the cyclic voltammograms obtained for the different pyrrhotite samples at pH 10 for the sweep from -800 to +700 mV.

The most prominent difference in the cyclic voltammograms for the different pyrrhotites is the large differences in current density which were correlated with the extent of the reactions. These can be directly related to the varying reactivity of the different pyrrhotite samples. Since the lowest current density occurred for Sudbury CCN non-magnetic pyrrhotite, it is indicative that it had the lowest reactivity of the samples examined. The current density for Nkomati mixed pyrrhotite was slightly larger and therefore the pyrrhotite was a little more reactive. The two magnetic pyrrhotite samples showed the greatest changes in current density and suggests that they were the most reactive. Magnetic Sudbury Gertrude West pyrrhotite however, showed the greatest changes in current density, and therefore the fastest reaction rates which indicates that it was the most reactive towards oxidation and reduction of the samples examined in this study.

## 5.4 Oxygen Uptake

Previous authors such as Spira and Rosenblum (1974), Greet and Brown (2000) and Johnson and Munro (2008) have recognised the significance of the oxygen demand of pyrrhotite rich ores in flotation. Consequently, a series of reactivity tests were performed to determine the oxygen uptake of the pyrrhotite samples investigated in this study. The tests were designed to measure the amount of dissolved oxygen in a slurry consumed through pyrrhotite oxidation. The tests were designed to simulate the conditions observed in the microflotation tests so that the results are comparable (Section 3.4, 3.5). Three sets of reagent conditions were explored, that consisted of no collector addition (collectorless), collector addition and collector plus activator addition, where copper sulfate was used for activation. Two collectors, namely SNPX and the longer chain length SIBX were used. The tests were carried out at pH 7 and pH 10. The mineralogical composition of the samples used is given in tables 3.1 and 3.3. Once the individual samples were suitably conditioned with reagents and the pH set to the desired pH, the mineral slurry was sparged with pure oxygen for a set time and then the decay of dissolved oxygen in the pyrrhotite slurry was measured. An exponential curve was fitted to the graph comparing the change in dissolved oxygen with time, and the coefficient of the slope of the curve used as the dissolved oxygen uptake factor. Table 5.1 summarises the calculated oxygen uptake factors obtained for the various pyrrhotite samples. An example of the calculation of the oxygen uptake factor, repeatability of the measurement and the raw data are given in Appendix B.

**Table 5.1**: Summary of oxygen uptake factors obtained in pyrrhotite reactivity tests for the various pyrrhotite samples. The associated $R^2$ is also given for the calculated oxygen uptake factor.

| **Pyrrhotite** | | **Nkomati MSB** Mixed | | **Phoenix** Magnetic | | **Sudbury CCN** Non-magnetic | | **Sudbury Gert West** Magnetic | |
|---|---|---|---|---|---|---|---|---|---|
| **Conditions** | **pH** | Factor | $R^2$ | Factor | $R^2$ | Factor | $R^2$ | Factor | $R^2$ |
| Collectorless | 7 | 15 | 0.998 | 29 | 0.997 | 9 | 0.999 | 17 | 0.998 |
| SNPX | 7 | 14 | 0.997 | 24 | 0.997 | 12 | 0.997 | 14 | 0.992 |
| SNPX + Cu | 7 | - | - | 16 | 0.991 | - | - | 8 | 0.983 |
| SIBX | 7 | 14 | 0.998 | 28 | 0.999 | 7 | 0.974 | 12 | 0.983 |
| SIBX + Cu | 7 | 18 | 0.998 | 16 | 0.997 | 12 | 0.997 | 9 | 0.982 |
| Collectorless | 10 | 60 | 0.998 | 110 | 0.995 | 8 | 0.999 | 36 | 0.995 |
| SNPX | 10 | 25 | 0.999 | 60 | 0.999 | 6 | 0.997 | 33 | 0.999 |
| SNPX + Cu | 10 | - | - | 28 | 0.995 | 2 | 0.981 | 14 | 0.998 |
| SIBX | 10 | 24 | 0.997 | 49 | 0.998 | 6 | 0.996 | 29 | 0.994 |
| SIBX + Cu | 10 | 17 | 0.999 | 31 | 0.999 | 10 | 0.999 | 13 | 0.998 |

### 5.4.1 Nkomati MSB Pyrrhotite

Following the conditioning of the Nkomati MSB mixed magnetic and non-magnetic pyrrhotite slurry with reagents, the pH was approximately neutral prior to pH modification for the associated mineral reactivity tests. The dissolved oxygen content of the mineral slurry after modification to pH 7 and prior to oxygen sparging varied between 2.3 and 5.7 ppm as shown in figure 5.13. The variability in initial dissolved oxygen content was likely a function of the conditioning procedure for each of the different tests given that different reagents were added for the various tests (SIBX, SNPX, Cu), each with their own respective conditioning times. Following sparging, the dissolved oxygen content of the slurry showed a progressive increase up to a maximum of 8.4 ppm for the SNPX test, 8.9 ppm for the collectorless test, 10.4 ppm for the SIBX test and up to 11.9 ppm for the SIBX with copper test. Once the maximum dissolved oxygen content had been reached, the dissolved oxygen levels showed a distinct decrease with time. The calculated oxygen uptake factors given in table 5.1 however, showed little difference between the different tests at pH 7. The highest factor was obtained for the SIBX with copper test ($O_2$ Uptake factor = 18) and the lowest for the SIBX and SNPX tests ($O_2$ Uptake factor = 14).

The dissolved oxygen contents of the slurry at pH 10 prior to sparging with oxygen were generally lower (0.4 – 2.0 ppm) than at pH 7 as shown in figure 5.14. Following oxygen sparging the dissolved oxygen content showed a progressive increase up to a maximum of 5.7 ppm for the collectorless test, 6.6 ppm for the SNPX test, 7.7 ppm for the SIBX with copper test and up to 8.6 ppm for the SIBX test. Once the maximum dissolved oxygen content had been reached, the decay of dissolved oxygen with time was fastest for the collectorless test (Uptake factor = 60), slightly slower for the xanthate tests ($O_2$ Uptake factor ~ 24) and slowest for the SIBX with copper test ($O_2$ Uptake factor = 17).

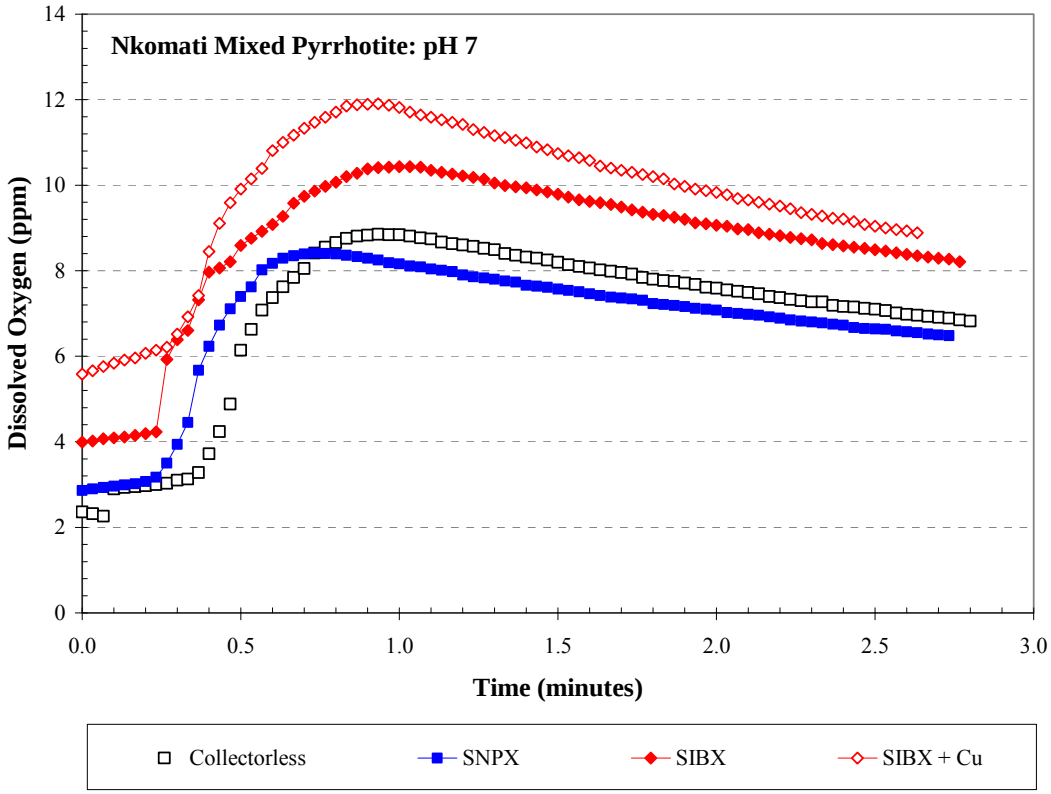


**Figure 5.13:** Change in dissolved oxygen with time for a slurry containing Nkomati MSB mixed pyrrhotite. Results are shown for the different reagent conditions at pH 7.

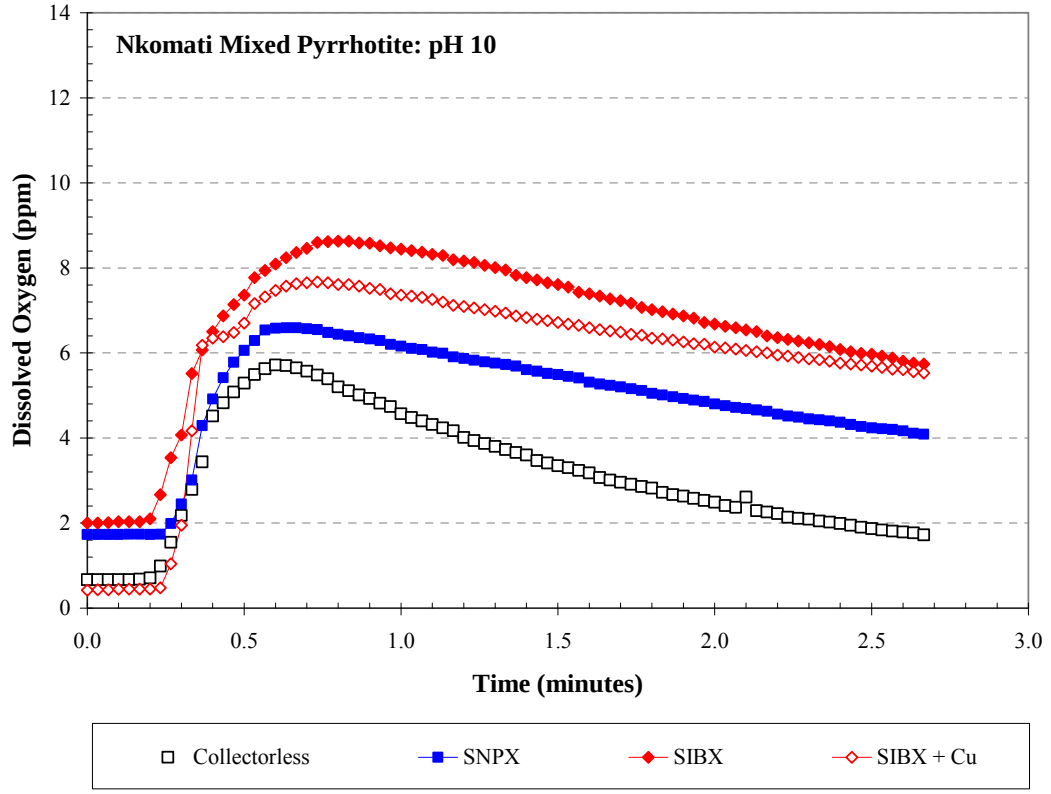


**Figure 5.14:** Change in dissolved oxygen with time for a slurry containing Nkomati MSB mixed pyrrhotite. Results are shown for the different reagent conditions at pH 10.

### 5.4.2 Phoenix Pyrrhotite

At pH 7, the natural dissolved oxygen content for a slurry of the Phoenix pyrrhotite prior to oxygen sparging was between 0 and 2 ppm as can be observed in figure 5.15. The natural pH of the slurry was ~ 5, prior to it being altered to the desired pH. Figure 5.15 shows that once the slurry had been sparged with pure oxygen, the dissolved oxygen content showed a steady increase until a point was reached where the rate of oxygen consumption by pyrrhotite oxidation was significant enough to cause a steady decline in the dissolved oxygen content.

At pH 7, the maximum dissolved oxygen content reached for the collectorless test was 6.78 ppm. Slightly higher maximum dissolved oxygen contents were obtained with SIBX (7.64 ppm), and slightly lower maximum dissolved oxygen contents for SNPX (6.88 ppm). With SIBX and copper addition, even higher maximum dissolved oxygen contents were obtained, whereas for SNPX with copper addition the lowest dissolved oxygen contents were measured at this pH.

The natural dissolved oxygen contents for Phoenix magnetic pyrrhotite at pH 10 are shown in figure 5.16 where it is evident that they were all less than 1 ppm and as such, even lower than at pH 7. For the collectorless test, the maximum dissolved oxygen content with sparging was the lowest of all (3.91 ppm) and the effect of reagent addition was to increase the maximum dissolved oxygen content. It is also apparent that at pH 10, the effect of copper addition with xanthate was to cause higher maximum dissolved oxygen contents (e.g. 6.25 ppm for SIBX and 7.16 ppm for SIBX + Cu).

The calculated oxygen uptake factors for the Phoenix magnetic pyrrhotite reactivity tests given in table 5.2 were as high as 29 at pH 7 and for pH 10, as high as 110. For both the pH conditions tested, the highest oxygen uptake factors were obtained for the collectorless tests ($O_2$ uptake factor = 29 at pH 7, 110 at pH 10). The effect of reagent addition was to decrease the oxygen uptake factor e.g. decrease to 24 at pH 7 for SNPX. A further decrease in oxygen uptake factor was observed with the addition of copper e.g. decrease to 16 at pH 7 for SNPX + Cu. The effect of an increase in pH was to cause a further increase in oxygen uptake factor, e.g. increase up to 60 for SNPX at pH 10. Similarly, the effect of copper addition at pH 10 was to cause another decrease in oxygen uptake factor, e.g. decrease to 28 for SNPX + Cu.

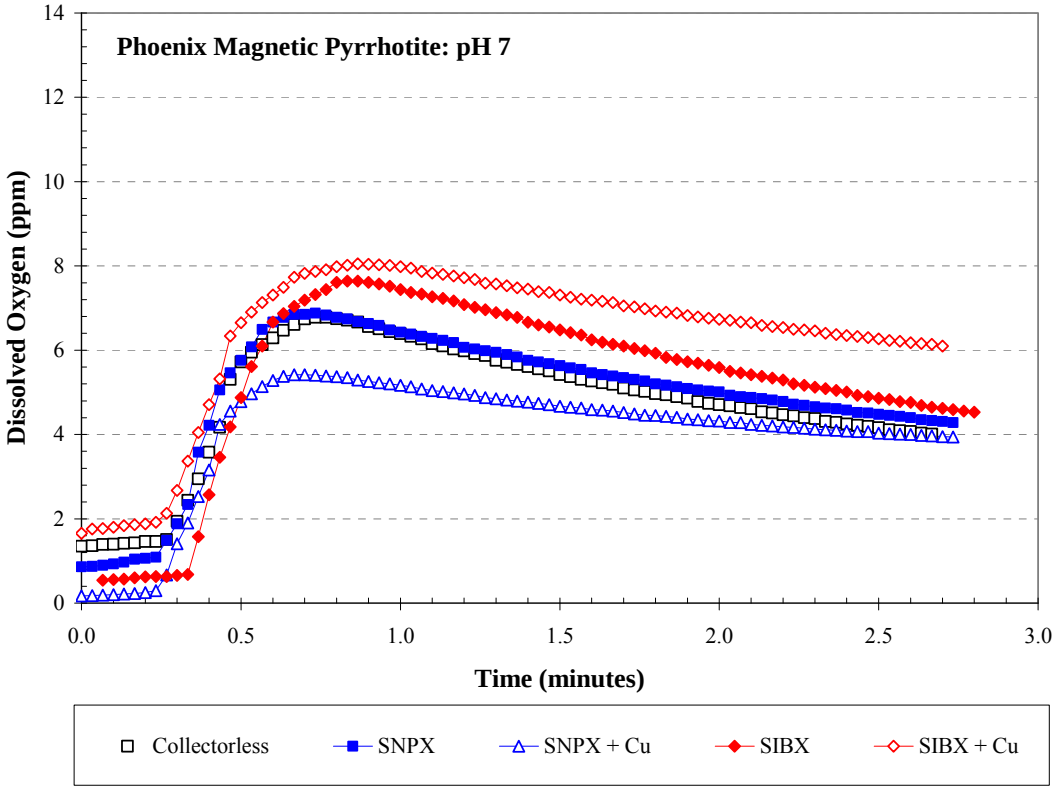


**Figure 5.15:** Change in dissolved oxygen with time for a slurry containing magnetic Phoenix pyrrhotite. Results are shown for the different reagent conditions at pH 7.

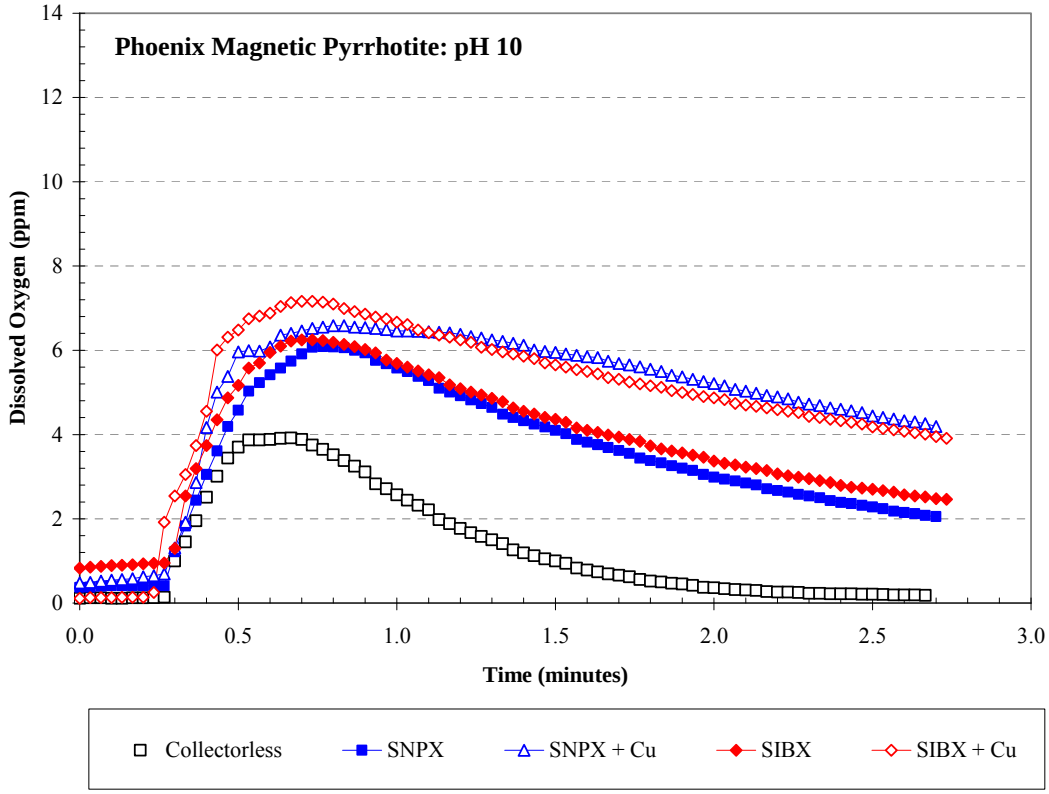


**Figure 5.16:** Change in dissolved oxygen with time for a slurry containing magnetic Phoenix pyrrhotite. Results are shown for the different reagent conditions at pH 10.

### 5.4.3 Sudbury Copper Cliff North Pyrrhotite

Following reagent conditioning, the natural pH measured for the Sudbury CCN non-magnetic pyrrhotite slurry was ~ 8 prior to pH modification associated with the mineral reactivity tests. The natural dissolved oxygen content at both pH 7 and 10 varied between 6 and 7.5 ppm as can be observed in figures 5.17 and 5.18. With oxygen sparging, the dissolved oxygen in the Sudbury CCN pyrrhotite slurry showed a rapid increase followed by a sudden, yet slow decay in dissolved oxygen due to the oxidation of the pyrrhotite in the slurry. The highest maximum dissolved oxygen content was obtained for the SIBX with copper test at pH 7 (13.3 ppm). For all the tests at pH 7, the consequent drop in dissolved oxygen content with time following oxygen sparging tended to be slow and therefore the calculated oxygen uptake factors were low (≤ 12; Table 5.1). Given the low oxygen uptake factors measured, it is unlikely that the differences observed for the different test conditions are significant for the Sudbury CCN non-magnetic pyrrhotite.

For all the tests performed at pH 10, the starting dissolved oxygen content was between 6.6 and 7.4 ppm then showed a sudden increase associated with oxygen sparging as shown in figure 5.18. The subsequent decay in dissolved oxygen due to pyrrhotite oxidation was generally very slow and the dissolved oxygen contents of the slurry remained between approximately 10 and 12 ppm. For the SIBX tests, the addition of copper caused an increase in maximum dissolved oxygen content (11.5 ppm for SIBX, 12.7 ppm for SIBX + Cu), and similarly for SNPX at pH 10. In terms of the calculated oxygen uptake factors, the addition of collector caused a decrease in uptake factor ($O_2$ uptake factor = 6 for both SNPX and SIBX) relative to the blank test ($O_2$ Uptake factor = 8). The addition of copper however had varying effects; an associated increase in oxygen uptake factor was observed for SIBX with copper addition (10) whereas for SNPX with copper addition, a decrease was observed (2). Similarly to at pH 7, the disparity in the calculated oxygen uptake factors for the CCN pyrrhotite is most likely a consequence of the error associated with the actual measurement.

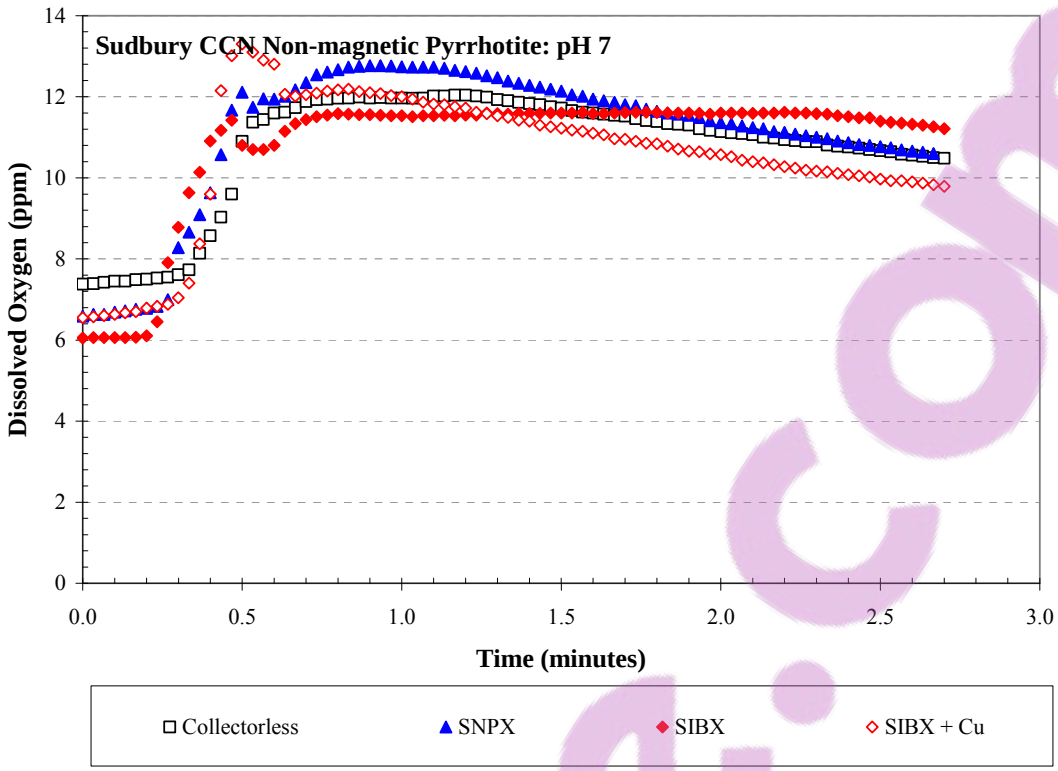


**Figure 5.17:** Change in dissolved oxygen with time for a slurry containing non-magnetic Sudbury CCN pyrrhotite. Results are shown for the different reagent conditions at pH 7.

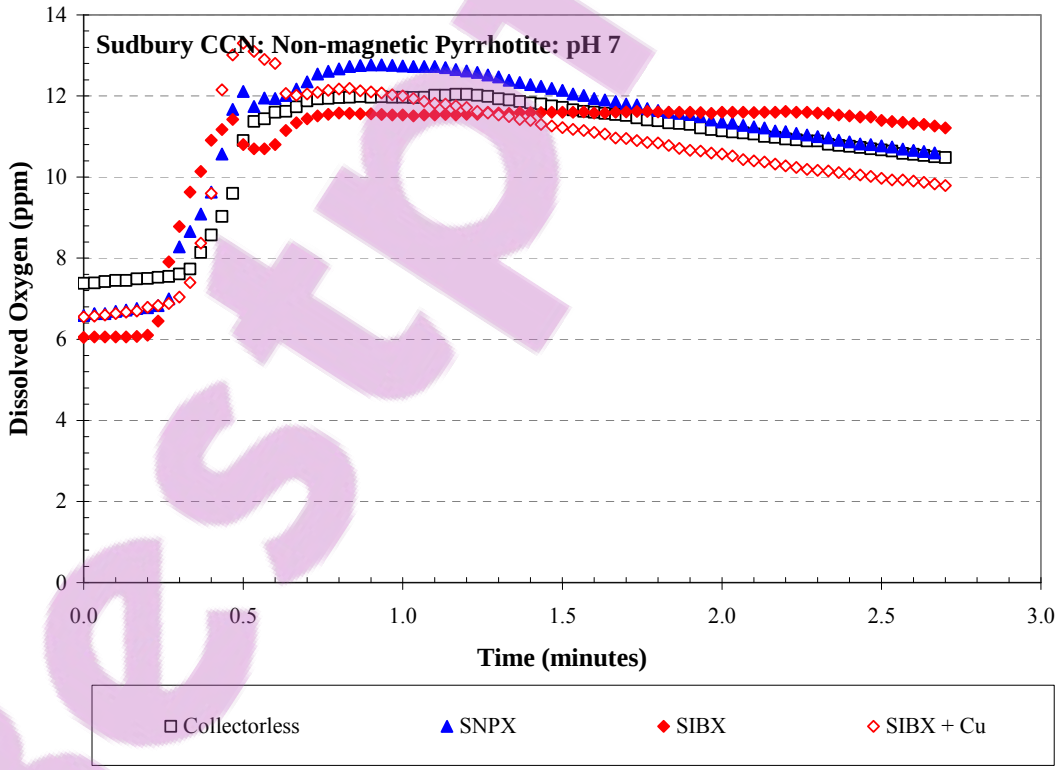


**Figure 5.18:** Change in dissolved oxygen with time for a slurry containing non-magnetic Sudbury CCN pyrrhotite. Results are shown for the different reagent conditions at pH 10.

### 5.4.4 Sudbury Gertrude West Pyrrhotite

Magnetic Sudbury Gertrude West pyrrhotite had a neutral pH (~ 7) when made into a mineral slurry prior to pH modification for the associated mineral reactivity tests. Prior to oxygen sparging the dissolved oxygen content of the mineral slurry varied between 1.8 and 3.6 ppm as shown in figure 5.19. Following sparging with oxygen, the dissolved oxygen content of the pyrrhotite slurry climbed to above 7.5 ppm, before the oxidation of pyrrhotite started to consume the dissolved oxygen in solution. At this point, the measured dissolved oxygen content of the slurry decreased at a relatively slow rate. For all tests other than the SNPX with copper test, slightly lower maximum dissolved oxygen contents were measured relative to the collectorless test.

In terms of the rate of dissolved oxygen consumption as quantified by the calculated oxygen uptake factor given in table 5.1, the highest factor was obtained for the collectorless test ($O_2$ Uptake factor = 17) and lower factors were obtained for tests with reagent addition. For both the SNPX and SIBX tests, the addition of copper caused an associated decrease in pyrrhotite reactivity (i.e. slower rate of $O_2$ decay) and lower oxygen uptake factors were obtained (e.g. $O_2$ Uptake factor = 12 for SIBX, 9 for SIBX + Cu).

It is noted that the slurry containing Gertrude West magnetic pyrrhotite was more reactive at pH 10 relative to pH 7 as shown in figure 5.20. The maximum dissolved oxygen contents measured for all the test conditions were lower at pH 10 (< 8.2 ppm) than at pH 7 (up to 9.8 ppm). It is also apparent that the slopes of the graphs in figure 5.20 were steeper for the tests at pH 10 than at pH 7 and which were manifested by the difference in calculated oxygen uptake factors for the Gertrude West pyrrhotite. In general, the calculated oxygen uptake factors at pH 10 were approximately double that from at pH 7, e.g. $O_2$ Uptake factor = 17 at pH 7, 36 at pH 10 for collectorless test. Calculated oxygen uptake factors were also lower with the addition of SIBX (29) or SNPX (33), and even lower still, with the addition of copper ($O_2$ Uptake factor = 13 for SIBX + Cu, 14 for SNPX + Cu).

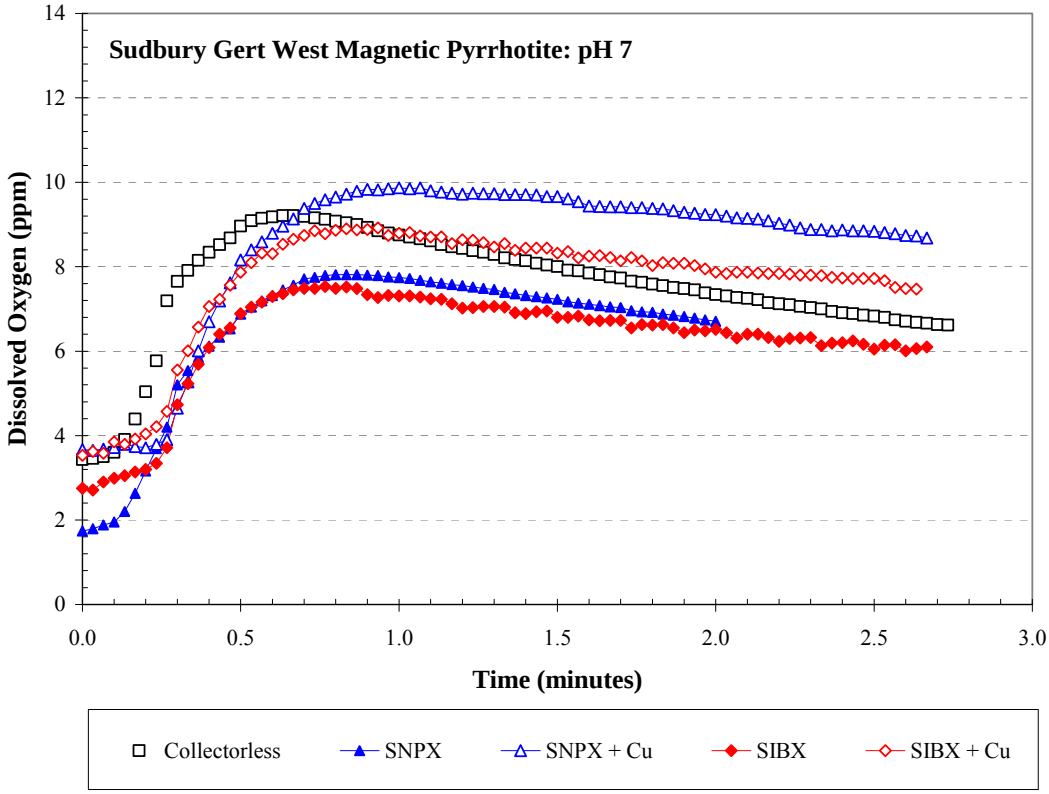


**Figure 5.19:** Change in dissolved oxygen with time for a slurry containing magnetic Sudbury Gertrude West pyrrhotite. Results are shown for the different reagent conditions at pH 7.

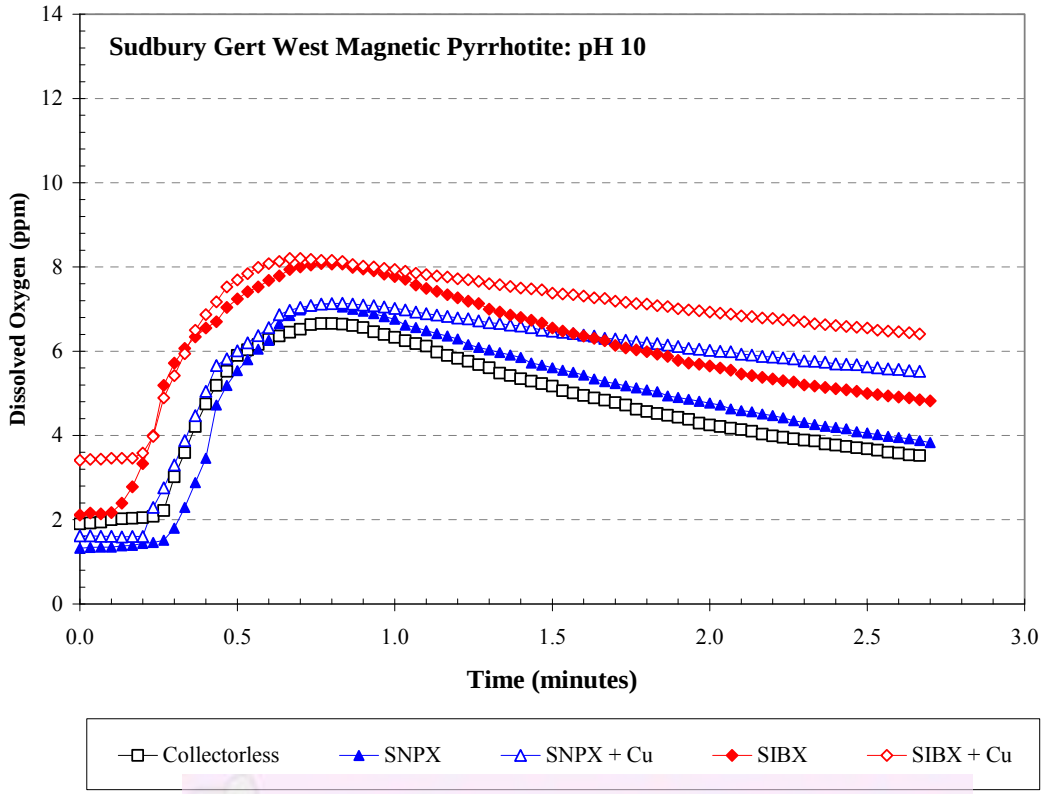


**Figure 5.20:** Change in dissolved oxygen with time for a slurry containing magnetic Sudbury Gertrude West pyrrhotite. Results are shown for the different reagent conditions at pH 10.

### 5.4.5 Comparison of the Oxygen Uptake of Pyrrhotite Samples

A comparison of the change in dissolved oxygen content with time for the four pyrrhotite slurries investigated is shown for pH 7 and pH 10 in figures 5.21 and 5.22, respectively. For comparative purposes, the results from only the collectorless tests are shown so that the interpretation is not complicated by the interaction of the reagents with the pyrrhotite surface. Figure 5.21 shows that at pH 7, the natural dissolved oxygen content was quite different for the slurries of the four pyrrhotite samples. The natural dissolved oxygen content of Phoenix magnetic pyrrhotite was lowest, the Nkomati mixed pyrrhotite was slightly higher, the magnetic Sudbury Gertrude West pyrrhotite was even higher, and the Sudbury CCN non-magnetic pyrrhotite was by far the highest of all. Following sparging with oxygen, the maximum dissolved oxygen contents of the pyrrhotite slurries showed a similar ordering; Phoenix magnetic pyrrhotite was the lowest (6.8 ppm), the Nkomati mixed pyrrhotite was slightly higher (8.8 ppm), the magnetic Sudbury Gertrude West pyrrhotite was even higher (9.2 ppm) and the Sudbury CCN non-magnetic pyrrhotite was by far the highest (12.0 ppm). This order was in turn reversed when the oxygen uptake factors are compared, in that the pyrrhotite with the highest dissolved oxygen contents (Sudbury CCN) had the lowest oxygen uptake factor (9), those with intermediate dissolved oxygen contents (Nkomati, Sudbury Gertrude West) had moderate oxygen uptake factors (~15), and the pyrrhotite with the lowest dissolved oxygen content (Phoenix) had the highest oxygen uptake factor (29).

Figure 5.22 shows that the relative differences in mineral reactivity between slurries of the four pyrrhotite samples at pH 7 were conserved at pH 10, although the differences were more extreme. For the magnetic and mixed pyrrhotite samples, the natural dissolved oxygen content was distinctly lower at pH 10 (< 2 ppm) and even approached zero for the Phoenix magnetic pyrrhotite. The natural dissolved oxygen content of the non-magnetic Sudbury CCN appeared to be relatively unaffected by a change in pH. In terms of the uptake of dissolved oxygen in solution through pyrrhotite oxidation, magnetic Phoenix pyrrhotite was the greatest ($O_2$ Uptake factor = 110), mixed Nkomati pyrrhotite was slightly less ($O_2$ uptake factor = 60), magnetic Sudbury Gertrude West was even less ($O_2$ uptake factor = 36) and the non-magnetic Sudbury CCN pyrrhotite was the lowest ($O_2$ uptake factor = 8). This indicates that the non-magnetic Sudbury CCN pyrrhotite was the least reactive of the pyrrhotite samples examined and had the lowest propensity for oxygen consumption via pyrrhotite oxidation.

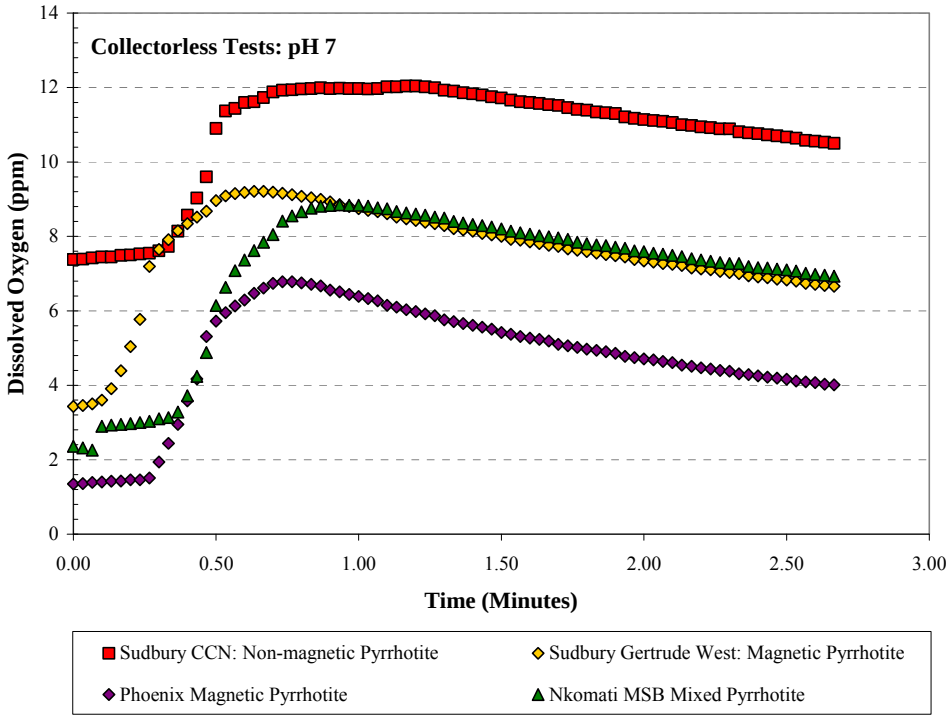


**Figure 5.21**: Change in dissolved oxygen content with time for slurries of all the pyrrhotite samples at pH 7 shown for the collectorless tests.

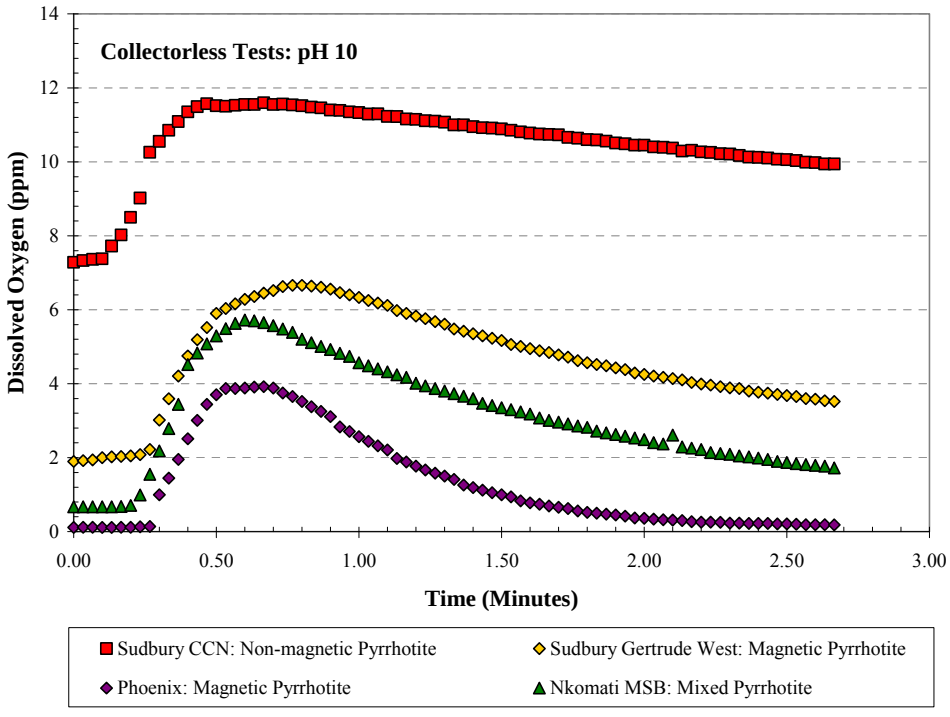


**Figure 5.22:** Change in dissolved oxygen content with time for slurries of all the pyrrhotite samples at pH 10 shown for the collectorless tests.

Comparison of the oxygen uptake factors at pH 7 for slurries of the four pyrrhotite samples examined under various reagent conditions illustrated in figures 5.23 and 5.24 shows that the Phoenix magnetic pyrrhotite always had the highest oxygen uptake factor for the conditions investigated. Similarly, the calculated oxygen uptake factors were almost always the lowest for the non-magnetic Sudbury CCN pyrrhotite, whereas the calculated oxygen uptake factors were generally slightly lower and similar for the magnetic Gertrude West and mixed Nkomati pyrrhotite samples.

The general trend observed at pH 7 with respect to the effect of reagent addition on the calculated oxygen uptake factor was that the factor got smaller since the addition of collector retarded the decay of oxygen in the pyrrhotite slurry (Figure 5.23, 5.24). Similarly, even though the trend appears to be somewhat tentative, the addition of copper to the solution caused a further drop in the oxygen uptake factor, suggesting the decay of oxygen in the pyrrhotite slurry was retarded even more.

Comparison of the calculated oxygen uptake factors in the collectorless oxygen uptake tests of the four pyrrhotite slurries at pH 10 illustrated in figures 5.25 and 5.26 similarly shows that the Phoenix magnetic pyrrhotite always had the highest oxygen uptake factor. In contrast, the oxygen uptake factors were always the lowest for the non-magnetic Sudbury CCN pyrrhotite slurry whereas oxygen uptake factors were somewhere in between for the magnetic Sudbury Gertrude and mixed Nkomati pyrrhotite samples. In general, the effect of collector addition on the reactivity for oxygen consumption of all the pyrrhotite slurries at pH 10 was to reduce their reactivity as shown by the decrease in calculated oxygen uptake factors. In general, the reactivity of the pyrrhotite with SNPX addition was greater than with SIBX addition. The effect of copper addition in conjunction with SIBX or SNPX addition was to cause a further decrease in pyrrhotite reactivity as evidenced by the subsequent decrease in oxygen uptake figures. It is evident however, that the oxygen uptake factors for the non-magnetic Sudbury CCN pyrrhotite showed little change that could be correlated with the effect of reagent addition which is an indication of the relatively unreactive nature of this pyrrhotite sample.

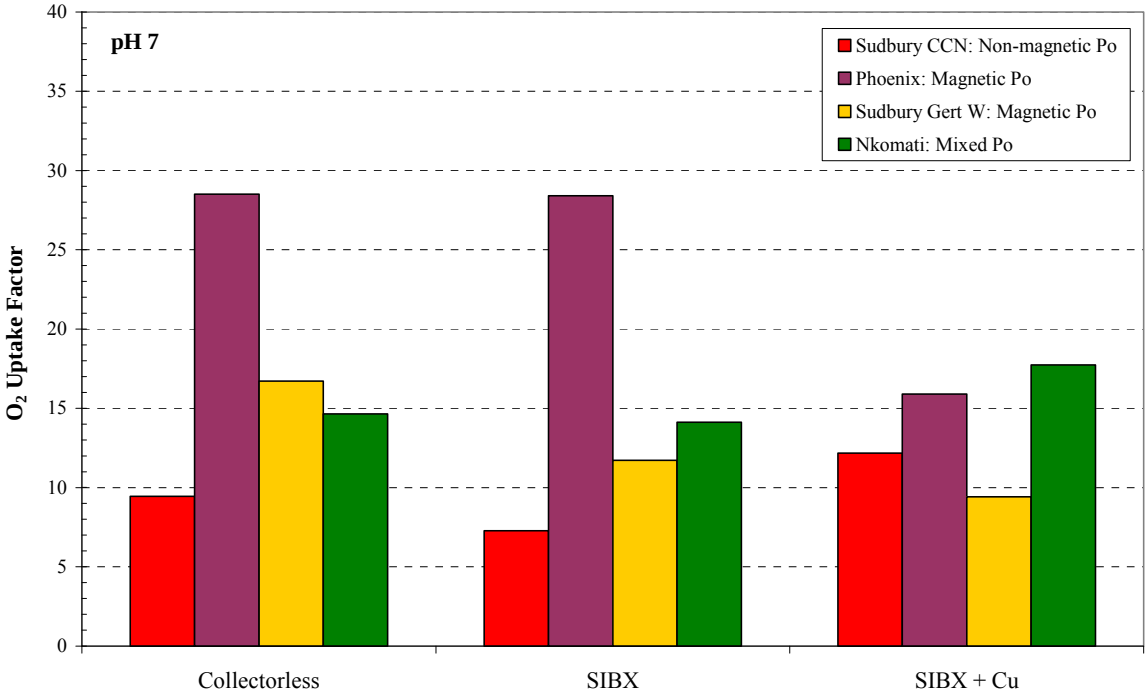


**Figure 5.23**: Comparison of the dissolved oxygen uptake factor for slurries of all the pyrrhotite samples at pH 7 shown for SIBX collector tests.

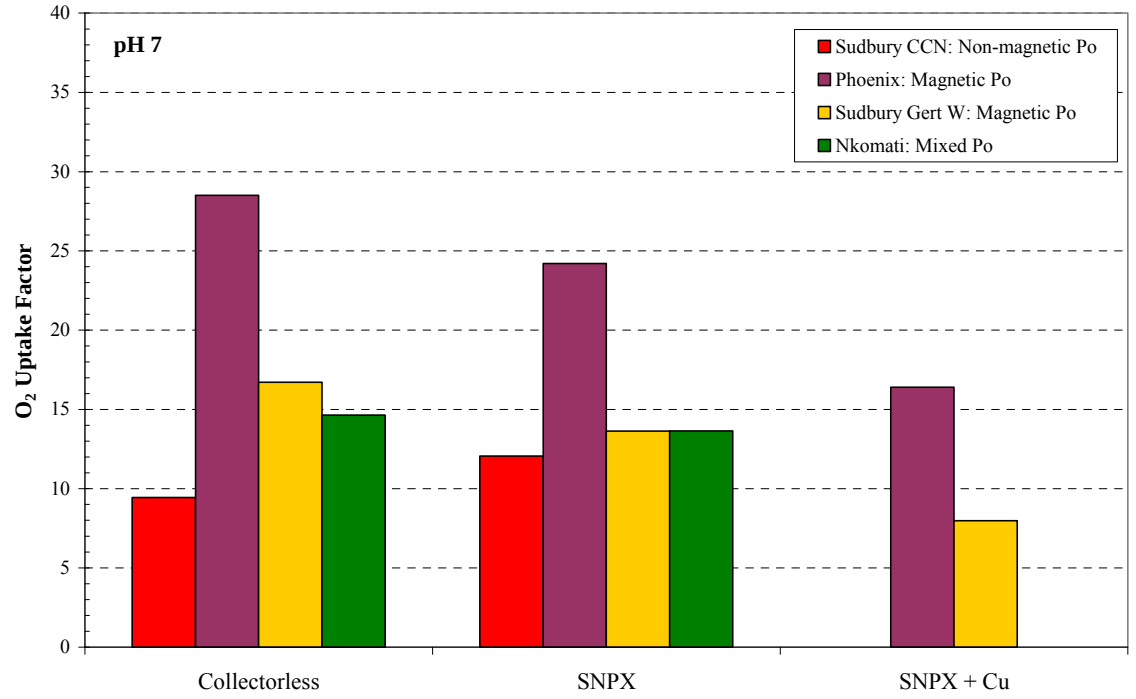


**Figure 5.24:** Comparison of the dissolved oxygen uptake factor for slurries of all the pyrrhotite samples at pH 7 shown for SNPX collector tests.

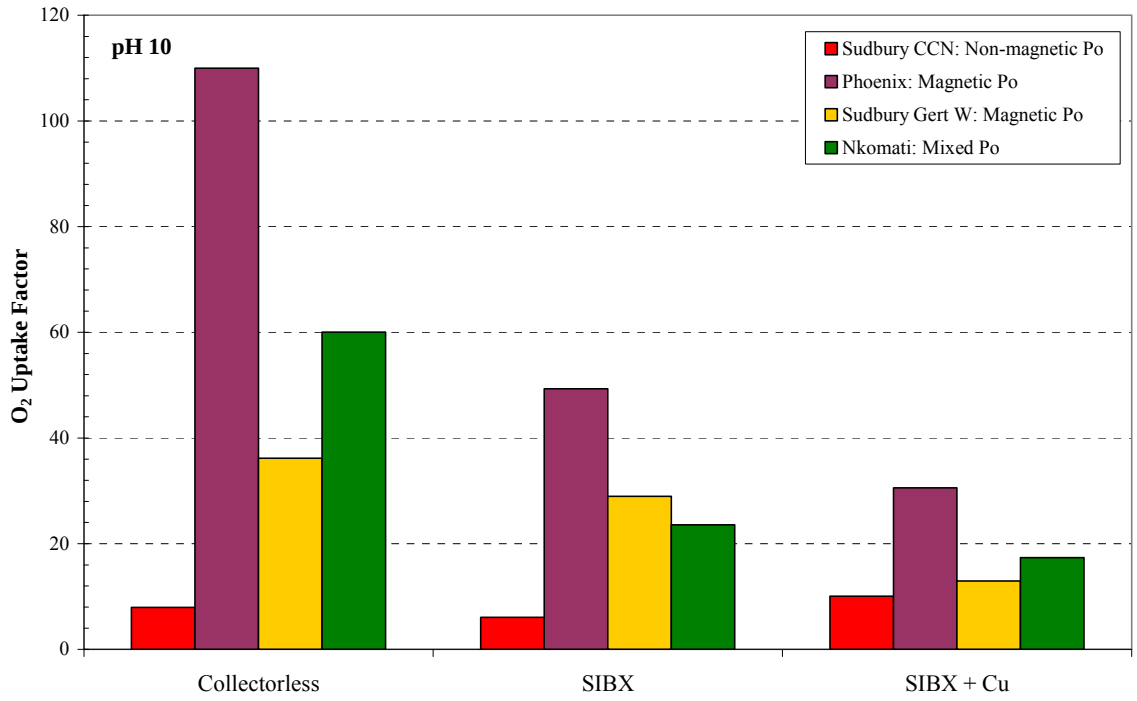


**Figure 5.25:** Comparison of the dissolved oxygen uptake factor for slurries of all pyrrhotite samples at pH 10 shown for SIBX collector tests.

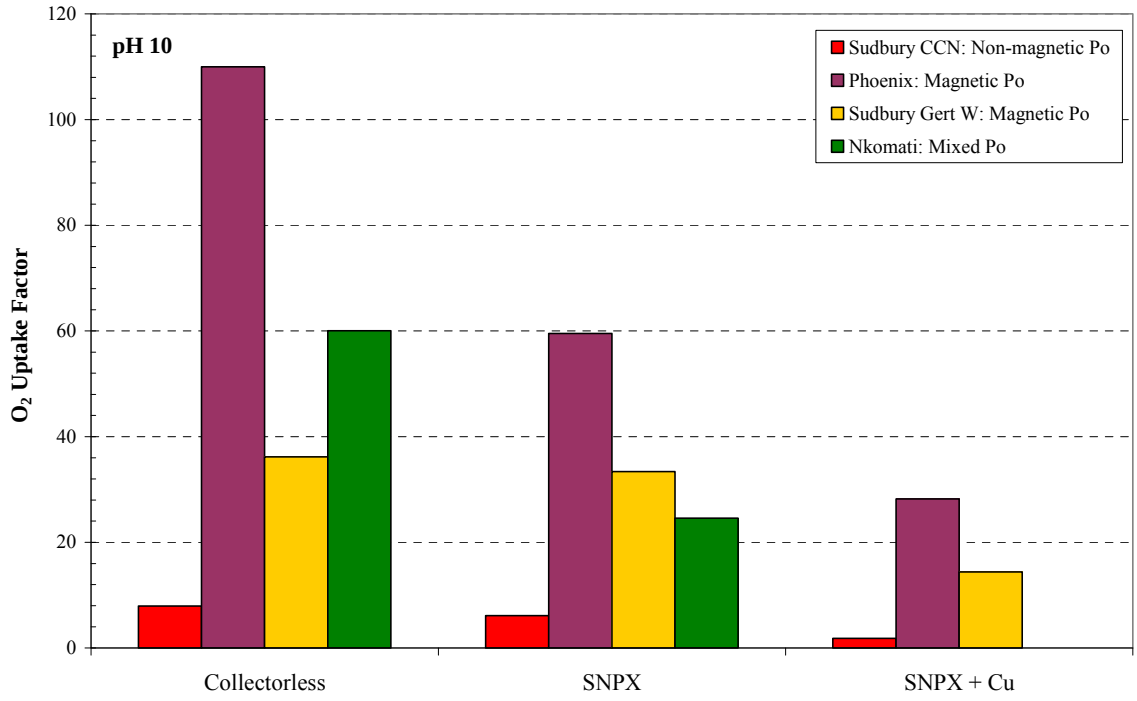


**Figure 5.26:** Comparison of the dissolved oxygen uptake factor for slurries of all pyrrhotite samples at pH 10 shown for SNPX collector tests.

## 5.5 Key findings

Key features noted with respect to the reactivity of pyrrhotite from selected nickel and platinum group element ore deposits were as follows:

Open circuit potential measurements performed on electrodes of the four pyrrhotite samples at pH 7 were relatively similar to each other, although the Sudbury CCN non-magnetic pyrrhotite was observed to show the highest open circuit potential (170 mV). At pH 10, better resolution occurred between open circuit potential measurements of the different pyrrhotite electrodes due to differences in electrochemical reaction rates. The highest open circuit potential was obtained for the Sudbury Gertrude West magnetic pyrrhotite sample (116 mV) and which indicated that the pyrrhotite electrode was the most oxidised of the samples examined. Phoenix magnetic pyrrhotite and Nkomati MSB mixed pyrrhotite had slightly lower and similar open circuit potentials (~ 43mV), and the lowest open circuit potential was obtained for the Sudbury CCN non-magnetic pyrrhotite (15 mV).

Two anodic and three cathodic reactions were noted in the cyclic voltammetry studies of the four pyrrhotite electrodes at pH 7. At pH 10, three anodic and two cathodic reactions were noted in the cyclic voltammetry studies. These reactions were common to all four pyrrhotite samples except for the Sudbury CCN non-magnetic pyrrhotite that did not show the anodic reaction A3 at ~ -200mV at pH 10. Significant differences were observed in current density that were related to differences in electrochemical reaction rates and pyrrhotite reactivity. Sudbury CCN non-magnetic pyrrhotite showed the smallest change in current density, Nkomati MSB mixed pyrrhotite showed slightly greater changes in current density and Phoenix magnetic pyrrhotite showed even greater changes in current density. The Gertrude West magnetic pyrrhotite showed the greatest changes in current density and was therefore the most reactive of the pyrrhotite samples investigated.

The rate of dissolved oxygen uptake from slurries containing the four different pyrrhotite samples increased when the pH was increased from 7 to 10. e.g. The slurry containing Phoenix magnetic pyrrhotite with no collector, showed an increase in the oxygen uptake factor from 29 to 110 due to the increase in reactivity with the increase in hydroxide ion concentration.

The rate of dissolved oxygen uptake from slurries containing the four different pyrrhotite samples decreased with the addition of collector to the slurry e.g. the slurry containing Phoenix magnetic pyrrhotite, showed a decrease in the oxygen uptake factor from 110 to 49 associated with the addition of SIBX at pH 10. The pyrrhotite slurry was noted to be more reactive for the shorter chain length SNPX collector relative to SIBX.

The rate of dissolved oxygen uptake from slurries containing the four different pyrrhotite samples generally decreased with copper activation e.g. the slurry containing Phoenix magnetic pyrrhotite, showed a decrease in the oxygen uptake factor from 49 to 31 associated with copper activation in conjunction with SIBX addition at pH 10.

At both pH 7 and 10, the dissolved oxygen uptake was greatest for the slurry containing the Phoenix magnetic pyrrhotite ($O_2$ uptake factor = 110 at pH 10). At both pH 7 and 10, the dissolved oxygen uptake was the lowest for the slurry containing the Sudbury CCN non-magnetic pyrrhotite ($O_2$ uptake factor = 8 at pH 10). The dissolved oxygen uptake was somewhere in between for the Sudbury Gertrude West magnetic and Nkomati MSB mixed pyrrhotite. At pH 10 however, the slurry containing the Nkomati MSB mixed pyrrhotite showed a slightly greater rate of dissolved oxygen uptake ($O_2$ uptake factor = 60) than the slurry containing Sudbury Gertrude West magnetic pyrrhotite ($O_2$ uptake factor = 36).

# Chapter 6

# PYRRHOTITE MICROFLOTATION

## 6.1 Introduction

As described in Chapter 2, a reasonable understanding exists with regard to the mechanism and species which lend pyrrhotite its floatability but the accounts comparing the floatability of the different pyrrhotite types are in conflict (Section 2.6.3). Since the aim of this research was to develop the relationship between pyrrhotite mineralogy and flotation performance, it is necessary to *explore and compare the flotation performance of magnetic and non-magnetic pyrrhotite*, which is the aim of this chapter. Microflotation tests were selected as the preferred experimental method to compare pyrrhotite flotation since the methodology allows for the flotation of pure sulfide samples. An additional benefit derived from the use of the microflotation, is that no interpretation of the interaction and dynamics between the froth and pulp phases is necessary since there is no froth phase in the microflotation tests (Bradshaw and O'Connor, 1996).

In order to investigate the floatability of pyrrhotite, microflotation tests of the Nkomati MSB mixed pyrrhotite, Phoenix magnetic pyrrhotite, Sudbury CCN non-magnetic pyrrhotite and Sudbury Gertrude and Gertrude West magnetic pyrrhotite samples (Tables 3.1, 3.3) were performed under selected conditions. Flotation tests were conducted with no collector addition (collectorless), collector addition (SIBX or SNPX) and collector plus activator addition (SIBX + Cu, SNPX + Cu). Hydrous copper sulfate ($CuSO_4.5H_20$) was used as a source of copper ions in this study. All tests were conducted with minimal guar depressant (10 ppm) in order to assist with the slime cleaning of pyrrhotite prior to flotation. Due to the very small masses recovered during microflotation tests, chemical assays were not possible for every test condition investigated and therefore the pyrrhotite recovery could not be calculated for every set of tests. Therefore, final mass recovery was chosen as the indicator of pyrrhotite flotation performance for all the samples investigated. It should be noted that the calculated

pyrrhotite recovery in itself was based on the assumption that all the nickel was accounted for by pentlandite recovery, and therefore the calculated pyrrhotite recovery may be slightly underestimated. Additional weaknesses of this assumption are that anomalous pyrrhotite grades are sometimes obtained, given that solid solution nickel was present in varying amounts in the pyrrhotite in this study (Section 4.4), but is the best which was possible within the limitations of this study. Table 6.1 presents a summary of the final mass and calculated pyrrhotite and pentlandite recovery, as well as final pentlandite concentrate grade for the microflotation tests. The complete set of flotation results is presented in Appendix C.

**Table 6.1:** Summary table of the average final mass, pyrrhotite and pentlandite recovery from microflotation tests of the different pyrrhotite samples. The average final pentlandite grade is also given.

| Pyrrhotite Sample | Conditions | | Collector-less | SNPX | SNPX+ Cu | SIBX | SIBX + Cu |
|---|---|---|---|---|---|---|---|
| Nkomati MSB Pyrrhotite Mix | pH 7 | Mass Rec (%) | 2.87 | 85.4 | 80.3 | 88.1 | 86.6 |
| | | Po Rec (%) | - | 90.1 | 84.9 | 92.4 | 90.9 |
| | | Pent Rec (%) | - | 90.5 | 85.0 | 93.8 | 92.0 |
| | | Pent Grade (%) | - | 7.00 | 7.33 | 7.21 | 7.39 |
| | pH 10 | Mass Rec (%) | 2.03 | 3.85 | 10.6 | 5.93 | 34.5 |
| | | Po Rec (%) | - | - | - | - | - |
| | | Pent Rec (%) | - | - | 15.2 | - | 37.3 |
| | | Pent Grade (%) | - | - | 8.79 | - | 8.39 |
| Phoenix Magnetic Pyrrhotite | pH 7 | Mass Rec (%) | 6.15 | 51.8 | 70.3 | 66.3 | 59.5 |
| | | Po Rec (%) | - | 51.7 | 70.4 | 66.4 | 59.8 |
| | | Pent Rec (%) | 14.1 | 62.9 | 74.5 | 73.0 | 67.0 |
| | | Pent Grade (%) | 1.36 | 0.78 | 0.72 | 0.74 | 0.76 |
| | pH 10 | Mass Rec (%) | 2.71 | 9.56 | 42.7 | 5.54 | 83.8 |
| | | Po Rec (%) | - | - | 44.2 | - | - |
| | | Pent Rec (%) | 5.21 | 16.0 | 52.5 | 14.4 | 87.6 |
| | | Pent Grade (%) | 1.43 | 1.19 | 0.74 | 1.72 | 0.69 |
| Sudbury CCN Non-magnetic Pyrrhotite | pH 7 | Mass Rec (%) | 36.1 | 51.6 | 74.5 | 68.6 | 84.6 |
| | | Po Rec (%) | - | 57.7 | 85.4 | 79.1 | 95.1 |
| | | Pent Rec (%) | - | 74.6 | 91.6 | 89.7 | 96.4 |
| | | Pent Grade (%) | 0.61 | 0.56 | 0.48 | 0.49 | 0.44 |
| | pH 10 | Mass Rec (%) | 27.0 | 39.2 | 54.2 | 32.7 | 79.8 |
| | | Po Rec (%) | 31.2 | 46.4 | 60.9 | - | 91.2 |
| | | Pent Rec (%) | 42.1 | 58.1 | 79.4 | 47.5 | 96.4 |
| | | Pent Grade (%) | 0.61 | 0.56 | 0.58 | 0.71 | 0.48 |

**Table 6.1:** Continued.

| Pyrrhotite Sample | Conditions | | Collector-less | SNPX | SNPX+ Cu | SIBX | SIBX + Cu |
|---|---|---|---|---|---|---|---|
| Sudbury Gertrude Magnetic Pyrrhotite | pH 7 | Mass Rec (%) | 4.79 | 10.2 | 17.6 | 14.7 | 32.8 |
| | | Po Rec (%) | - | - | - | - | - |
| | | Pent Rec (%) | - | - | - | - | - |
| | | Pent Grade (%) | - | - | - | - | - |
| | pH 10 | Mass Rec (%) | 5.57 | 4.44 | 5.14 | 5.17 | 17.4 |
| | | Po Rec (%) | - | - | - | - | - |
| | | Pent Rec (%) | - | - | - | - | - |
| | | Pent Grade (%) | - | - | - | - | - |
| Sudbury Gertrude West Magnetic Pyrrhotite | pH 7 | Mass Rec (%) | 1.36 | 14.7 | 21.9 | 28.4 | 41.8 |
| | | Po Rec (%) | - | - | - | - | 38.8 |
| | | Pent Rec (%) | - | 33.2 | 29.4 | 56.3 | 58.3 |
| | | Pent Grade (%) | - | 30.0 | 18.9 | 34.7 | 22.3 |
| | pH 10 | Mass Rec (%) | 1.36 | 3.53 | 4.80 | 3.77 | 7.12 |
| | | Po Rec (%) | - | - | - | - | - |
| | | Pent Rec (%) | - | - | - | - | - |
| | | Pent Grade (%) | - | - | - | - | - |

## 6.2 Mineralogy of Flotation Feed Samples

Prior to the interpretation of the flotation performance of the various pyrrhotite samples, the mineralogical characteristics of the microflotation feed samples were characterised with a combination of QXRD and MLA techniques (Section 3.2). The more comprehensive MLA results are shown in figures 6.1 to 6.4, so that the role of mineral liberation can be evaluated.

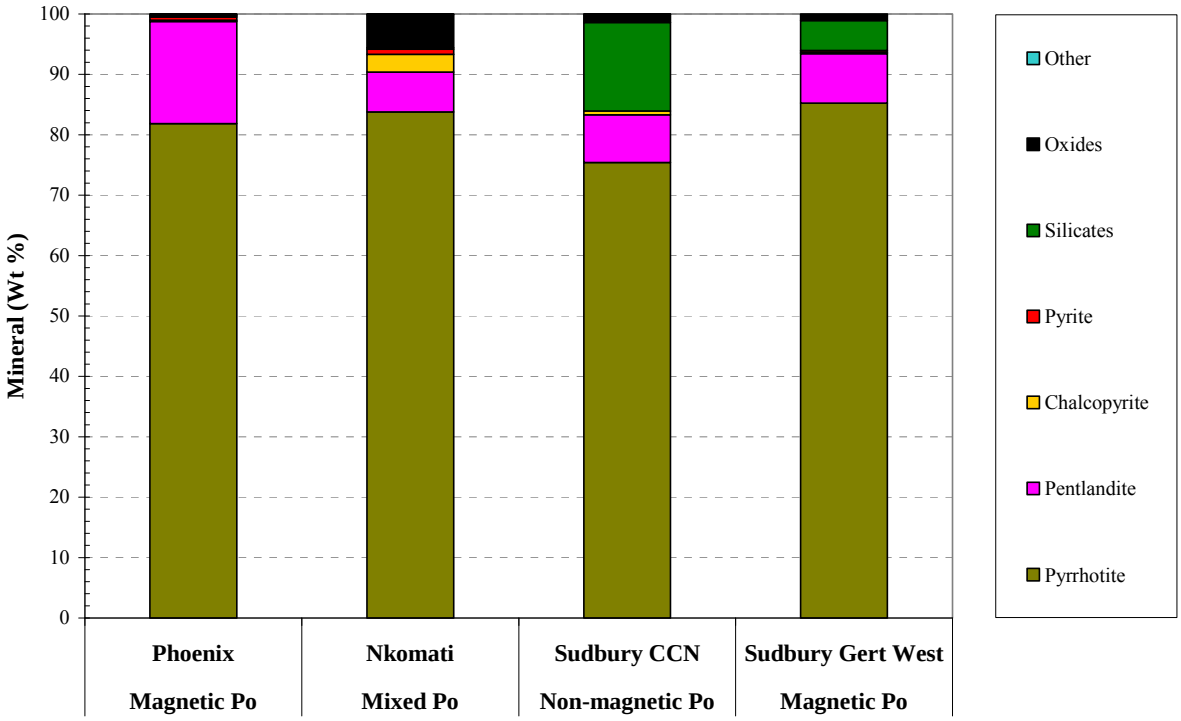


**Figure 6.1**: Composition of microflotation feed samples for the Nkomati, Sudbury CCN and Sudbury Gertrude West pyrrhotite ores as determined by MLA. The composition of the Phoenix pyrrhotite oxygen uptake sample determined by MLA is also shown and can be assumed to be representative of the Phoenix pyrrhotite microflotation feed sample.

It is evident from figure 6.1 that the pyrrhotite content of all the microflotation feed samples was greater than 75 wt % (see also Table 3.3). The magnetic Sudbury Gertrude West flotation feed sample had the highest pyrrhotite content (85.2 wt %). The concentration of pentlandite in the flotation feed samples varied between 6.61 wt % (Nkomati MSB) and 16.9 wt % (Phoenix). The proportion of chalcopyrite was very low in the flotation feed samples (< 0.66 wt %), except for the Nkomati flotation feed sample which had a chalcopyrite content of 2.29 wt %. Similarly, pyrite content was very low for all the flotation feed samples (< 0.86 wt %).

No pyrite was detected in the Sudbury CCN non-magnetic flotation feed sample. The total base metal sulfide content of the flotation feed samples was the lowest for Sudbury CCN (84.0 wt %), higher for both Sudbury Gertrude West (94.0 wt %) and Nkomati MSB (94.2 wt %), and highest for the Phoenix microflotation feed sample (99.5 wt %). Magnetite was the greatest non-sulfide mineral that contributed to the Nkomati MSB flotation feed sample (5.49 wt %), whereas the silicate minerals (amphibole, biotite, plagioclase and quartz) were the major diluents for both the Sudbury CCN and Gertrude West flotation feed samples (Figure 6.1; Table 3.3).

MLA false colour images of the particle types forming the microflotation feed samples of the various pyrrhotite samples are shown in figure 6.2. Similarly to figure 6.1, these images demonstrate that the microflotation feed samples were dominated by pyrrhotite with some contribution from pentlandite. The Phoenix pyrrhotite sample consisted of pyrrhotite with abundant locked flame pentlandite and only minor liberated granular pentlandite (Figure 6.2a). The Nkomati flotation feed sample also consisted of locked flame pentlandite hosted by pyrrhotite (Figure 6.2b), although considerably less than the Phoenix microflotation feed sample. The Nkomati flotation feed sample also contained some liberated magnetite whereas chalcopyrite occurred in composite particles with pyrrhotite and pentlandite. Pyrrhotite in the Sudbury CCN flotation sample was generally liberated and contained only minor locked flame pentlandite (Figure 6.2c). The pentlandite more commonly occurred as liberated granular pentlandite particles. Silicate gangue minerals in the Sudbury CCN flotation feed sample were generally liberated from the BMS. Similarly to the Sudbury CCN flotation feed sample, Sudbury Gertrude West consisted of liberated pyrrhotite and liberated granular pentlandite (Figure 6.2d). Only minor locked flame pentlandite was apparent. Silicate gangue minerals in the Gertrude West flotation feed sample were also liberated from the BMS.

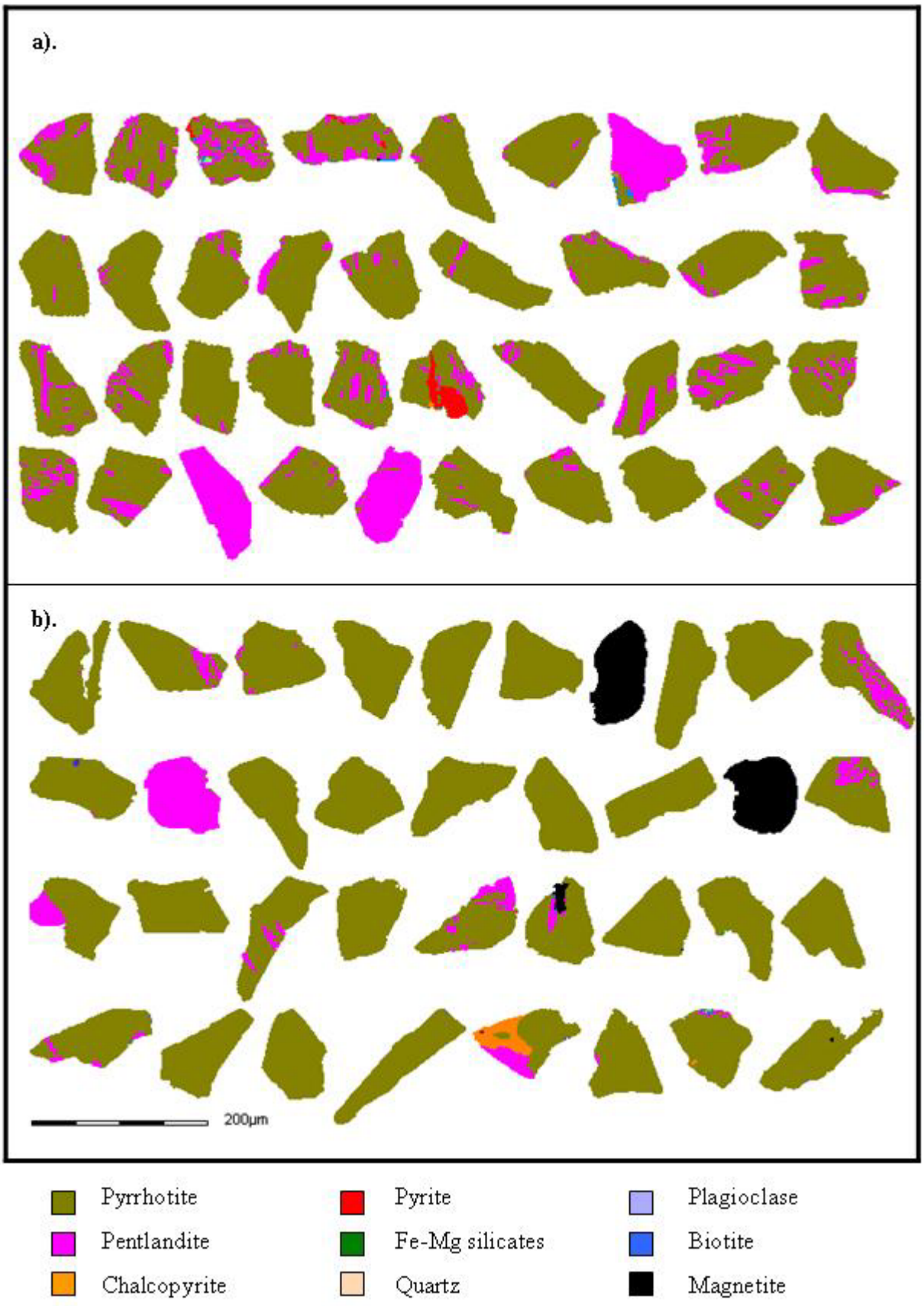


**Figure 6.2:** MLA particle images of microflotation feed samples shown for (a) Phoenix magnetic pyrrhotite (b) Nkomati mixed pyrrhotite, (c) Sudbury CCN non-magnetic pyrrhotite and (d) Sudbury Gertrude West magnetic pyrrhotite.

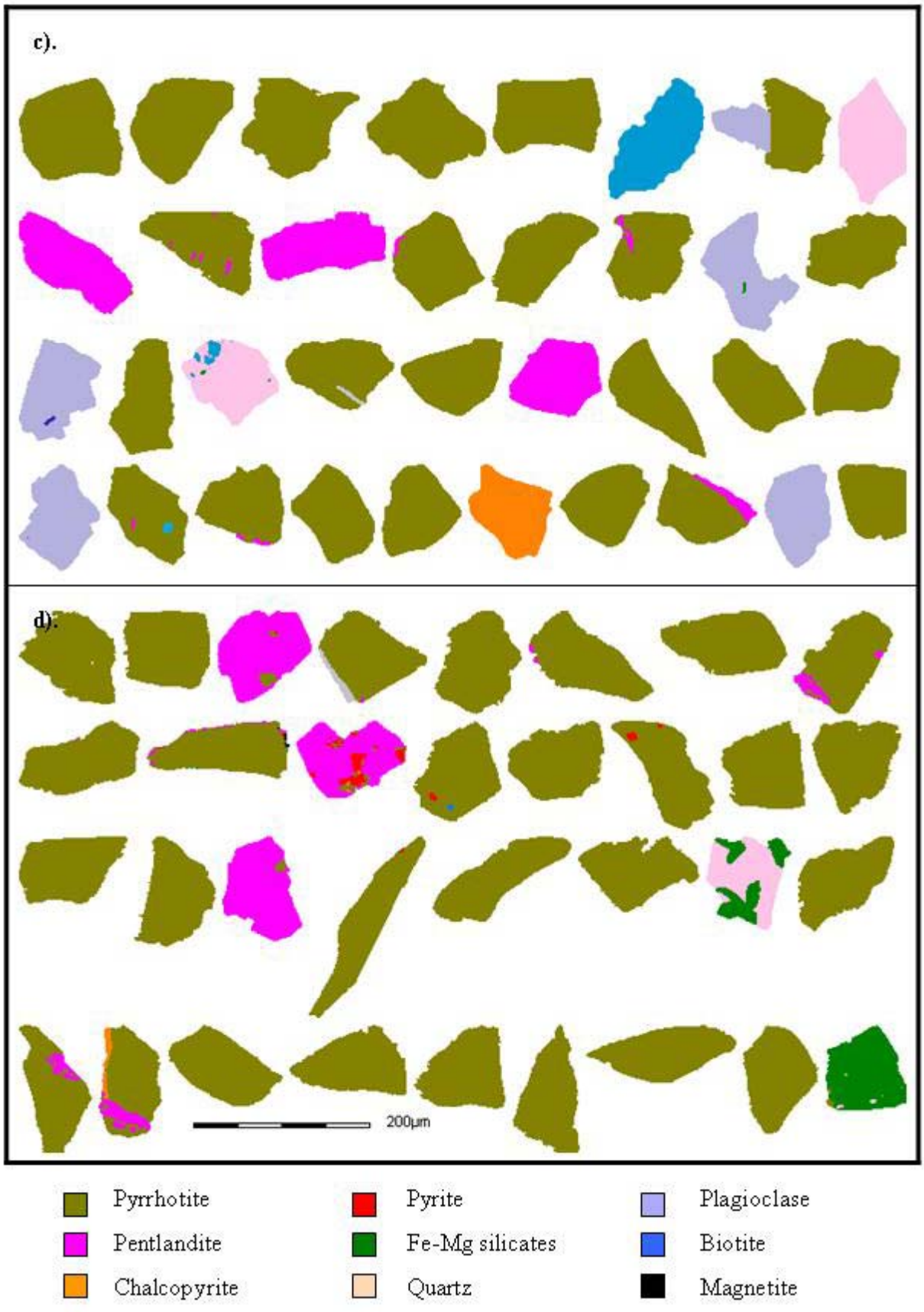


**Figure 6.2:** Continued.

In order to quantify the observations made from the particle images shown in figure 6.2, the liberation characteristics of pyrrhotite and pentlandite are shown for the microflotation feed samples in figures 6.3 and 6.4, respectively. Pyrrhotite was over 90% liberated (> 95 % area exposed) in the Sudbury CCN and Gertrude West microflotation feed samples (Figure 6.3). Pyrrhotite in the Nkomati microflotation feed sample was only slightly less liberated (88.4 % liberated), whereas Phoenix had considerably lower pyrrhotite liberation (50.7 % liberated). This was due to the significant proportion of locked flame pentlandite in the Phoenix pyrrhotite particles and which is evidenced by the pentlandite liberation characteristics (Figure 6.4). The lowest proportion of liberated pentlandite particles occurred in the Phoenix microflotation feed sample (48.5 % liberated). Pentlandite in the Nkomati microflotation feed sample was only slightly more liberated (53.6 %) due to the fact that less flame pentlandite occurred locked in the pyrrhotite. 77.1 % of the pentlandite particles in the Sudbury Gertrude West microflotation feed were liberated, and 89.3% of the pentlandite particles in the Sudbury CCN microflotation feed sample were liberated (Figure 6.4).

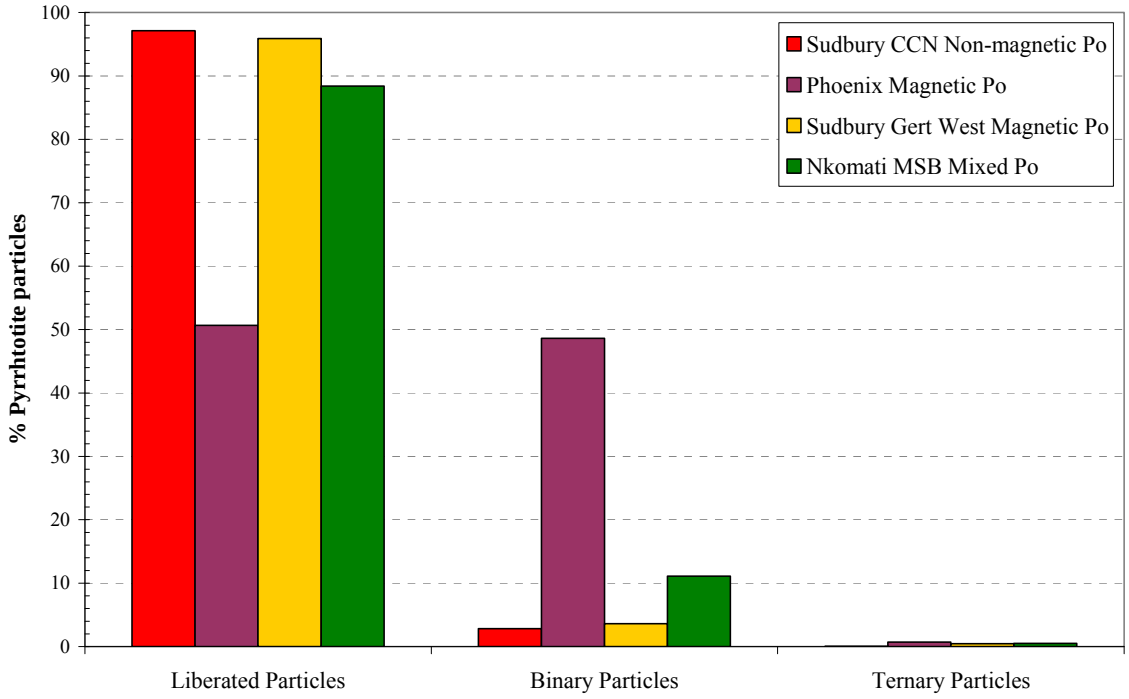


**Figure 6.3:** Proportion of pyrrhotite in microflotation feed samples as liberated (> 95 % area exposed), binary or ternary particles.

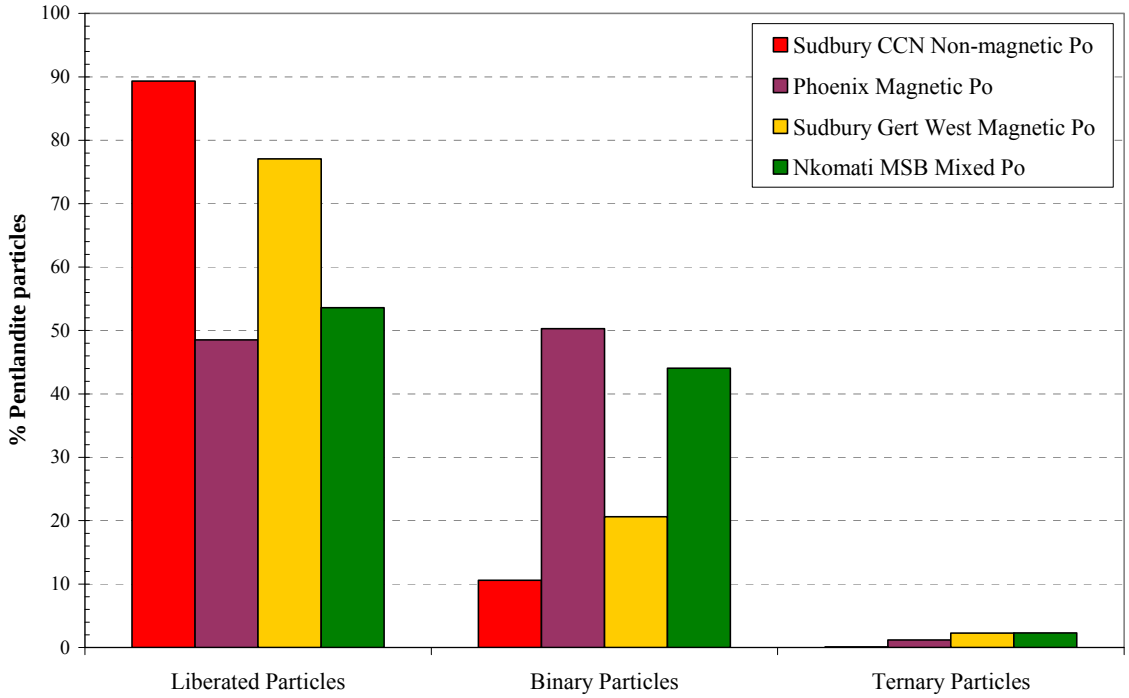


**Figure 6.4:** Proportion of pentlandite in microflotation feed samples as liberated (> 95% area exposed), binary or ternary particles.

## 6.3 Nkomati MSB Pyrrhotite

Nkomati MSB mixed pyrrhotite showed poor natural or collectorless floatability at pH 7 as illustrated in figure 6.5, where the mass recovery of the blank flotation test was only 2.87 %. The Nkomati pyrrhotite however, responded very well to the addition of reagents and resulted in a dramatic increase in flotation recovery up to ~ 80 %. Little difference was observed between the conditions of the respective flotation tests with reagent addition. Copper addition appeared to have had no significant impact on the floatability of the Nkomati mixed pyrrhotite at pH 7. For the SNPX flotation test with copper activation, a slightly lower overall recovery of pyrrhotite was obtained during flotation (decrease from 85.4 to 80.3 % recovery).

Similarly to the microflotation results at pH 7, the natural floatability of Nkomati pyrrhotite at pH 10 shown in figure 6.6 was very poor (2.03 % recovery). The addition of xanthate collector caused a subtle improvement in overall pyrrhotite floatability up to ~ 5 % mass recovery. Nkomati pyrrhotite floatability was further improved by the addition of copper in conjunction with SNPX (10.6 % recovery). The effect of copper activation in conjunction with the stronger SIBX collector caused a further increase in mass recovery up to 34.5 %, but this was still well below the flotation recovery obtained at pH 7.

Compared to the actual mass recovery, the calculated pyrrhotite recovery for Nkomati pyrrhotite for the various flotation tests given in table 6.1 was ~ 5 % higher than the mass recovery. Similarly, pentlandite recovery was also ~ 5 % higher than the mass recovery. The grade of pentlandite in the concentrates collected in the microflotation test was between 7 and 8 wt %. Therefore, it needs to be considered that the good flotation performance of the Nkomati pyrrhotite induced by reagent addition was somewhat influenced by the recovery of pentlandite to the concentrate.

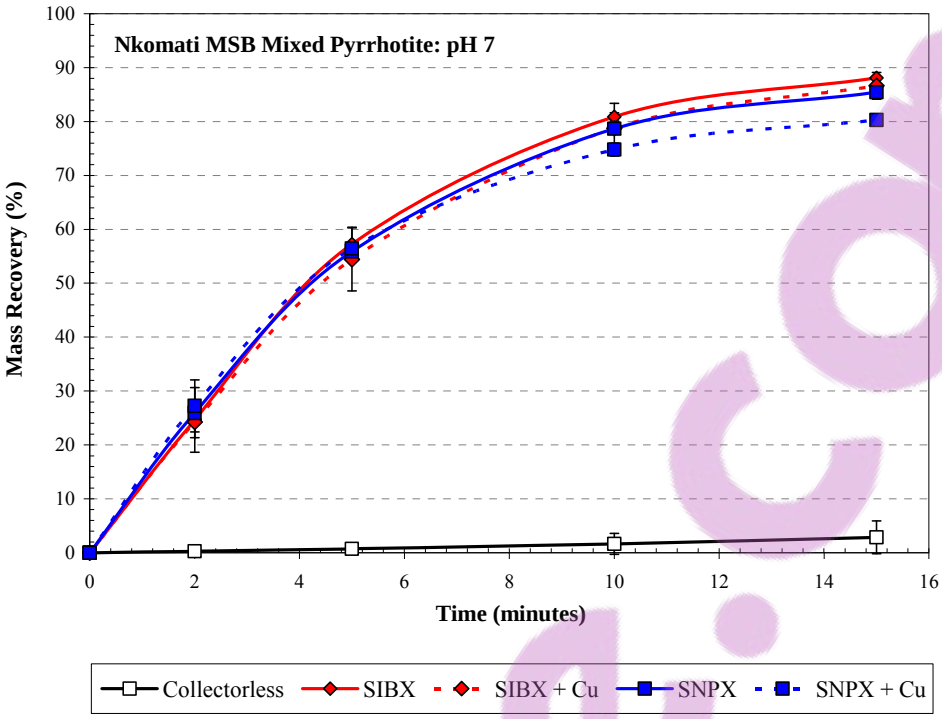


**Figure 6.5:** Mass recovery versus time from microflotation tests of Nkomati MSB mixed pyrrhotite at pH 7. The 2σ standard deviation is also shown.

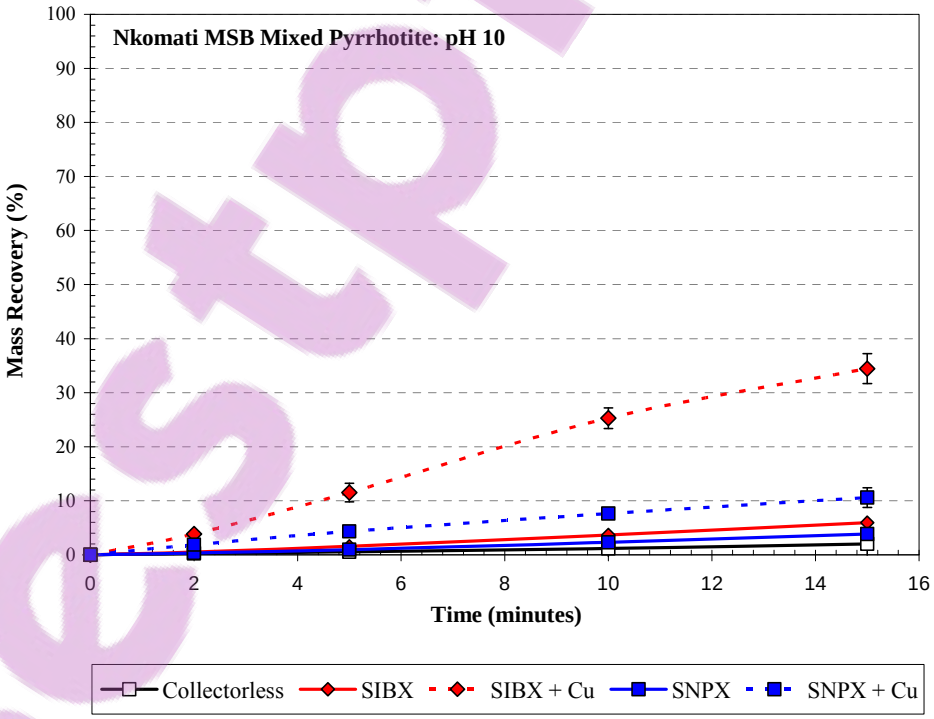


**Figure 6.6:** Mass recovery versus time from microflotation tests of Nkomati MSB mixed pyrrhotite at pH 10. The 2σ standard deviation is also shown.

## 6.4 Phoenix Pyrrhotite

Phoenix magnetic pyrrhotite showed poor collectorless floatability at pH 7 as illustrated in figure 6.7, where the final mass recovery obtained in microflotation tests was only 6.15%. The addition of collector had a marked effect on flotation performance both in terms of flotation kinetics and of the final recovery (> 50 % recovery). A higher mass recovery of 66.3 % was obtained for the longer chain length SIBX collector in comparison to the slightly shorter chain length SNPX collector where the recovery was only 51.8 %. The effect of copper activation was mixed, and only had a positive influence on flotation recovery when used in conjunction with SNPX where the recovery increased to 70.3 %.

The increase in pH up to 10 during flotation caused Phoenix magnetic pyrrhotite to have even poorer natural floatability than at pH 7 due to the increase in hydroxide ion concentration, as can be observed in figure 6.8. At pH 10, the final mass recovery of pyrrhotite was only 2.71 %. The addition of collector at this pH did not improve the flotation recovery of pyrrhotite since the maximum flotation recovery for both SIBX and SNPX collectors was less than 10 %. The effect of copper activation however was most apparent and caused a rapid increase in flotation kinetics (recovery of between 30 and 50 % within the first 5 minutes of flotation). The final pyrrhotite recovery obtained for the copper activation tests was greater when SIBX (83.8% recovery) was used as collector relative to SNPX (42.7% recovery).

The calculated pyrrhotite recovery of Phoenix pyrrhotite for selected flotation tests is shown in table 6.1. For the test conditions examined, the calculated pyrrhotite recovery was almost identical to the mass recovery indicating that the final mass recovery is a suitable indicator of Phoenix pyrrhotite flotation performance. It is also evident from table 6.1 that pentlandite recovery was ~ 7 % higher than the mass or calculated pyrrhotite recovery. Since the final pentlandite grade of the concentrates was less than 1.5 wt %, the proportion of pentlandite diluting the concentrate was relatively negligible. Based on the pentlandite liberation shown in figure 6.4, it is more than likely that the majority of the pentlandite recovered was locked flame pentlandite in association with pyrrhotite.

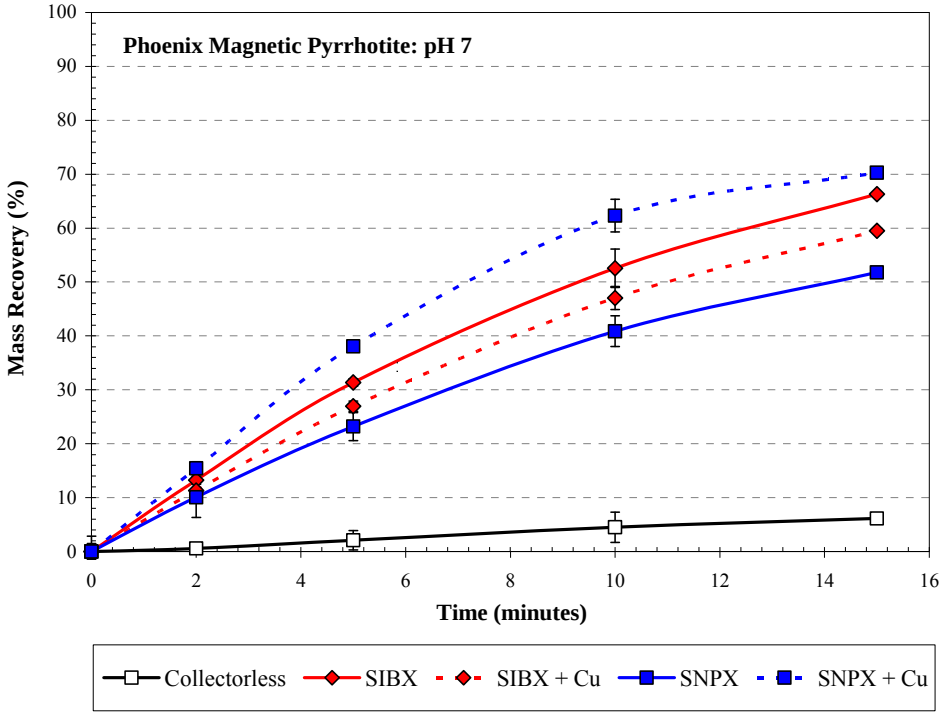


**Figure 6.7:** Mass recovery versus time from microflotation tests of Phoenix magnetic pyrrhotite at pH 7. The 2σ standard deviation is also shown.

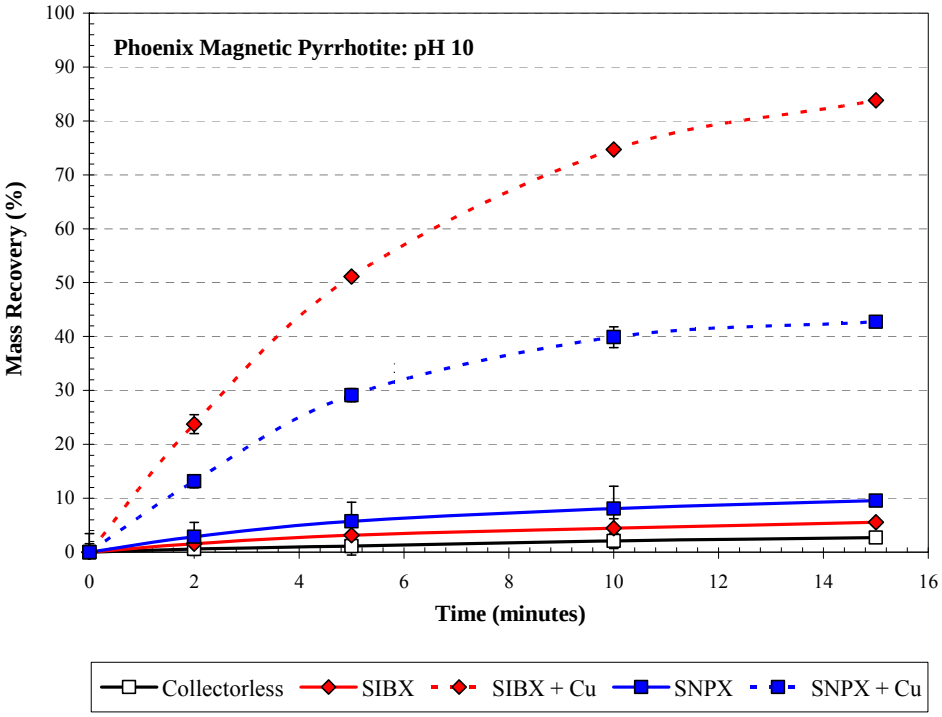


**Figure 6.8:** Mass recovery versus time from microflotation tests of Phoenix magnetic pyrrhotite at pH 10. The 2σ standard deviation is also shown.

## 6.5 Sudbury Copper Cliff North Pyrrhotite

Sudbury Copper Cliff North non-magnetic pyrrhotite showed moderate collectorless floatability at pH 7 as shown in figure 6.9. The final pyrrhotite recovery obtained under these conditions was 36.1 % and it is notable that a linear relationship appears to exist between pyrrhotite recovery and time. Pyrrhotite recovery was improved with the addition of SNPX (51.6 % recovery) and even more so with SIBX addition (68.6 % recovery). Unlike the linear relationship observed between pyrrhotite recovery and time for the collectorless flotation test, the addition of copper in conjunction with collector caused a distinct improvement in flotation kinetics where the typical exponential shaped recovery versus time curve was observed.

The flotation results of Sudbury CCN at pH 10 are shown in figure 6.10 where it is evident that the final pyrrhotite mass recovery of ~ 36 % obtained with collector addition was only slightly improved relative to the collectorless flotation test where 27.0 % recovery was obtained. The addition of copper in conjunction with SNPX collector caused further improvement in pyrrhotite floatability (54.5 % recovery) and even more so for the SIBX collector (79.8 % recovery).

The calculated pyrrhotite recovery for the flotation tests of Sudbury CCN pyrrhotite given in table 6.1 was between 5 and 10 % higher than the mass recovery. Similarly, the pentlandite recovery was on the order of ~ 15 % higher than the mass recovery which suggests that pentlandite recovery is significant. However, even though pentlandite recovery was significant, it did negatively affect the grade of pyrrhotite in the concentrate since the maximum pentlandite grade obtained was only 0.61 wt %. Therefore, final mass recovery can be accepted as a suitable indicator of pyrrhotite flotation performance (Table 6.1).

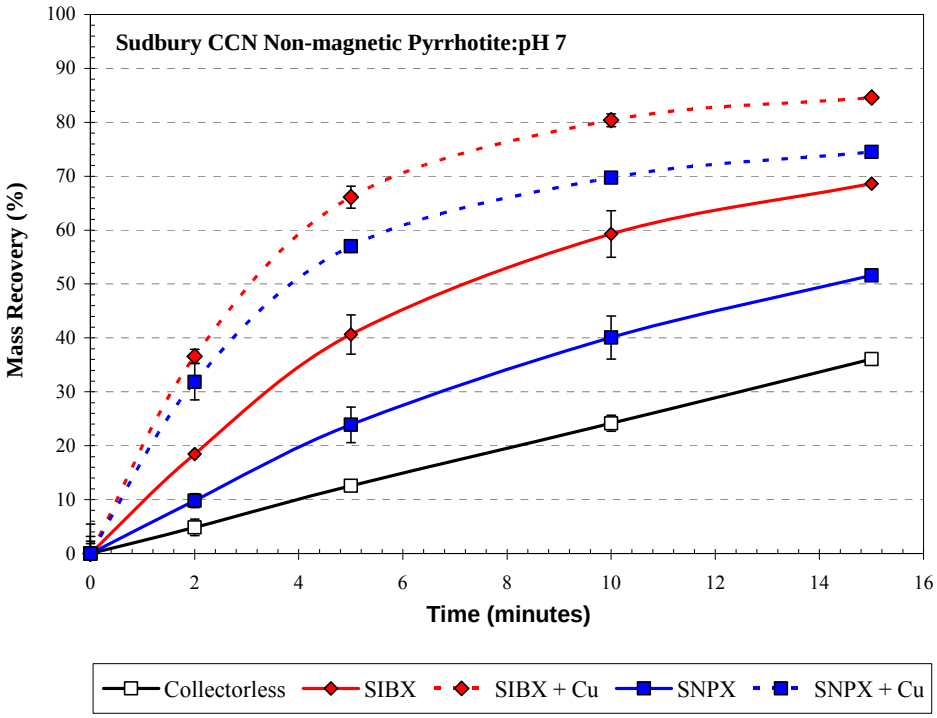


**Figure 6.9:** Mass recovery versus time from microflotation tests of Sudbury CCN non-magnetic pyrrhotite at pH 7. The 2σ standard deviation is also shown.

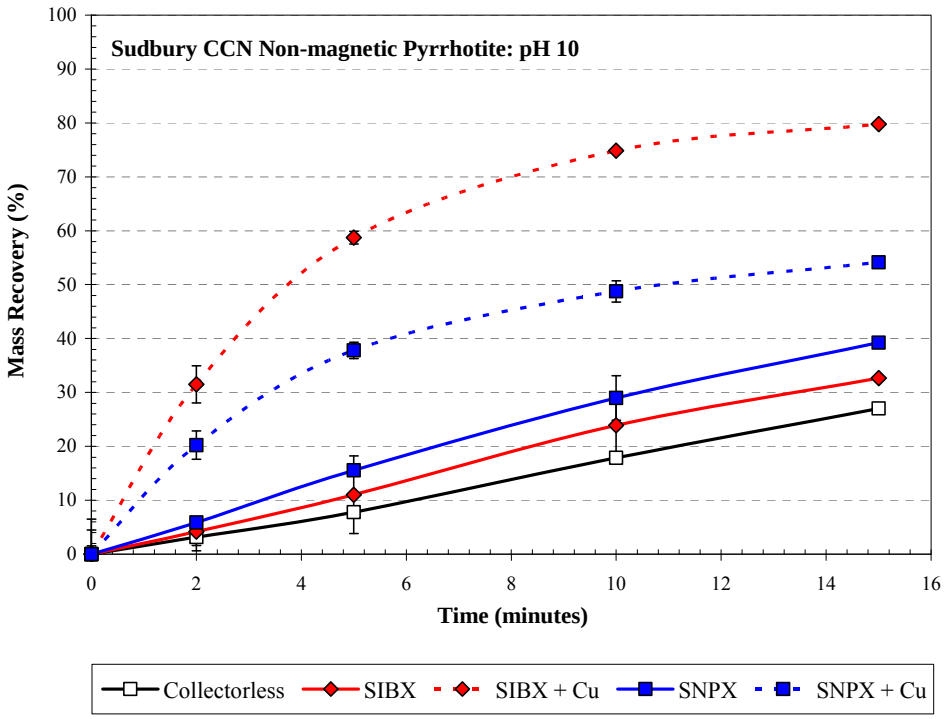


**Figure 6.10:** Mass recovery versus time from microflotation tests of Sudbury CCN non-magnetic pyrrhotite at pH 10. The 2σ standard deviation is also shown.

## 6.6 Sudbury Gertrude and Gertrude West Pyrrhotite

The natural floatability of Sudbury Gertrude magnetic pyrrhotite at pH 7 tended to be very poor as can be observed in figure 6.11, where the final mass recovery obtained was only 4.79 %. The addition of reagents (collector ± copper) appeared to have relatively limited effect on the floatability of the Gertrude pyrrhotite. Even the addition of the stronger SIBX collector with copper activation caused only a minor improvement in floatability (32.8 % recovery). In order to confirm that the Gertrude pyrrhotite had not been unduly oxidised during sample preparation a new Gertrude sample was sourced and prepared, namely Gertrude West pyrrhotite. The flotation results of the new Gertrude West pyrrhotite shown in figure 6.12 were remarkably similar to that of the Gertrude pyrrhotite at pH 7. Poor natural floatability was also observed for Gertrude West pyrrhotite (1.36 % recovery). The addition of reagents however, did cause some minor improvement in pyrrhotite floatability. The addition of copper only caused a very slight improvement in pyrrhotite floatability when used in conjunction with SNPX and SIBX (increase from 14.7 to 21.9 %, and 28.4 to 41.8 % recovery respectively).

For both the Gertrude and Gertrude West pyrrhotite samples, collectorless pyrrhotite flotation was very poor at pH 10 as is shown in figures 6.13 and 6.14, respectively. For both these pyrrhotite samples, the flotation recovery even for tests with reagent addition was less than 7 %. The only exception however, occurred for the Gertrude pyrrhotite for which the addition of both SIBX and copper caused an improvement in flotation recovery up to 17.4 %.

Due to the poor floatability of the Gertrude and Gertrude West pyrrhotite under all the test conditions investigated, very low masses were recovered and therefore detailed chemical assays were not possible. The pyrrhotite recovery could only be calculated for the flotation test of the Gertrude West pyrrhotite at pH 7 with SIBX and copper activation. The calculated pyrrhotite recovery for this particular test was 38.8 % which was slightly lower than the actual mass recovery 41.8 %, but most likely within the error of the analysis. However, it is evident from table 6.1 that the pentlandite recovery could be up to double that of the mass recovery. Since the final pentlandite grade varied between 19 and 30 wt %, it can be concluded that the poor flotation performance of the Gertrude and Gertrude West pyrrhotite was actually even more severe than the mass recovery results shown in figures 6.11 to 6.14 would suggest, since the recovery of pentlandite significantly contributed to the total mass recovery.

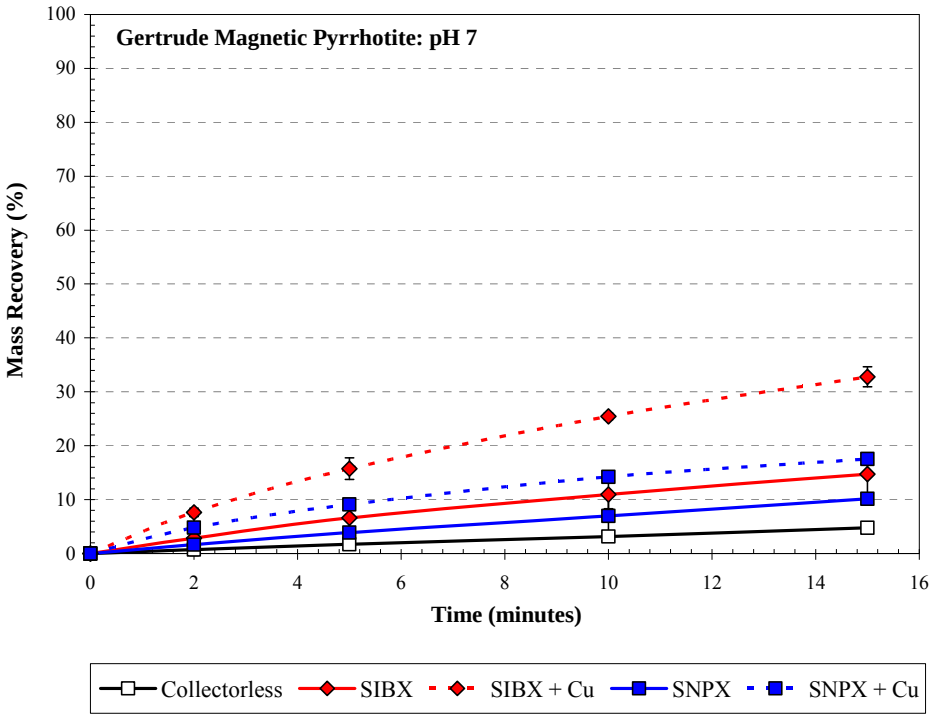


**Figure 6.11:** Mass recovery versus time from microflotation tests of Sudbury Gertrude magnetic pyrrhotite at pH 7. The 2σ standard deviation is also shown.

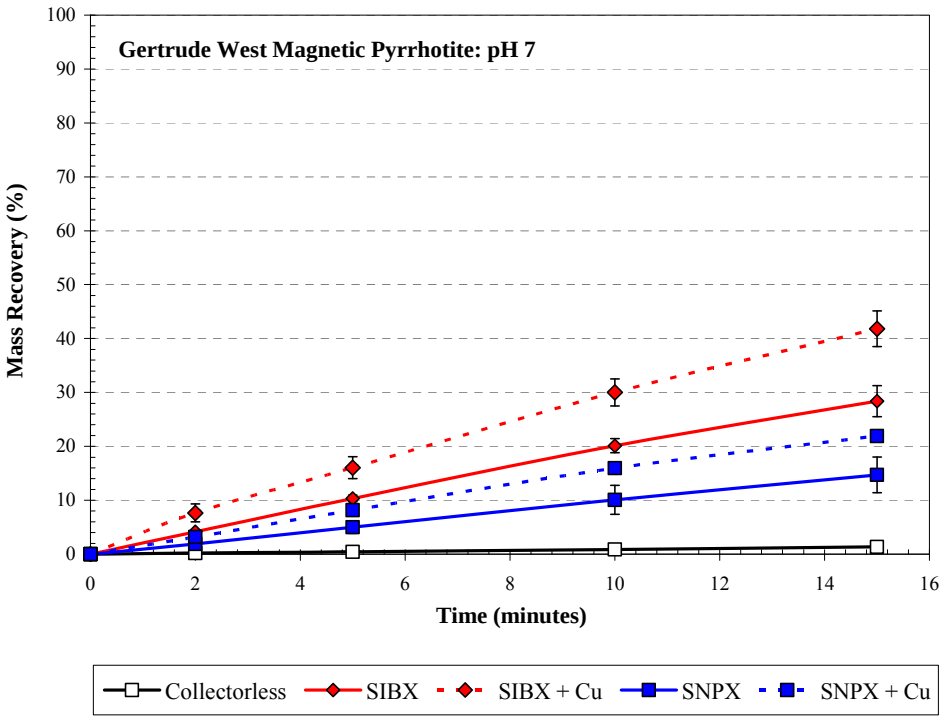


**Figure 6.12:** Mass recovery versus time from microflotation tests of Sudbury Gertrude West magnetic pyrrhotite at pH 7. The 2σ standard deviation is also shown.

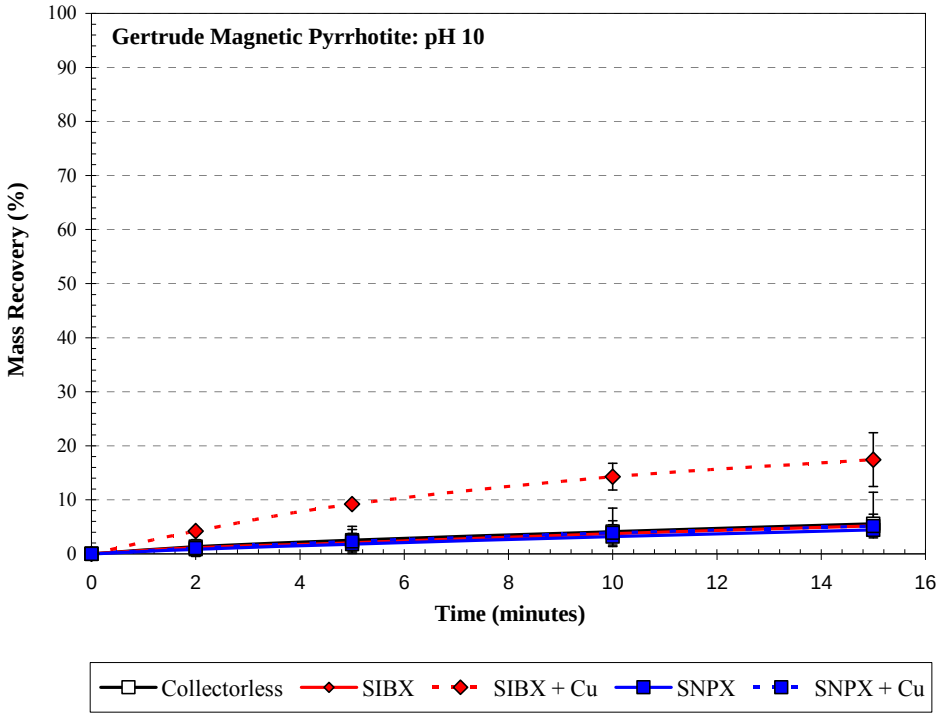


**Figure 6.13:** Mass recovery versus time from microflotation tests of Sudbury Gertrude magnetic pyrrhotite at pH 10. The 2σ standard deviation is also shown.

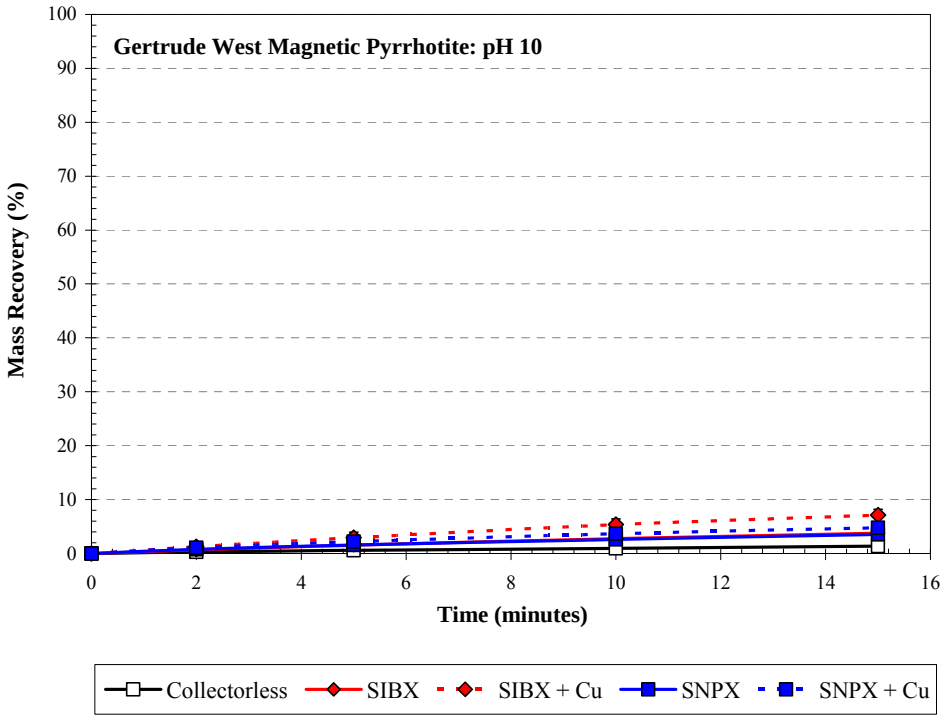


**Figure 6.14:** Mass recovery versus time from microflotation tests of Sudbury Gertrude West magnetic pyrrhotite at pH 10. The 2σ standard deviation is also shown.

## 6.7 Comparison of the Floatability of Pyrrhotite Samples

In order to compare the differences in floatability between magnetic, non-magnetic and mixed pyrrhotite samples, the final mass recovery from the different test conditions is shown for comparison in figures 6.15 - 6.18. It is noted that the feed composition of the pyrrhotite samples for the microflotation tests was variably contaminated with additional sulfide minerals such as pentlandite (Figures 6.1 - 6.4) that would have contributed to the mass recovery during flotation. Since the contribution of pentlandite to the mass recovery during the flotation tests has already been examined for the individual pyrrhotite samples (Table 6.1), and shown generally not to be an issue for all samples other than Gertrude and Gertrude West pyrrhotite, further comparisons are performed based on final mass recovery.

Non-magnetic Sudbury CCN pyrrhotite showed the greatest natural floatability or degree of collectorless flotation of all the pyrrhotite samples tested in this study at pH 7 (Figure 6.15). In comparison to the collectorless flotation recovery of the magnetic pyrrhotite and mixed pyrrhotite samples (Sudbury Gertrude and Gertrude West, Phoenix and Nkomati MSB, respectively), the 36.1 % mass recovery obtained for the Sudbury CCN non-magnetic pyrrhotite was by far the greatest. No consistent relationship between the natural flotation recovery of magnetic and mixed pyrrhotite samples can be observed from figure 6.15. This suggests that none of them showed preferentially greater natural floatability to the other (< 6.15 % recovery).

With the addition of SIBX collector to the flotation system at pH 7, the floatability of all the pyrrhotite samples showed a dramatic increase as evidenced by the high total mass recovery of pyrrhotite (Figure 6.15). The final mass recovery of Sudbury CCN non-magnetic and Phoenix magnetic pyrrhotite was fairly similar (~ 67 % recovery), whereas the Nkomati mixed pyrrhotite was the most floatable (88 % recovery). Both the magnetic Sudbury Gertrude and Gertrude West pyrrhotite samples showed very poor mass recovery during flotation, even with the addition of SIBX collector (< 28 % recovery). Based on the contribution of pentlandite to the mass recovery in the Gertrude and Gertrude West samples during flotation (Section 6.4), it can be surmised that the poor floatability of this pyrrhotite was even more severe than the mass recovery would suggest.

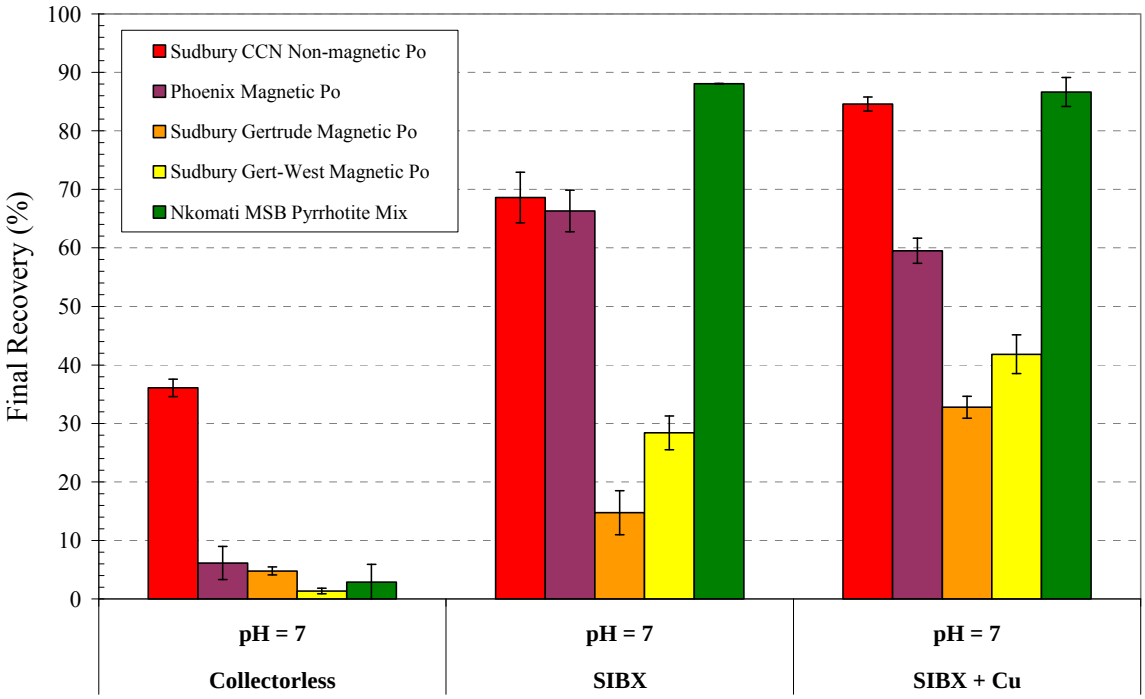


**Figure 6.15:** Comparison of the final flotation mass recovery for all pyrrhotite samples at pH 7 shown for SIBX collector tests. The 2σ standard deviation is also shown.

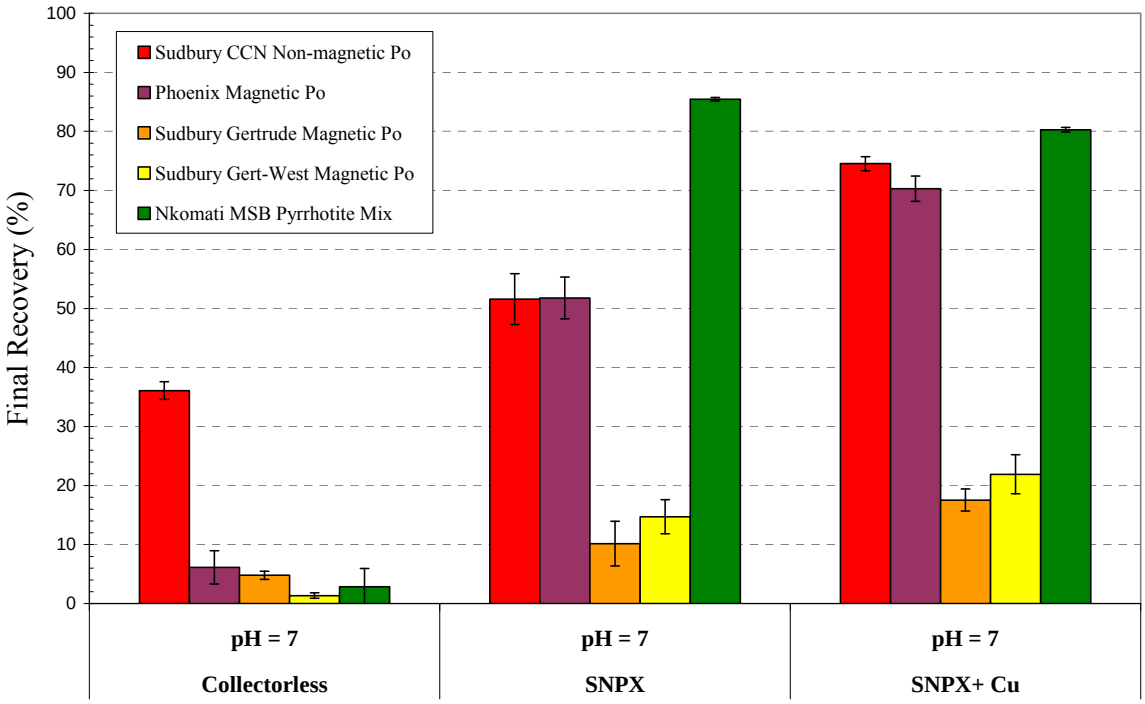


**Figure 6.16:** Comparison of the final flotation mass recovery for all pyrrhotite samples at pH 7 shown for SNPX collector tests. The 2σ standard deviation is also shown.

The addition of the slightly shorter chain length SNPX collector to the flotation system at pH 7 caused similar changes in floatability for the pyrrhotite samples as SIBX, although the effects were not quite so dramatic (Figure 6.16). For example, the addition of SIBX caused an increase in flotation recovery of Sudbury CCN non-magnetic pyrrhotite from 31% recovery (collectorless flotation), to 68.6 %, whereas the addition of SNPX only caused an increase up to 51.6 % recovery.

The effect of copper activation on pyrrhotite floatability in conjunction with the addition of SIBX collector for all the pyrrhotite samples at pH 7 shown in figure 6.15 was quite variable. Some pyrrhotite samples showed increased floatability or improved recovery (Sudbury CCN, Sudbury Gertrude and Gertrude West), whereas others showed negligible improvement (Phoenix, Nkomati MSB). The effect of copper activation on pyrrhotite floatability with the addition of SNPX collector was generally similar to the tests with SIBX collector (Figure 6.16). However, it is noted that the Phoenix magnetic pyrrhotite showed a distinct improvement in flotation performance when copper activation occurred in the presence of SNPX collector.

The collectorless flotation recovery of all the pyrrhotite samples at pH 10 is shown in figure 6.17, and it is evident that the floatability is lower than at pH 7. The non-magnetic Sudbury CCN pyrrhotite sample was still the most floatable of all the pyrrhotite samples as evidenced by its good natural floatability (27.0 % recovery) relative to the other magnetic pyrrhotite and mixed pyrrhotite samples (< 5.5 % recovery). The addition of either SIBX or SNPX at pH 10 served to only significantly improve the floatability of the non-magnetic Sudbury CCN pyrrhotite, whereas the addition of collector in conjunction with copper influenced the floatability of all the pyrrhotite samples (Figures 6.17, 6.18). The recovery of non-magnetic Sudbury CCN pyrrhotite increased from 32.6 to 79.8 % with copper activation, magnetic Phoenix pyrrhotite increased from 5.54 to 83.8 % with copper activation and the mixed Nkomati pyrrhotite recovery increased from 5.93 to 34.5%. Even the magnetic Gertrude and Gertrude West pyrrhotite sample showed some minor improvement in flotation recovery e.g. increase from 5.17 to 17.4 % recovery for Gertrude pyrrhotite. It is also noted that the effect of copper activation was far greater for the longer chain length SIBX collector than the shorter SNPX collector. The flotation recovery showed an almost two fold increase for SIBX relative to the small increase in floatability evidenced for the SNPX collector (e.g. increase from 39.2 to 54.2 % recovery for non-magnetic Sudbury CCN pyrrhotite).

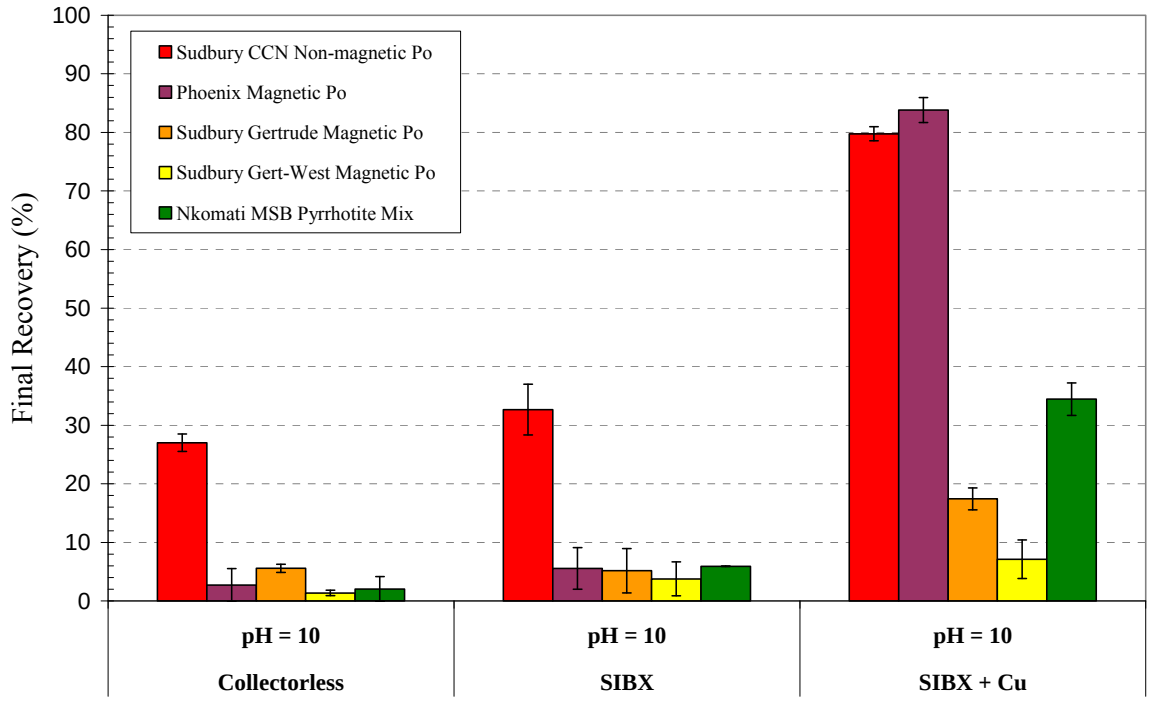


**Figure 6. 17:** Comparison of the final flotation mass recovery for all pyrrhotite samples at pH 10 shown for SIBX collector tests. The 2σ standard deviation is also shown.

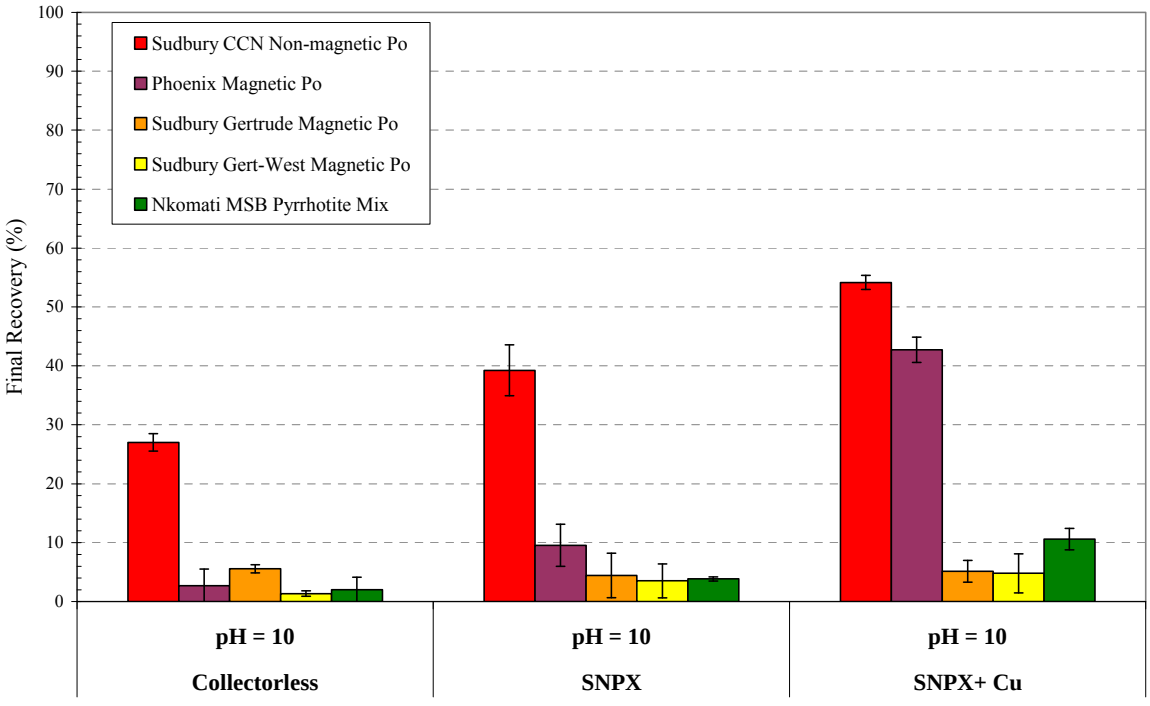


**Figure 6.18:** Comparison of the final flotation mass recovery for all pyrrhotite samples at pH 10 shown for SNPX collector tests. The 2σ standard deviation is also shown.

## 6.8 Key findings

Key features noted with respect to the microflotation of pyrrhotite from selected nickel and platinum group element ore deposits were as follows:

MLA analysis of the feed samples prepared for microflotation tests of the Nkomati MSB mixed pyrrhotite, Phoenix magnetic pyrrhotite, Sudbury CCN non-magnetic pyrrhotite, Sudbury Gertrude and Gertrude West magnetic pyrrhotite showed that all samples were comprised of greater than 75 wt % pyrrhotite and greater than 84 wt % sulphides. Pyrrhotite liberation was noted to be quite variable, Sudbury CCN non-magnetic pyrrhotite and Sudbury Gertrude West magnetic pyrrhotite were over 90 % liberated, Nkomati MSB pyrrhotite was 88.4 % liberated whereas the Phoenix magnetic pyrrhotite was only 50.7 % liberated. The lower pyrrhotite liberation in the Nkomati and Phoenix pyrrhotite flotation feed samples was due to the presence of locked flame pentlandite. Pentlandite liberation for these two pyrrhotite samples was only ~ 50 % compared to Sudbury CCN and Sudbury Gertrude West pentlandite that was greater than 77 % liberated.

The collectorless flotation for all pyrrhotite samples was observed to be greater at pH 7 instead of pH 10 e.g. the Phoenix magnetic pyrrhotite showed a decrease in collectorless flotation recovery from 6.15 to 2.71 % with an increase in pH.

The flotation recovery for all pyrrhotite samples increased with the addition of collector at pH 7 e.g. the Phoenix magnetic pyrrhotite showed an increase in flotation recovery from 6.15 to 51.8 wt % with the addition of SNPX collector at pH 7. Sudbury CCN non-magnetic pyrrhotite was the only pyrrhotite sample to show a significant increase in flotation recovery with the addition of collector at pH 10. e.g. increase in flotation recovery from 27.0 to 39.2 wt % with the addition of SNPX collector. The flotation recovery was generally greater for the longer chain length SIBX collector relative to SNPX collector due to the increased hydrophobicity of SIBX relative to SNPX.

In general, the flotation recovery of the pyrrhotite samples increased with copper activation, but was heavily influenced by pyrrhotite mineralogy, pH and collector chain length. Nearly all pyrrhotite samples other than the Nkomati MSB mixed pyrrhotite showed an increase in flotation recovery due to copper activation at pH 7, but it was noted that the results were

more consistent for copper activation in conjunction with the shorter chain length SNPX collector e.g. the Phoenix magnetic pyrrhotite showed an increase in flotation recovery from 51.8 to 70.3 wt % due to copper activation in conjunction with SNPX addition at pH 7. At pH 10, some pyrrhotite samples showed an increase in flotation recovery due to copper activation, but only for the longer chain length SIBX collector. Only those pyrrhotite samples that already had improved floatability due to SNPX addition were positively affected by copper activation e.g. the Phoenix magnetic pyrrhotite showed an increase in flotation recovery from 9.56 to 42.7 wt % due to copper activation in conjunction with SNPX addition at pH 10.

The Sudbury CCN non-magnetic pyrrhotite showed the greatest collectorless flotation recovery at pH 7 and 10 (36.1 and 27.0 % recovery) compared to the other pyrrhotite samples. No significant differences were observed between the collectorless flotation recovery of the other magnetic and mixed pyrrhotite samples at pH 7 or 10 (< 6.15 % recovery). The addition of reagents at pH 7 caused a marked influence in the flotation recovery of the non-magnetic Sudbury CCN, magnetic Phoenix and mixed Nkomati MSB pyrrhotite samples (e.g. up to 88.1 % recovery for Nkomati MSB mixed pyrrhotite at pH 7 with SIBX addition). The addition of reagents at pH 10 however, only caused a marked influence in the flotation recovery for the Sudbury CCN non-magnetic and Phoenix magnetic pyrrhotite. The magnetic Sudbury Gertrude and Gertrude West pyrrhotite samples showed the poorest overall flotation recovery of all the pyrrhotite samples examined with reagent addition; where the maximum recovery obtained for the Sudbury Gertrude West pyrrhotite sample was only 41.8 % with copper activation in conjunction with SIBX addition at pH 7.

# Chapter 7

# DISCUSSION

---

## 7.1 Introduction

This chapter develops the relationship between the mineralogy of pyrrhotite from selected nickel and platinum group element ore deposits, and flotation performance based on the mineralogical characterisation of pyrrhotite (Chapter 4), measurement of its reactivity towards oxidation (Chapter 5) and measurement of its flotation performance (Chapter 6). The chapter is subdivided into sections, each of which address one of the key questions proposed in Section 1.3. Once the relationship between pyrrhotite mineralogy and flotation performance has been investigated, some final implications of this relationship are given.

## 7.2 Variation in Pyrrhotite Mineralogy

The aim of this section is to answer the first key question; "H*ow does the mineral association, mineral chemistry and crystallography vary between magnetic and non-magnetic pyrrhotite*." Based on the variation observed in composition, crystallography and mineral association of magnetic and non-magnetic pyrrhotite samples examined in this study, some generalisations regarding pyrrhotite as a mineral can be made. In order to do this, it is easiest to use a classification system for the different pyrrhotite types which accounts for the composition of pyrrhotite in terms of its mineral association. The classification system proposed is based on several other systems given by Zapletal (1972) and Arnold (1967), but the one used in this work integrates detailed pyrrhotite mineral compositional and crystallographic information and is shown in table 7.1

The basis of this classification system is the division of pyrrhotite occurrences on their mineral association. Pyrrhotite occurrences can be subdivided as either *single phase* pyrrhotite with no association to troilite or another pyrrhotite phase, or as *two phase* pyrrhotite which shares an association to an additional pyrrhotite phase. The degree of nickel association is only shown as solid solution nickel in pyrrhotite in table 7.1, even though the association to pentlandite is of importance in all the pyrrhotite samples examined in this study (e.g. Section 4.2, Figure 6.3, 6.4).

Using the classification given in table 7.1, the first group of pyrrhotite occurrences corresponds to the very iron rich non-magnetic 6C pyrrhotite of composition $Fe_{11}S_{12}$ and which coexisted with stoichiometric FeS or 2C troilite. This occurrence corresponds to the Impala Merensky Reef pyrrhotite sample *IMP-2* examined that had an average atomic metal content of 47.9 ± 0.47 %, and average sulfur content of 52.1 ± 0.47 %. This pyrrhotite occurrence showed the least enrichment in solid solution nickel.

The next pyrrhotite occurrence in the proposed classification system shown in table 7.1 is comprised of single phase non-magnetic or single phase magnetic pyrrhotite. The Sudbury CCN pyrrhotite was the only example of single phase non-magnetic pyrrhotite examined in this study (47.2 ± 0.38 atomic metal %, 52.8 ± 0.38 atomic sulfur %), whereas several occurrences of single phase magnetic pyrrhotite were recognised. These included the Sudbury

**Table 7. 1:** Summary table of the mineralogy and crystallography of the pyrrhotite occurrences in this study. xC represents the pyrrhotite superstructure determined on the basis of the cell parameters or interpreted from mineral chemistry. The average atomic metal, atomic metal / sulfur ratio and weight % nickel contents of magnetic and non-magnetic pyrrhotite with their associated number of analyses (No) and 2σ standard deviation are also given.

| PYRRHOTITE SAMPLE | | Ideal comp. | xC | No. | At. Metal % Ave | At. Metal % 2σ | At. Metal / S % Ave | At. Metal / S % 2σ | Wt Nickel % Ave | Wt Nickel % 2σ |
|---|---|---|---|---|---|---|---|---|---|---|
| **2 PHASE** | | | | | | | | | | |
| **Troilite and Non-magnetic Po** | | | | | | | | | | |
| Merensky: Impala (*IMP-2)* | Troilite | FeS | 2C - Hex | 21 | 49.4 | *(0.67)* | 0.976 | *(0.026)* | 0.12 | (0.18) |
| Merensky: Impala (*IMP-2)* | Non-mag Po | $Fe_{11}S_{12}$ | 6C - ? | 101 | 47.9 | *(0.46)* | 0.918 | *(0.017)* | 0.22 | (0.07) |
| **1 PHASE** | | | | | | | | | | |
| **1 Phase: Non-magnetic Pyrrhotite** | | | | | | | | | | |
| Sudbury: CCN | Non-mag Po | $Fe_9S_{10}$ | 5C - Ortho | 201 | 47.2 | *(0.38)* | 0.894 | *(0.014)* | 0.75 | (0.19) |
| **1 PHASE** | | | | | | | | | | |
| **Magnetic Pyrrhotite** | | | | | | | | | | |
| Sudbury: Gertrude | Magnetic Po | $Fe_7S_8$ | 4C - Mon | 194 | 46.4 | *(0.32)* | 0.867 | *(0.011)* | 0.82 | (0.19) |
| Sudbury: Gertrude West | Magnetic Po | $Fe_7S_8$ | 4C - Mon | 68 | 46.4 | *(0.37)* | 0.865 | *(0.013)* | 0.78 | (0.12) |
| Merensky: Impala *(IMP-1)* | Magnetic Po | $Fe_7S_8$ | 4C - Mon | 103 | 46.5 | *(0.40)* | 0.870 | *(0.014)* | 0.67 | (0.27) |
| Nkomati: MMZ (*MMZ-4)* | Magnetic Po | $Fe_7S_8$ | 4C - Mon | 42 | 46.5 | *(0.32)* | 0.870 | *(0.011)* | 1.10 | (0.18) |
| Tati: Phoenix | Magnetic Po | $Fe_7S_8$ | 4C - Mon | 203 | 46.5 | *(0.33)* | 0.869 | *(0.011)* | 1.06 | (0.67) |
| **2 PHASE** | | | | | | | | | | |
| **Non-magnetic and Mag Po** | | | | | | | | | | |
| Nkomati: MSB & *MMZ-1* | Non-mag Po | $Fe_9S_{10}$ | 5C - Ortho | 115 | 47.2 | *(0.33)* | 0.895 | *(0.012)* | 0.75 | (0.10) |
| Nkomati: MSB & *MMZ-1* | Magnetic Po | $Fe_7S_8$ | 4C - Mon | 72 | 46.6 | *(0.35)* | 0.873 | *(0.012)* | 0.43 | (0.18) |
| Non-magnetic pyrrhotite | | $Fe_{11}S_{12}$ | 6C | 101 | 47.9 | *(0.46)* | 0.918 | *(0.017)* | 0.22 | (0.07) |
| Non-magnetic pyrrhotite | | $Fe_9S_{10}$ | 5C | 316 | 47.2 | *(0.36)* | 0.895 | *(0.013)* | 0.75 | (0.16) |
| Magnetic pyrrhotite | | $Fe_7S_8$ | 4C | 699 | 46.5 | *(0.36)* | 0.869 | *(0.013)* | 0.84 | (0.57) |

Gertrude, Gertrude West, Impala Merensky Reef (sample *IMP-1*), Nkomati MMZ (sample *MMZ-4*) and Phoenix pyrrhotite samples. The average atomic metal and sulfur contents of these single phase 4C magnetic pyrrhotite occurrences of ideal composition close to $Fe_7S_8$ fell within the standard deviation of one another (~ 46.5 atomic metal %, ~ 53.5 atomic sulfur %). Single phase magnetic pyrrhotite occurrences were more nickel rich (0.67 – 1.10 wt % Ni) than single phase non-magnetic pyrrhotite (0.75 ± 0.19 wt % Ni).

The final type of pyrrhotite occurrence proposed here consists of intergrown magnetic and non-magnetic pyrrhotite as observed in the Nkomati MSB and MMZ sample *MMZ-1*. Ideal pyrrhotite compositions of the 4C magnetic phase were close to $Fe_7S_8$ and showed little compositional difference in terms of atomic metal (46.6 ± 0.35 %) and atomic sulfur (53.4 ±

0.35 %) contents to single phase magnetic pyrrhotite. Coexisting non-magnetic 5C $Fe_9S_{10}$ pyrrhotite also showed little compositional difference in terms of atomic metal and sulfur contents (47.2 ± 0.33; and 52.8 ± 0.33 %, respectively) to single phase non-magnetic pyrrhotite. The most notable difference however, was in terms of the solid solution nickel content. Magnetic pyrrhotite that coexisted with non-magnetic pyrrhotite was less enriched in nickel than the non-magnetic phase (0.43 and 0.75 wt % Ni, respectively for Nkomati pyrrhotite). Two phase magnetic pyrrhotite intergrown with non-magnetic pyrrhotite was also significantly less enriched in nickel than single phase magnetic pyrrhotite.

In the study of Arnold (1967) which examined the mineralogy of 82 different natural pyrrhotite samples from around the world, 73 % of the samples were mixtures of intergrown magnetic (monoclinic) and non-magnetic ("hexagonal") pyrrhotite. The remaining pyrrhotite samples were either single phase magnetic (9 % monoclinic), single phase non-magnetic (13 % "hexagonal") or two phase non-magnetic pyrrhotite ("hexagonal") intergrown with troilite (5 %). Since the focus of this study is on the detailed examination of pyrrhotite mineralogy from several locations as opposed to a simple examination of the mineralogy of pyrrhotite from multiple locations, comparison cannot be made as to whether the results of this study are consistent with those of Arnold (1967) with respect to the frequency of the different pyrrhotite occurrences.

However, it is possible to compare the range in atomic metal compositions of the different pyrrhotite types with the compilations published by Carpenter and Desborough (1964) and Arnold (1967). The majority of the compositions given in these compilations were based on either bulk chemical measurements or using the x-ray spacing method of Arnold and Reichen (1962). No distinction was provided by these compilations between the composition of magnetic and non-magnetic pyrrhotite, but rather a bulk pyrrhotite composition for the two intergrown phases is given. Therefore, the importance of the data from this study is that it has been obtained using microbeam x-ray analysis methods (EMP; Section 3.2.4), that allowed for spot analysis of the different pyrrhotite phases.

Comparison of the atomic metal content between pyrrhotite examined in this study with that of Carpenter and Desborough (1964) shows that there is good overlap for non-magnetic pyrrhotite, although non-magnetic pyrrhotite in this study extends beyond 47.8 atomic metal % (Figure 7.1a). This can be accounted by the fact that no 6C $Fe_{11}S_{12}$ pyrrhotite was

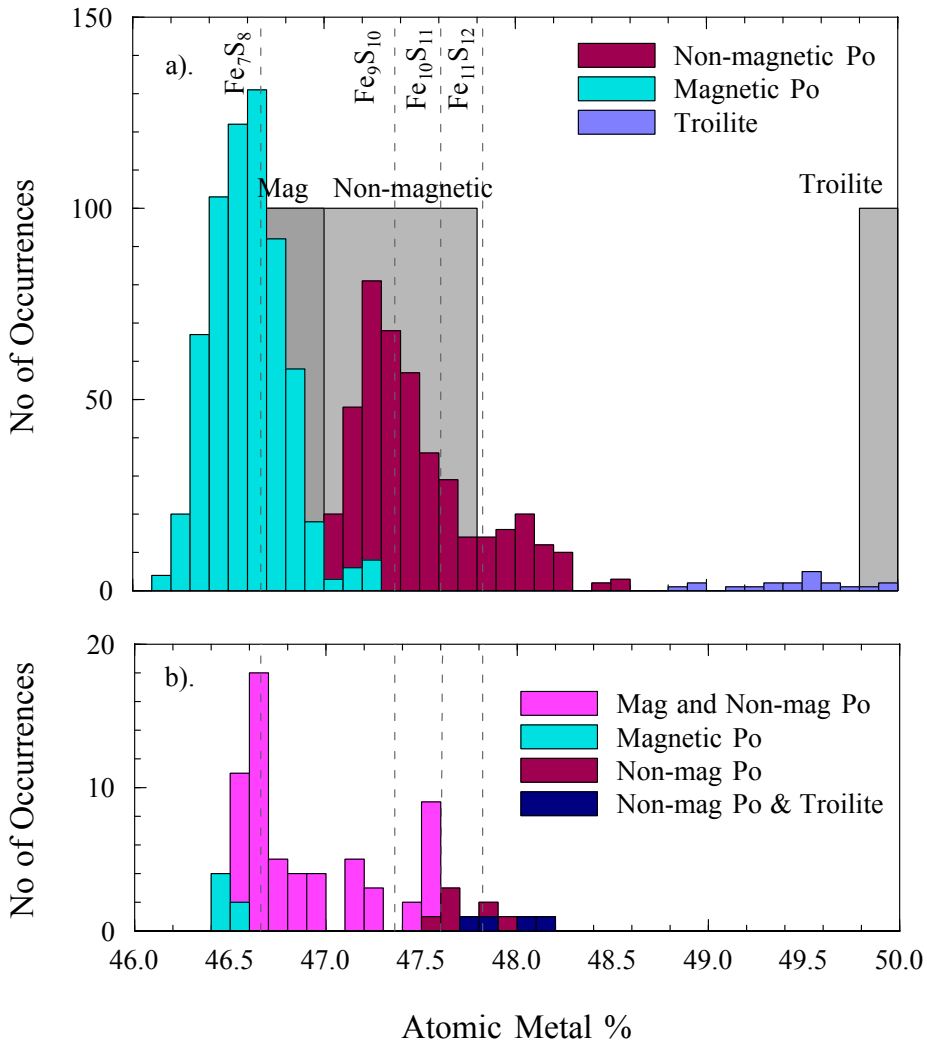


**Figure 7. 1:** (a) Comparison of the atomic metal content for all magnetic and non-magnetic pyrrhotite occurrences examined in this study. Grey bars illustrate atomic metal contents for pyrrhotite as given in Carpenter and Desborough (1964). (b) Comparison of the atomic metal contents given in Arnold (1967) as determined by the x-ray spacing method. Compositions given for "magnetic and non-magnetic pyrrhotite" and "non-magnetic pyrrhotite and troilite" pyrrhotite represent the bulk chemical composition of the two intergrown pyrrhotite phases. Note the change in scale on the y-axis between (a) and (b).

examined in the study of Carpenter and Desborough (1964). The poor overlap between the troilite compositions is due to the analytical difficulties experienced in analysing Merensky Reef troilite (Section 4.4). The composition of magnetic pyrrhotite in this study was also broader than that given by Carpenter and Desborough (1964) in terms of some of the more atomic metal poor compositions (< 46.5 atomic metal %). This is most likely accounted for by the fact that the detailed variation in pyrrhotite compositions within an ore deposit have been examined in this study (i.e. the intra pyrrhotite compositional variation) as opposed to the

variation between pyrrhotite deposits (i.e. the inter pyrrhotite compositional variation) as studied by Carpenter and Desborough (1964). As such, the compositional variation in magnetic pyrrhotite from any particular location is expected to show a close to Gaussian distribution (Figure 7.1a)

Comparison of the atomic metal compositions of the pyrrhotite in this study with those given by Arnold (1967) as illustrated in figure 7.1b broadly shows a similar range in composition. However, the comparison is limited by the size of the data set of Arnold (1967) and that there was no discrimination between the compositions of intergrown magnetic and nonmagnetic pyrrhotite that represents 73 % of the pyrrhotite examined in the study.

The complete dataset of mineral compositions from the pyrrhotite samples in this study are shown as a histogram of their metal / sulfur ratios in figure 7.2 in order to examine the variation in composition of the mineral pyrrhotite. Metal / sulfur ratios of Merensky Reef troilite are also shown for comparison but due to the small size of the dataset, they are only shown for reference. The three pyrrhotite compositions recognised in this study comprising 4C $Fe_7S_8$, 5C $Fe_9S_{10}$ and 6C $Fe_{11}S_{12}$, where the 5C and 6C pyrrhotites are part of the NC group of pyrrhotites are shown as distinct groups. A Gaussian distribution function has been fitted to each of the pyrrhotite compositions based on the mean composition and standard deviation of the pyrrhotite analyses (Table 7.1). Based on figure 7.2, three important observations with respect to the mineralogy of pyrrhotite can be made.

Firstly, it is evident from figure 7.2 and table 7.1 that the most frequently occurring metal / sulfur ratio for magnetic $Fe_7S_8$ pyrrhotite is 0.869, and the ratio for non-magnetic $Fe_9S_{10}$ pyrrhotite is 0.895, both of which are slightly more deficient in iron than the theoretical ratio (metal / sulfur = 0.875 for $Fe_7S_8$, 0.900 for $Fe_9S_{10}$). Therefore it is necessary to determine whether this is statistically relevant or is an analytical artefact due to the precision of the measurement. During the EMP analysis, a synthetic troilite standard was prepared to check the calibration of the pyrrhotite analysis routine (Section 3.2.4). On the basis that the synthetic troilite standard was homogenous, the error in the metal / sulfur ratio associated with repeat analyses of the standard can be used to determine the precision of the technique. Since the $2\sigma$ standard deviation calculated for the metal / sulfur ratio obtained from repeat analyses of the troilite standard was 0.01 (Section 3.2.4), this means that the most frequently occurring metal

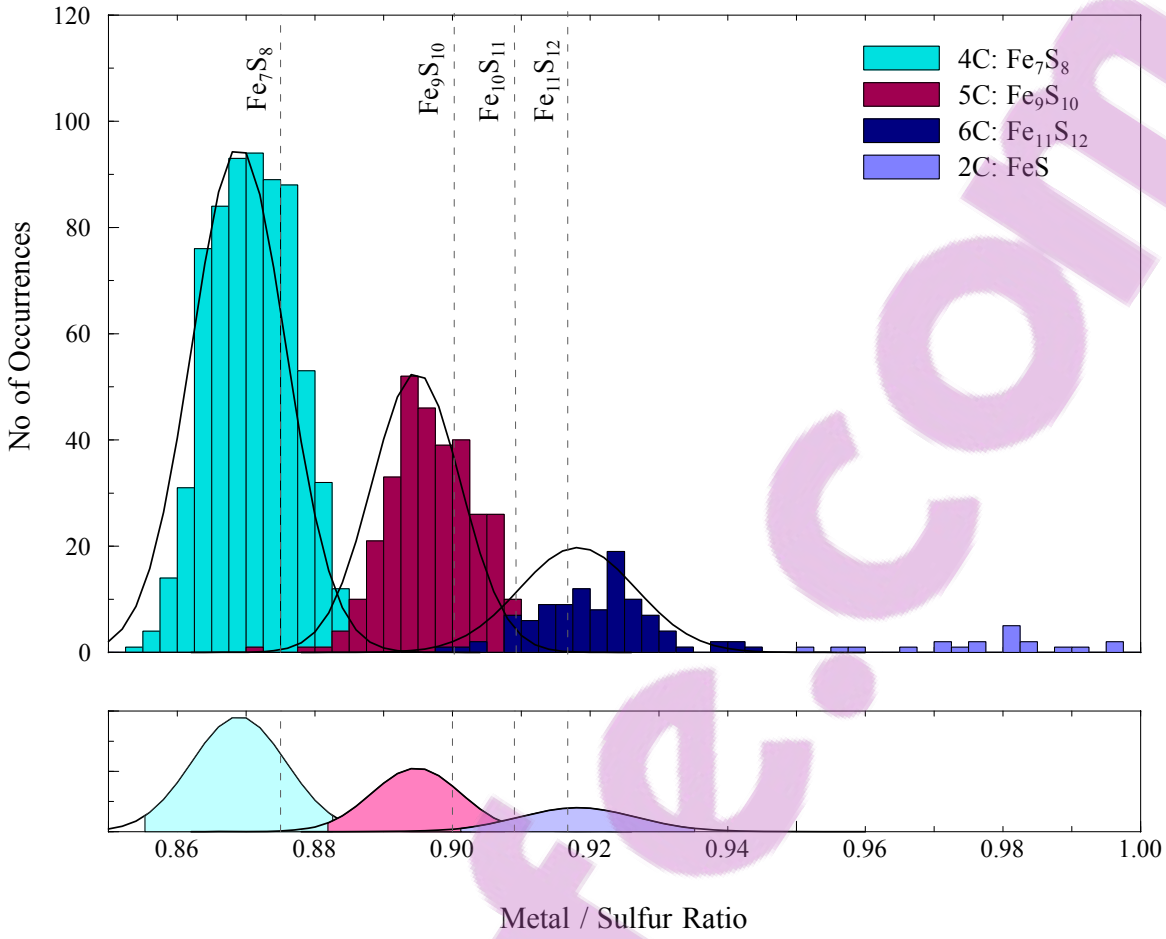


**Figure 7.2**: Comparison of the atomic metal to sulfur ratios for all 4C magnetic ($Fe_7S_8$) and NC non-magnetic pyrrhotite ($Fe_9S_{10}$, $Fe_{11}S_{12}$) occurrences examined in this study. The normal or Gaussian distribution function corresponding to the mean metal / sulfur ratios given in table 7.1 is also shown. The area under the Gaussian function which represents metal / sulfur ratios within 2σ of the mean are shown in colour in the bottom inset.

/ sulfur ratios for magnetic and non-magnetic pyrrhotite fall within the precision which the EMP allows. Therefore the observation that the most frequently occurring metal / sulfur ratio for magnetic and non-magnetic pyrrhotite in this study is slightly more depleted in iron than the ideal is not significant.

Secondly, it is evident from figure 7.2, that the naturally occurring magnetic 4C $Fe_7S_8$ pyrrhotite analysed in this study shows a range of atomic metal to sulfur ratios that approaches a Gaussian distribution. Similarly, it is evident that the naturally occurring magnetic 5C $Fe_9S_{10}$ pyrrhotite analysed in this study shows a range of atomic metal to sulfur ratios that approaches a Gaussian distribution. Even though the distribution of metal to sulfur

ratios for 6C $Fe_{11}S_{12}$ pyrrhotite were slightly skewed to more positive values due to troilite contamination, the histogram approaches a Gaussian distribution. This implies that a degree of non-stoichiometry is present in naturally occurring pyrrhotite.

Thirdly, it is evident from figure 4.24 that there is some overlap in the distribution of the metal to sulfur ratios between naturally occurring 4C $Fe_7S_8$, 5C $Fe_9S_10$ and 6C $Fe_{11}S_{12}$ pyrrhotite. In particular, the distribution functions for the $Fe_9S_{10}$ and $Fe_{11}S_{12}$ pyrrhotite are noted to show some overlap that encompasses the field of $Fe_{10}S_{11}$ pyrrhotite. However, no 11C $Fe_{10}S_{11}$ pyrrhotite was encountered in this study even though it has been previously described by others (e.g. Morimoto *et al*., 1970). The absence of $Fe_{10}S_{11}$ pyrrhotite in this study is attributed to the analytical precision of the EMP. Since the calculated two sigma standard deviation in the metal to sulfur ratio of troilite was 0.01 (Section 3.2.4), it indicates that the EMP is unable to distinguish between $Fe_9S_{10}$ (metal / sulfur = 0.900) and $Fe_{10}S_{11}$ (metal / sulfur = 0.909). Similarly, the EMP is unable to distinguish between $Fe_{10}S_{11}$ (metal / sulfur = 0.909) and $Fe_{11}S_{12}$ (metal / sulfur = 0.917). In theory though, discrimination between $Fe_9S_{10}$ and $Fe_{11}S_{12}$ is possible. On the basis that both the mineral chemistry and crystallographic studies showed that non-magnetic Sudbury CCN pyrrhotite was 5C $Fe_9S_{10}$ pyrrhotite some confidence can be placed in the results of this study.

However, in order to determine whether the degree of overlap between 4C magnetic and NC non-magnetic pyrrhotite (5C, 6C, and 11C) is real, the field that encompasses the 2σ standard deviation (95% confidence interval) for the composition of naturally occurring 4C, 5C and 6C pyrrhotite samples is shown in the bottom inset of figure 7.2. Since these calculated fields overlap one another, it suggests that the coincidence in metal / sulfur ratios between some 4C and NC pyrrhotite is real. The implication of this is that certain metal / sulfur ratios exist in nature where there is a probability that either 4C or NC pyrrhotite can. Similarly, there must be a probability that for certain metal / sulfur ratios, 5C, 6C or 11C pyrrhotite can form (even if they cannot be distinguished analytically from one another with ease).

Therefore, the mechanism by which the pyrrhotite structure is able to accommodate non-stoichiometry is of interest. Two potential options exist that allow the pyrrhotite structure to accommodate non-stoichiometry. The first of which is based upon the presence of partially occupied iron sites. The crystal structure solutions proposed for stoichiometric magnetic 4C $Fe_7S_8$ pyrrhotite consist of alternating fully occupied layers with vacancy containing layers

(Tokonami *et al.*, 1972; Powell *et al.*, 2004). Within the 4C pyrrhotite crystal structure, the vacancy layers consist of either fully occupied or completely vacant iron sites (Figure 4.10a). In contrast, the crystal structure proposed for naturally occurring 5C pyrrhotite from Sudbury CCN by De Villiers *et al*. (Submitted), consisted of no fully occupied layers. Instead each layer contained a series of fully occupied and partially occupied iron sites. Several different partial occupancies were also proposed for the 5C Sudbury CCN pyrrhotite structure. On this basis, it is possible that natural pyrrhotite is able to accommodate non-stoichiometry. Therefore, it would be anticipated that the exact partial occupancy of iron sites is variable between individual pyrrhotite crystals.

An additional mechanism to account for the non-stoichiometry present in pyrrhotite is by the presence of non-integral or incommensurate pyrrhotite types. Morimoto *et al.* (1975b) described pyrrhotite crystals from Kishu mine in Japan that were mixtures of 4C, 4.88C and 5C pyrrhotite types. Morimoto *et al.* (1975b) also described pyrrhotite crystals from the Kohmori mine that were mixtures of NC and 2C pyrrhotite with *N* varying between 5.36 and 5.80. Therefore, the possibility also exists that the non-stoichiometry observed in pyrrhotite samples from this study could be accounted for by the presence of some non-integral pyrrhotite types intergrown with the stoichiometric 4C or 5C pyrrhotite superstructures. However, since pyrrhotite mineral chemistry was used to interpret pyrrhotite superstructure based on the relationship of Morimoto *et al.* (1970), should there have been any non-integral pyrrhotite types present within the samples analysed, they would not have been identified. This does not apply to the pyrrhotite samples analysed by single crystal x-ray diffraction by which it would be possible to recognise non-integral pyrrhotite types.

## 7.3 Effect of Ore Deposit Formation on Pyrrhotite Mineralogy

The aim of this section is to answer the second key question; "H*ow does ore deposit formation affect the mineralogy of pyrrhotite*." Based on the results of Chapter 4; the following are considered important attributes of the mineralogy of the pyrrhotite ore samples examined:

(i) The magnetic properties, crystallography and mineral chemistry of pyrrhotite.
(ii) The identity of the minerals and relative proportions of the individual sulfide, oxide and silicate minerals present.
(iii) The textural properties of the minerals present (grain size, shape) as well as their association to the other minerals present. This would include different types of intergrowth textures between the minerals.

Since the focus of this study is on pyrrhotite, only the mineralogy of the sulfide contingent and how it is affected by ore deposit formation will be concentrated upon. Pyrrhotite samples in this study were selected from magmatic nickel and platinum group element ore deposits (Section 2.1) which are commonly accepted to have formed from the crystallisation of a monosulfide solid solution (MSS; Naldrett *et a*l, 1967; Naldrett and Kullerud, 1967; Kelly and Vaughan, 1983). The two main parameters that control the key attributes of the pyrrhotite mineralogy noted above are the bulk composition and cooling history of the MSS, each of which will be further evaluated.

The phase diagram for the FeS to $FeS_2$ system given in figure 2.8 (Kissin and Scott, 1982; Wang and Salveson, 2005) in section 2.2 shows that the type and composition of pyrrhotite formed is controlled by the bulk composition of the MSS. It is noted that the bulk composition in turn is heavily influenced by sulfur fugacity ($fS_2$). According to Toulmin and Barton (1964), the mole fraction of FeS in the system FeS-$S_2$ was determined by both sulfur fugacity and temperature. Figure 2.8 shows that for equilibrium crystallisation of pyrrhotite from the MSS with a bulk composition of 48.5 atomic % iron, the formation of non-magnetic NC pyrrhotite coexisting with troilite is likely. For a slightly lower bulk composition of 47.5 atomic % iron, the formation of non-magnetic NC pyrrhotite is likely. For an even lower bulk composition of 47.0 atomic % iron, the formation of non-magnetic NC pyrrhotite coexisting

with magnetic 4C pyrrhotite is expected. For the lowest atomic % iron contents, the formation of 4C magnetic pyrrhotite coexisting with pyrite is expected.

Since the intergrowth textures between magnetic 4C and non-magnetic NC pyrrhotite types described in this study (Section 2.7, 4.2) were generally lamellae-like features and not irregular intergrowths, they are primary textures indicative of the cooling history of the MSS. These textures are related to the sub-solidus exsolution of magnetic pyrrhotite from a non-magnetic pyrrhotite host. Similarly, the formation of troilite coexisting with non-magnetic NC pyrrhotite is through exsolution. Since the intergrowth textures were noted in Section 4.2 to be crystallographically controlled, it further confirms that they formed through sub-solidus exsolution from the MSS. Exsolution lamellae of magnetic 4C pyrrhotite hosted by non-magnetic NC pyrrhotite could be further developed by lamellae coarsening due to annealing as a result of slow cooling (Brady, 1987). Examples of this type of lamellae coarsening were readily noticeable in the mixed pyrrhotite samples such as the Nkomati MSB or MMZ pyrrhotite. Box work textures were also observed in the Nkomati MSB and Phoenix pyrrhotite samples (Section 4.2), and which Lianxing and Vokes (1996) argued to represent the more advanced stages of lamellae coarsening. Crystal defects such as the twinning noted for some of the pyrrhotite samples examined in Section 4.2 are also a function of the cooling history of the pyrrhotite.

This shows that both the bulk composition and cooling history of the MSS influence the magnetic properties, composition and crystallography of each pyrrhotite phase. Similarly, these factors also influence the nature of the intergrowth patterns between pyrrhotite types and determine whether two phase non-magnetic NC pyrrhotite coexisting with troilite, single phase non-magnetic NC pyrrhotite, two phase non-magnetic NC pyrrhotite coexisting with magnetic 4C pyrrhotite or single phase magnetic 4C pyrrhotite according to the classification scheme given in table 7.1 is formed.

The MSS can be further extended to account for the contribution of nickel to the iron-sulfur system. It is well known from both petrographic and experimental evidence that pentlandite formation occurs via exsolution from the MSS (e.g. Naldrett *et al.*, 1967; Ramdohr, 1969; Kelly and Vaughan, 1983; Fleet, 2006), and the exsolution of pentlandite from pyrrhotite in the samples examined in this study would be no exception. The experimental studies of Kelly and Vaughan (1983) showed the dependency of pentlandite exsolution on the metal / sulfur

ratio and cooling time (Figure 2.13). It is evident from figure 2.13 that the formation of flame pentlandite lamellae was preceded in time by the exsolution of pentlandite blebs and blades on grain boundaries and fractures. Flame pentlandite formation was however, restricted to those experimental studies which had the highest metal / sulfur ratio (metal / sulfur = 0.981).

The composition of pyrrhotite samples used in microflotation tests was shown to contain differing proportions of pentlandite that varied between 6.61 wt % (Nkomati MSB mixed pyrrhotite) and 16.9 wt % (Phoenix magnetic pyrrhotite; Table 3.1, 3.3). However, of greater importance to pyrrhotite flotation performance was the difference in pentlandite liberation. Petrographic examination of the pyrrhotite samples in Section 4.2 showed that the Phoenix magnetic pyrrhotite hosted abundant flame pentlandite, Nkomati MSB contained slightly less flame pentlandite whereas only minor flame pentlandite was noted for the Sudbury pyrrhotite samples. MLA analysis of the flotation feed samples confirmed this difference in the amount of flame pentlandite between the pyrrhotite samples. Pentlandite in the Phoenix magnetic pyrrhotite samples was only 48.5 % liberated, was 53.6 % liberated in the Nkomati MSB pyrrhotite and was over 75 % liberated for the Sudbury pyrrhotite samples. Using pentlandite liberation as a proxy for the proportion of flame pentlandite, it can be concluded that the MSS from which the Phoenix pyrrhotite formed, had a sufficiently high metal / sulfur ratio and a long, slow cooling history that allowed the formation of abundant flame pentlandite. In contrast, it can be concluded the initial metal / sulfur ratios of the Sudbury pyrrhotite samples was possibly not as high, or that the cooling time was slightly more rapid and did not allow for the formation of abundant flame pentlandite.

Localised exsolution of flame pentlandite was also sometimes associated with the formation of monoclinic pyrrhotite. Kelly and Vaughan (1983) described how the localised removal of a metal rich component (pentlandite) from the MSS caused the zone surrounding the area of flame pentlandite exsolution to be more sulfur rich, with the consequent formation of rims of the more sulfur rich pyrrhotite phase (magnetic pyrrhotite) surrounding the pentlandite flames. This was observed in both the Nkomati and Sudbury pyrrhotite samples examined in this study (Section 4.2) and has previously been described by authors such as Naldrett and Kullerud (1967).

In the experimental studies of Naldrett *et al.* (1967) on the MSS, it was similarly shown that pentlandite exsolution was dependent on the initial metal to sulfur ratio of the MSS. In

addition, Naldrett *et al.*, (1967) showed that pentlandite exsolution was dependent on the nickel content of the MSS which in turn affects the composition of pyrrhotite. During the cooling of the MSS, the composition of the MSS continually changes with pentlandite exsolution. The residual nickel content of the MSS however, represents the amount of solid solution nickel substituting for iron and hosted by pyrrhotite (Naldrett *et al.*, 1967; Kelly and Vaughan, 1983). As part of the mineralogical characterisation of pyrrhotite, it was shown that the solid solution nickel content varied between pyrrhotite type, although some correlation existed between nickel content and pyrrhotite association (Table 7.1). For single phase pyrrhotite occurrences, non-magnetic pyrrhotite was less nickel rich than magnetic pyrrhotite. For two phase pyrrhotite occurrences, the host phase was generally more nickel rich than the exsolved phase, i.e. the nickel content of non-magnetic pyrrhotite from which magnetic pyrrhotite lamellae had exsolved was more nickel rich than the magnetic pyrrhotite exsolution lamellae (e.g. Nkomati MSB, MMZ sample *MMZ-4* pyrrhotite).

Other impurity minerals or elements that may be associated with the bulk composition of the MSS include pyrite, chalcopyrite, magnetite and the platinum group elements. If the bulk composition of the MSS was enriched in sulfur and had a sufficiently high $fS_2$, the formation of pyrite coexisting with magnetic 4C pyrrhotite would be expected. This was observed for the magnetic pyrrhotite samples in this study (Merensky Reef sample *IMP-1*, Nkomati MSB and MMZ, Phoenix and Sudbury Gertrude and Gertrude West pyrrhotite). No pyrite was noted in the non-magnetic NC pyrrhotite samples examined (Merensky sample *IMP-2*; Sudbury CCN). Given the compatibility of the platinum group elements in a sulfide liquid compared to the silicate fraction, the MSS could also have some association to the platinum group elements (Crockett *et al.*, 1997). If the bulk composition of the MSS was enriched in the platinum group elements then the cooling history would determine whether the platinum group elements occurred in solid solution with pyrrhotite or pentlandite. The formation of discrete platinum group minerals would be a consequence of a fractional crystallisation cooling history.

The effect of the bulk composition and cooling history of the MSS are considered to be the most important features controlling the primary mineralogy of pyrrhotite. Although not necessarily a very significant feature in the samples analysed in this study, the role of secondary processes and their effect on the mineralogy of pyrrhotite should be mentioned. This includes oxidation, hydrothermal alteration and weathering. Depending on the partial

pressure of oxygen during the cooling of the MSS, oxidation may also be relevant during primary ore formation.

Pyrrhotite is known to be associated with magnetite and which can be related to the oxygen fugacity ($fO_2$) in the Fe-S-O system and hence the bulk composition of the system. The experimental studies of Kullerud (1957) showed that below $675^0$C, ferrous iron in pyrrhotite could be oxidised to ferric iron with the resultant formation of magnetite if oxygen was introduced to the system. This reaction could be followed by the subsequent formation of pyrite from the excess sulfur (Kullerud, 1957; Naldrett and Kullerud, 1967). It was also shown by Kullerud (1957) and Desborough and Carpenter (1965) that "hexagonal" pyrrhotite could be converted to monoclinic pyrrhotite and magnetite at relatively high $fO_2$. Magnetite was noted to occur in association for all of the pyrrhotite samples examined in this study other than the Merensky Reef pyrrhotite, where the oxide phase was chromite. For the Nkomati MMZ pyrrhotite, magnetite occurred as discrete grains as well as very fine-grained rod like inclusions (Section 4.2). It has also previously been shown that the crystal structures of monoclinic and "hexagonal" pyrrhotite may contain some oxygen (Graham and Mc Kenzie, 1987). This provides further evidence to suggest that $fO_2$ may be an important influence on the bulk composition of the system from which pyrrhotite forms.

Alternatively, "hexagonal" pyrrhotite can be converted to monoclinic pyrrhotite by hydrothermal alteration processes (Desborough and Carpenter, 1965). Lianxing and Vokes (1996) attributed the development of irregular intergrowth textures between magnetic and non-magnetic pyrrhotite due to this type of alteration. Although the formation of magnetic pyrrhotite rims surrounding non-magnetic pyrrhotite was not observed for the samples examined in this study, it does not preclude that this may be an important mechanism controlling the mineralogy of pyrrhotite for some ore deposits. Liebenberg (1970) noted the formation of monoclinic pyrrhotite along cracks and grain boundaries of "hexagonal" pyrrhotite in samples examined from the Bushveld Complex. Mackinawite ($Fe_{(1+X)}S$) has also been known to form during the secondary alteration of pyrrhotite (Ramdohr, 1969; Liebenberg, 1970).

Silicate minerals were not focussed upon here since the majority of the pyrrhotite samples studied were massive in nature. However, the silicate minerals may well influence the flotation performance of pyrrhotite. Two hydrous ferromagnesian silicate minerals in

particular that commonly form through alteration of magmatic sulfide deposits are known to have a detrimental effect on flotation performance of these ores. Talc is a naturally hydrophobic mineral and although only present in small quantities in the Merensky Reef, is known to have a disproportionately detrimental effect on flotation performance, particularly due to its froth stabilising properties (Shortridge, 2002; Wiese *et al*., 2005). Talc has previously been shown to form through the alteration of orthopyroxene (Hemley *et al.*, 1977; Nesbitt and Bricker, 1978; Viti *et al.*, 2005) which is the major gangue mineral in the Merensky Reef ore. Talc was also reported as a problematic mineral in the processing of the Sudbury ores (Lotter *et al.*, 2008). Serpentine on the other hand, forms through the alteration of olivine (Hemley *et al.*, 1977). The presence of serpentine in the processing of nickel ores may cause severe rheological problems due to its fibrous nature and effect on the yield stress of the ore slurry (Senior and Thomas, 2005; Burdukova *et al.*, 2008).

## 7.4 Effect of Mineralogy on Pyrrhotite Reactivity

The aim of this section is to answer the third key question, "*How does the reactivity of magnetic and non-magnetic pyrrhotite differ and can these differences be accounted for by the crystallography, mineral chemistry and mineral association of pyrrhotite?*" In order to do this, the results from the open circuit potential, cyclic voltammetry and oxygen uptake experiments in Chapter 5 are first reviewed and discussed in order to understand the nature of the pyrrhotite surface in the different experiments. These results need to be interpreted with care since if the reaction rates are so rapid, an apparently "unreactive" surface which has already been passivated may be detected upon measurement. Only once these results have been interpreted, can any attempt be made to develop the relationship between pyrrhotite mineralogy and reactivity.

Based on the literature review the reaction product of pyrrhotite that most commonly forms under standard oxidising conditions is ferric hydroxide. Since the measurement conditions of the open circuit potential and cyclic voltammetry studies did not include any interaction with flotation reagents, the results can be directly interpreted to give an indication of the difference in reactivity of the pyrrhotite samples due to their mineralogy. Since the differences between the various electrodes were more significant at pH 10 than pH 7 due to the increase in electrochemical reaction rates at the higher hydroxide ion concentrations (Janzen, 1996; Chirita *et al.*, 2008), differences in pyrrhotite reactivity due to mineralogy are best interpreted using the results of the tests at pH 10 (Section 5.2, 5.3).

On this basis, non-magnetic Sudbury CCN pyrrhotite was the most unreactive of the pyrrhotite samples examined in this study. Non-magnetic Sudbury CCN pyrrhotite showed the lowest open circuit potential of the samples examined which suggests the surface of the pyrrhotite electrode was covered with the lowest amount of ferric hydroxide species (Section 5.2.1). Non-magnetic Sudbury CCN pyrrhotite also showed the smallest changes in current density associated with the REDOX reactions in the cyclic voltammetry studies that indicate that the pyrrhotite was not very reactive.

Magnetic Sudbury Gertrude West pyrrhotite was the most reactive of the pyrrhotite samples examined. Since the open circuit potential measurements obtained at pH 10 for the magnetic Sudbury Gertrude West pyrrhotite electrode were by far the highest (Section 5.2.1), it can be

concluded that the surface of the electrode was covered with the greatest proportion of ferric hydroxide species. This was likely due to the very reactive nature of the Gertrude West magnetic pyrrhotite and the consequent formation of ferric hydroxides following rapid oxidation. The cyclic voltammetry studies confirmed the very reactive nature of the Sudbury Gertrude West magnetic pyrrhotite due to the fact that it was the pyrrhotite sample that showed the greatest changes in current density (Section 5.3.5).

The magnetic Phoenix pyrrhotite sample was also relatively reactive towards oxidation although the reaction rates were not as rapid as for the magnetic Sudbury Gertrude West pyrrhotite sample. Open circuit potential measurements obtained for the Phoenix magnetic pyrrhotite were somewhere in between the unreactive non-magnetic Sudbury CCN and very reactive Sudbury Gertrude West pyrrhotite (Section 5.2.1). Similarly, the current density obtained in the cyclic voltammetry studies of the Phoenix magnetic pyrrhotite electrode was significantly greater than the unreactive non-magnetic Sudbury CCN and less reactive than the magnetic Sudbury Gertrude West pyrrhotite (Section 5.3.5).

The reactivity of the Nkomati MSB mixed magnetic and non-magnetic pyrrhotite sample is considered to be in between that of the reactive magnetic Phoenix pyrrhotite and the unreactive non-magnetic Sudbury CCN pyrrhotite samples. Although little difference was observed in open circuit potential between the mixed Nkomati and magnetic Phoenix pyrrhotite electrodes at pH 10 (Section 5.2.1), significantly lower current densities were measured for the REDOX reactions of the Nkomati pyrrhotite in comparison to the Phoenix magnetic pyrrhotite. Significantly higher current densities were obtained in the cyclic voltammetry studies of the Nkomati pyrrhotite relative to the non-magnetic Sudbury CCN pyrrhotite. This indicates that the Nkomati mixed pyrrhotite was less reactive than the Phoenix magnetic pyrrhotite and more reactive than the non-magnetic Sudbury CCN pyrrhotite.

Similarly to the interpretation of the open circuit potential and cyclic voltammetry studies, the results of the oxygen uptake studies are best interpreted at pH 10 in the absence of flotation reagents in order to identify differences in reactivity due to mineralogy. The relatively unreactive character of the non-magnetic Sudbury CCN pyrrhotite was confirmed by the oxygen uptake studies where the lowest oxygen uptake factor was obtained for the Sudbury CCN pyrrhotite relative to the other pyrrhotite samples examined (Section 5.4.5). Next to the

non-magnetic Sudbury CCN pyrrhotite, the lowest oxygen uptake factor was obtained at pH 10 for the slurry of the magnetic Sudbury Gertrude West pyrrhotite (Section 5.4.5). The low oxygen uptake factor obtained for the magnetic Sudbury Gertrude West pyrrhotite slurry is interpreted to be due to the fact that it was already covered by ferric hydroxide species and passivated at the time of measurement due to its very reactive character as evidenced by the open circuit potential and cyclic voltammetry studies. It is probable that despite careful sample preparation for the oxygen uptake tests, sufficient opportunity was available for the oxidation of the very reactive Sudbury Gertrude West pyrrhotite. In contrast, the sample preparation procedure used in manufacturing pyrrhotite electrodes for the cyclic voltammetry studies was able to expose a fresh layer of Gertrude West pyrrhotite at the start of each measurement such that its very reactive nature was recorded by the cyclic voltammetry studies. The very reactive nature of the Sudbury Gertrude West and Gertrude pyrrhotite was also noted during the preparation of the cut pyrrhotite surfaces used for the photomicrographs of the pyrrhotite samples shown in figure 3.3. With the period of a week, the Gertrude and Gertrude West pyrrhotite sample surfaces showed considerable tarnishing whereas, those of the other pyrrhotite surfaces remained relatively fresh.

The highest oxygen uptake factor was obtained for the slurry of the Phoenix magnetic pyrrhotite sample and which confirms its reactive nature. It is also of interest to note, that the slurry containing the Phoenix magnetic pyrrhotite had the lowest dissolved oxygen content of the samples investigated prior to sparging the slurry with oxygen (Section 5.4.5). This indicates that prior to sparging the solution with oxygen, the pyrrhotite had already depleted the available oxygen in solution during oxidation. No indication was obtained from the reactivity studies to suggest that the Phoenix magnetic pyrrhotite surface was already passivated.

Similarly to the open circuit potential and cyclic voltammetry studies, the oxygen uptake factor of the Nkomati MSB mixed pyrrhotite was greater than the non-magnetic Sudbury CCN pyrrhotite and lower than the magnetic Phoenix pyrrhotite. This indicates that the reactivity of the intergrown magnetic and non-magnetic pyrrhotite was in between that of magnetic and non-magnetic pyrrhotite.

The relative differences in reactivity between the pyrrhotite samples were generally conserved with the addition of flotation reagents. The results from Section 5.4 showed that the pulp

oxygen content was generally higher and the dissolved oxygen uptake factor lower for a pyrrhotite slurry conditioned with xanthate collector relative to a slurry with no collector. Previous studies that have examined the change in pulp dissolved oxygen content on an operating plant at the point of reagent addition have showed little change in dissolved oxygen content. Buswell *et al.* (2002) showed little difference in dissolved oxygen content of the pulp with xanthate addition on a platinum plant, but this was attributed to the very low sulfide content (1 %) of the Merensky Reef ore. Ekmekci *et al.* (2003) also showed little difference in dissolved oxygen content at the point of xanthate addition for a Turkish pyrite ore. However, since dissolved oxygen measurements from this work corresponded with the point of the initiation of flotation following conditioning (Section 3.4.4; 4.5.1), the results are not entirely comparable to previous research. Results in this study are interpreted to represent the state of the pulp subsequent to the electrochemical interactions between the pyrrhotite samples with collector.

The decreased reactivity of the pyrrhotite slurry conditioned with xanthate was attributed to the formation of a surface coating most likely corresponding to several monolayers that would have protected the pyrrhotite surface from further oxidation. Sparging of the pulp with oxygen therefore caused an increase in pulp dissolved oxygen content and decrease in the oxygen uptake factor since the amount of oxygen consumption through pyrrhotite oxidation was limited. This is consistent with the interpretation of Spira and Rosenblum (1974), although the decrease noted in oxygen demand for the pyrrhotite ore in their study was due to sodium cyanide addition that was similarly argued to restrict the access of oxygen to the pyrrhotite surface.

The dissolved oxygen content was also generally lower and the oxygen uptake factors higher, when the shorter chain length SNPX was used as a collector (Table 5.1). In addition to the difference in solubility product between xanthate collectors of varying chain lengths (M.C. Fuerstenau, 1982), it would be expected that they would show differences in oxidation rate. Harris and Finkelstein (1977) investigated the amount of oxygen consumed with the addition of xanthate to chalcocite. They showed a consistent change in the rate of oxygen consumption corresponding with xanthate chain length. The rate of oxygen consumption was far greater for the longer chain length hexyl, amyl and butyl xanthate relative to the propyl and ethyl xanthate. Since the time required for the oxidation of SIBX to its dixanthogen species would be less than that required for SNPX, it is expected that the time required to form a surface

layer of dixanthogen on pyrrhotite would be longer for the latter. Prior to complete dixanthogen surface coverage, the pyrrhotite surface would still be able to interact with oxygen and prone to oxidation. This scenario is proposed to account for the difference in oxygen uptake factor between SNPX and SIBX addition to the pyrrhotite slurry. During the additional time required for dixanthogen formation from SNPX, the pyrrhotite would still have been reactive and prone to oxidation which is evidenced by the slightly higher oxygen uptake factor.

Similarly to the reduction in pyrrhotite reactivity with collector addition, the addition of copper caused a further decrease in oxygen uptake factor. This effect was only manifested for the magnetic Phoenix and Sudbury Gertrude West pyrrhotite samples where the oxygen uptake factor was approximately halved due to copper addition. Using ToF-SIMS, Gerson and Jasieniak (2008) showed that following copper addition, the surface of pyrrhotite was covered with an adsorbed layer of copper. Comparison of the degree of surface oxidation using ToF-SIMS also showed that pyrrhotite samples that had been exposed to copper showed significantly lower proportions of oxidation products (e.g. lower O/S ratio) relative to pyrrhotite with no copper activation. The reduction in oxygen uptake factor due to copper addition in conjunction with collector is therefore attributed to the formation of an adsorbed layer of copper, and formation of a hydrophobic copper collector species that protected the pyrrhotite surface from further oxidation.

On the whole, the mineral reactivity studies have shown that non-magnetic pyrrhotite is relatively unreactive whereas magnetic pyrrhotite is reactive. The studies have also shown that definite differences exist in the reactivity of magnetic pyrrhotites derived from different ores. The reactivity of mixed magnetic and non-magnetic pyrrhotite was in between that of pure magnetic and non-magnetic pyrrhotite most likely due to the combined contribution of the reactive magnetic pyrrhotite intergrown with the unreactive non-magnetic pyrrhotite. Therefore, it is now of interest to explore possible mechanisms that could allow for the crystallography, mineral chemistry and mineral association of pyrrhotite to influence its reactivity.

*Crystallography*

Pyrrhotite is known to oxidise rapidly and therefore it is of relevance to review the oxidation mechanism. As described in Chapter 2, Pratt *et al.* (1994) proposed a mechanism for pyrrhotite oxidation by which the only movement of species during the reaction was the transfer of electrons from the crystal lattice and the diffusion of iron towards the surface ferric oxyhyroxide layer. Pratt *et al.* (1994) argued that the most reactive sites for oxygen reduction were associated with the ferric iron sulfur bonds and the vacancies in the pyrrhotite crystal lattice. The presence of vacancies would likely facilitate electron transfer as well as the diffusion of iron through the crystal lattice to the surface, thereby assisting the oxidation reaction. Since the magnetic pyrrhotite structure has more vacancies relative to the non-magnetic pyrrhotite, it is hypothesised that that the greater abundance of vacancies accelerates the oxidation process for magnetic pyrrhotite relative to non-magnetic pyrrhotite. For the samples examined in this study, this would theoretically relate to 1 vacancy for every 8 iron sites for the magnetic 4C $Fe_7S_8$ Phoenix and Sudbury Gertrude West pyrrhotite samples, whereas only 1 in 10 iron sites would be vacant for the non-magnetic 5C $Fe_9S_{10}$ Sudbury CCN pyrrhotite.

The presence of vacancies and their role in facilitating more rapid oxidation and greater reactivity for magnetic pyrrhotite relative to non-magnetic pyrrhotite is in agreement with the results of the oxidation studies of Gerson and Jasieniak (2008) and Lehmann *et al.* (2000). Gerson and Jasieniak (2008) observed more rapid oxidation of monoclinic pyrrhotite relative to “hexagonal” pyrrhotite with ToF-SIMS. Lehmann *et al.* (2000) measured both larger rate constants and lower activation energy for the oxidation of monoclinic relative to “hexagonal” pyrrhotite. The results from this study are not in disagreement with Janzen (1996) where no correlation was found between oxidation rate and crystallography. However, since the experiments of Janzen (1996) were performed on pyrrhotite derived from multiple provenances, it is likely that the dataset was not sensitive enough in order to isolate these differences. The oxygen demand tests of Spira and Rosenblum (1974) also showed a greater oxygen demand for non-magnetic pyrrhotite relative to magnetic Noranda pyrrhotite. Spira and Rosenblum (1974) did however comment that the non-magnetic pyrrhotite sample was most likely troilite and so direct comparison with the results of this study is not necessarily possible.

*Mineral Chemistry*

Both oxygen and ferric iron are known to be oxidising agents of pyrrhotite (Hamilton and Woods, 1981; Janzen, 1996; Belzile *et al.*, 2004) and so the presence of both these species within the pyrrhotite structure needs to be evaluated. Ferric iron was also noted by Janzen (1996) to be a much stronger oxidising agent than oxygen. The ideal formula for magnetic and non-magnetic pyrrhotite has been argued to contain both ferrous and ferric iron. The presence of both these iron species would then maintain the charge balance due to the variation of the relative proportions of these two cations (Bertaut, 1953; Pratt *et al.*, 1994; Mikhlin and Tomashevich, 2005). Therefore, magnetic pyrrhotite of formula $Fe^{3+}_2Fe^{2+}_5S^{2-}_8$ ($Fe_7S_8$) contains proportionally more ferric iron in its structure than non-magnetic pyrrhotite of formula $Fe^{3+}_2Fe^{2+}_7S^{2-}_{10}$ ($Fe_9S_{10}$). Consequently, it could be expected that magnetic pyrrhotite is more prone to oxidation than non-magnetic pyrrhotite because of the greater proportion of ferric iron acting as an oxidising agent within its structure.

In the case of oxygen as an oxidising agent, the results of the mineralogical characterisation of pyrrhotite in Chapter 4 provide more than sufficient evidence to suggest that oxygen in the form of magnetite is often associated with pyrrhotite. The most well developed example of this was the presence of very fine grained elongate rod-like inclusions of magnetite hosted by pyrrhotite in the Nkomati MMZ samples (Section 4.2.2). On the basis of this observation, it can be concluded that oxygen is present during the crystallisation of the MSS and formation of pyrrhotite. Therefore, it is not implausible that some minor proportion of oxygen could have been accommodated within the pyrrhotite crystal structure. The results of the nuclear microprobe analyses of Graham and Mc Kenzie (1987) showed the presence of detectable amounts of oxygen of ~ 0.05 wt % within both monoclinic and “hexagonal” pyrrhotite. The presence of trace amounts of dissolved oxygen in the pyrrhotite crystal structure is proposed here as a possible mechanism to account for the differences in reactivity between magnetic pyrrhotite samples derived from different ore deposits. Therefore, if the Sudbury Gertrude West magnetic pyrrhotite sample contained a greater concentration of oxygen within its structure than the Phoenix magnetic pyrrhotite sample, it could be expected that the greater oxygen content would facilitate the oxidation reaction thereby increasing the reactivity of the magnetic Sudbury Gertrude West pyrrhotite. This is clearly an area for further investigation (see Chapter 8).

It is recognised that the concentration of trace oxygen within the pyrrhotite crystal structure is not necessarily correlated with the actual proportion of magnetite present in the sample. The MLA results of the microflotation feed and oxygen uptake samples (Table 3.3 ) showed only minor differences in magnetite concentration between the magnetic Sudbury Gertrude West (0.61 wt % magnetite) and Phoenix pyrrhotite (0.19 wt %). It is noted that the Nkomati MSB pyrrhotite had the highest proportion of magnetite (5.49 wt %), yet this pyrrhotite was noted to be less reactive than the magnetic Sudbury Gertrude West and Phoenix pyrrhotite samples.

The mineralogical characterisation also showed that the solid solution nickel content in pyrrhotite was variable (Table 7.1). In the study of Kwong (1993), a semi-quantitative correlation was found between nickel and cobalt content and oxidation rate for monoclinic pyrrhotite. Pyrrhotite samples enriched in nickel and cobalt were found to oxidise slightly slower. This was most likely due to the positive effective charge as a result of the donor defects caused by the substitution of cobalt and nickel for iron (Janzen, 1996). Since cobalt concentrations were relatively negligible for the pyrrhotite samples analysed in this study, the focus is on nickel. The implication of a positive effective charge within the vicinity of nickel substitution sites would be to retard the movement of electrons, thereby inhibiting the oxidation process. This is another additional mechanism to potentially account for the difference in reactivity observed between magnetic pyrrhotite samples derived from different ore bodies. The average solid solution nickel content of Phoenix pyrrhotite (1.06 ± 0.67 wt % Ni) was found to be slightly greater than for the magnetic Sudbury Gertrude West (0.82 ± 0.19 wt % Ni). It is possible that the resultant positive effective charge was greater in the Phoenix pyrrhotite and helped to stabilise the pyrrhotite structure. In contrast, the positive effective charge was not as significant in the magnetic Sudbury Gertrude West pyrrhotite and therefore it would have been prone to more severe oxidation as observed.

*Mineral Association*

In this study, only the Nkomati MSB and MMZ (sample *MMZ-4*) pyrrhotite consisted of intergrown magnetic and non-magnetic pyrrhotite. In the study of Arnold (1967) on the range in composition and structure of naturally occurring terrestrial pyrrhotites however, 73 % of the samples examined were mixtures of monoclinic and “hexagonal” pyrrhotite. Therefore, the association between magnetic and non-magnetic pyrrhotite is relatively important when evaluating the effect of mineral association on the reactivity of pyrrhotite in general. Due to the conductive or semi-conductive nature of the sulfide minerals, they may facilitate electron

transfer when they come into contract with one another, thereby creating a galvanic cell. The presence of a galvanic interaction could cause more severe oxidation than expected for the anodic mineral compared to that expected if the mineral occurred on its own. Since magnetic and non-magnetic pyrrhotite are commonly intergrown with one another, they could be considered prime candidates for the creation of a galvanic cell. Middlings or locked particles are known to suffer from galvanic effects more so than liberated particles (Almeida and Giannetti, 2003). A galvanic interaction between two minerals however, is dependent on the difference in rest potential of the two sulfide minerals and only when the difference is sufficiently high enough between the anodic and cathodic minerals, will there be a galvanic current. Even though differences have been noted here between the reactivity of magnetic and non-magnetic pyrrhotite, these are by no means comparable to the scale of the differences that are experienced during the operation of a true galvanic cell (Ekmekci and Demirel, 1997). Therefore, it is considered unlikely that galvanic interactions are effective between magnetic and non-magnetic pyrrhotite.

The reactivity of the mixed magnetic and non-magnetic Nkomati MSB pyrrhotite was observed to be in between that of the reactive Phoenix magnetic pyrrhotite and unreactive non-magnetic Sudbury CCN pyrrhotite. Therefore, even though a galvanic interaction is unlikely between intergrown magnetic and non-magnetic pyrrhotite, the effect of intergrown pyrrhotite does influence pyrrhotite reactivity. The effect of intergrown pyrrhotite appears to cause the resultant reactivity to be in between that of the reactive magnetic and unreactive non-magnetic pyrrhotite components.

Pyrrhotite samples in this study were observed to occur in association with other sulfide minerals of which the association to pentlandite was the strongest. Minor associations to chalcopyrite and pyrite were also noted. Therefore, the importance of galvanic effects between pyrrhotite and these minerals does need consideration, especially since the abovementioned minerals are more noble than pyrrhotite (Rand, 1977). In the weathering experiments conducted on real ores samples by Kwong (1993), rapid alteration due to oxidation of pyrrhotite was most noticeable for the monoclinic pyrrhotite sample that contained the greatest amount of pyrite (15 %). Similarly, results of flotation studies that have investigated the effect of galvanic interactions on floatability have only shown galvanic interactions to be effective when the proportion of the cathodic mineral is relatively high (e.g. Cheng and Iwasaki, 1992; Nakazawa and Iwasaki, 1995; Ekmekci and Demirel, 1997). Since

pentlandite is the only volumetrically significant sulfide in the pyrrhotite samples investigated, galvanic interactions between pyrrhotite and pentlandite need to be evaluated.

SEM images of the pyrrhotite electrodes used for the mineral reactivity tests showed some pentlandite contamination of the electrodes (Figure 3.7) and similarly, so did the MLA and QXRD analyses of the pyrrhotite samples (Tables 3.1, 3.3). MLA analyses of the Phoenix magnetic pyrrhotite sample showed that it contained the greatest amount of pentlandite contamination (16.9 wt % pent) relative to the other pyrrhotite samples investigated (6.61 – 8.21 wt % pent). Since galvanic interactions are most effective when the anodic and cathodic minerals are in contact with one another, the pyrrhotite samples with the lowest degree of pentlandite liberation would be expected to experience the strongest galvanic interaction. Phoenix magnetic pyrrhotite showed the lowest pentlandite liberation (48.5 % liberated particles) relative to the other pyrrhotite samples examined (53.6 -89.3 % liberated particles) due to the abundant locked flame pentlandite. However, the results of the pyrrhotite reactivity tests did not give any conclusive indication that the reactivity of the Phoenix pyrrhotite was significantly increased due to galvanic interactions with pentlandite. The most reactive pyrrhotite sample was the Sudbury Gertrude West pyrrhotite for which the pentlandite was 77.1 % liberated. Therefore, these results are argued to show negligible influence of galvanic effects on the reactivity of pyrrhotite. This does not necessarily mean that the flotation performance could not be adversely affected by a galvanic interaction between pentlandite and pyrrhotite. This will be further investigated in Section 7.5.

## 7.5 Effect of Mineralogy on Pyrrhotite Flotation Performance

The aim of this section is to answer the fourth key question, "*How does the flotation performance of magnetic and non-magnetic pyrrhotite differ and can these differences be accounted for by the crystallography, mineral chemistry and mineral association of pyrrhotite?*" In order to do this, the results from the microflotation tests in Chapter 6 are first reviewed and discussed in order to understand the interactions of the pyrrhotite surface with the flotation reagents. Only once these results have been interpreted, can any attempt be made to develop the relationship between pyrrhotite mineralogy and flotation performance.

As described in Section 2.4.2, some mild oxidation is required for the collectorless flotation of pyrrhotite. A variety of species varying between elemental sulfur, polysulfides, metal deficient sulfides to a stable $Fe(OH)S_2$ intermediate species have all been proposed to provide the necessary hydrophobicity for the collectorless flotation of pyrrhotite (Hamilton and Woods, 1981; Heyes and Trahar, 1984; Hodgson and Agar, 1984; Buckley and Woods, 1985; Legrand *et al.*, 2005a). However, extensive oxidation is well known to be detrimental to the flotation performance of pyrrhotite due to the formation of hydrophilic ferric hydroxide species (e.g. Rao and Finch, 1991; Kelebek, 1993). Although ferric hydroxide species were not actively identified on the surface of pyrrhotite during the flotation tests in this study, their presence is inferred as the reason for poor pyrrhotite flotation. Therefore, the interpretation of the flotation results needs to account for the balance between mild and severe oxidation that causes differences in pyrrhotite floatability with the propensity of the different pyrrhotite samples for oxidation i.e. their reactivity.

The degree of collectorless flotation was generally very low for all the pyrrhotite samples in this study other than the non-magnetic Sudbury CCN pyrrhotite sample. This suggests that the degree of oxidation experienced by the Sudbury CCN pyrrhotite was just mild enough to cause the production of hydrophobic species such as elemental sulfur or polysulfides. This agrees with the results of the mineral reactivity tests that showed the non-magnetic Sudbury CCN pyrrhotite was the most unreactive of the samples examined. In contrast, more extensive oxidation probably occurred for the magnetic and non-magnetic pyrrhotite due to their increased reactivity (Section 7.4), resulting in the formation of hydrophilic ferric hydroxides species that prevented the particles from being recovered during flotation. Since the

collectorless flotation of the magnetic and mixed pyrrhotite samples was so poor, no significant differences were observed between the samples that were related to their mineralogy. Similarly, since the collectorless flotation was so poor for the magnetic and mixed pyrrhotite samples, no significant differences were observed that were related to pH. Only the non-magnetic Sudbury CCN pyrrhotite showed a decrease in its collectorless floatability that could be attributed to the increase in electrochemical reaction rates and increase in the amount of hydrophilic ferric hydroxides at the greater hydroxide ion concentration (pH 10).

The floatability of all the pyrrhotite samples was significantly improved with the addition of xanthate collector. This is attributed to collector adsorption on the pyrrhotite surface followed by oxidation and formation of the dixanthogen species ($MX_2$) which is known to render pyrrhotite its hydrophobicity during flotation (Allison *et al.*, 1972; Fornasiero *et al.*, 1995; Bozkurt *et al.*, 1998). Kelebek (1993) suggested that mild oxidation of the pyrrhotite surface promoted the amount of surface sites available for xanthate adsorption, the production of elemental sulfur and the oxidation of xanthate to dixanthogen. Extensive oxidation however, would have shifted the balance so that the layer of hydrophilic ferric hydroxides covering the surface of the pyrrhotite would have been too thick to allow for sufficient xanthate adsorption. Therefore differences in the floatability of the different pyrrhotite samples with collector addition are interpreted to be influenced by the reactivity of pyrrhotite for oxidation.

With the addition of collector, non-magnetic Sudbury CCN pyrrhotite was still one of the most floatable pyrrhotites of the samples investigated at both pH 7 and 10, although a reduction in floatability was observed at the higher pH. This is once again attributed to the increase in concentration of ferric hydroxides at pH 10 and is in agreement with the Barsky relationship where $[X^-]/[OH^-] = K$ (Kelebek *et al.*, 2007). Differences in the floatability of the magnetic and mixed magnetic and non-magnetic pyrrhotite samples also became more evident. The magnetic Sudbury Gertrude and Gertrude West pyrrhotite samples showed the poorest flotation recovery of all the pyrrhotite samples. This was interpreted to be the result of severe oxidation of the Gertrude and Gertrude West pyrrhotite samples due to their very reactive nature (Section 7.4). It suggests that the surface of the pyrrhotite was already passivated and covered with hydrophilic ferric hydroxides prior to the addition of collector so that no interaction between the reagent and the pyrrhotite surface was possible.

The microflotation studies showed that the floatability of the Phoenix magnetic pyrrhotite was considerably better than the magnetic Sudbury Gertrude and Gertrude West pyrrhotite samples in the presence of a collector. This suggests that oxidation of the magnetic Phoenix pyrrhotite samples was less intense than the Gertrude and Gertrude West pyrrhotite so that some interaction between the pyrrhotite surface with xanthate was possible. At pH 7, the microflotation recovery of the Phoenix magnetic pyrrhotite in the presence of collector was virtually equal to the non-magnetic Sudbury CCN pyrrhotite. At pH 10, however the reactive nature of the Phoenix pyrrhotite was significantly increased due to the increase in pH, so that interaction with the collector was inhibited and its flotation performance was poor. A similar argument is able to account for the good flotation performance of the Nkomati MSB mixed pyrrhotite at pH 7 and the poor flotation performance at pH 10 in the presence of a collector.

The microflotation recovery of the different pyrrhotite samples was also greater for the longer chain length SIBX collector than the shorter chain length SNPX collector. Longer chain length xanthate collectors are known to have lower solubility products in water and therefore are more hydrophobic (M.C. Fuerstenau, 1982). This increase in hydrophobicity with the longer chain length SIBX collector was therefore attributed for the improved flotation performance of pyrrhotite with SIBX. An additional mechanism that could account for the lower recovery of pyrrhotite using the shorter chain length SNPX collector is related to the xanthate oxidation rate. The lower oxidation rate of the shorter chain length SNPX relative to SIBX (Section 5.5; Harris and Finkelstein, 1977) could also allow for more extensive oxidation of pyrrhotite thereby increasing the concentration of ferric hydroxides and impairing its floatability.

The effect of copper activation on the flotation recovery of the different pyrrhotite samples was mixed and showed a dependence on pyrrhotite mineralogy, pH and collector chain length. The inherent mechanism behind the improvement in pyrrhotite flotation performance with copper activation is through the adsorption of cupric copper onto the pyrrhotite surface and its rapid reduction to cuprous copper (Section 2.4.4). Following xanthate addition to the system, a hydrophobic copper - xanthate - hydroxide species most likely formed which rendered the pyrrhotite hydrophobic. The exact nature of this species is unknown and remains the subject of debate in the literature (e.g. Chandra and Gerson, 2009). It has also been shown that oxidation of the pyrrhotite surface prior to copper addition negatively interferes with the copper activation mechanism (Gerson and Jasieniak, 2008).

At pH 7, all of the pyrrhotite samples other than the Nkomati MSB mixed pyrrhotite showed some improvement in flotation performance due to copper activation. Even the magnetic Sudbury Gertrude and Gertrude West pyrrhotite samples showed some improvement in flotation performance even though they are considered to have been the most oxidised. Only the Nkomati MSB mixed pyrrhotite showed negligible improvement in flotation performance with copper addition, which was probably due to the fact that its flotation performance with collector at pH 7 was already excellent.

At pH 10 however, only the non-magnetic Sudbury CCN and Phoenix magnetic pyrrhotite samples showed a distinct improvement in flotation performance at pH 10 due to copper activation in conjunction with SIBX or SNPX collector addition. The magnetic Sudbury Gertrude and Gertrude West and Nkomati MSB pyrrhotite samples showed a very minor improvement in flotation performance at pH 10 due to copper activation and only when in conjunction with the addition of the stronger SIBX collector. This suggests that at pH 10, the Gertrude, Gertrude West and Nkomati pyrrhotite samples were much more reactive due to the increase in pH, and the effect of prior surface oxidation was detrimental to copper activation.

The microflotation results for the tests with copper activation at pH 10 of the Phoenix magnetic and Nkomati mixed pyrrhotite however, were not consistent with what was expected based on the relative reactivity of these pyrrhotite samples. It was expected that the Phoenix magnetic pyrrhotite would have been negatively affected by oxidation and therefore copper activation during flotation would not have occurred. It is also unclear why copper activation was not significant in the flotation performance of the mixed Nkomati MSB pyrrhotite at pH 10. Given its excellent flotation performance at pH 7 and its relatively unreactive character towards oxidation, it was anticipated that the Nkomati pyrrhotite would have shown a significant improvement in flotation performance due to copper activation. This suggests that understanding copper activation on the different pyrrhotite samples is relatively complex.

The microflotation results are generally consistent with those from the mineral reactivity studies and show that pyrrhotite floatability is primarily controlled by the degree of oxidation of the pyrrhotite surface. In general, the unreactive non-magnetic pyrrhotite showed the best floatability. The flotation performance of magnetic pyrrhotite was variable according to its origin but in general, showed poorer flotation performance than non-magnetic pyrrhotite. The

flotation performance of mixed magnetic and non-magnetic pyrrhotite was in between magnetic and non-magnetic pyrrhotite. Therefore, the same factors that influence the propensity of the different pyrrhotite types for oxidation, must affect their flotation performance although not necessarily in the same manner. Consequently, the effect of crystallography, mineral chemistry and mineral association are reviewed again.

*Crystallography*

In Section 7.4, it was argued that magnetic pyrrhotite is more reactive towards oxidation than non-magnetic pyrrhotite due to the greater proportion of vacancies in its crystal structure that facilitate the oxidation reaction. Consequently, the increased oxidation of magnetic pyrrhotite and formation of hydrophilic ferric hydroxides is proposed to account for its poorer flotation performance relative to non-magnetic pyrrhotite. The results from this study are in agreement with the account of Iwasaki (1988) from Harada (1967; In Japanese), that "hexagonal" pyrrhotite was more floatable than monoclinic pyrrhotite when the sample was oxidised. Harada (1967) also noted that freshly ground monoclinic pyrrhotite was more floatable. Given the sample preparation procedure used in this study whereby microflotation studies were performed on a selected pyrrhotite size fraction which had been prepared in advance (Section 3.5), flotation of a freshly ground sample was not possible. The results from this study are in partial agreement with Kalahdoozan (1996), where it was found that "hexagonal" pyrrhotite was more floatable than monoclinic pyrrhotite at pH 10. At pH 7, however, monoclinic pyrrhotite was more floatable. In the study of M.F. He *et al.* (2008), it was shown that monoclinic pyrrhotite was more floatable through a range of pH conditions in the presence of xanthate collector. However, since M.F. He *et al.* (2008) used pyrrhotite derived from lead zinc ores in their flotation experiments, the influence of pyrrhotite origin may account for the differences in flotation performance.

Both the results of this study and the literature suggest that a relationship exists between pyrrhotite crystallography, degree of oxidation and copper activation during flotation (Kalahdoozan, 1996; Wiese *et al.*, 2005; Gerson and Jasieniak, 2008; M.F. He *et al.*, 2008). Gerson and Jasieniak (2008) clearly showed that preoxidation is detrimental to the efficiency of copper activation and that copper activation stabilised the surface of pyrrhotite from further oxidation. On the basis that magnetic pyrrhotite is more reactive to oxidation, it is expected to be more sensitive to copper activation. Yet, the results of this study have shown that any pyrrhotite sample with a magnetic pyrrhotite component (including mixed pyrrhotite) does

not necessarily behave according to what would be expected from its reactivity towards oxidation. For some pyrrhotite samples, such as the magnetic monoclinic Phoenix pyrrhotite, the effect of copper activation is very significant in improving its flotation performance. Results of flotation studies from the literature have suggested that monoclinic pyrrhotite is more "sensitive" to copper activation. Kalahdoozan (1996) showed that the effect of changes in collector concentration with copper activation were more significant to the flotation performance of monoclinic pyrrhotite than "hexagonal" pyrrhotite. M.F. He *et al.* (2008) showed greater improvement in the flotation performance of monoclinic pyrrhotite with copper activation at pH 10 than "hexagonal" pyrrhotite. Wiese *et al.* (2007) also showed the effect of copper activation on pyrrhotite flotation differed according to whether the pyrrhotite was derived from the Impala or Lonmin Merensky Reef mine. Figure 7.3 shows that copper activation caused minor improvement in the flotation performance of pyrrhotite derived from the Impala Platinum mine, whereas the improvement in flotation performance with copper activation on the Lonmin pyrrhotite was significant.

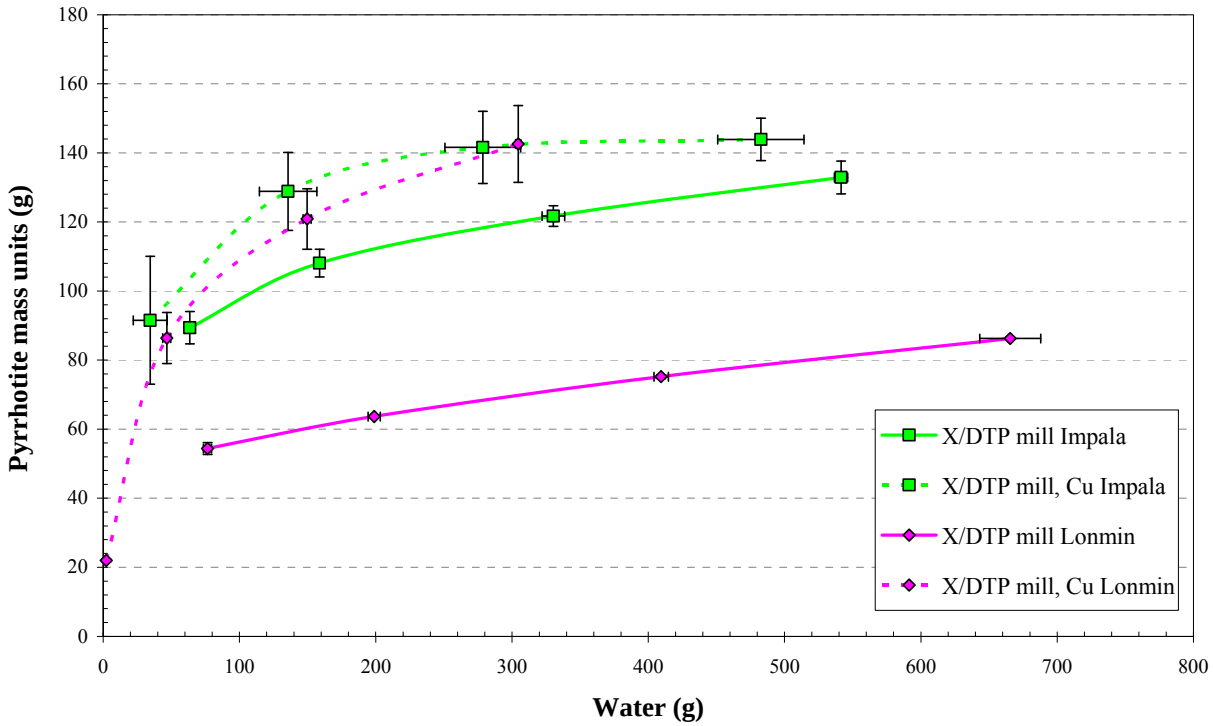


**Figure 7.3:** Comparison of the difference in calculated mass units of pyrrhotite recovered in batch flotation tests of Impala and Lonmin Merensky Reef ore for tests with and without copper activation. X represents xanthate and DTP, dithiophosphate. Adapted from Wiese *et al.* (2005) and Wiese (Unpublished data).

In order to determine whether there were significant mineralogical differences between the pyrrhotite from the two Merensky Reef ores, pyrrhotite concentrates from the flotation test results shown in figure 7.3 were prepared for mineralogical characterisation (J. Wiese, Pers. Comm. 2005). Mineral chemistry results of the different pyrrhotite samples analysed by Bushell (2005) have been reworked here, and are now presented in figure 7.4 as a histogram of metal to sulfur ratios. The entire pyrrhotite data set from this study is shown for reference in figure 7.4.

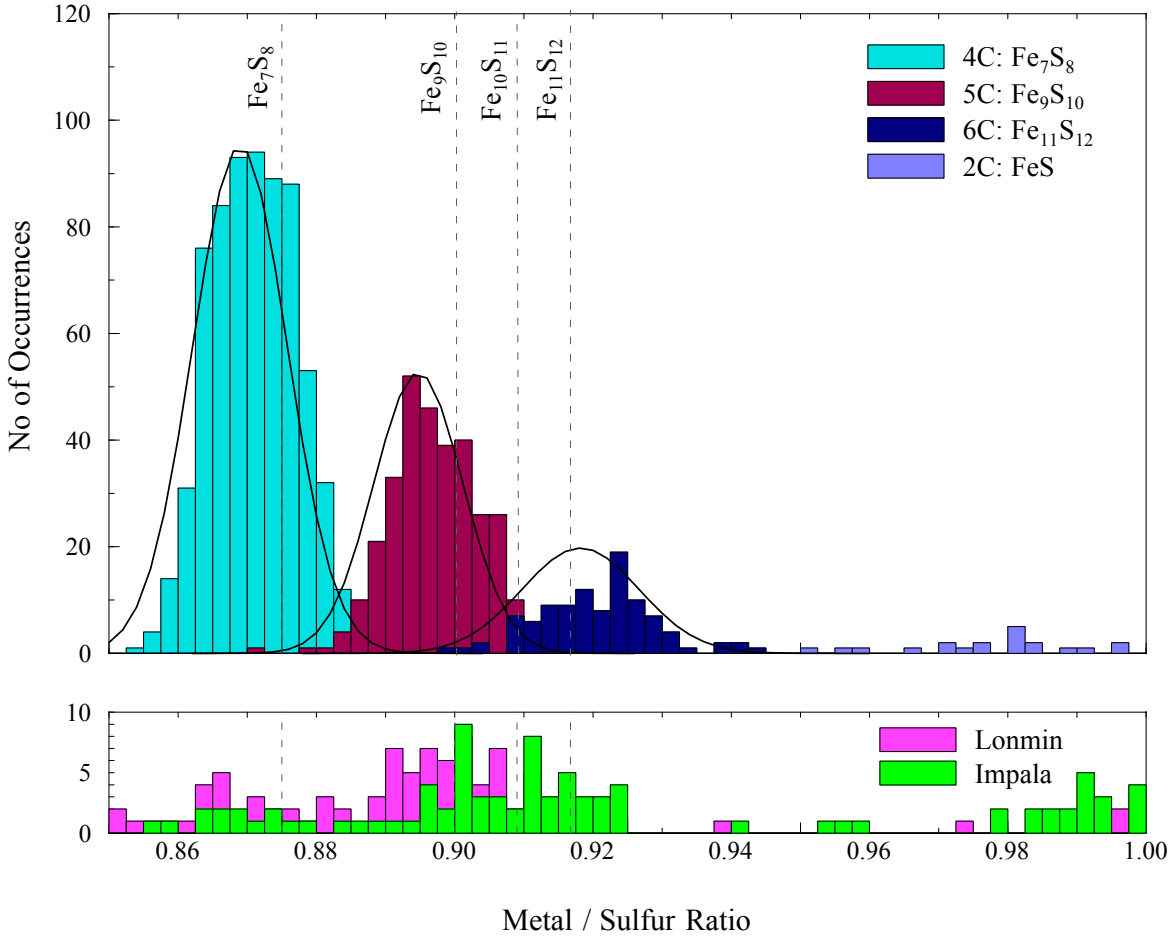


**Figure 7.4:** Comparison of the metal to sulfur ratio of pyrrhotite from batch flotation tests of Lonmin and Impala Merensky Reef pyrrhotite with pyrrhotite analyses from this study. Impala and Lonmin pyrrhotite metal to sulfur ratios were recalculated from Bushell (2005) based on pyrrhotite samples derived from batch flotation tests by Wiese *et al.* (2005) and Wiese (Unpublished data).

It is evident from figure 7.4 that the pyrrhotite population from both the Impala and Lonmin Merensky Reef mines is comprised of magnetic pyrrhotite ($Fe_7S_8$), non-magnetic pyrrhotite

(most likely $Fe_9S_{10}$) and troilite (FeS), although the abundance of each of these phases varies. Even though the pyrrhotite populations are relatively small, it is evident that a greater proportion of the pyrrhotite samples analysed from the Lonmin Merensky ore contained slightly lower metal / sulfur ratios than the Impala Merensky pyrrhotite. This suggests that there may be more magnetic pyrrhotite present in the Lonmin Merensky ore. The presence of a greater proportion of magnetic pyrrhotite in the Lonmin ore may account for its significant improvement in flotation performance with copper activation if magnetic pyrrhotite is more sensitive to copper activation. This effect could be enhanced if the magnetic pyrrhotite was secondary in origin and occurred as magnetic pyrrhotite rims surrounding non-magnetic pyrrhotite with which the copper could interact. If the magnetic pyrrhotite formed through hydrothermal alteration of "hexagonal pyrrhotite" (Desborough and Carpenter, 1965), the formation of magnetic pyrrhotite rims surrounding non-magnetic pyrrhotite may have occurred and which was previously described for Bushveld pyrrhotite by Liebenberg (1970).

These results suggest that magnetic pyrrhotite is more sensitive to copper activation but the underlying mechanism is considered to be complex. Some correlation to surface preoxidation probably does exist (Gerson and Jasieniak, 2008), but other mechanisms such as the role of pulp oxidation potential (He *et al.*, 2005), surface defect properties (e.g. Harris and Richter, 1985) or preferential copper adsorption on to particular crystallographic sites may well be important factors that need further investigation

*Mineral Chemistry*

As argued in Section 7.4, the presence of a greater proportion of ferric iron in the magnetic pyrrhotite structure likely increases the reactivity of magnetic pyrrhotite and particularly so since ferric iron is a stronger oxidising agent than oxygen. Consequently, the increased reactivity of magnetic pyrrhotite relative to non-magnetic pyrrhotite results in the increased formation of hydrophilic iron hydroxides that impair its floatability. Similarly, the presence of oxygen within the pyrrhotite structure could also be an oxidising agent to pyrrhotite. This might account for the differences in the reactivity and flotation performance between the different magnetic pyrrhotite samples (Phoenix, Sudbury Gertrude and Gertrude West). An additional mechanism that could account for the differences in the flotation response of the magnetic Phoenix and magnetic Sudbury Gertrude and Gertrude West pyrrhotite samples is the concentration of solid solution nickel. The creation of a positive effective charge in the vicinity of these sites of substitution would likely retard the oxidation (Section 7.4) and

formation of ferric hydroxide species on the pyrrhotite surface, thereby reducing its floatability. This is consistent with the flotation results obtained by Chanturia *et al.* (2004) where the floatability of iron rich, cobalt rich and nickel rich pentlandite was investigated. Chanturia *et al.* (2004) found that nickel rich and cobalt rich pentlandite were more floatable than iron rich pentlandite, which they suggested was due to differences in open circuit potential and the preferential formation of hydrophobic species on the nickel rich pentlandite.

*Mineral Association*

Given the importance of the association between magnetic and non-magnetic pyrrhotite occurring as intergrowths with one another in terms of the general occurrence of pyrrhotite (Arnold, 1967), so their effect on flotation performance is of interest. The microflotation results of the Nkomati MSB mixed magnetic and non-magnetic pyrrhotite was similar to the non-magnetic Sudbury CCN and magnetic Phoenix pyrrhotite samples at pH 7 in the presence of collector and copper activation. This suggests that similarly to its mineral reactivity, the floatability of the Nkomati mixed pyrrhotite was governed by the floatability of the intergrown magnetic and non-magnetic pyrrhotite phases. At pH 10 however, the decrease in the flotation performance of the Nkomati pyrrhotite was most likely due the stronger influence of the floatability of the magnetic pyrrhotite component that was adversely affected by the increase in hydroxide concentration.

The mineral association between pyrrhotite and pentlandite may also be important with respect to the possibility of galvanic interactions and particularly so for composite particles. The results from the reactivity studies however, gave no conclusive indication that the reactivity of pyrrhotite was adversely affected by a galvanic interaction with pentlandite (Chapter 5, Section 7.4). Galvanic interaction between pyrrhotite and pentlandite is expected to be detrimental to pyrrhotite flotation since pentlandite is the more noble of the two minerals. The addition of xanthate to the system may be of further detriment to pyrrhotite flotation since the anodic oxidation of xanthate to dixanthogen preferentially occurs on pentlandite (Bozkurt *et al.*, 1998). S.H. He *et al.* (2008) proposed a galvanic interaction as one of the mechanisms to account for the difference in pentlandite flotation between the magnetic and non-magnetic streams at the Clarabelle Mill in Sudbury. Due to the greater concentration of pyrrhotite in the magnetic stream, it was proposed that a galvanic interaction would cause the preferential oxidation of pyrrhotite relative to pentlandite, causing the improved pentlandite recovery noted. In this study, it is only really applicable to investigate the effect of

galvanic interactions between pyrrhotite samples which are similar in magnetic character. Due to the greater proportion of flame pentlandite and lower pentlandite liberation in the Phoenix magnetic pyrrhotite sample relative to the Sudbury Gertrude and Gertrude West pyrrhotite samples, it would be expected that if a galvanic interaction was significant, the floatability of the Phoenix magnetic pyrrhotite would be more adversely affected. However, the results of the microflotation studies showed that the presence of pentlandite enhanced the floatability of the Phoenix pyrrhotite sample. Consequently an additional mechanism needs to be investigated.

Various studies have described how the flotation rate of pyrrhotite is slower than pentlandite (e.g. Buswell and Nicol, 2002; Miller *et al.*, 2005). On the basis that pentlandite is more floatable than pyrrhotite, a mechanism for the flotation of composite pyrrhotite and pentlandite particles is proposed. This mechanism would be directly applicable to account for the improved floatability of pyrrhotite samples containing abundant locked flame pentlandite. It is proposed that preferential collector adsorption and bubble – particle attachment occurs at sites where unliberated pentlandite is partially exposed on the surface of the composite particle. Therefore, the recovery of pyrrhotite during flotation would be by virtue of its association to pentlandite. This mechanism of composite particle flotation would be relevant to the Phoenix magnetic pyrrhotite and the Nkomati MSB mixed pyrrhotite. It provides an additional mechanism to account for the differences in floatability between the magnetic Phoenix and Sudbury Gertrude and Gertrude West pyrrhotite samples. It may be an additional explanation to account for the difference in flotation performance of the Phoenix magnetic pyrrhotite relative to the Nkomati MSB mixed pyrrhotite at pH 10. Given that the liberation of pentlandite in the Nkomati mixed pyrrhotite sample is slightly greater than the Phoenix magnetic pyrrhotite, the composite particle flotation would not be as strong for the Nkomati pyrrhotite and therefore its flotation recovery with collector addition was poor. Since copper activation is known not to have any influence on pentlandite flotation (Senior *et al.*, 1995; Wiese *et al.*, 2007), the effect of pentlandite activation by copper in improving the flotation of pyrrhotite can be ruled out as a mechanism influencing the success of copper activation of pyrrhotite.

Another mechanism related to the presence of pentlandite associated with pyrrhotite is that caused by the release of nickel ions from pentlandite and inadvertent activation of pyrrhotite. The inadvertent activation of pyrrhotite from nickel ions has previously been described for the

Sudbury ores by Yoon *et al.* (1995) and Xu and Wilson (2000). It is possible that the flotation performance of those pyrrhotite samples containing significant locked flame pentlandite would be improved due to inadvertent activation by nickel ions associated with the flame pentlandite. This provides yet another mechanism that may account for the differences in the flotation performance of the Phoenix magnetic pyrrhotite to the Sudbury Gertrude and Gertrude West pyrrhotite samples.

## 7.6 Implications of this Study

As described in Chapter 1, the aim of this study was to develop the relationship between pyrrhotite mineralogy and flotation performance. The motivation behind this research was that mineral processing operations treating pyrrhotite need to manipulate pyrrhotite flotation performance. This is in accordance to whether pyrrhotite needs to be actively recovered due to its association with the platinum group elements and minerals (e.g. Merensky Reef, South Africa) or rejected in order to control circuit throughput and concentrate grade and thereby reduce excess sulfur dioxide smelter emissions (e.g. Sudbury, Canada).

The results of this study have shown that good flotation performance was achieved by the non-magnetic pyrrhotite and suggests that the recovery of this type of pyrrhotite should not be problematic for processing operations targeting pyrrhotite flotation recovery. In contrast, the recovery of the reactive magnetic pyrrhotite is likely to be more problematic. In order to optimise the recovery of magnetic pyrrhotite, the effect of surface oxidation and copper activation need to be more clearly understood. Investigation of mechanisms to prevent the extensive oxidation and formation of hydrophilic ferric hydroxide species on the surface of magnetic pyrrhotite that impair its floatability is needed. Similarly, investigation of the properties that influence the success of copper activation on magnetic pyrrhotite is needed in order to optimise the flotation of this pyrrhotite phase.

The results of this study have shown that the poorest flotation performance was achieved by the most reactive pyrrhotite sample towards oxidation. Therefore, for processing operations targeting pyrrhotite rejection during flotation, the role of oxidation is of particular interest. Although the use of oxygen as a pyrrhotite depressant has previously been evaluated (e.g. Kelebek, 1993), it does not appear to have been implemented in flotation operations where DETA or TETA in conjunction with sodium metabisulfite is the favoured pyrrhotite depressant (Lawson *et al*., 2005). This is probably due to the large amount of space required to actively oxidise pyrrhotite in terms of conditioning tanks, and that too much oxidation would be detrimental to pentlandite recovery. Given the unreactive nature of non-magnetic pyrrhotite this would not be advised. The results from this study suggest that it should not be too difficult to actively oxidise very reactive magnetic pyrrhotite, and perhaps the use of oxidation should be reevaluated as a depressant for these reactive pyrrhotite types. An additional benefit of using oxygen as a pyrrhotite depressant is that it is not only relatively

inexpensive but is also environmentally friendly. Since pyrrhotite flotation performance was also heavily influenced by the presence of locked flame pentlandite, a change in the grind size and liberation characteristics of pyrrhotite and pentlandite should also be evaluated as a mechanism to assist in manipulating pyrrhotite flotation performance.

Finally, the importance of process mineralogy as a whole is to be able to better understand and optimise flotation performance. Although prediction of flotation performance is not necessarily possible from the results of this study, the results do provide a means to understand and optimise pyrrhotite flotation performance. Simple measurements of well controlled experiments that have been of the most use in this study and that can be readily repeated are those which determine pyrrhotite identity, the identity and relative proportions of minerals in the sample and the oxygen uptake of the mineral slurry. Pyrrhotite identity can easily be determined with the use of hand magnet (magnetic versus non-magnetic), optical microscopy with the magnetic colloid method (magnetic versus non-magnetic) or powder XRD (monoclinic versus orthorhombic). Depending on the nature of the sample and the analyst, the identity and relative proportions of the minerals in the sample can similarly be determined with the use of optical microscopy, powder XRD or automated SEM techniques (QEMSCAN, MLA). Oxygen uptake measurements have also been of benefit and are simple to carry out given that only a dissolved oxygen probe and TPS meter are required. However, these measurements need to be interpreted with care, especially if the pyrrhotite is so reactive that it is readily passivated.

# Chapter 8

# CONCLUSIONS AND RECOMMENDATIONS

---

## 8.1 Conclusions

The aim of this thesis was to develop the relationship between pyrrhotite mineralogy and flotation performance based on a thorough characterisation of pyrrhotite from selected nickel and platinum group element ore deposit in terms of their mineralogy and mineral reactivity. It is considered that the aim of this thesis has been addressed since a clearer understanding of this relationship now exists. This thesis has shown what the critical parameters are that influence pyrrhotite reactivity and hence flotation performance. Various mechanisms to account for the differences in pyrrhotite reactivity and flotation performance have been proposed.

Based upon the examination of the mineral association, crystallography and mineral chemistry of pyrrhotite, the variation in mineralogy between magnetic and non-magnetic pyrrhotite was described by the proposed classification scheme:

i). *Two phase pyrrhotite:* Non-magnetic 6C $Fe_{11}S_{12}$ pyrrhotite intergrown with 2C FeS troilite (Impala Merensky sample *IMP-2*).

(ii). *Single phase pyrrhotite:* Non-magnetic 5C $Fe_9S_{10}$ pyrrhotite (Sudbury CCN).

(iii). *Two phase pyrrhotite:* Magnetic 4C $Fe_7S_8$ intergrown with non-magnetic pyrrhotite 5C $Fe_9S_{10}$ (Nkomati MSB, Nkomati MMZ sample *MMZ-4*)

(iv). *Single phase pyrrhotite*: Magnetic 4C $Fe_7S_8$ pyrrhotite (Impala Merensky sample *IMP-1*, Nkomati MMZ sample *MMZ-1*, Phoenix, Sudbury Gertrude and Gertrude West).

Single crystal analysis of the magnetic Impala Merensky sample *IMP-1* and Phoenix pyrrhotite samples confirmed they were monoclinic. Single crystal analysis of the non-magnetic Sudbury CCN pyrrhotite proved that 5C $Fe_9S_{10}$ pyrrhotite was actually

orthorhombic in contrast to its commonly accepted crystallography as “hexagonal” pyrrhotite. Using the unique mineral chemistry dataset derived in this research, it was shown that the average atomic metal / sulfur ratios obtained for magnetic 4C $Fe_7S_8$ was 0.869 ± 0.013 (n = 699), for non-magnetic 5C $Fe_9S_{10}$ was 0.895 ± 0.013 (n = 316) and for non-magnetic 6C $Fe_{11}S_{12}$ was 0.918 ± 0.017 (n = 101). The histogram comparing metal / sulfur ratios of all the pyrrhotite samples analysed showed a continuum of metal / sulfur ratios for each of the pyrrhotite superstructures. Some minor overlap in composition between pyrrhotite superstructures was observed and determined to be statistically significant. These features were interpreted to be representative of non-stoichiometry in the pyrrhotite mineral structure.

Based upon the examination of the mineral association, crystallography and mineral chemistry of pyrrhotite, it was argued that these features were primarily controlled by ore deposit formation. It was argued that the pyrrhotite superstructure and composition; intergrowth textures between magnetic and non-magnetic pyrrhotite, non-magnetic pyrrhotite and troilite, pyrrhotite and pentlandite; and the relative abundance of each sulfide phase, were influenced by the bulk composition and cooling history of the monosulfide solid solution (MSS) from which the pyrrhotite crystallised. Additional attributes of pyrrhotite mineralogy that were inferred to be important were the presence of oxygen during the crystallisation of the MSS (as evidenced by the presence of magnetite) and hydrothermal alteration of non-magnetic pyrrhotite to magnetic pyrrhotite (as evidenced by descriptions of magnetic pyrrhotite rims surrounding non-magnetic pyrrhotite in the literature).

Using open circuit potential, cyclic voltammetry and oxygen uptake measurements the reactivity of magnetic and non-magnetic pyrrhotite was investigated at pH 7 and 10. Non-magnetic Sudbury CCN pyrrhotite was the most unreactive of the pyrrhotite samples investigated, whereas magnetic pyrrhotite was considerably more reactive. Magnetic Sudbury Gertrude West was interpreted to be so reactive that the surfaces were already oxidised and passivated at the time of the oxygen uptake measurement, whereas the reactivity of Phoenix magnetic pyrrhotite was not as extreme. The reactivity of the Nkomati MSB pyrrhotite was in between non-magnetic Sudbury CCN and magnetic Phoenix due to the combined contribution of intergrown magnetic and non-magnetic pyrrhotite. Addition of flotation reagents to the pyrrhotite slurry caused a decrease in the reactivity of the pyrrhotite samples that was attributed to the formation of an adsorbed surface layer that protected the pyrrhotite from further oxidation.

Based upon carefully controlled microflotation studies of pyrrhotite under selected conditions, the flotation performance of magnetic and non-magnetic pyrrhotite was investigated at pH 7 and 10. Differences in the flotation performance of the different pyrrhotite samples were primarily attributed to their relative reactivity towards oxidation and formation of hydrophilic ferric hydroxides on the surface of pyrrhotite particles. Where pyrrhotite oxidation was more severe, it appeared that any interaction of the flotation reagents (SIBX, SNPX or copper sulfate) with the pyrrhotite surface was not possible as evidenced by the poor flotation performance of these pyrrhotite samples, especially at the higher pH. The non-magnetic Sudbury CCN pyrrhotite was the most floatable of the samples examined, whereas the magnetic Sudbury Gertrude and Gertrude West pyrrhotite samples showed the poorest flotation performance. Phoenix magnetic pyrrhotite also showed good flotation performance, whereas the flotation performance of the Nkomati MSB mixed pyrrhotite was only good at pH 7.

The key mineralogical characteristics of pyrrhotite that were interpreted to affect its reactivity and flotation performance were crystallography, mineral chemistry and mineral association. On the basis that magnetic pyrrhotite has more vacancies in its crystal structure than non-magnetic pyrrhotite (1 in 8 iron sites versus 1 in 10 iron sites), it was proposed that the presence of these vacancies facilitates the oxidation reaction and accounts for the increased reactivity of magnetic pyrrhotite. The greater proportion of ferric iron in the magnetic pyrrhotite structure relative to the non-magnetic pyrrhotite ($2Fe^{3+}$ out of 7 cations versus $2Fe^{3+}$ out of 9 cations) was also argued to act as a stronger oxidising agent for magnetic pyrrhotite and accounts for its increased reactivity. Differences in the reactivity and flotation performance between magnetic pyrrhotite samples were postulated to be linked to the solid solution nickel content and its effect on positive effective charge that would likely retard pyrrhotite oxidation. Although not measured in this study, the influence of trace amounts of oxygen in the pyrrhotite structure could also influence the reactivity of magnetic pyrrhotite. Given the association of pyrrhotite with magnetite, it is known that $fO_2$ is important during crystallisation and cooling of the MSS and therefore it is not unlikely that some trace amount of oxygen may have been accommodated in the pyrrhotite crystal structure. The association of pyrrhotite with pentlandite was very important since pyrrhotite flotation could be positively influenced by the flotation of composite particles comprised of abundant locked flame pentlandite. Nickel ions derived from the locked flame pentlandite could also assist in the activation of pyrrhotite and further improve its flotation performance. The mineral association

between pyrrhotite types was noted to be important since the reactivity and flotation performance of mixed pyrrhotite was likely controlled by the contribution of the intergrown magnetic and non-magnetic pyrrhotite components.

This study has also shown the usefulness of process mineralogy as a field of research in aiding the understanding of pyrrhotite flotation performance. Although the process mineralogy measurements performed here cannot necessarily predict flotation performance, they can assist in the understanding and potential optimisation of pyrrhotite flotation performance according to whether the recovery or rejection of pyrrhotite is targeted. Simple mineralogical and mineral reactivity measurements which have been of the most use in developing this relationship between mineralogy and flotation performance include the identification of pyrrhotite type (magnetic versus non-magnetic), determination of the relative proportions of minerals in a sample and investigation of the oxygen uptake.

## 8.2 Recommendations

In light of the findings of this thesis, several recommendations for future research are made below:

- Quantitative analysis of platinum group elements in pyrrhotite with laser ablation ICP-MS or PIXE methods using synthetic sulfide standards doped with the platinum group elements in order to determine whether there is a relationship between pyrrhotite type and PGE content.

- Further sampling of pyrrhotite from the Merensky Reef to comprehensively explore the compositional variation of pyrrhotite in this ore deposit, and confirm the presence of intergrown magnetic and non-magnetic pyrrhotite phases that was not encountered in the samples examined in this study.

- Single crystal analysis of a 6C $Fe_{11}S_{12}$ pyrrhotite crystal in order to determine and solve its crystal structure. With the addition of the 6C crystal structure to the pyrrhotite crystal structure database, naturally occurring 4C, 5C and 6C pyrrhotite structures would be available for quantitative powder XRD using Rietveld refinement.

- Validation of the pyrrhotite mapping procedure using EBSD and further QEMSCAN or MLA analysis methods to establish a procedure which can routinely be used for mineralogical analysis of metallurgical samples.

- The use of nuclear microprobe techniques to measure oxygen in magnetic and non-magnetic pyrrhotite samples and determine whether a correlation between oxygen content and reactivity exists.

- The use of EDTA, pH and Eh measurements in conjunction with oxygen uptake studies on pyrrhotite samples may provide further insight into pyrrhotite oxidation. The use of ToF-SIMS would also be of interest to confirm differences in the extent of oxidation of pyrrhotite samples examined in this study.

- Further electrochemical measurements such as cyclic voltammetry or electrical impedance spectroscopy to evaluate the interactions of the different pyrrhotite samples with flotation reagents. The assignment of the appropriate equations to the various REDOX reaction is also necessary.

- Further electrochemical and flotation studies to examine the effect of the galvanic interaction on pentlandite flotation performance.

- Further investigation into the mechanism of copper activation on pyrrhotite and the factors that influence its success, particularly for magnetic pyrrhotite.

- Laboratory scale batch flotation tests on pyrrhotite samples in order confirm the results of this study and determine the influence of additional variables such as the effect of grinding media, silicate mineralogy and presence of a froth phase on pyrrhotite flotation. Subsequent MLA or QEMSCAN analysis of metallurgical samples would also be beneficial.

- Key ideas from this research should be extended to the application of pyrrhotite flotation in other nickel deposits (e.g. Noris'lk Talnakh, Russia) and lead zinc type ore deposits in order to determine whether the same mineralogical factors also influence pyrrhotite flotation.

- Key ideas from this research should be extended into the field of acid mine drainage research in order to determine whether pyrrhotite mineralogy is a controlling factor in acid producing potential.

# Chapter 9

## REFERENCES

Adam K., Iwasaki I. 1984. Grinding media-sulfide mineral interaction and its effect on flotation. In: PR Richardson, SS Srinivasan and R Woods (eds.) *Electrochemistry in Mineral and Metal Processing*. pp. 66-80. (ECS: Pennington, NJ, USA).

Adkins S.J., Pearse M.J. 1992. The influences of collector chemistry on kinetics and selectivity in base-metal sulphide flotation. *Minerals Engineering* 5: 295-310.

African Oxygen Limited (Afrox). 2008. *RN in Flotation*. Patent: 2008/09676. South Africa.

Allison S.A., Goold L.A., Nicol M.J., Granville A. 1972. A determination of the products of reaction between various sulfide minerals and aqueous xanthate solution, and a correlation of the products with electrode rest potentials. *Metallurgical Transactions* 3: 2513-2618.

Almeida C.M.V.B., Giannetti B.F. 2003. The electrochemical behaviour of pyrite-pyrrhotite mixtures. *Journal of Electroanalytical Chemistry* 553: 27-34.

Arnold R.G. 1967. Range in composition and structure of 82 natural terrestrial pyrrhotites. *Canadian Mineralogist*: 31-50.

Arnold R.G., Reichen L.E. 1962. Measurement of the metal content of naturally occurring, metal-deficient, hexagonal pyrrhotite by an x-ray spacing method. *American Mineralogist* 47: 105-111.

Ballhaus C., Sylvester P.J. 2000. Noble metal enrichment processes in the Merensky Reef, Bushveld Complex. *Journal of Petrology* 41: 545-561.

Ballhaus C., Ulmer P. 1995. Platinum-group elements in the Merensky Reef: II. Experimental solubilities of platinum and palladium in $Fe_{1-x}S$ from 950 to 450$^0$C under controlled $fS_2$ and $fH_2$. *Geochimica et Cosmochimica Acta* 59: 4881-4888.

Batt A.P. 1972. Nickel distribution in hexagonal and monoclinic pyrrhotite. *Canadian Mineralogist* 11: 892-897.

Baum W., Lotter N.O., Whittaker P.J. 2006. Process Mineralogy - A new generation for ore characterisation and plant optimization. Paper presented at *SME Annual Meeting*, Colorado.

Becker M., Mainza A.M., Powell M.S., Bradshaw D.J., Knopjes B. 2008. Quantifying the influence of classification with the 3-product cyclone on liberation and recovery of PGMs in UG2 ore. *Minerals Engineering* 21: 549-558.

Becker M., Kitenge J.K., Bradshaw D.J. 2005. *The relationship between Reactivity Number™ and flotation for a pyrrhotite rich ore*. University of Cape Town, Cape Town.

Belzile N., Chen Y.-W., Cai M.-F., Li Y. 2004. A review of pyrrhotite oxidation. *Journal of Geochemical Exploration* 84: 65-76.

Bertaut P.E.F. 1953. Contribution a l'Etude des Structures Lacunaires: La pyrrhotine. *Acta Crystallographica* 6: 557-561.

Bitter F. 1932. Experiments on the nature of ferromagnetism. *Physical Review* 41: 507-515.

Bojcevski D., Vink L., Johnson N.W., Landmark V., Johnston M., Mackenzie J., Young M.F. 1998. Metallurgical characterization of George Fisher ore textures and implications for Mineral Processing. In: *Mine to Mill*. pp. 29-41. (AusIMM: Brisbane).

Botha P.W.S.K., Butcher A.R. 2008. *Mapping of magnetic and non-magnetic pyrrhotite using novel QEMSCAN® backscattered electron brightness contrast settings*. Intellection, Brisbane.

Bozkurt V., Xu Z., Finch J.A. 1998. Pentlandite / pyrrhotite interaction and xanthate adsorption. *International Journal of Mineral Processing* 52: 203-214.

Brady J.B. 1987. Coarsening of fine-scale exsolution lamellae. *American Mineralogist* 72: 697-706.

Bradshaw D.J., O'Connor C.T. 1996. Measurement of the sub-process of bubble loading in flotation. *Minerals Engineering* 9: 443-448.

Brough C. 2008. An investigation into the process mineralogy of the Merensky Reef at Northam Platinum Limited. MSc thesis, University of Cape Town.

Brown M., Dinham P. 2006. Benchmark quality investigation on automated mineralogy: A discussion of some preliminary data. Paper presented at *MEI Automated Mineralogy 07*, Brisbane.

Buckley A.N., Woods R. 1985. X-ray photoelectron spectroscopy of oxidized pyrrhotite surfaces. 1 Exposure in air. *Applications of Surface Science* 22/23: 280-287.

Bullock E.S., Gounelle M., Lauretta D.S., Grady M.M., Russell S.S. 2005. Mineralogy and texture of Fe-Ni sulfides in CI1 chondrites: Clues to the extent of aqueous alteration on the CI1 parent body. *Geochimica et Cosmochimica Acta* 69: 2687-2700.

Burdukova E., Becker M., Ndlovu B., Mokgethi D., Deglon D. 2008. Relationship between slurry rheology and its mineralogical content. In: *24th International Mineral Processing Congress*. pp. 2169-2178. (Science Press: Beijing).

Bushell C. 2005. *Mineralogical characterisation of Merensky Reef pyrrhotite*. Mintek, Johannesburg.

Buswell A.M., Bradshaw D.J., Harris P.J., Ekmekci Z. 2002. The use of electrochemical measurements in the flotation of a platinum group minerals (PGM) bearing ore. *Minerals Engineering* 15: 395-404.

Buswell A.M., Nicol M.J. 2002. Some aspects of the electrochemistry of the flotation of pyrrhotite. *Journal of Applied Electrochemistry* 32: 1321-1329.

Cabri L.J., Rudashevsky N.S., Rudashevsky V.N. 2008. Current approaches for the process mineralogy of platinum group element ores and tailings. In: *9th International Congress for Applied Mineralogy*. pp. 9-17. (AusIMM: Brisbane).

Cabri L.J., Sylvester P.J., Tubrett M.N., Peregoedova A., LaFlamme J.H.G. 2003. Comparison of LAM-ICP-MS and micro-pixe results for palladium and rhodium in selected samples of Noril'sk and Talnakh sulfides. *Canadian Mineralogist* 41: 321-329.

Carpenter R.H., Bailey A.C. 1973. Application of Ro and Ar measurements to the study of pyrrhotite and troilite. *American Mineralogist* 58: 440-443.

Carpenter R.H., Desborough G.A. 1964. Range in solid solution and structure of naturally occurring troilite and pyrrhotite. *American Mineralogist* 49: 1350-1365.

Cawthorn R.G. 1999. The platinum and palladium resources of the Bushveld Complex. *South African Journal of Science* 95: 481-489.

Cawthorn R.G., Lee C.A., Schouwstra R.P., Mellowship P. 2002. Relationship between PGE and PGM in the Bushveld Complex. *Canadian Mineralogist* 40: 311-328.

Chandra A.P., Gerson A.R. 2009. A review of the fundamental studies of the copper activation mechanisms for selective flotation of the sulfide minerals, sphalerite and pyrite. *Advances in Colloid and Interface Science* 145: 97-110.

Chanturia V.A., Makarov V., Forsling W., Makarov D., Vasil'eva T., Trofimenko T., Kuznetsov V. 2004. The effect of crystallochemical peculiarities of nickel sulphide minerals on flotation of copper-nickel ore. *International Journal of Mineral Processing* 74: 289-301.

Charland A., Kormos L., Whittaker P., Arrue-Canales C., Fragomeni D., Lotter N., Mackey P., Anes J. 2006. A case study for integrated use of automated mineralogy in plant optimization: The Falconbridge Montcalm Concentrator. Paper presented at *MEI Automated Mineralogy*, Brisbane.

Cheng X., Iwasaki I., Smith K.A. 1994. An electrochemical study on cathodic decomposition behaviour of pyrrhotite in deoxygenated solutions. *Minerals and Metallurgical Processing* 11: 160-167.

Cheng X., Iwasaki I. 1992. Effect of chalcopyrite and pyrrhotite interaction on flotation separation. *Minerals and Metallurgical Processing* 9: 73-79.

Chirita P., Descostes M., Schlegel M.L. 2008. Oxidation of FeS by oxygen-bearing acidic solutions. *Journal of Colloid and Interface Science* 321: 84-95.

Clark A.H. 1966. Stability field of monoclinic pyrrhotite. *Transactions AIME* B232: 278-280.

Craig J.R., Vaughan D.J. 1981. *Ore microscopy and ore petrography*. John Wiley and Sons: New York.

Crockett J.H., Fleet M.E., Stone W.E. 1997. Implications of composition for experimental partitioning of platinum-group elements and gold between sulfide liquid and basalt melt: The significance of nickel content. *Geochimica et Cosmochimica Acta* 61: 4139-4149.

Cruz R., Gonzalez I., Monroy M. 2005. Electrochemical characterization of pyrrhotite reactivity under simulated weathering conditions. *Applied Geochemistry* 20: 109-121.

Desborough G.A., Carpenter R.H. 1965. Phase relations of pyrrhotite. *Economic Geology* 60: 1431-1450.

De Villiers J.P.R., Liles D., Becker M. In Prep. The crystal structure of a naturally occurring 4C pyrrhotite from the Merensky Reef, its chemistry and vacancy distribution.

De Villiers J.P.R., Liles D., Becker M. Submitted. The crystal structure of a naturally occurring 5C pyrrhotite from Sudbury, its chemistry and vacancy distribution. *American Mineralogist*.

De Villiers J.P.R., Verryn S. 2008. Modern x-ray diffraction methods for process optimization in the minerals industry - Case studies. In: *9th International Congress of Applied Mineralogy*. pp. 265-276. (AusIMM: Brisbane).

Eales H.V., Cawthorn R.G. 1996. The Bushveld Complex. In: RG Cawthorn (ed.) *Layered Intrusions*. pp. 181-229. (Elsevier: Amsterdam).

Ekmekci Z. 2008. *Electrochemistry in sulphide mineral flotation*. Electrochemistry Course Notes.

Ekmekci Z., Becker M., Bagki Tekes E., Bradshaw D.J. The relationship between pyrrhotite mineralogy and electrochemistry. Submitted for presentation at the *83rd ACS Colloid and Surface Science Symposium*, New York.

Ekmekci Z., Bradshaw D.J., Harris P.J., Aslan A., Hassoy H. 2003. The value and limitations of electrochemical measurements in sulphide mineral flotation. In: FM Doyle, GH Kelsall and R Woods (eds.) *Electrochemistry in Mineral and Metal Processing*. pp. 1-13. (ECS: Pennington, NJ, USA).

Ekmekci Z., Demirel H. 1997. Effects of galvanic interaction on collectorless flotation behaviour of chalcopyrite and pyrite. *International Journal of Mineral Processing* 52: 31-48.

Evans H.T. 1970. Lunar troilite: Crystallography. *Nature* 30: 621-623.

Fandrich R., Gu Y., Burrows D., Moeller K. 2007. Modern SEM-based mineral liberation analysis. *International Journal of Mineral Processing* 84: 310-320.

Farquhar J. 1986. The Western Platinum Mine. In: CR Annhaeusser and S Maske (eds.) *Mineral Deposits of Southern Africa*. pp. 1135-1142. (GSSA: Johannesburg).

Farrow C.E.G., Lightfoot P.C. 2002. Sudbury PGE revisited: Toward an integrated model. In: LJ Cabri (ed.) *The Geology, Geochemistry, Mineralogy and Mineral Beneficiation of the Platinum Group Elements*. pp. 273-297. (CIM: Montreal).

Finkelstein N.P. 1997. The activation of sulphide minerals for flotation: A review. *International Journal of Mineral Processing* 52: 81-120.

Fleet M.E. 1971. The crystal structure of a pyrrhotite ($Fe_7S_8$). *Acta Crystallographica* B27: 1864-1867.

Fleet M.E. 2006. Phase equilibria at high temperatures. In: DJ Vaughan (ed.) *Sulfide Mineralogy and Geochemistry*. pp. 365-419. (MSA: Washington DC, USA).

Fornasiero D., Montalti M., Ralston J. 1995. Kinetics of adsorption of ethyl xanthate on pyrrhotite: In-situ UV and infrared spectroscopic studies. *Journal of Colloid and Interface Science* 172: 467-478.

Francis C.A., Craig J.R. 1976. Pyrrhotite: the *n*A (or 2*A*, 3*C*) superstructure reviewed. *American Mineralogist* 61: 21-25.

Fuerstenau D.W. 1982. Activation in the flotation of sulphide minerals. In: RP King (ed.) *Principles of Flotation* pp. 183-198. (SAIMM: Johannesburg).

Fuerstenau M.C. 1982. Chemistry of collectors in solution. In: RP King (ed.) *Principles of Flotation*. pp. 1-16. (SAIMM: Johannesburg).

Gain S.B., Mostert A.B. 1982. The geological setting of the platinoid and base metal sulfide mineralization in the Platreef of the Bushveld Complex in Drenthe, North of Potgietersrus. *Economic Geology* 77: 1395-1404.

Gaudin A.M. 1939. *Principles of Mineral Dressing*. McGraw-Hill Book Company: New York.

Gauert C.D.K. 2001. Sulphide and oxide mineralisation in the Uitkomst Complex, South Africa: Origin in a magma conduit. *Journal of African Earth Sciences* 32: 149-161.

Gauert C.D.K., De Waal S.A., Wallmach T. 1995. Geology of the ultrabasic to basic Uitkomst complex, eastern Transvaal, South Africa: An overview. *Journal of African Earth Sciences* 21: 553-570.

Gerson A., Jasieniak M. 2008. The effect of surface oxidation on the Cu activation of pentlandite and pyrrhotite. In: *24th International Mineral Processing Congress*. pp. 1054-1063. (Science Press: Beijing).

Gottlieb P. 2008. The revolutionary impact of automated mineralogy on mining and mineral processing. In: *24th International Mineral Processing Congress*. pp. 165-174. (Science Press: Beijing).

Graham A.R. 1969. Quantitative determination of hexagonal and monoclinic pyrrhotites by x-ray diffraction. *Canadian Mineralogist* 10: 4-24.

Graham J., Bennett C.E.G., van Riessen A. 1987. Oxygen in Pyrrhotite: 1. Thermomagnetic behaviour and annealing of pyrrhotites containing small quantities of oxygen. *American Mineralogist* 72: 599-604.

Graham J., Mc Kenzie A.D. 1987. Oxygen in Pyrrhotite: 2. Determination of oxygen in natural pyrrhotites. *American Mineralogist* 72: 605-609.

Greet C.J., Brown S. 2000. Oxygen demand testing - A new laboratory procedure. Paper presented at *7th Mill Operators' Conference*, Kalgoorlie.

Greet C.J., Small G.L., Steiner P., Grano S. 2004. The Magotteaux Mill®: investigating the effect of grinding media on pulp chemistry and flotation performance. *Minerals Engineering* 17: 891-896.

Gu Y. 2003. Automated scanning electron microscope based mineral liberation analysis, an introduction to the JKMRC / FEI Mineral Liberation Analyser. *Journal of Minerals and Materials Characterization and Engineering* 2: 33-41.

Harada T. 1967. Variation in floatability of pyrrhotites. *Nippon Kogyo Kaishi* 83: 656-660.

Hamilton I.C., Woods R. 1981. An investigation of surface oxidation of pyrite and pyrrhotite by linear potential sweep voltammetry. *Journal of Electroanalytical Chemistry* 118: 327-343.

Hamilton I.C., Woods R. 1984. A voltammetric study of the surface oxidation of sulfide minerals. In: PR Richardson, SS Srinivasan and R Woods (eds.) *Electrochemistry in Mineral and Metal Processing*. pp. 259-302. (ECS: Pennington, N.J., USA).

Harris P.J., Finkelstein N.P. 1977. *The interaction of chalcocite, oxygen and xanthates*. National Institute for Metallurgy, 1896, Johannesburg.

Harris P.J., Richter K. 1985. The influence of surface defect properties on the activation and natural floatability of sphalerite. In: KSE Forssberg (ed.) *Flotation of Sulphide Minerals*. pp. 141-157. (Elsevier: Amsterdam).

He M.F., Qin W.Q., Liz W.Z., Chen Y.J., Lai C.H. 2008. Research on flotation performances of polymorphic pyrrhotite. In: *24th International Mineral Processing Congress*. pp. 1153-1160. (Science Press: Beijing).

He S.H., Fornasiero D., Skinner W. 2005. Correlation between copper-activated pyrite flotation and surface species: Effect of pulp oxidation potential. *Minerals Engineering* 18: 1208-1213.

He S.H., Grano S., Manoucheri H.M., Taylor A., Lawson V. 2008. The critical influence of pulp oxygen content on the separation of pentlandite from pyrrhotite in two process streams of the Clarabelle Mill of VALE INCO, Sudbury, Canada. In: *International Mineral Processing Congress*. pp. 1028-1037. (Science Press: Beijing).

Hemley J.J., Montoya J.W., Shaw D.R., Luce R.W. 1977. Mineral equilibria in the MgO-$SiO_2$-$H_2O$ System: II Talc-antigorite-forsterite-anthophyllite-enstatite stability relations and some geologic implications in the system. *American Journal of Science* 277: 353-383.

Henley K.J. 1983. Ore-dressing mineralogy - a review of techniques, applications and recent developments. In: JPR De Villiers and PA Cawthorn (eds.) *Proceedings of the International Congress of Applied Mineralogy 1981*. pp. 175-200. (GSSA: Johannesburg).

Heyes G.W., Trahar W.J. 1984. The flotation of pyrite and pyrrhotite in the absence of conventional collectors. In: PR Richardson, SS Srinivasan and R Woods (eds.) *Electrochemistry in Mineral and Metal Processing*. pp. 219-232. (ECS: Pennington, NJ, USA).

Hoal K.O. 2008. Getting the Geo into Geomet. *SEG Newsletter* 73: 11-15.

Hodgson M., Agar G.E. 1984. An electrochemical investigation into the natural flotability of pyrrhotite. In: PR Richardson, SS Srinivasan and R Woods (eds.) *Electrochemistry in Mineral and Metal Processing*. pp. 185-201. (ECS: Pennington, NJ, USA).

Hodgson M., Agar G.E. 1989. Electrochemical investigations into the flotation chemistry of pentlandite and pyrrhotite: Process water and xanthate interactions. *Canadian Metallurgical Quarterly* 28: 189-198.

Irving J.D. 1906. University training of engineers in economic geology: Discussion. *Economic Geology* 1: 77-82.

Iwasaki I. 1988. Flotation behaviour of pyrrhotite in the processing of copper-nickel ores. In: GP Tyroler and CA Landolt (eds.) *Extractive Metallurgy of Nickel and Cobalt*. pp. 272-292. (TMS: Warrendale, PA, USA).

Janzen M.P. 1996. Role of ferric iron, trace metal content, and crystal structure on pyrrhotite oxidation. MSc thesis, University of Waterloo.

Johnson R.H., Blowes D.W., Robertson W.D., Jambor J.L. 2000. The hydrogeochemistry of the Nickel Rim mine tailings impoundments, Sudbury, Ontario. *Journal of Contaminant Hydrology* 41: 49-80.

Johnson N.W., Munro P.D. 2008. Methods for assigning domains in the primary sulfide zone of a sulfide orebody. In: *9th International Congress for Applied Mineralogy*. pp. 597-603. (AusIMM: Brisbane).

Johnson R.S. 1986. The Phoenix and Selkirk nickel-copper sulphide ore deposits, Tati Greenstone belt, Eastern Botswana. In: CR Annhaeusser and S Maske (eds.) *Mineral Deposits of Southern Africa*. pp. 243-248. (GSSA: Johannesburg).

Jones C.F., LeCount S., Smart R.S.C. 1992. Compositional and structural alteration of pyrrhotite surfaces in solution, XPS and XRD studies. *Applied Surface Science* 55: 65-85.

Kalahdoozan M. 1996. Adsorption and flotation characteristics of hexagonal and monoclinic pyrrhotite. PhD thesis, Queens University.

Keays R.R., Lightfoot P.C. 2004. Formation of Ni-Cu-Platinum group mineralization in the Sudbury impact melt sheet. *Mineralogy and Petrology* 82: 217-258.

Kelebek S. 1993. The effect of oxidation on the flotation behaviour of nickel-copper ores. Paper presented at *XVIII Mineral Processing Congress*, Sydney.

Kelebek S., Nanthakumar B., Katsabanis P.D. 2007. Oxidation of complex Ni-Cu sulphide ores and its implication for flotation practice. *Canadian Metallurgical Quarterly* 46: 279-284.

Kelebek S., Thompson J.M., Tukel C. 2005. The impact of copper activation on the scavenging of Ni-Cu sulfide ores. In: *Centenary of Flotation Symposium*. pp. 869-873. (AusIMM: Brisbane).

Kelebek S., Tukel C. 1999. The effect of sodium metabisulfite and triethylenetetramine system on pentlandite-pyrrhotite separation. *International Journal of Mineral Processing* 57: 135-152.

Keller-Besrest F., Collin G., Comes R. 1982. Structure and planar faults in the defective NiAs-type compound 3C $Fe_7S_8$. *Acta Crystallographica* B38: 296-303.

Kelly A.P., Vaughan D.J. 1983. Pyrrhotine-pentlandite ore textures: a mechanistic approach. *Mineralogical Magazine* 47: 453-463.

Kerr, A. 2008. Personal Communication, Vale INCO.

Khan A., Kelebek S. 2004. Electrochemical aspects of pyrrhotite and pentlandite in relation to their flotation with xanthate. Part I: Cyclic voltammetry and rest potential measurements. *Journal of Applied Electrochemistry* 34: 849-856.

King R.P. 1982. *Principles of Flotation*. SAIMM: Johannesburg.

Kinloch E.D. 1982. Regional trends in the platinum-group mineralogy of the Critical Zone of the Bushveld Complex, South Africa. *Economic Geology* 77: 1328-1347.

Kirjavinen V., Schreithofer N., Heiskanen K. 2002. Effect of some process variables on flotability of sulfide nickel ores. *International Journal of Mineral Processing* 65: 59-72.

Kissin S.A., Scott S.D. 1982. Phase relations involving pyrrhotite below $350^0$C. *Economic Geology* 77: 1739-1754.

Klimpel R. 1984. Froth flotation: The kinetic approach. In: *Proceedings of Mintek 50*. (SAIMM: Johannesburg).

Koto K., Morimoto N., Gyobu A. 1975. The superstructure of the Intermediate pyrrhotite. I. Partially disordered distribution of metal vacancy in the 6C type, $Fe_{11}S_{12}$. *Acta Crystallographica* B31: 2759-2764.

Kullerud G. 1957. Phase relations in the Fe-S-O system *Carnegie Institute of Washington Year Book* 56: 198-200.

Kwong Y.T.J. 1993. *Prediction and prevention of acid rock drainage from a geological and mineralogical perspective*. NRCan, Ottawa.

Kwong Y.T.J., Swerhone G.W., Lawrence J.R. 2003. Galvanic sulphide oxidation as a metal-leaching mechanism and its environmental applications. *Geochemistry: Exploration, Environment, Analysis* 3: 337-343.

Lawson V., Kerr A.N., Shields Y., Wells P.F., Xu M., Dai Z. 2005. Improving pentlandite pyrrhotite separation at INCO's Clarabelle Mill. In: *Centenary of Flotation Symposium*. pp. 875-885. (AusIMM: Brisbane).

Leeb-Du Toit A. 1986. The Impala platinum mines. In: CR Annhaeusser and S Maske (eds.) *Mineral Deposits of Southern Africa*. pp. 1091-1106. (GSSA: Johannesburg).

Legrand D.L., Bancroft G.M., Nesbitt H.W. 2005a. Oxidation/alteration of pentlandite and pyrrhotite surfaces at pH 9.3: Part I. Assignment of XPS spectra and chemical trends. *American Mineralogist* 90: 1042-1054.

Legrand D.L., Bancroft G.M., Nesbitt H.W. 2005b. Oxidation of pentlandite and pyrrhotite surfaces at pH 9.3: Part 2 Effect of xanthates and dissolved oxygen. *American Mineralogist* 90: 1055-1061.

Lehmann M.N., Kaur P., Pennifold R.M., Dunn J.G. 2000. A comparative study of the dissolution of hexagonal and monoclinic pyrrhotites in cyanide solution. *Hydrometallurgy* 55: 255-273.

Lehner S., Savage K., Ciobanu M., Cliffel D.E. 2007. The effect of As, Co and Ni impurities on pyrite oxidation kinetics: An electrochemical study of synthetic pyrite. *Geochimica et Cosmochimica Acta* 71: 2491-2509.

Leppinen J.O. 1990. FTIR and flotation investigation of the adsorption of ethyl xanthate on activated and non-activated sulfide minerals. *International Journal of Mineral Processing* 30: 245-263.

Letard I., Sainctavit P., Deudon C. 2007. XMCD at Fe $L_{2,3}$ edges and S K edges on $Fe_7S_8$. *Physics and Chemistry of Minerals* 34: 113-120.

Li C., Naldrett A.J., Rucklidge J.C. 1993. Concentrations of platinum-group elements and gold in sulfides from the Strathcona deposit, Sudbury, Ontario. *Canadian Mineralogist* 30: 523-531.

Li C., Ripley E.M., Maier W.D., Gomwe T.E.S. 2002. Olivine and sulfur isotopic compositions of the Uitkomst Ni-Cu sulfide ore-bearing complex, South Africa: Evidence for sulfur contamination and multiple magma emplacements. *Chemical Geology* 188: 149-159.

Lianxing G., Vokes F.M. 1996. Intergrowths of hexagonal and monoclinic pyrrhotites in some sulphide ores from Norway. *Mineralogical Magazine* 60: 303-316.

Liebenberg L. 1970. The sulphides in the layered sequence of the Bushveld Igneous Complex. In: *Symposium on the Bushveld Igneous Complex and other layered intrusions*. pp. 108-207. (GSSA: Johannesburg).

Lotter N.O., Bradshaw D.J., Kormos L.J., Becker M., Parolis L.A.S. 2008. A discussion of the occurrence and undesirable flotation behaviour of orthopyroxene and talc in the processing of mafic deposits. *Minerals Engineering* 21: 905-912.

Lotter N., Whittaker P.J., Kormos L., Stickling J.S., Wilkie G.J. 2002. The development of process mineralogy at Falconbridge Limited, and the application to the Raglan Mill. Paper presented at the *34th Annual Meeting of the Canadian Mineral Processors*, Ottawa.

Magyarosi Z., Watkinson D.H., Jones P.C. 2002. Mineralogy of Ni-Cu-Platinum-Group-Element sulfide ore in the 800 and 810 Ore bodies, Copper Cliff South Mine, and P-T-X Conditions during the formation of platinum-group-minerals. *Economic Geology* 97: 1471-1486.

Maier W.D., Barnes S.-J., Chinyepi G., Barton M.J., Eglington B., Setshedi I. 2008. The composition of magmatic Ni-Cu-(PGE) sulfide deposits in the Tati and Selebi-Phikwe belts of eastern Botswana. *Mineralium Deposita* 43: 37-60.

Makovicky E. 2006. Crystal structures of sulfides and other chalcogenides. In: DJ Vaughan (ed.) *Sulfide Mineralogy and Geochemistry*. pp. 7-125. (MSA: Washington DC, USA).

Malysiak V., O' Connor C.T., Ralston J., Gerson A., Coetzer L.P., Bradshaw D.J. 2002. Pentlandite - feldspar interaction and its effect on separation by flotation. *International Journal of Mineral Processing* 66: 89-106.

Mbonambi M.J. 2009. On the selective flotation of pentlandite. MSc thesis, University of Cape Town.

Mendiratta N.K. 2000. Kinetic studies of sulfide mineral oxidation and xanthate adsorption. PhD thesis, Virginia Polytechnic and State University.

Mikhlin Y., Tomashevich Y. 2005. Pristine and reacted surfaces of pyrrhotite and arsenopyrite as studied by X-ray absorption near-edge structure spectroscopy. *Physics and Chemistry of Minerals* 32: 19-27.

Mikhlin Y.L., Kuklinskiy A.V., Pavlenko N.I., Varnek V.A., Asanov I.P., Okotrub A.V., Selyutin G.E., Solovyev L.A. 2002. Spectroscopic and XRD studies of the air degradation of acid-reacted pyrrhotites. *Geochimica et Cosmochimica Acta* 66: 4057-4067.

Miller J.A., Li C., Davidtz J.C., Vos F. 2005. A review of pyrrhotite flotation chemistry in the processing of PGM ores. *Minerals Engineering* 18: 855-865.

Morimoto N., Gyobu A., Mukaiyama H., Izawa E. 1975a. Crystallography and stability of pyrrhotites. *Economic Geology* 70: 824-833.

Morimoto N., Gyobu A., Tsukuma K., Koto K. 1975b. Superstructure and nonstoichiometry of intermediate pyrrhotite. *American Mineralogist* 60: 240-248.

Morimoto N., Nakazawa H., Nishiguchi K., Tokonami M. 1970. Pyrrhotites: Stoichiometric compounds with composition $Fe_{n-1}S_n$ ($n > 8$). *Science* 168: 964-966.

Mycroft J.R., Nesbitt H.W., Pratt A.R. 1995. X-ray photoelectron and Auger electron spectroscopy of air-oxidized pyrrhotite: Distribution of oxidized species with depth. *Geochimica et Cosmochimica Acta* 59: 721-733.

Nagaraj D.R., Brinen J.S. 1996. SIMS and XPS study of the adsorption of sulfide collectors on pyroxene: a case for inadvert metal in activation. *Colloids and Surfaces A: Physicochemical and Engineering Aspects* 116: 241-249.

Nakano A., Tokonami M., Morimoto N. 1979. Refinement of 3C pyrrhotite, $Fe_7S_8$. *Acta Crystallographica* B35: 722-724.

Nakazawa H., Iwasaki I. 1995. Effect of pyrite-pyrrhotite contact on their floatabilities. *Minerals and Metallurgical Processing* 2: 206-211.

Nakazawa H., Morimoto N. 1971. Phase relations and superstructures of pyrrhotite, $Fe_{1-x}S$. *Materials and Research Bulletin* 6: 345-358.

Naldrett A.J. 1969. A portion of the system Fe-S-O between 900 and $1080^0$C and its application to ore magmas. *Journal of Petrology* 10: 171-201.

Naldrett A.J. 1989. *Magmatic Sulfide Deposits*. Oxford University Press: New York.

Naldrett A.J. 2004. *Magmatic Sulfide Deposits*. Springer: Berlin.

Naldrett A.J., Craig J.R., Kullerud G. 1967. The central portion of the Fe-Ni-S system and its bearing on pentlandite exsolution in iron-nickel sulfide ores. *Economic Geology* 62: 826-847.

Naldrett A.J., Kullerud G. 1967. A study of the Strathcona Mine and its bearing on the origin of the nickel-copper ores of the Sudbury District, Ontario. *Journal of Petrology* 9: 453-531.

Naldrett A.J., Singh J., Krstic S., Li C.S. 2000. The mineralogy of the Voisey's Bay Ni-Cu-Co deposit, northern Labrador, Canada: Influence of oxidation state on textures and mineral compositions. *Economic Geology* 95: 889-900.

Nel E., Valenta M., Naude M. 2005. Influence of open circuit regrind milling on UG2 ore composition and mineralogy at Impala's UG2 concentrator. *Minerals Engineering* 18: 785-790.

Nesbitt H.W., Bricker O.P. 1978. Low temperature alteration processes affecting ultramafic bodies *Geochimica et Cosmochimica Acta* 42: 403-409.

Nicol M.J. 1984. An electrochemical study of the interaction of copper (II) ions with sulphide minerals. In: PR Richardson, SS Srinivasan and R Woods (eds.) *Electrochemistry in Mineral and Metal Processing*. pp. 152-168. (ECS: Pennington, NJ, USA).

Orlova T.A., Stupnikov V.M., Kresan A.L. 1988. Mechanism of oxidative dissolution of sulphides. *Zhurnal Prikladnoi Khimii* 61: 2172-2177.

Penberthy C.J., Merkle R.K.W. 1999. Lateral variations in the platinum-group element content and mineralogy of the UG2 Chromitite layer, Bushveld Complex. *South African Journal of Geology* 102: 240-250.

Petruk W. 2000. *Applied Mineralogy in the Mining Industry*. Elsevier: Amsterdam.

Pierce L., Buseck P.R. 1974. Electron imaging of pyrrhotite superstructures. *Science* 186: 1209-1212.

Pietrobon M.C., Grano S.R. 2001. Pyrrhotite depression for enhanced pentlandite / pyrrhotite selectivity at the Strathcona Concentrator, Falconbridge Limited, Canada. In: JA Finch, SR Rao and L Huang (eds.) *Interactions in Mineral Processing*. pp. 153-167. (CIM: Montreal).

Posfai M., Dodony I. 1990. Pyrrhotite superstructures. Part I: Fundamental structures of the *NC* (N = 2, 3, 4 and 5) type. *European Journal of Mineralogy* 2: 525-528.

Posfai M., Sharp T.G., Kontny A. 2000. Pyrrhotite varieties from the 9.1km deep borehole of the KTB project. *American Mineralogist* 85: 1406-1415.

Powell A.V., Vaqueiro P., Knight K.S., Chapon L.C., Sanchez R.D. 2004. Structure and magnetism in synthetic pyrrhotite $Fe_7S_8$: A powder neutron-diffraction study. *Physical Review B* 70: 014415-1 -014415-12.

Pratt A.R., Muir I.J., Nesbitt H.W. 1994. X-ray photoelectron and Auger electron spectroscopic studies of pyrrhotite and mechanism of air oxidation. *Geochimica et Cosmochimica Acta* 58: 827-841.

Prestidge C.A., Ralston J., Smart R.S.C. 1993. The competitive adsorption of cyanide and ethyl xanthate on pyrite and pyrrhotite surfaces. *International Journal of Mineral Processing* 38: 205-233.

Ramdohr P. 1969. *The ore minerals and their intergrowths*. Pergamon Press: Oxford.

Rand D.A.J. 1977. Oxygen reduction of sulphide minerals. Part III. Comparison of activities of various copper, iron, lead and nickel mineral electrodes. *Journal of Electroanalytical Chemistry* 83: 19-32.

Rao S.R., Finch J.A. 1991. Adsorption of amyl xanthate at pyrrhotite in the presence of nitrogen and implications in flotation. *Canadian Metallurgical Quarterly* 30: 1-6.

Raudsepp M., Pani E., Kern A. 2002. Quantitative phase analysis of sulfide-bearing mine wastes using the Rietveld method and X-ray Powder diffraction data. *Powder Diffraction in Mining and Minerals* 27: 10-12.

Rickard J.H., Watkinson D.H. 2001. Cu-Ni-PGE mineralization within the Copper Cliff Offset Dike, Copper Cliff North Mine, Sudbury, Ontario: Evidence for multiple stages of emplacement. *Exploration and Mining Geology* 10: 111-124.

Rousell D.H., Fedorowich J.S., Dressler B.O. 2003. Sudbury Breccia (Canada): A product of the 1850Ma Sudbury Event and host to footwall Cu-Ni-PGE ore deposits. *Earth Science Reviews* 60: 147-174.

Rumball J.A., Richmond G.D. 1996. Measurement of oxidation in a base metal flotation circuit by selective leaching with EDTA. *International Journal of Mineral Processing* 48: 1-20.

SACS 1980. *Stratigrapy of Southern Africa. Part 1: Lithostratigraphy of South Africa, South West Africa/Namibia, and the Republics of Bophuthatswana, Transkei, and Venda*. Geological Survey of South Africa.

Schouwstra R.P., Kinloch E.D., Lee C.A. 2000. A short geological review of the Bushveld Complex. *Platinum Metals Review* 44: 33-39.

Scott R.G., Benn K. 2002. Emplacement of sulfide deposits in the Copper-Cliff Offset dike during collapse of the Sudbury Crater Rim: Evidence from magnetic fabric studies. *Economic Geology* 97: 1447-1458.

Senior G.D., Thomas S.A. 2005. Development and implementation of a new flow sheet for the flotation of a low grade nickel ore. *International Journal of Mineral Processing* 78: 49-61.

Senior G.D., Trahar W.J., Guy P.J. 1995. The selective flotation of pentlandite from a nickel ore. *International Journal of Mineral Processing* 43: 209-234.

Shackleton N.J. 2003. The role of complexing agents in the flotation of pentlandite-pyroxene mixtures. MSc thesis, University of Cape Town.

Shackleton N.J., Malysiak V., O'Connor C.T. 2007. Surface characteristics and flotation behaviour of platinum and palladium arsenides. *International Journal of Mineral Processing* 85: 25-40.

Shima H., Naldrett A.J. 1975. Solubility of sulfur in an ultramafic melt and the relevance of the system Fe-S-O. *Economic Geology* 70: 960-967.

Shortridge P.G. 2002. The influence of polymeric charge and structure, molecular weight and ionic conditions on depressant ability to reduce the natural floatability of talc. MSc thesis, University of Cape Town.

Skala R., Cisarova I., Drabek M. 2006. Inversion twinning in troilite. *American Mineralogist* 91: 917-921.

Skinner W.M., Nesbitt H.W., Pratt A.R. 2004. XPS identification of bulk hole defects and itinerant Fe 3d electrons in natural troilite (FeS). *Geochimica et Cosmochimica Acta* 68: 2259-2263.

Spira P., Rosenblum F. 1974. The oxygen demand of flotation pulps. In: *6th Annual Meeting of the Canadian Mineral Processors*. pp. 74-106. (CIM: Ottawa).

Steger H.F. 1982. Oxidation of sulfide minerals VII. Effect of temperature and relative humidity on the oxidation of pyrrhotite. *Chemical Geology* 35: 281-295.

Steger H.F., Desjardins L.E. 1978. Oxidation of sulfide minerals, 4. Pyrite, chalcopyrite, and pyrrhotite. *Chemical Geology* 23: 225-237.

Stillwell F.L., Edwards A.B. 1945. The mineral composition of the Black Star copper ore body, Mount Isa, Queensland. *Proceedings of the Australian Institute of Mining and Metallurgy* 139: 149-159.

Sugaki A., Kitakaze A. 1998. High form of pentlandite and its thermal stability. *American Mineralogist* 83: 133-140.

Sutherland K.L., Wark I.W. 1955. *Principles of Flotation* AusIMM: Melbourne.

Szentpéteri K., Watkinson D.H., Molnár F., Jones P.C. 2002. Platinum-group elements-Co-Ni-Fe sulfarsenides and mineral paragenesis in Cu-Ni-platinum-group element deposits, Copper Cliff North area, Sudbury, Canada. *Economic Geology* 97: 1459-1470.

Tao D.P., Richardson P.E., Luttrell G.H., Yoon R.-H. 2003. Electrochemical studies of pyrite oxidation and reduction using fresh-fractured electrodes and rotating ring-disc electrodes. *Electrochimica Acta* 48: 3615-3623.

Theart H.F.J., de Nooy C.D. 2001. The platinum group minerals in two parts of the massive sulphide body of the Uitkomst Complex, Mpumalanga, South Africa. *South African Journal of Geology* 104: 287-300.

Theodossiou A. 1965. Measurements of the Hall effect and resistivity in pyrrhotite. *Physical Review* 137: A1321.

Thomas J.E., Skinner W.M., Smart R.S.C. 2003. A comparison of the dissolution behaviour of troilite with iron(II) sulfides, implications of structure. *Geochimica et Cosmochimica Acta* 67: 831-843.

Thomas J.E., Smart R.S.C., Skinner W.M. 2000. Kinetic factors for oxidative and non-oxidative dissolution of iron sulfides. *Minerals Engineering* 13: 1149-1159.

Tokonami M., Nishiguchi K., Morimoto N. 1972. Crystal structure of a monoclinic pyrrhotite ($Fe_7S_8$). *American Mineralogist* 57: 1066-1080.

Toulmin P., Barton P.B. 1964. A thermodynamic study of pyrite and pyrrhotite. *Geochimica et Cosmochimica Acta* 28: 641-671.

Tremblay, E. 2007. Personal Communication, Vale INCO.

Vanyukov A.V., Razumovskaya N.N. 1979. Hydrothermal oxidation of pyrrhotites. *Izv. Vyssh. Uchelon. Zaved., Tsvetn.Metall.* 6: 605-610.

Vaughan D.J., Schwarz E.J., Owens D.R. 1971. Pyrrhotites from the Strathcona Mine, Sudbury, Canada: A thermomagnetic and mineralogical study. *Economic Geology* 66: 1131-1144.

van Zyl A.M. 1996. The sulphides of the Uitkomst Complex, Badplaas, South Africa. MSc thesis, University of Pretoria.

Viljoen M.J., Hieber R. 1986. The Rustenburg Section of Rustenburg Platinum Mines Limited, with reference to the Merensky Reef. In: CR Annhaeusser and S Maske (eds.) *Mineral Deposits of Southern Africa*. pp. 1107-1134. (GSSA: Johannesburg).

Viljoen M.J., Theron J., Underwood B., Walters B.M., Weaver J., Peyerl W. 1986. The Amandebult section of Rustenburg Platinum mines Limited, with reference to the Merensky

Reef. In: CR Annhaeusser and S Maske (eds.) *Mineral Deposits of Southern Africa*. pp. 1041-1060. (GSSA: Johannesburg).

Viti C., Mellini M., Rumori C. 2005. Exsolution and hydration of pyroxenes from partially serpentinized harzburgites. *Mineralogical Magazine* 69: 491-507.

Viring R.G., Cowell M.W. 1999. The Merensky Reef on Northam Platinum Limited. *South African Journal of Geology* 102: 192-208.

Vos F. 2006. The role of long chain trithiocarbonates in the optimisation of Impala Platinum's flotation circuit. MSc thesis, University of Pretoria.

Walters S.G. 2008. An overview of new integrated geometallurgical research. In: *9th International Congress for Applied Mineralogy*. pp. 79-82. (AusIMM: Brisbane).

Wang H., Salveson I. 2005. A review on the mineral chemistry of the non-stoichiometric iron sulphide, $Fe_{1-x}S$ ($0 \leq x \leq 0.125$): Polymorphs, phase relations and transitions, electronic and magnetic structures. *Phase Transitions* 78: 547-567.

Weisener C., Gerson A. 2000. An investigation of the Cu(II) adsorption mechanism on pyrite by ARXPS and SIMS. *Minerals Engineering* 13: 1329-1340.

Wells P.F., Kelebek S., Burrows M.J., Suarez D.F. 1997. Pyrrhotite rejection at Falconbridge's Strathcona Mill. In: JA Finch, SR Rao and I Holubec (eds.) *Processing of Complex Ores: Mineral Processing and the Environment*. pp. 51-62. (CIM: Montreal).

Wiese, J.G. Unpublished Data.

Wiese, J.G. 2005. Personal Communication, University of Cape Town.

Wiese J.G., Becker M., Bradshaw D.J., Harris P.J. 2007. Interpreting the role of reagents in the flotation of platinum-bearing Merensky ores. *South African Institute of Mining and Metallurgy* 107: 29-36.

Wiese J.G., Harris P.J., Bradshaw D.J. 2005. The influence of the reagent suite on the flotation of ores from the Merensky Reef. *Minerals Engineering* 18: 189-198.

Wightman E., Evans C.L., Vizcarra T., Sandoval G. 2008. Process Mineralogy as a tool in modelling mineral processing operations. In: *9th International Congress for Applied Mineralogy*. pp. 475-481. (AusIMM: Brisbane).

Wills B.A., Napier-Munn, T.J. 2006. *Will's Mineral Processing Technology: An introduction to the practical aspects of ore treatment and mineral recovery*. Elsevier: Amsterdam.

Wuensch B.J. 1963. On the superstructure and twinning of pyrrhotite. *Mineralogical Society of America Special Paper* 1: 157-162.

Wyckoff R.W.G. 1963. *Crystal Structures*. Interscience: London.

Xu M., Wilson S. 2000. Investigation of seasonal metallurgical shift at INCO's Clarabelle Mill. *Minerals Engineering* 13: 1207-1218.

Yakhontova L.K., Nesterovich L.G., Grudev A.P. 1983. New data on natural oxidation of pyrrhotite. *Vestnik Moskovskogo Universiteta Geologiya* 38: 41-44.

Yamamoto M., Iwata T., Iwata M. 1959. Domain patterns on ferromagnetic pyrrhotite crystal. *Science Reports of the Research Institutes, Tohoku University* 11: 21-29.

Yoon R.-H., Basilio C.I., Marticorena M.A., Kerr A.N., Stratton-Crawley, R. 1995. A study of the pyrrhotite depresssion mechanism by diethylenetriamine. *Minerals Engineering* 8: 807-816.

Young R.A. 1995. Introduction to the Rietveld Method. In: RA Young (ed.) *The Rietveld Method*. pp. 1-38. (Oxford University Press: New York).

Zapletal K. 1969. Connection of some magnetic properties with the phase composition of natural pyrrhotites. *Studia geophysica et geodata* 13: 191-197.

Zapletal K. 1972. On the magnetic phases of natural pyrrhotites *Studia geophysica et geodata* 16: 167-208.